

Copyright

by

John Zihong Li

2017

**The Thesis Committee for John Zihong Li
Certifies that this is the approved version of the following thesis:**

**Fracture Spatial Arrangement in Tight Gas Sandstone and
Shale Reservoir Rocks**

**APPROVED BY
SUPERVISING COMMITTEE:**

Supervisor:

Stephen E. Laubach

Co-Supervisor:

Julia F. W. Gale

William L. Fisher

Charles Kerans

**Fracture Spatial Arrangement in Tight Gas Sandstone and
Shale Reservoir Rocks**

by

John Zihong Li

Thesis

Presented to the Faculty of the Graduate School of

The University of Texas at Austin

in Partial Fulfillment

of the Requirements

for the Degree of

Master of Science in Geological Sciences

The University of Texas at Austin

August 2017

Dedication

To Mom

Acknowledgements

I am immensely grateful to my supervisors Dr. Julia F.W. Gale and Dr. Stephen E. Laubach for their insightful advising and kind support through my graduate geoscience study. I thank Prof. Randall A. Marrett for developing Normalized Correlation Count and providing its software vital to my research. I also thank my committee members Prof. William L. Fisher and Prof. Charles Kerans for thesis review. For the tight gas sandstone section as a paper in the Journal of Structural Geology, I am grateful to B.B. DeJarnett for image log access, to S.J. Wilkins and Anadarko Petroleum Corporation for core access, and to L.K. Copley for contributing to the initial spatial analysis of core fracture data. I am also grateful to E. Ukar, S.R. Forstner, J.N. Hooker, and M. Shuster for comments on the earlier drafts of the TGS manuscript and to Clare E. Bond, David A. Ferrill, and William M. Dunne for thorough reviews. For the shale section, I thank the associated sponsors of FRAC for image logs from the Neuquén Basin and the Horn River Basin. Funding for the Marcellus Shale project was provided by Research Partnership to Secure Energy for America (RPSEA) through the “Ultra-Deepwater and Unconventional Natural Gas and Other Petroleum Resources” program authorized by the U.S. Energy Policy Act of 2005. Range Resources Appalachia LLC provided core and well data.

This study on fracture spatial arrangement is funded in part by grant DE-FG02-03ER15430 from Chemical Sciences, Geosciences and Biosciences Division, Office of Basic Energy Sciences, Office of Science, U.S. Department of Energy, by the Fracture Research and Application Consortium, by the Geology Foundation of the Jackson School of Geosciences at The University of Texas at Austin. It is also supported in part by the Edward C. and Caroline Beaumont Named Grant of the AAPG Foundation.

Abstract

Fracture Spatial Arrangement in Tight Gas Sandstone and Shale Reservoir Rocks

John Zihong Li, M.S. Geo. Sci.

The University of Texas at Austin, 2017

Supervisor: Stephen E. Laubach

Co-Supervisor: Julia F. W. Gale

A new statistical analytical method was applied to quantify the spatial arrangement of fractures in sandstones and shales. Results show that spatial arrangements of fractures in the subsurface have a wide range of patterns and that fracture clusters are prevalent. The Upper Cretaceous Frontier Formation is a naturally fractured gas-producing sandstone in Wyoming. East-west-striking regional fractures sampled using image logs and cores from three horizontal wells exhibit clustered patterns, whereas data collected from outcrop have patterns that are indistinguishable from random. Image log data analyzed with the correlation count method shows clusters ~35 m wide and spaced ~ 50 to 90 m apart as well as clusters up to 12 m wide with periodic inter-cluster spacings. A hierarchy of cluster sizes exists; arrangement within clusters is likely fractal. Regionally, random and statistically more clustered than random patterns exist in the same upper to lower shoreface depositional facies. These rocks have markedly different structural and burial histories, so regional differences in degree of clustering are unsurprising. Application to shale reservoirs

further link fracture clusters and spatial arrangements with reservoir mechanical stratigraphy: Vaca Muerta Formation shale shows strong control of fracture cluster locality by reservoir mechanical properties; Middle Devonian shales in the Horn River Basin identify spatial arrangement and cluster dimensions associated with preferred wellbore intervals; Marcellus Formation shale shows spatial arrangement controlled by mechanical bed thickness. Our results show that quantifying and identifying patterns as statistically more or less clustered than random delineate differences in fracture patterns that are not otherwise apparent but that may influence petroleum and water production, and therefore may be economically important.

Table of Contents

List of Tables	xi
List of Figures	xiii
SECTION I: OVERVIEW	1
Chapter 1: Fracture Spatial Arrangement	1
SECTION II: FRACTURE SPATIAL ARRANGEMENT IN A TIGHT GAS SANDSTONE	3
Chapter 2: Geologic Setting of Tight Gas Sandstone Example	3
Chapter 3: Datasets and Methods for Sandstone Study	11
3.1 Horizontal well image logs, Wyoming	11
3.2 Horizontal Well VM-Cores, Wyoming.....	16
3.3 Outcrop data, Wyoming.....	16
3.4 General Spatial analysis methods	17
Chapter 4: Results: Wyoming.....	21
4.1 Rock Island 4-H observations.....	23
4.2 Sidewinder 1-H observations.....	23
4.3 Sidewinder 2-H observations.....	23
4.4 Core observations, Wyoming.....	24
4.5 Outcrop observations, Wyoming	25
4.6 Intensity and spatial arrangement, Wyoming	26
4.6.1 Intensity and correlation count, Wyoming subsurface data.....	28
4.6.2 Intensity and correlation count, Wyoming outcrop data.....	35
Chapter 5: Discussion: Tight Gas Sandstone.....	36
5.1 Cluster patterns in sandstone example.....	36
5.2 Causes of spatial arrangement patterns, Wyoming.....	44
5.3 Comment on fractured layer/bed thickness from Wyoming outcrop...47	
5.4 Implications for reservoir characterization, Frontier Formation TGS .49	

Chapter 6: Conclusions: Tight Gas Sandstone.....	50
SECTION III: FRACTURE SPATIAL ARRANGEMENT IN SHALES.....	52
Chapter 7: Geologic Backgrounds of Shale Studies	52
7.1 Vaca Muerta Formation shale, Argentina.....	52
7.2 Middle and Late Devonian shales, Canada.....	55
7.3 Marcellus Formation shale, USA.....	55
Chapter 8: Datasets and Methods for Shale Studies	58
Chapter 9: Results and Discussion: Neuquén Basin	60
9.1 Intensity and spatial arrangement, Neuquén Basin.....	60
9.1.1 Intensity and correlation count, Well VM-A	60
Set 1 fractures, VM-A.....	62
Set 2 fractures, VM-A.....	66
9.1.2 Intensity and correlation count, Well VM-B	71
9.1.3 Intensity and correlation count, Well VM-C	74
9.2 Interpretation and discussion, Neuquén Basin.....	76
9.2.1 Interpretation: Well VM-A	76
9.2.2 Interpretation: Well VM-B	77
9.2.3 Interpretation: Well VM-C	77
9.2.4 Discussion: Neuquén Basin wells.....	78
Chapter 10: Results and Discussion: Horn River Basin	80
10.1 Intensity and spatial arrangement, Horn River Basin	80
10.1.1 Intensity and correlation count, Well HRB-1	80
Conductive fracture sets, HRB-1	83
Resistive fracture sets, HRB-1	91
Other fracture sets, HRB-1	101
10.1.2 Intensity and correlation count, Well HRB-2	109
Conductive fracture sets, HRB-2	112
Sealed fracture sets, HRB-2.....	120
Natural fracture supersets, HRB-2.....	128

10.2 Interpretation and discussion, Horn River Basin	133
10.2.1 Interpretation: Well HRB-1	138
Conductive fracture sets, HRB-1	138
Resistive fracture sets, HRB-1	139
10.2.2 Interpretation: Well HRB-2	140
Conductive fracture sets, HRB-2	140
Sealed fracture sets, HRB-2	141
10.2.3 Discussion: Horn River Basin wells	143
Well HRB-1	145
Well HRB-2	147
Causes of spatial arrangement patterns, Horn River Basin.....	149
Chapter 11: Results and Discussion: Appalachian Basin	152
11.1 Intensity and spatial correlation results, Appalachian Basin	152
11.2 Interpretation: Gulla 10H.....	154
11.3 Discussion: Gulla 10H	155
SECTION IV: SUMMARY	156
Chapter 12: Fracture Spatial Arrangement Insights through Normalized Correlation Count.....	156
Appendix: Vaca Muerta Formation Shale Fracture Petrography	158
References.....	166

List of Tables

Table 3-1	Descriptive statistics of fractures in Rock Island 4-H image log. Upper shoreface approximately 4663.4 m – 4785.4 m; lower shoreface approximately 4785.4 m – 5025.2 m. Fracture intensity values normalized to correct for difference in facies’ interval length.19
Table 4-1	Descriptive statistics for conductive fracture spacings in Frontier Formation acquired from wells, outcrop images, and cores. 4H = Rock Island 4H; 1H = Sidewinder 1H; 2H = Sidewinder 2H. CR = Core; CR1, 2, and 3 from 4H (1 and 2 in upper shoreface, 3 in lower shoreface); CR4 from 1H. Oc2 = Hogsback outcrop. Coefficient of variation, Cv, calculated as σ/μ , where σ is the standard deviation of fracture spacings and μ is the mean (Gillespie et al., 1993); if coefficient of variation is near 1 then fracture arrangement is indistinguishable from random, but a value greater than 1 indicates clustering and a value less than 1 indicates anti-clustering.22
Table 5-1	Summary of NCC interpretation for fractures in Frontier image logs, cores, and outcrop. RI4H = Rock Island 4H; SW1H = Sidewinder 1H; SW2H = Sidewinder 2H. Cluster width within parenthesis indicates width of internal clusters. *Well name or outcrop locality. †Average orientation and local set classification.37
Table 9-1	Statistical summaries of selected image log fracture sets in Well VM-A, VM-B, and VM-C. UVM = Upper Vaca Muerta.....61

Table 9-2	Summary of NCC interpretation for selected fracture sequences in Vaca Muerta image logs. Numbers within parentheses indicates attributes of internal clusters. UVM = Upper Vaca Muerta.....	78
Table 10-1	Statistical summaries on image log fracture sets in Horn River Basin Well HRB-1. Fracture sets in red contain NCC results for select internal high intensity interval(s) and are presented in Figures 10-64 to 10-67 for cross-well comparison.	81
Table 10-2	Statistical summaries on image log fracture sets in Horn River Basin Well HRB-2. Fracture sets in red contain NCC results for select internal high intensity interval(s) and are presented in Figures 10-64 to 10-67 for cross-well comparison.	110
Table 10-3	Summary of NCC interpretation for selected fracture sequences in Horn River Basin horizontal wellbore image logs. Spatial arrangement styles in parentheses are interpreted for NCC on selected internal clusters. Numbers within parentheses indicates attributes of internal clusters identified from corresponding NCC results.....	144
Table 11-1	Statistical summaries on image log fracture sets in Gulla 10H. Note that the NCC results for sets other than Natural-All are omitted due to incomplete curves from small sample sizes.....	152

List of Figures

Figure 2-1 Greater Green River Basin, Wyoming, showing Well VM-A outcrop locations, scanline dimensions, and representative image log. (a) Sub-basins, uplifts and Well VM-And outcrop locations. Wells: Rock Island 4-H (RI4H), Sidewinder 1-H (SW1H), Sidewinder 2-H (SW2H), Table Rock (TR) field, Sweetwater County, Wyoming. NNE well trajectories are indicated. Rose diagrams show fractures strikes (from Laubach et al., 2016). Outcrops Oc1 and Oc2 shown in Figures 2-2 and 2-3 respectively. Orientation diagram shows main fracture strikes in Kemmerer section, Hogsback outcrop belt. K, Kemmerer, Wyoming. Inset: Location of Greater Green River Basin in western U.S. Background image: Google Earth. (b) Representative lengths of observation scanlines: outcrop scanline length from Oc2; image log length from RI4H and core lengths from RI4H. For the Rock Island 4-H well, readily interpreted image log data exists from measured depth (MD) 4663.4 m to 5025.2 m. (c) Representative section of FMI image log from RI4H showing fracture traces (F) and bedding (B).....4

Figure 2-2 Fractures in outcrop and core, Frontier Formation. (a) Fracture traces in north-northeast trending outcrop (Oc1), west-dipping pavement northeast of Kemmerer, Wyoming, Google Earth dated 9/1/2014. Three main fracture trends are evident. Spacings of east- or east-northeast-striking fractures (F) were measured here and in Oc2, directly north along the outcrop belt. L1, L2 mark separate marine sandstone lenses. Part of contact is dashed. (b) Fracture face, east-northeast striking fracture from outcrop south of Kemmerer. Calcite (cc) filling fractures is compatible with formation of these fractures in the subsurface. Comparator is 10 cm long. (c) Same outcrop as in b; F, fracture face. Tall fractures (H) span the thickness of the sandstone; entire thickness of which is not shown. (d) Frontier Formation bed surface with fractures traces (F), Muddy Gap, Wyoming, northeast of core location. Fractures have trace lengths many tens of meters long. Here, spacing between traces (arrow) is ca. 5 m. Fractured bed thickness is ca. 20 m. (e) Core from Rock Island 4-H horizontal core, in the depth interval 15454-15464 ft (4710-4713 m) (Core 2). Beds are approximately parallel to the long dimension of the core; arrow marks top of core, core diameter ca. 4 inches (10 cm).....7

Figure 2-3 Fracture traces, western Green River Basin, outcrop 2 (Oc2 in Figure 2-1). Background Google Earth image where fractures were traced. Red lines mark fracture traces, black lines represent scanlines. Location map after Lorenz and Laubach (1994). Fracture clusters (called swarms; Laubach, 1992, their Figures 4 and 9) are visible in other outcrops on the opposite, steeply east-dipping fold limb.9

Figure 3-1 Occurrence versus distance (stick) plots of fractures visible in image logs, core and outcrop. Zero represents beginning of scanline. Black vertical lines are opening-mode fractures (some with evidence of reactivation in core data sets); FL, red lines are faults recognized by offset beds on image logs. Horizontal scale in meters. Vertical dimension of lines is arbitrary; Laubach et al. (2016) report aperture size versus distance plots for cored intervals (their figure 4). Inset numbers are fractures per meter (F/m).14

Figure 3-2 Fracture spacing histograms for image logs, cores, and outcrop. Image log and core plots generated from spacing of conductive fractures aggregated from all wells. A few very low frequencies (0 to 1) for large spacings (> 10 m) omitted for clarity. All show high frequency of sub-meter spacings with varying degrees of distribution spread.15

Figure 3-3 Cumulative frequency versus fracture spacing for all data sets. Frequencies approaching zero beyond 1 m, 5 m, and 10 m omitted for optimal display as in Figure 5.20

Figure 4-1 CorrCount result for Rock Island 4-H conductive fractures. (a) Normalized fracture intensity variation of Set 1. Fracture intensity is the number of fractures per unit length along a scanline (Ortega et al., 2006). (b) Normalized correlation count Set 1 fractures in RI4H. Length scales are logarithmically graduated. Sparse Set 2 observations precluded analysis. For this and subsequent figures, ‘0 m’ signifies arbitrary start of scanline. Highlighted areas mark parts of curve outside 95% confidence interval.29

Figure 4-2 Sidewinder 1-H conductive fracture sets CorrCount results. (a) Intensity of Set 1. (b) Correlation count of Set 1. (c) Intensity of Set 2. There is a peak at ~100 m. The two largest peaks in the intensity plot are spaced ~100 apart, and the smaller peaks are spaced at ~15 m. (d) Correlation count of Set 2. Set 1 correlation count patterns exhibit low amplitude, and predominantly statistically significant patterns throughout. Set 2 correlation count results have a decreasing elevated section followed by peaks and troughs over larger length scales. Highlighted areas mark parts of curve outside 95% confidence interval.....30

Figure 4-3 Sidewinder 2-H conductive fracture sets CorrCount results. (a) Intensity of Set 1. (b) Correlation count of Set 1. There is a minor trough over 9.5 m and a major trough over 20 m. (c) Intensity of Set 2. (d) Correlation count of Set 2. All correlation count results have a decreasing elevated section followed by peaks and troughs over larger length scales. Highlighted areas mark parts of curve outside 95% confidence interval.31

Figure 4-4 Cores, Frontier Formation sandstone, CorrCount results. (a) Intensity for Cores 1 and 2. (b) Correlation count of Cores 1 and 2. (c) Intensity of Core 3. (d) Correlation count of Core 3. (e) Intensity of Core 4. (f) Correlation count of Core 4. All correlation count results exhibit distinctive peaks for small length scales but are overall confined within the 95% confidence interval. Highlighted areas mark parts of curve outside 95% confidence interval.....33

Figure 4-5 Outcrop, east-striking fractures, Frontier sandstone Oc2, CorrCount results. (a) Intensity result. (b) Correlation count result. Both plots Well VM-Confined within upper- and lower confidence limits and are therefore practically indistinguishable from random. Highlighted areas mark parts of curve outside 95% confidence interval.....35

Figure 5-1 Comparison of CorrCount results. Normalized correlation count = 1 suggests correlation indistinguishable from random. Log scale, windowing set to 1. Highlighted areas mark parts of curve outside 95% confidence interval. (a) Comparison of normalized correlation count results between image logs. All results show similar exponential decrease in spatial correlation for length scales less than 10 m. RI4H = Rock Island 4-H, SW1H = Sidewinder 1-H, SW2H = Sidewinder 2-H. (b) Comparison of normalized correlation count results between cores and outcrop. Peak-and-trough signals differ from the continuous interval pattern for image log results.41

Figure 7-1 (a) Neuquén Basin location map with distribution of selected major compressional structures. Present-day S_{Hmax} trends approximately E-W. Modified from Howell et al. (2005) and Guzmán et al. (2007). (b) Generalized Early Jurassic to Early Cretaceous basinal stratigraphic column. Vaca Muerta Formation shale in red. Modified from Vergani et al. (1995).53

Figure 7-2 Subvertical opening-mode natural fracture in Vaca Muerta Formation shale petrographic thin section under optical microscope in crossed polar view. Wall-to-wall distance in figure averages approximately 3.5 mm. Fracture is filled by twinned anhedral calcite cements.54

Figure 7-3	(a) Horn River Basin and the Liard Basin to its west, northeastern British Columbia, western Canada. The west-dipping Bovie normal fault zone divides the two basins. Modified from Wright et al. (1994), Ross and Bustin (2008), and Dunphy and Campagna (2011). (b) Generalized Middle to Late Devonian stratigraphic section of the Horn River Basin. Muskwa, Otter Park, and Evie Shales highlighted in red. Modified from Ross and Bustin (2008).	56
Figure 7-4	(a) Location of the Appalachian Basin and the surface and subsurface extent of the Marcellus Formation shale, eastern USA. Modified from USGS Marcellus Shale Assessment Team (2011) and Ciezobka (2013) (b) Generalized Middle Devonian stratigraphic section of Northern Central Appalachian Basin. Marcellus Formation shale highlighted in red. Modified from USGS Marcellus Shale Assessment Team (2011).	57
Figure 9-1	Intensity of all Set 1 natural fractures, Well VM-A.	62
Figure 9-2	Correlation count of all Set 1 natural fractures, Well VM-A.	63
Figure 9-3	Intensity of Set 1 natural fractures in Zone 2, Well VM-A.	64
Figure 9-4	Correlation count of Set 1 natural fractures in Zone 2, Well VM-A.	64
Figure 9-5	Intensity of Set 1 natural fractures in Zone 4, Well VM-A.	65
Figure 9-6	Correlation count of Set 1 natural fractures in Zone 4, Well VM-A.	66
Figure 9-7	Intensity of all Set 2 natural fractures, Well VM-A.	67
Figure 9-8	Correlation count of all Set 2 natural fractures, Well VM-A.	67
Figure 9-9	Intensity of Set 2 natural fractures in Zone 4, Well VM-A.	68
Figure 9-10	Correlation count of Set 2 natural fractures in Zone 4, Well VM-A.	69
Figure 9-11	Intensity of Set 2 natural fractures in Zone 3-2, Well VM-A.	70

Figure 9-12	Correlation count of Set 2 natural fractures in Zone 3-2, Well VM-A.	70
Figure 9-13	Intensity of all image log natural fractures, Well VM-B.	72
Figure 9-14	Correlation count of all image log natural fractures, Well VM-B.	72
Figure 9-15	Intensity of natural fractures in Zone 5, Well VM-B.	73
Figure 9-16	Correlation count of natural fractures in Zone 5, Well VM-B.	73
Figure 9-17	Intensity of Upper Vaca Muerta closed fractures, Well VM-C.	75
Figure 9-18	Correlation count of Upper Vaca Muerta closed fractures, Well VM-C.	75
Figure 10-1	(a) Well HRB-1 inclination versus Measured Depth (m). (b) Change in inclination value with respect to best fit regression value. (c) True Vertical Depth (TVD) of the wellbore with respect to Measured Depth. Measured Depth interval begins at the first healed fracture observed.	82
Figure 10-2	Intensity of conductive continuous fractures, Well HRB-1.	84
Figure 10-3	Correlation count of conductive continuous fractures, Well HRB-1.	84
Figure 10-4	Correlation count of conductive continuous fractures, intensity plot position 400 to 600 m, Well HRB-1.	85
Figure 10-5	NCC of conductive continuous fractures, intensity plot position 900 to 1100 m, Well HRB-1.	85
Figure 10-6	Intensity of conductive discontinuous fractures, Well HRB-1.	86
Figure 10-7	Correlation count of conductive discontinuous fractures, Well HRB-1.	87
Figure 10-8	Intensity of conductive bed-bound fractures, Well HRB-1.	88
Figure 10-9	Correlation count of conductive bed-bound fractures, Well HRB-1.	88
Figure 10-10	Intensity of all conductive fractures, Well HRB-1.	90
Figure 10-11	Correlation count of all conductive fractures, Well HRB-1.	90

Figure 10-12 Correlation count of all conductive fractures, intensity plot position 900 to 1100 m, Well HRB-1.....	91
Figure 10-13 Intensity of all resistive fractures, Well HRB-1.....	92
Figure 10-14 Correlation count of all resistive fractures, Well HRB-1.	92
Figure 10-15 Intensity of resistive Set 1 fractures, Well HRB-1.	93
Figure 10-16 Correlation count of resistive Set 1 fractures, Well HRB-1.	94
Figure 10-17 Intensity of resistive Set 2 fractures, Well HRB-1.	95
Figure 10-18 Correlation count of resistive Set 2 fractures, Well HRB-1.	96
Figure 10-19 Correlation count of resistive Set 2 fractures, intensity plot position 450 to 650 m, Well HRB-1.....	96
Figure 10-20 Intensity of Set 2 resistive continuous fractures, Well HRB-1.....	97
Figure 10-21 Correlation count of Set 2 resistive continuous fractures, Well HRB-1.	98
Figure 10-22 Intensity of resistive discontinuous fractures, Well HRB-1.	99
Figure 10-23 Correlation count of resistive discontinuous fractures, Well HRB-1.....	99
Figure 10-24 Intensity of resistive bed-bound fractures, Well HRB-1.	100
Figure 10-25 Correlation count of resistive bed-bound fractures, Well HRB-1.....	101
Figure 10-26 Intensity of drilling induced fractures, Well HRB-1.	102
Figure 10-27 Correlation count of drilling induced fractures, Well HRB-1.	103
Figure 10-28 Correlation count of drilling induced fractures, intensity plot position 550 to 750 m, Well HRB-1.....	103
Figure 10-29 Intensity of drilling induced fractures and continuous conductive fractures, Well HRB-1.	105
Figure 10-30 NCC plot of Well HRB-1 drilling fractures & continuous conductive fractures.....	105

Figure 10-31	Intensity of all natural Set 1 fractures, Well HRB-1.....	107
Figure 10-32	Correlation count of all natural Set 1 fractures, Well HRB-1.....	107
Figure 10-33	Intensity of faults, Well HRB-1.....	108
Figure 10-34	Correlation count of faults, Well HRB-1.....	108
Figure 10-35	(a) Well HRB-2 inclination versus Measured Depth (m). (b) Change in inclination value with respect to best fit regression value. (c) True Vertical Depth of the wellbore with respect to Measured Depth. Measured Depth interval begins at the first sealed fracture observed.	111
Figure 10-36	Intensity of all conductive fractures, Well HRB-2.	112
Figure 10-37	Correlation Count of all conductive fractures, Well HRB-2.	113
Figure 10-38	Intensity of conductive Set 1 fractures, Well HRB-2.	114
Figure 10-39	Correlation count of conductive Set 1 fractures, Well VM-A.	115
Figure 10-40	Correlation count of conductive Set 1 fractures, intensity plot position 0 to 600 m, Well HRB-2.....	115
Figure 10-41	Intensity of conductive Set 2 fractures, Well HRB-2.	116
Figure 10-42	Correlation count of conductive Set 2 fractures, Well HRB-2.	117
Figure 10-43	Correlation count of conductive Set 2 fractures, intensity plot position 820 to 1060 m, Well HRB-2.....	117
Figure 10-44	Intensity of conductive Set 3 fractures, Well HRB-2.	119
Figure 10-45	Correlation count of conductive Set 3 fractures, Well HRB-2.....	119
Figure 10-46	Correlation count of conductive Set 3 fractures, intensity position 0 to 80 m, Well HRB-2.	120
Figure 10-47	Intensity of all sealed fractures, Well HRB-2.....	121
Figure 10-48	Correlation count of alls fractures, Well HRB-2.	121
Figure 10-49	Intensity of sealed Set 1 fractures, Well HRB-2.....	123

Figure 10-50	Correlation count of sealed Set 1 fractures, Well HRB-2.....	123
Figure 10-51	Correlation count of sealed Set 1 fractures, intensity position 100 to 350 m, Well HRB-2.	124
Figure 10-52	Intensity of sealed Set 2 fractures, Well HRB-2.....	125
Figure 10-53	Correlation count of sealed Set 2 fractures, Well HRB-2.....	125
Figure 10-54	Correlation count of sealed Set 2 fractures, intensity position 0 to 650 m, Well HRB-2.	126
Figure 10-55	Intensity of sealed Set 3 fractures, Well HRB-2.....	127
Figure 10-56	Correlation count of sealed Set 3 fractures, Well HRB-2.....	127
Figure 10-57	Correlation count of sealed Set 3 fractures, intensity position 20 to 220 m, Well HRB-2.	128
Figure 10-58	Intensity of all Set 1 natural fractures, Well HRB-2.....	129
Figure 10-59	Correlation count of all Set 1 natural fractures, Well HRB-2.....	129
Figure 10-60	Intensity of all Set 2 natural fractures, Well HRB-2.....	130
Figure 10-61	Correlation count of all Set 2 natural fractures, Well HRB-2.....	131
Figure 10-62	Intensity of all Set 3 natural fractures, Well HRB-2.....	132
Figure 10-63	Correlation count of all Set 3 natural fractures, Well HRB-2.....	132
Figure 10-64	Comparing fracture intensities from conductive fracture sets in Wells HRB-1 and HRB-2. TVD vs MD plots (a) and (e) provided as horizontal wellbore trajectory approximation. N = number of fractures in a given sequence. Cv = coefficient of variation. Red boxes indicate high fracture intensity intervals further analyzed separately with NCC. Horizontal axes are column-wise aligned. Vertical axes are not aligned.	134

Figure 10-65 Comparing NCC results from conductive fracture sets in Wells HRB-1 and HRB-2. N = number of fractures in a given sequence. Cv = coefficient of variation. Red insets show correlation count results from analyzing high fracture intensity intervals in individual sets. Horizontal axes are column-wise aligned. Vertical axes not aligned.135

Figure 10-66 Comparing fracture intensities from resistive or healed (i.e. sealed) fracture sets in Wells HRB-1 and HRB-2. TVD vs MD plots (a) and (d) provided as horizontal wellbore trajectory approximation. N = number of fractures in a given sequence. Cv = coefficient of variation. Red boxes indicate high fracture bintensity intervals further analyzed separately with NCC. Horizontal axes are column-wise aligned. Vertical axes not aligned.....136

Figure 10-67 Comparing NCC results from resistive or healed (i.e. sealed) Set 1, 2, 3 fractures in Wells HRB-1 and HRB-2. N = number of fractures in a given sequence. Cv = coefficient of variation. Red insets show correlation count results from analyzing high fracture intensity intervals within individual sets. Horizontal axes are column-wise aligned. Vertical axes not aligned.....137

Figure 11-1 Intensity of all natural fractures, Gulla 10H.153

Figure 11-2 Correlation count of all natural fractures, Gulla 10H.154

SECTION I: OVERVIEW

Chapter 1: Fracture Spatial Arrangement

Natural opening-mode fractures are widespread in unconventional reservoirs. In tight gas sandstones, differences in fracture attributes profoundly influence fluid flow and associated gas and water producibility (Laubach, 2003; Cumella and Scheevel, 2008; Olson et al., 2009; Solano et al., 2011). Fractures are also widespread in shales (Gale et al., 2014). Yet obtaining representative subsurface data on opening-mode fractures by sampling is extremely challenging, and serious inherent limitations of sampling diffuse fracture arrays lead to data that are commonly biased and incomplete. In particular, although vertical fractures may have lengths of hundreds of meters or more, their narrow widths and spacings of centimeters to tens or hundreds of meters apart leads them being readily missed by vertical wells. In contrast, wells drilled approximately in the plane of bedding – ‘horizontal wells’ – and outcrops sample fracture occurrence more systematically and provide valuable information. Collecting data from horizontal wells is expensive, and such data sets in the public domain are rare, leading to reliance on outcrop observations despite concerns that differences in loading histories may make some outcrops unreliable guides to the subsurface fracture orientations, densities, and spatial distributions.

Fracture spacing is defined as the perpendicular distance between two fractures in the same set (Price, 1966; Priest and Hudson, 1976). Commonly, spacings for a system of near-vertical fractures are measured along a straight line of observation (scanline) orthogonal to fracture strike. Descriptive statistics, frequency distributions (e.g. Narr and Suppe, 1991), coefficient of variation, a measure of the irregularity of fracture spacing (e.g. Gillespie et al., 1999; 2001), and interval counting (e.g. Gillespie et al., 1993; Walsh and

Watterson, 1993) provide numerical characterization of fracture spacings. These methods do not account for sequences of spacings along the scanline.

Spatial arrangement describes fracture positions in space, including whether fractures are clustered, randomly placed or evenly spaced, fundamental attributes that need assessment to help guide many subsurface engineering practices such as well planning and hydraulic fracture treatment design. In Section II, I investigate opening-mode fracture spatial arrangement patterns within Upper Cretaceous Frontier Formation tight gas sandstones using data acquired from horizontal image logs as well as from cores and outcrop. I analyze fracture occurrence data with the Normalized Correlation Count method (NCC; Marrett et al., 2017; including CorrCount software), which accounts for the sequences of spacings, and compare results with conventional spacing analysis methods (descriptive statistics; coefficient of variation). Previous examination of the cores and well logs used in this study identified that the fractures are unevenly spaced (Lorenz et al., 2005), but the patterns have not previously been quantified. In Section III, I further investigate opening-mode fracture spatial arrangement patterns in three different shale reservoir rocks – the Vaca Muerta Formation shale, the Evie, Otter Park, and Muskwa shale members of the Horn River Formation and the Woodbend/Winterburn Group, and the Marcellus Formation shale – similarly through analyzing image log fracture sequential spacings with NCC. My results for a sandstone example (Li et al., 2017 and Section II) and for shales (Section III) show regional contrasts in fracture clustering patterns as well as contrast between fracture sets by degree of sealing and strike, and help illuminate why differing clustering patterns exist in fracture arrays.

SECTION II: FRACTURE SPATIAL ARRANGEMENT IN A TIGHT GAS SANDSTONE

The Upper Cretaceous Frontier Formation is a naturally fractured gas-producing sandstone in Wyoming. For east-striking regional fractures sampled using image logs and cores from three horizontal wells and from outcrop, NCC results show that clustered patterns characterize deep-seated fractures whereas patterns indistinguishable from random occur in outcrop. A hierarchy of cluster sizes exists, and arrangement within clusters is likely fractal. Random and statistically more clustered than random patterns exist in the same upper to lower shoreface depositional facies, but from rocks having markedly different structural and burial histories. Although the origins of regional differences in degree of clustering are unknown, our results show that quantifying spatial arrangement delineates potentially economically important differences in fracture patterns that are not otherwise apparent.

Chapter 2: Geologic Setting of Tight Gas Sandstone Example

The Greater Green River Basin in southwestern Wyoming, USA was part of the foreland basin of the east-vergent, Mid- to Late Cretaceous Sevier (or western Wyoming) thin-skinned fold and thrust belt (Jordan, 1981; Wiltschko and Dorr, 1983) (Figure 2-1). Basement-involved (Laramide) folds and faults subdivided the foreland during the Tertiary (English and Johnson, 2004). DeJarnett et al. (2001) provide an east-west seismic line across the basin, and Dutton et al. (1995) show a basin-wide structure map.

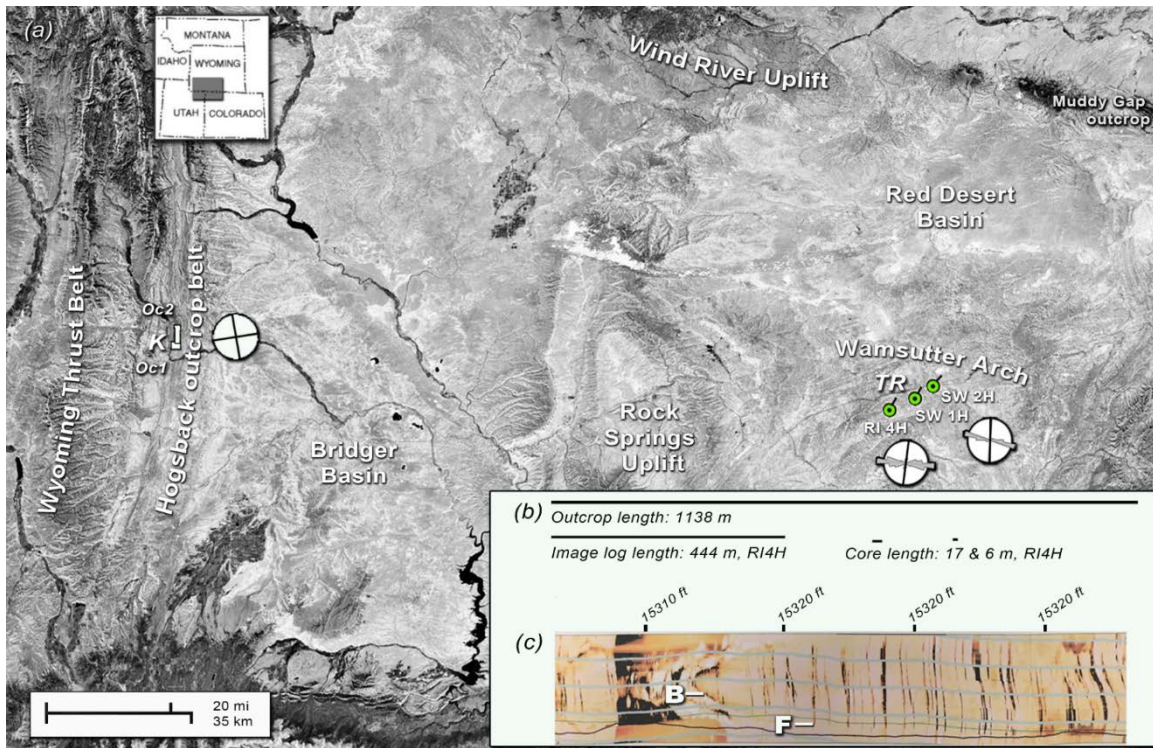


Figure 2-1 Greater Green River Basin, Wyoming, showing Well VM-A outcrop locations, scanline dimensions, and representative image log. (a) Sub-basins, uplifts and Well VM-A outcrop locations. Wells: Rock Island 4-H (RI4H), Sidewinder 1-H (SW1H), Sidewinder 2-H (SW2H), Table Rock (TR) field, Sweetwater County, Wyoming. NNE well trajectories are indicated. Rose diagrams show fracture strikes (from Laubach et al., 2016). Outcrops Oc1 and Oc2 shown in Figures 2-2 and 2-3 respectively. Orientation diagram shows main fracture strikes in Kemmerer section, Hogsback outcrop belt. K, Kemmerer, Wyoming. Inset: Location of Greater Green River Basin in western U.S. Background image: Google Earth. (b) Representative lengths of observation scanlines: outcrop scanline length from Oc2; image log length from RI4H and core lengths from RI4H. For the Rock Island 4-H well, readily interpreted image log data exists from measured depth (MD) 4663.4 m to 5025.2 m. (c) Representative section of FMI image log from RI4H showing fracture traces (F) and bedding (B).

My data come from directionally drilled horizontal wells in the Greater Green River Basin in a distal foreland setting, and from outcrops on the western side of the basin

adjacent to the thrust front (Figures 2-1 to 2-3). Both data sets are from areas of gently dipping beds. The wells target the Upper Cretaceous (Cenomanian-Turonian) Frontier Formation, which comprises multiple fluvial and marine shoreface sandstone members that are mainly very fine to medium-grained litharenites to sublitharenites (Cobban and Reeside, 1952; Merewether, 1983; DeJarnett et al., 2001). The marine shoreface sandstones range from 9 to more than 35 m thick and have blanket geometry. The relatively quartz-rich and clay-mineral-poor upper shoreface intervals are typically less than 6 m thick (Cobban and Reeside, 1952; Dutton et al., 1995). On the western side of the basin, in outcrop, the Frontier Formation is about 90 m thick, underlain by the Mowry Shale and overlain by the Hilliard Shale. Our outcrop and core data are from similar Frontier Formation facies, but considerable regional stratigraphic variations and differences in burial history need to be accepted (i.e., Dutton et al., 1995).

Sandstone members of the Frontier Formation are of interest in petroleum exploration and development (Dutton et al., 1995; Hennings et al., 2000). In 1998 and 1999, the Greater Green River Basin Production Improvement Project (GGRBPIP) led by the U.S. Department of Energy and Union Pacific Resources drilled the slant wells Rock Island 4-H (RI4H) and Sidewinder 1-H and 2-H (SW1H and SW2H) in the Frontier sandstone in the Table Rock Field in east-central Green River Basin (DeJarnett et al., 2001; Lorenz et al., 2005; Laubach et al., 2016). Beds here are nearly flat lying and well trajectories in zones of interest are nearly horizontal. RI4H, SW1H, and SW2H were investigated with image logs, but only RI4H and SW1H were cored. RI4H set a record of having the highest gas flow capacities up to then in the Frontier (DeJarnett et al., 2001) and ended up producing approximately 10.1 BCF of natural gas by 2007 (Coleman, 2008).

SW1H intersected the same fracture sets but had high water production. Engineering and geological context for these wells is described by DeJarnett et al. (2001).

In RI4H, image logs were collected in the measured depth (MD) interval from 4581.1 m to 5025.2 m, have clear resistivity contrast features first appearing at 4663.4 m (Figure 2-2). Three cores were retrieved from within this interval: two from the mid to upper shoreface facies of the Frontier (Cores 1 and 2) and one from the lower shoreface facies (Core 3) (Lorenz et al. 2005; Laubach et al., 2016). The core in SW1H (Core 4) was taken from the lower shoreface of the Frontier Formation (DeJarnett et al., 2001). All cores contain opening-mode fractures that are primarily subvertical and bed-normal. Fractures have a range of opening displacement sizes – kinematic aperture, the perpendicular distance from one fracture wall to the other – and are variably lined or filled with quartz cement. Two sets of fractures are present. Set 1 strikes approximately east-west and Set 2 strikes approximately north-south (Lorenz et al., 2005; Laubach et al., 2016). Based on crosscutting relations, Set 1 is older than Set 2. Set 1 has slightly more quartz cement, but fractures of both sets retain open pore space in these wells (Laubach et al., 2016). Some Set 1 fractures have been reactivated in shear and a few small (>5 m offset) oblique-slip faults are present in core and more are evident on image logs (DeJarnett et al., 2001). Wells were drilled at a high angle to Set 1, which are thus more completely sampled than Set 2; most of our analysis focuses on the older Set 1 fractures.

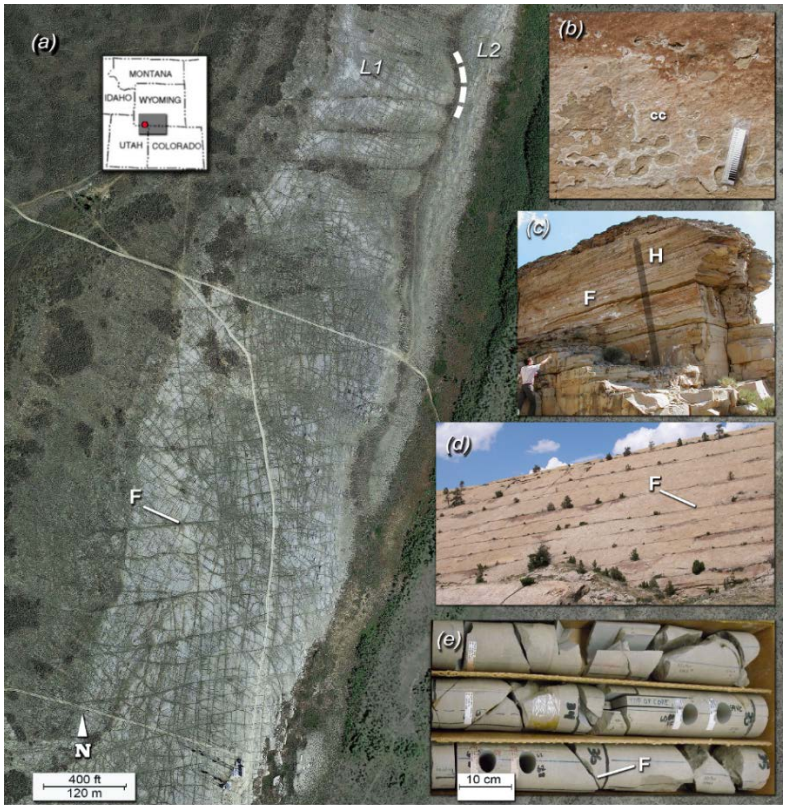


Figure 2-2 Fractures in outcrop and core, Frontier Formation. (a) Fracture traces in north-northeast trending outcrop (Oc1), west-dipping pavement northeast of Kemmerer, Wyoming, Google Earth dated 9/1/2014. Three main fracture trends are evident. Spacings of east- or east-northeast-striking fractures (F) were measured here and in Oc2, directly north along the outcrop belt. L1, L2 mark separate marine sandstone lenses. Part of contact is dashed. (b) Fracture face, east-northeast striking fracture from outcrop south of Kemmerer. Calcite (cc) filling fractures is compatible with formation of these fractures in the subsurface. Comparator is 10 cm long. (c) Same outcrop as in b; F, fracture face. Tall fractures (H) span the thickness of the sandstone; entire thickness of which is not shown. (d) Frontier Formation bed surface with fractures traces (F), Muddy Gap, Wyoming, northeast of core location. Fractures have trace lengths many tens of meters long. Here, spacing between traces (arrow) is ca. 5 m. Fractured bed thickness is ca. 20 m. (e) Core from Rock Island 4-H horizontal core, in the depth interval 15454-15464 ft (4710-4713 m) (Core 2). Beds are approximately parallel to the long dimension of the core; arrow marks top of core, core diameter ca. 4 inches (10 cm).

I selected north-south-striking Frontier Formation outcrops on the western margin of the basin to sample fractures having the same generally east-west strike as those most prevalent in core (Figure 2-3). Previous studies of the outcrops concluded that north-south and east-west-striking fracture sets are regional in extent and, based on local calcite mineral fills, likely formed in the subsurface (Laubach, 1992; Lorenz and Laubach, 1994). For outcrops, I examined fractures in the same depositional facies as those in core, mid- to upper and lower shoreface marine sandstones. Outcrop fractures are, however, above the easternmost thrust of the western Wyoming fold-and-thrust belt, whereas our core samples are more than 170 km east in a distal foreland basin setting on the Wamsutter arch. Outcrops are in the west-dipping (ca. 15 degrees) limb of an asymmetric east-vergent syncline above the easternmost frontal thrust of the fold-and-thrust belt. These west-dipping beds likely tilted without passing through a fold hinge (Delphia and Bombolakis, 1988). Cores are from the backlimb of a gentle, west-vergent anticline.

Outcrop and core fractures also differ in cement petrology (Laubach et al., 2016). Calcite fill is prevalent in outcrop fractures although it may postdate fracture opening, whereas quartz is the primary and earliest cement in both cored fracture sets. This quartz was deposited during and after fracture opening. The relative timing of north-south- and east-west-striking fractures in outcrop is opposite to that found in cores, suggesting that the east-west-striking fractures in outcrop and core are not the same age despite sharing common orientations. Absolute timing of cored fractures has been estimated using fluid inclusion trapping temperatures tied to thermal history (Laubach et al., 2016), but no comparable estimates exist for the outcrop fractures.



Figure 2-3 Fracture traces, western Green River Basin, outcrop 2 (Oc2 in Figure 2-1). Background Google Earth image where fractures were traced. Red lines mark fracture traces, black lines represent scanlines. Location map after Lorenz and Laubach (1994). Fracture clusters (called swarms; Laubach, 1992, their Figures 4 and 9) are visible in other outcrops on the opposite, steeply east-dipping fold limb.

Though opening-mode fractures have been documented at outcrop using trace maps and for core using occurrence or aperture versus distance plots (e.g. Laubach, 1992; Lorenz and Laubach, 1994; Laubach et al., 2016), spatial arrangement of fractures has not been quantified at any scale prior to this study.

Chapter 3: Datasets and Methods for Sandstone Study

Subsurface data comprises observations of fracture traces on paper image logs that were collected in the late 1990s (DeJarnett et al., 2001) (Figure 2-1c) as well as fracture sequences measured in core (Laubach et al., 2016) (Figure 2-2e). Outcrop fractures were sequentially measured on Google Earth images (sub-meter resolution; narrow fractures are clearly visible; Figures 2-2, 2-3) in areas where fractures had previously been measured in the field (Laubach 1992; Lorenz and Laubach, 1994). Comparison of outcrop-based measurements with Google Earth-based measurements for this location indicates that, in this case, detection of fractures is not markedly degraded by using remote images to measure spacing values compared to measurements made on the ground. Opening displacements and mineral fills, however, are rarely clearly preserved owing to weathering and resolution. Fractures in the cored interval and the outcrops, at least locally, have similar kinematic aperture size ranges. In both cases, fractures are large enough to be readily visible without microscopy; microfractures are rare (e.g. Copley, 2015; Anders et al., 2014) and can be omitted from assessment of size distributions.

3.1 HORIZONTAL WELL IMAGE LOGS, WYOMING

Electrical and acoustic image logs are widely used in the oil and gas industry for reservoir characterization (e.g. Pöppelreiter et al., 2010). Our source of fracture spatial observations in uncored wells are horizontal image logs – that is, image logs from well segments that are approximately parallel to bedding, collected using Schlumberger’s Formation MicroImager (FMI) at 5 and 25 inch scales from wells RI4H, SW1H, and SW2H (DeJarnett et al., 2001). An electrical image log is a map of micro-resistivity variations along a borehole wall (Ekstrom et al., 1987; Lofts and Bourke, 1999). In horizontal image

logs, fractures intersecting the wellbore at high angles can be distinguished from low angle bedding planes by their appearance as low-amplitude sinusoids cutting across bedding (Lofts et al., 1997) (Figure 2-1c). Compared to vertical wells, slant and horizontal wells can capture more vertical or steeply dipping fractures, allowing measurement of fracture spatial arrangement provided that those fractures strike at a high angle to the wellbore. A horizontal image log can therefore be used as a scanline to calculate subsurface fracture spacings using measured depths and appropriate geometrical corrections.

I picked traces by hand and compiled fracture measured depths in spreadsheets. Modern workstation-based image log analysis (e.g., Ponziani et al., 2013) is more efficient than extraction of data from paper logs, and manipulation of the resistivity data can in some circumstances yield aperture estimates (Luthi and Souhaité, 1990), but these capabilities were unavailable for our vintage observational dataset. The lack of modern workstation trace picking capability may have slightly reduced the lateral accuracy of our picks, although discrepancies are probably too small to affect our results. Each paper image log came with annotations of the calculated strikes and dips of features crossing wellbores, as well as a classification of features, e.g. conductive, resistive, or drilling-induced fractures; faults; bedding planes. Image log fractures are categorized using this classification. Although interpreting the origin of different types of fractures on image logs is subject to uncertainty, the most prevalent type of fracture in each well is sufficiently pervasive to govern our results; combining or separating conductive or resistive fractures for example does not change the spatial patterns substantially. Comparing image logs with core shows that the distinction between conductive versus resistive fractures in my example does not reliably differentiate degree of open fracture pore space visible in core. For Set 1,

comparison of cores and logs suggests that resistive fractures include those that were reactivated in shear and consequently have negligible continuous open pore space.

Once sorted and separated by orientations and types, the measured depths for neighboring features were used to calculate spacings and spatial patterns (Figures 3-1, 3-2). The Terzaghi (1965) correction was applied to each fracture strike to account for obliquity bias. The correction resulted in insignificant changes in the large majority of the distances between east-west-striking Set 1 fractures in RI4H and SW1H, most of which strike within +/- 10 degrees of perpendicular to the wellbore. The correction resulted in significant changes in the distances between Set 2 fractures striking approximately north-south at low angles to the horizontal wellbores (e.g. Figures 4-1c and 4-2c).

Although fracture kinematic apertures can be physically measured in outcrops and sometimes in cores, apertures cannot be measured on the paper image logs used in our study. I used a single nominal size of 1 mm as the aperture input, a dimension compatible with core observations (Laubach et al., 2016) and approximately an order of magnitude smaller than the smallest spacing measured in the image log, and thus too small to affect analysis results using the CorrCount software. Both the calculated spatial patterns and the preselected aperture were used as inputs for the Normalized Correlation Count calculations. Lack of aperture data precluded using some of the capabilities of the Marrett et al. (2017) analysis protocol, or of comparing results with fracture size distribution frequency as discussed by Putz-Perrier and Sanderson (2008).

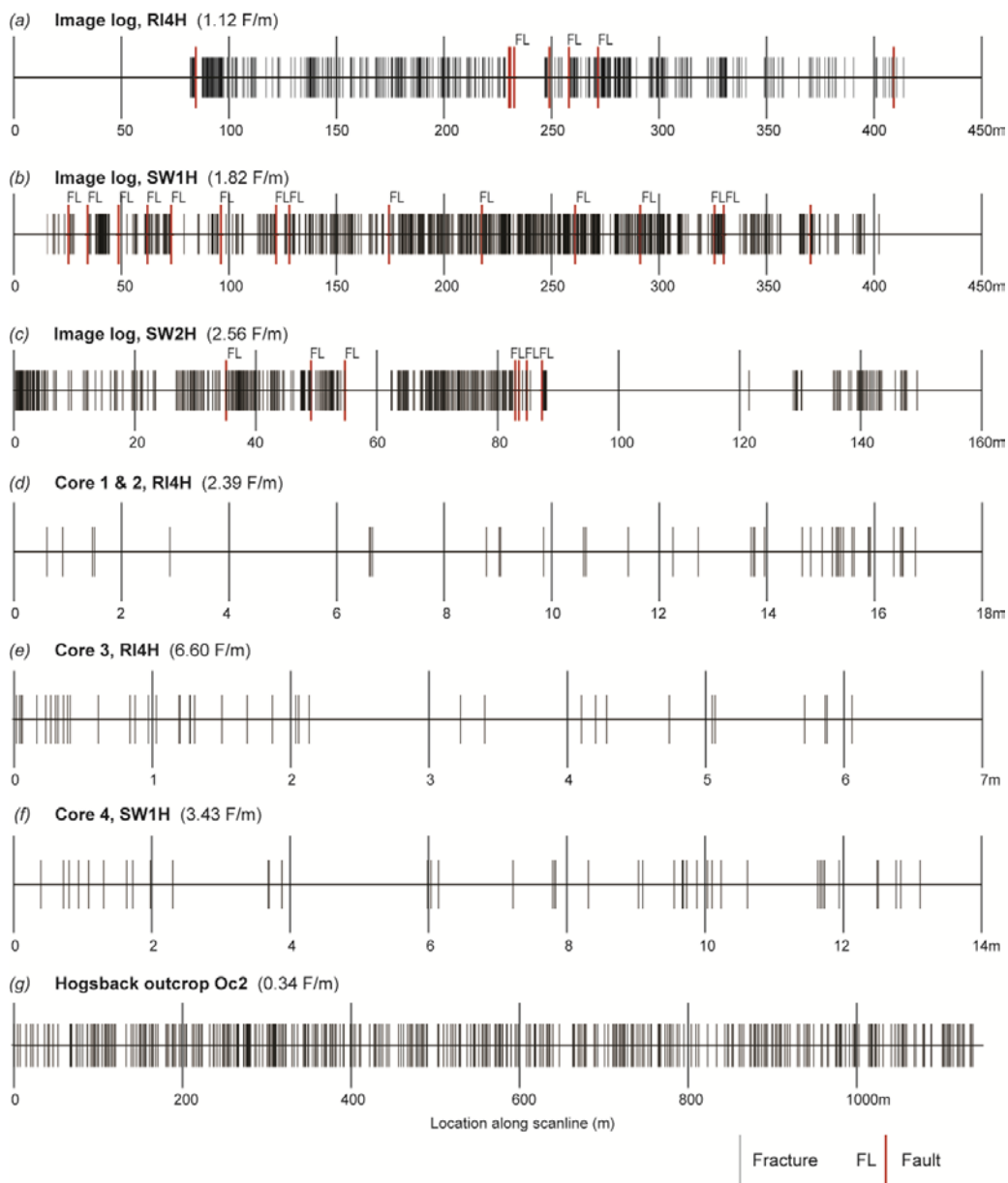


Figure 3-1 Occurrence versus distance (stick) plots of fractures visible in image logs, core and outcrop. Zero represents beginning of scanline. Black vertical lines are opening-mode fractures (some with evidence of reactivation in core data sets); FL, red lines are faults recognized by offset beds on image logs. Horizontal scale in meters. Vertical dimension of lines is arbitrary; Laubach et al. (2016) report aperture size versus distance plots for cored intervals (their figure 4). Inset numbers are fractures per meter (F/m).

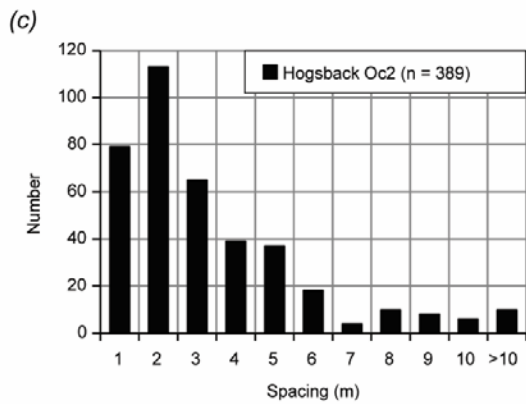
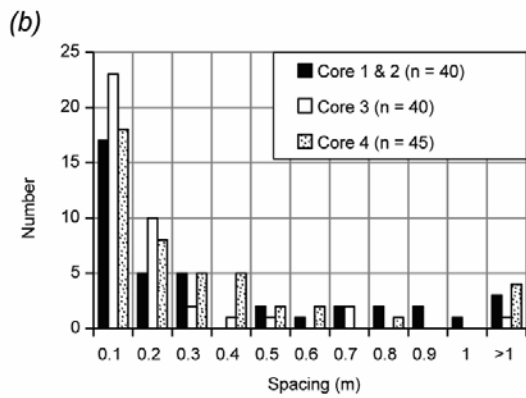
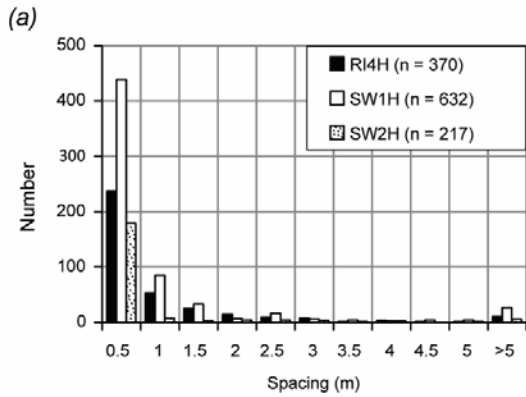


Figure 3-2 Fracture spacing histograms for image logs, cores, and outcrop. Image log and core plots generated from spacing of conductive fractures aggregated from all wells. A few very low frequencies (0 to 1) for large spacings (> 10 m) omitted for clarity. All show high frequency of sub-meter spacings with varying degrees of distribution spread.

3.2 HORIZONTAL WELL VM-CORES, WYOMING

Three horizontal cores (Cores 1, 2, 3) were taken in RI4H and one horizontal core (Core 4) was taken in SW1H. Laubach et al. (2016) documented measured and true vertical depths at which fractures occur in each core, with results comparable to the previous core description of Lorenz et al. (2005) where uneven spacing was noted. Cores 1, 2, and 3 total 23.9 m long and contain 76 discrete fractures, whereas Core 4 is 18.3 m long and contains 40 discrete fractures (Copley, 2015; Laubach et al., 2016).

3.3 OUTCROP DATA, WYOMING

At least three sets of fractures are visible in Frontier Formation sandstone outcrops along the ca. 100-km long Hogsback escarpment (Laubach, 1991; 1992; Lorenz and Laubach, 1994) (Figure 2-3). Some sandstones in these outcrops are in the same part of the Frontier Formation stratigraphic section and are of the same facies as those penetrated by the Rock Island and the Sidewinder wells, although rocks in these widely separated localities have experienced different depositional, burial and tectonic histories. In outcrop, fractures in the east-west-striking and locally younger set, termed “J2” by Lorenz and Laubach (1994), are prevalent through the entire length of Hogsback exposure. J2 fractures are variable in length, ranging from sub-meter to many tens of meters long (Laubach et al., 2016) although in the outcrops where we measured spacing, fracture lengths are censored by outcrop widths of 200 m or less. Fractures in the east-west-striking J2 set are well captured in satellite images (Figures 2-2, 2-3).

Fracture patterns along the Hogsback escarpment have substantial diversity and are locally complex (Lorenz and Laubach, 1994). Two outcrops, Oc1 and Oc2, having fairly simple patterns, were selected for fracture spacing characterization (Figures 2-1 and 2-3).

According to the interpretation of Lorenz and Laubach (1994), these outcrops have the least overprint from thrust-related folding. I focus on the pattern in Oc2, which is representative of both outcrops. Using Google Earth's built-in tools, I traced fractures in outcrops, drew NNE-trending scanlines perpendicular to the traces (Figure 2-2), and recorded consecutive distances between fractures. Sandstones along the outcrop are subdivided into well-defined lenticular bodies or lenses (Merewether, 1983) (Figure 2-2) that are smaller than outcrop dimensions, but image resolution of sandstone internal structure is sufficient to draw scanlines that are entirely within a given sandstone lens. Aperture sizes are of course not visible on the images, and apertures also are only rarely measurable in these outcrops. Therefore a nominal fracture aperture (1 mm) compatible with sparse outcrop observations and matching that used in image log analysis was used in my spatial analysis.

3.4 GENERAL SPATIAL ANALYSIS METHODS

The Normalized Correlation Count technique (NCC; Marrett et al., 2017) provides a quantitative analysis of the degree to which fractures are clustered, and can distinguish between even spacing (periodic or anticlustered), clusters arising due to random fracture arrangement, and clustering that is stronger than a random signal. NCC uses distances between all pairs of fractures including non-nearest neighbors and thus accounts for the sequence of fracture spacings along the scanline. Accounting for sequential positions and sizes of fractures provides information on cluster distribution to cluster internal structure. I also used a standard measure of spatial clustering, coefficient of variation (Cv) (e.g. Gillespie et al., 1999). Cv equals σ/μ where σ is the standard deviation of spacings and μ

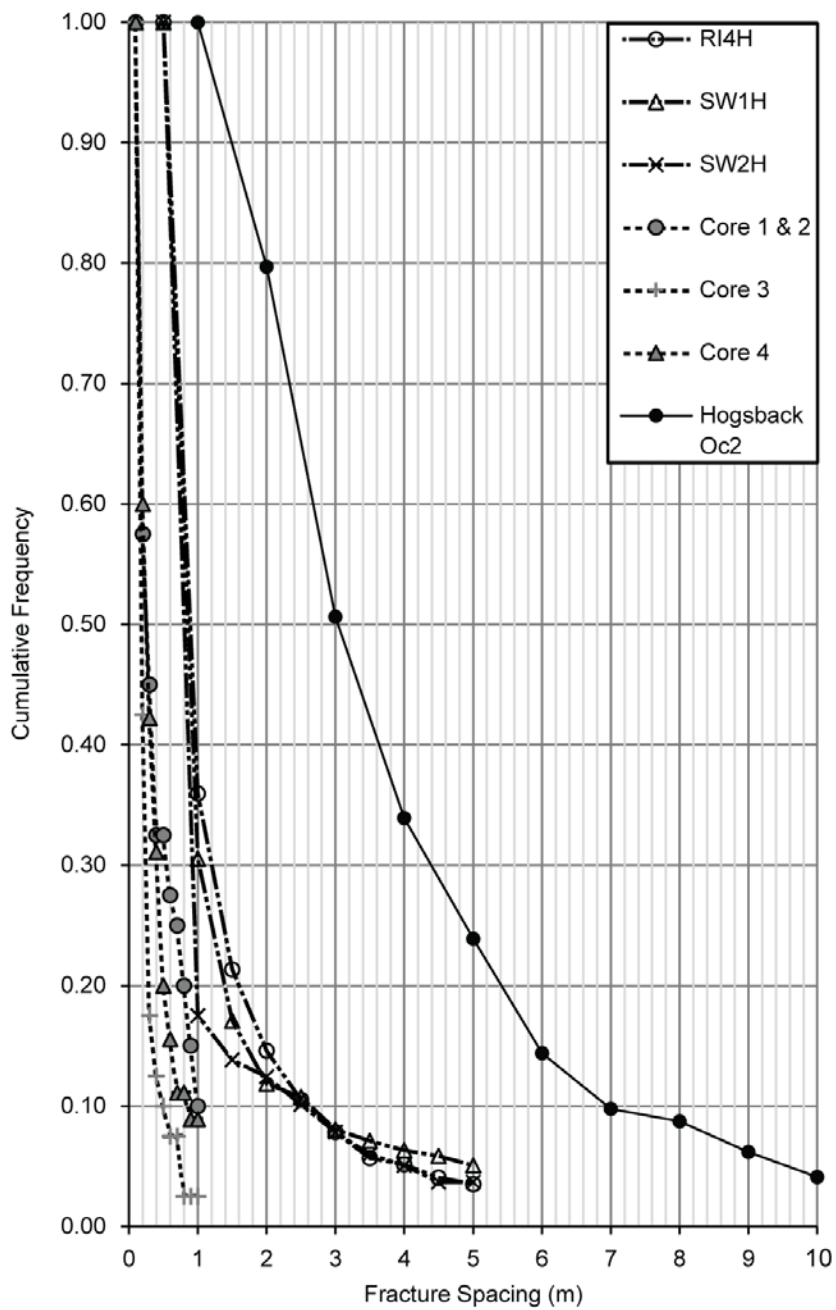
is the mean. Perfectly periodic fracture spacing produces a Cv of zero, and Cv increases with increasing irregularity of spacing (Tables 1 and 2; Figures 3-1 to 3-3).

NCC is based on correlation sum, or the two-point correlation function (Bonnet et al., 2001), that calculates the proportion of fracture pairs in a set, including pairs of non-neighboring fractures, separated by a distance less than each given length scale λ_k in a logarithmically or linearly graduated series of length scales. A correlation count assigned for a given λ_k is defined as the fraction of all fracture pairs for which the pair's spacing falls between λ_{k+m} and λ_{k-m} (Marrett et al., 2017), essentially the difference between the correlation sum of λ_{k+m} and that of λ_{k-m} . The Marrett et al. (2017) NCC computer program, CorrCount, also provides analytical and Monte Carlo solutions for randomized input spacings (the program is freely available online; Marrett et al., 2017). A 95% confidence interval is constructed for the randomized sequence. If a length scale's corresponding correlation count falls either above or below the upper or lower confidence limits, the corresponding fracture spacing can be interpreted to be statistically significant.

Set	# Fractures, (total)	# Fractures, Upper Shoreface	# Fractures, Lower Shoreface	# Fault	# Conductive Fractures	# Resistive Fractures
Set 1 (EW)	413	204	209	7	369	37
Set 2 (NS)	86	29	57	1	17	68

Set	Fracture Intensity, Overall (fractures/m)	Fracture Intensity, U. Shoreface (fractures/m)	Fracture Intensity, L. Shoreface (fractures/m)	Spacing Range (m)	Spacing Average (m)	Spacing Median (m)
Set 1 (EW)	1.25	1.67	1.01	0.015 - 14.25	0.81	0.29
Set 2 (NS)	0.26	0.24	0.27	0.0346 - 50.91	2.51	0.27

Table 3-1 Descriptive statistics of fractures in Rock Island 4-H image log. Upper shoreface approximately 4663.4 m – 4785.4 m; lower shoreface approximately 4785.4 m – 5025.2 m. Fracture intensity values normalized to correct for difference in facies’ interval length.



QAe5347

Figure 3-3 Cumulative frequency versus fracture spacing for all data sets. Frequencies approaching zero beyond 1 m, 5 m, and 10 m omitted for optimal display as in Figure 5.

Chapter 4: Results: Wyoming

In the Frontier Formation sandstone, fracture spacings range from a few tens of centimeters to several meters in cores, approximately 100-300 centimeters in image logs and more in outcrop (Table 2; Figures 3-1 to 5-1). I measured and calculated 499, 733, and 382 spacings for all types and sets of fractures in RI4H, SW1H, and SW2H image logs, respectively. Only the spacings of fractures having a conductive image log response are presented. These are the most abundant in each of the wells. Although in general this selection might introduce bias, for this data set any bias is small for this data set owing to the predominance of this category of fracture as well as the close match between fractures visible in core and on image logs. Fracture spacings in core are markedly less numerous, with 40 spacings in Cores 1 and 2, 40 in Core 3, and 45 in Core and 4, respectively owing to shorter lines of observation compared to image logs. The outcrop data set includes 389 fracture spacing measurements from scanline sampling of 390 fractures.

Spatial distributions show high occurrence of sub-meter to meter scale inter-fracture distances in all datasets, with outcrop having the largest range of spacing distribution from 0.3 m to 16 m (Figure 3-2). The NCC plots presented by Marrett et al. (2017) are generated from hundreds of fracture spacings. Null correlation counts at certain length scales arise if there are too few spacing measurements, leading to incomplete correlation count plots, and a less meaningful analysis of fracture spatial arrangement patterns. In this study, image log and outcrop scanlines are long and numbers of spacing measurements are comparable to those of Marrett et al., and therefore I conclude that the image logs and outcrops have enough data to reveal spatial patterns. Compared to the image log and outcrop scanlines, core scanlines are short and core data may be insufficient to

reveal patterns evident in longer scanlines. I used core data to interpret and calibrate image log fracture picks. Core data provide essential information on relative timing and fracture aperture information absent in image logs, and illuminate aspects of fine-scale spacing not apparent in image log data because these tools miss some of the narrowest fractures that are preferentially sealed (Lander and Laubach, 2015).

Source, Set	4H, Set 1	1H, Set 1	1H, Set 2	2H, Set 1	2H, Set 2	CR1&2, Set 1	CR3, Set 1	CR4, Set 1	Oc2, Set J2
Total corrected spacing (m)	426	402.9	172.3	149.5	45.63	16.80	6.097	13.15	1138
Spacing count	370	533	99	108	109	40	40	45	389
Mean spacing (m)	1.15	0.76	1.74	1.38	0.42	0.42	0.15	0.29	2.93
Standard deviation (m)	4.83	1.66	3.49	5.1	1.72	0.69	0.22	0.41	2.58
Cv	4.20	2.19	2.00	3.69	4.11	1.65	1.45	1.41	0.88

Table 4-1 Descriptive statistics for conductive fracture spacings in Frontier Formation acquired from wells, outcrop images, and cores. 4H = Rock Island 4H; 1H = Sidewinder 1H; 2H = Sidewinder 2H. CR = Core; CR1, 2, and 3 from 4H (1 and 2 in upper shoreface, 3 in lower shoreface); CR4 from 1H. Oc2 = Hogsback outcrop. Coefficient of variation, Cv, calculated as σ/μ , where σ is the standard deviation of fracture spacings and μ is the mean (Gillespie et al., 1993); if coefficient of variation is near 1 then fracture arrangement is indistinguishable from random, but a value greater than 1 indicates clustering and a value less than 1 indicates anti-clustering.

4.1 ROCK ISLAND 4-H OBSERVATIONS

A total of 499 fractures, including conductive and resistive opening-mode fractures as well as faults, were documented in the RI4H image log. Of the 499 fractures, 413 belong to the east-west-striking and locally oldest Set 1 and the other 86 fractures to the north-south-striking Set 2. The majority, 369 of the 413 Set 1 fractures, are conductive, whereas the majority (68 of 86) of Set 2 fractures are resistive (Table 1). Core analysis shows that fractures of both sets retain porosity (Laubach et al., 2016). Seven of the eight faults visible in the image log strike east-west, and all but one fault is in the lower shoreface facies of the Frontier sandstone beyond approximately MD 4801 m. No obvious systematic increase in fracture intensity (decrease in spacing) is evident near identified faults (Figure 3-1), unsurprising in that crosscutting relations in core show that faults postdate Set 1 fractures.

4.2 SIDEWINDER 1-H OBSERVATIONS

SW1H was drilled to the northeast of RI4H and targeted the Second Member of the Frontier Formation. DeJarnett et al. (2001) reported that the well was sidetracked after initially drilling out of Frontier sandstones into overlying shales. FMI logs are from the third lateral in the interval between 4724.7 m and 5135.9 m MD. The 18 meter-long horizontal core is from a different lateral (DeJarnett et al., 2001). Image logs record 721 fractures and 12 faults. Of the 630 conductive fractures, 532 are east-west-striking Set 1 fractures, and the other 98 are north-northwest-striking Set 2 fractures.

4.3 SIDEWINDER 2-H OBSERVATIONS

SW2H was drilled to the northeast of SW1H also into the Second Frontier sandstone in the backlimb of the Table Rock anticline. Cuttings indicate that much of the well was in the stratigraphically higher fluvial portion of the Second Frontier instead of the

marine sandstone drilled into by RI4H and SW1H (DeJarnett et al., 2001). No core was taken from this well. I documented 368 fractures and 13 faults from the FMI log from the 5044.4 m – 5193.8 m MD interval. A category of fracture pick that only appears in the SW2H report labeled “LQ” or “Low Quality”, meaning that they are indistinct and potentially not correctly identified as fractures. I separated these fractures from the more reliable conductive and resistive fractures. Unlike RI4H and SW1H, the number of conductive and resistive fractures for both sets is similar: 107 conductive fractures in Set 1 and 108 in Set 2.

4.4 CORE OBSERVATIONS, WYOMING

Four horizontal cores were collected. Cores 1 and 2 were taken in the mid- to upper shoreface Frontier sandstone whereas Cores 3 and 4 were taken in the lower shoreface facies (DeJarnett et al., 2001). In the four cores, Laubach et al. (2016) documented 121 Set 1 fractures and 12 Set 2 fractures. The number of Set 1 fractures is approximately an order of magnitude higher than the number of Set 2 fractures primarily owing to sampling bias as a result of set orientation relative to the wellbore. Spacing measurements were corrected for this effect.

Comparison shows that fractures in core are generally visible in image logs. Discrepancies between fracture occurrence in image logs and cores over the same interval of rock can occur owing to the fact that image logs (borehole wall) and cores sample slightly different rock volumes. The differences between core fracture observations from RI4H and SW1H and the corresponding image log intervals could also arise from under-picked image log fractures, as a result of variation in log resolution along or between wells that cannot be assessed for these vintage logs. Moreover, conductive and possibly wider

fractures, which are likely open and contain fluids, may be more readily visible on image logs than are mostly sealed narrow fractures. Set 1 fractures have a range of aperture sizes and concomitant range of degree of quartz fill (Laubach et al., 2016). On the other hand, as noted by Lorenz et al. (2005) for these cores, in some cases where closely spaced fractures occur in core and core integrity is degraded, image logs over the same interval may find more fractures than are readily distinguished in core. Obviously, where both are available, cores should be examined alongside image logs to confirm what types of fractures are being identified with the logging tool and to provide information on fracture apertures.

Quality or reliability of fracture picks affects spacing outcomes if picking biases are systematic. For large data sets of generally reliable image log, core, or outcrop data, problems with a few interpretations are unlikely to affect the overall pattern. Cores have the potential to reveal more narrow fractures and thus can be expected to differ somewhat from patterns on image logs.

4.5 OUTCROP OBSERVATIONS, WYOMING

Frontier Formation west-dipping outcrops along the Hogsback escarpment (Figure 2-1) have fractures are clearly visible in satellite imagery. At least three fracture sets are distinguishable by orientation and cross-cutting relationships (Laubach, 1992) (Figures 2-2 to 2-3); I focused on the broadly east-west-striking set that roughly parallels the best sampled set in our image log and core data sets.

Approximately 500 east-west-striking fractures with low (<10 percent) deviation in strike are visible in a single continuous Frontier sandstone depositional body (or lens) (Figure 2-3). I confined data collection to the lens, although fractures appear to be

contained within the overall sandstone interval, rather than being localized in the lens. Field work shows that the sandstone is about 15 m thick, and fractures span the sandstone layer, that is, the fractures are perfectly bed-bounded in the nomenclature of Hooker et al. (2013). In other words, fractured layer thickness here is about 15 m.

To document fracture spacing, I drew ten parallel, en echelon scanlines orthogonal to fracture strike over a total scanline interval of approximately 1138 m (Figure 2-3), intersecting 390 fractures. The direction normal to fracture strike is not exactly parallel to the long dimension of the outcrop (divergence ca. 20 degrees), and the purpose of the en echelon arrangement of scanlines is to remain within the sandstone. At each en echelon step the scanline terminates against the fracture on which the next scanline begins, allowing the measurement of a long, continuous spacing sequence with no missing fractures or double counting.

4.6 INTENSITY AND SPATIAL ARRANGEMENT, WYOMING

Occurrence versus distance (stick) diagrams (Figure 3-1), spacing histograms (Figure 3-2), and cumulative frequency (Figure 3-3) document a range of spacing sizes. Occurrence versus distances plots document a degree of uneven spacing in all data sets (Figure 3-1) and some high C_v values (Tables 2) suggest clustering. Here I present an analysis based on Normalized Correlation Count (Marrett et al., 2017) aimed at assessing whether these patterns can be quantified and distinguished from each other, and distinguished from random clustering.

The computer program CorrCount (Marrett et al., 2017) calculates fracture intensity and correlation count from measured spacings for selected, computer-generated length scales. The results are normalized by comparison to results for randomized spacings (See

Marrett et al. (2017) for explanation of the normalization method). Figures 4-1 to 4-5 show results for both Set 1 and Set 2 conductive fractures, except in the case of RI4H where only a few conductive fractures were sampled in Set 2 (17 versus 369 in Set 1).

In a normalized fracture intensity plot, the horizontal axis represents the distance in meters along the wellbore or scanline. The vertical axis represents fracture intensity. The calculated intensity values are normalized by expected intensity for randomly spaced fractures. Normalized fracture intensity that peaks above the upper 95% confidence limit (highlighted in the Figures) suggests that the intensity, at the 95% confidence level, is higher than it would be under the null hypothesis of random spatial arrangement.

In a Normalized Correlation Count plot (Figures 4-1 to 4-5), the vertical axis represents the degree to which the spacings at given length scales (horizontal axis) are more (peaks) or less (troughs) common than would be seen in a random distribution. All log-log scale NCC plots have uniform axis values for ease of comparison and interpretation. Marrett et al. (2017) identified and interpreted a range of pattern types including peaks, troughs, slopes, and plateaus, which we discuss after describing the patterns in our data.

The descriptive statistics and the coefficients of variation C_v calculated using CorrCount for the spacings in each of the fracture sets analyzed are summarized in Table 2 and Figures 3-1 and 3-2. The average spacings between image log fractures, ranging from 0.75 m in SW1H Set 1 to 1.74 m in SW1H Set 2, are at least twice as large as the average spacings of 0.15, 0.29, and 0.42 m for Cores 1, 2, 3, and 4, respectively. The average spacing of fractures in outcrop Oc1 and Oc2 is 2.93 m, nearly twice the largest image log average spacing. The coefficients of variations of all fracture sets except the Oc2 outcrop

set are above 1, with RI4H Set 1 having the largest value of 4.20, compatible with a range of degrees of clustering.

In the following, we first describe the pattern of spatial variability on NCC plots. We then describe what these patterns likely mean in terms of fracture spatial arrangement.

4.6.1 Intensity and correlation count, Wyoming subsurface data

For Set 1 in the normalized fracture intensity plot of RI4H (Figure 4-1a), major peaks occur at 90, 180, and 270 m along the wellbore. Minor peaks occur at 140 m and 205 m. Average peak width is approximately 35 m. Major troughs are observed at 230 and 310 m, and minor troughs at 350 and 380 m. In the Normalized Correlation Count plot (Figure 4-1b), there is a wide section elevated above the 95% confidence envelope with negative slope for length scales from 0.1 to approximately 35 m. Two overlapping peaks are observed at length scales of 50 m and 90 m. Normalized Correlation Count falls to 1 at the length scale of 145 m.

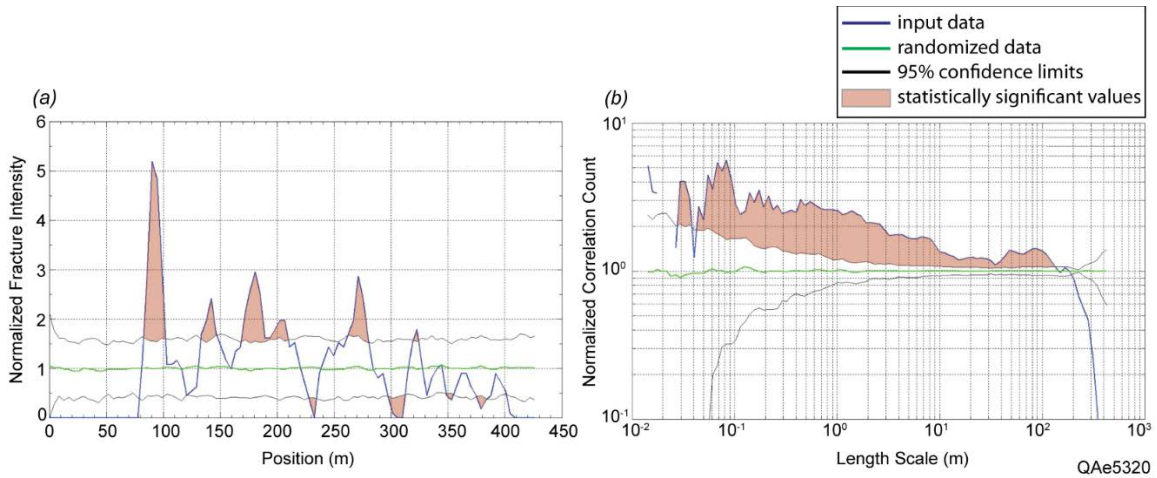


Figure 4-1 CorrCount result for Rock Island 4-H conductive fractures. (a) Normalized fracture intensity variation of Set 1. Fracture intensity is the number of fractures per unit length along a scanline (Ortega et al., 2006). (b) Normalized correlation count Set 1 fractures in RI4H. Length scales are logarithmically graduated. Sparse Set 2 observations precluded analysis. For this and subsequent figures, ‘0 m’ signifies arbitrary start of scanline. Highlighted areas mark parts of curve outside 95% confidence interval.

Set 1 in SW1H has a broad, statistically significant interval of high fracture intensity that extends from 210 m to 280 m, combining subsidiary peaks at 230, 245, 260, and 270 m (Figure 4-2a). The largest peak is at 290 m. An additional minor peak is at 190 m. A major trough beneath the lower confidence limit occurs at 80 m. A near-periodic distribution of troughs occurs at 310, 340, 365, and 385 m. Owing to overlaps it is difficult to quantify peak widths. The NCC plot is elevated for all length scales between 0.1 m and 120 m (Figure 4-2b). The Normalized Correlation Count drops to 1 at the length scale of approximately 135 m. Unlike the RI4H normalized correlation curve, which has a relatively constant negative slope through the elevated interval, the SW1H curve’s slope remains negative before the length scale of 3 m, then flattens to zero until length scale of 30 m where the slope becomes negative again. Several peaks are evident (Figure 4-2c).

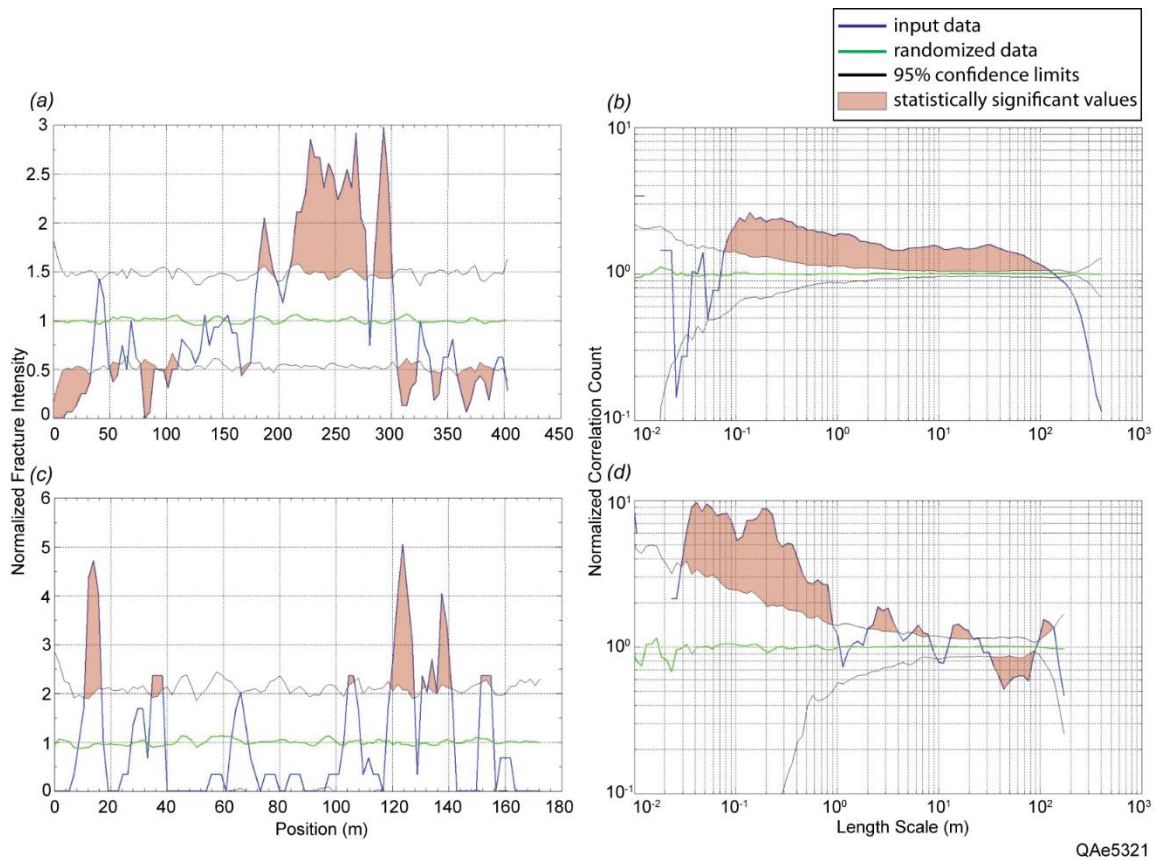


Figure 4-2 Sidewinder 1-H conductive fracture sets CorrCount results. (a) Intensity of Set 1. (b) Correlation count of Set 1. (c) Intensity of Set 2. There is a peak at ~ 100 m. The two largest peaks in the intensity plot are spaced ~ 100 apart, and the smaller peaks are spaced at ~ 15 m. (d) Correlation count of Set 2. Set 1 correlation count patterns exhibit low amplitude, and predominantly statistically significant patterns throughout. Set 2 correlation count results have a decreasing elevated section followed by peaks and troughs over larger length scales. Highlighted areas mark parts of curve outside 95% confidence interval.

The largest peak for Set 1 fractures in SW2H (Figure 4-3a) is at the beginning of the scanline. Statistically significant peaks also appear at 39 m, 53 m, and 65 m, with diminishing peak magnitudes. A wide, near-zero intensity interval extends from 92 to 135 m. In the NCC plot (Figure 4-3b), the statistically significant part of the curve is confined

between the length scales of 0.1 m and approximately 4 m and has a negative slope. Spatial correlation decreases to 1 after 4 m. Subsequent peaks appear at 6 m, 12 m, and 36 m with increasing amplitudes.

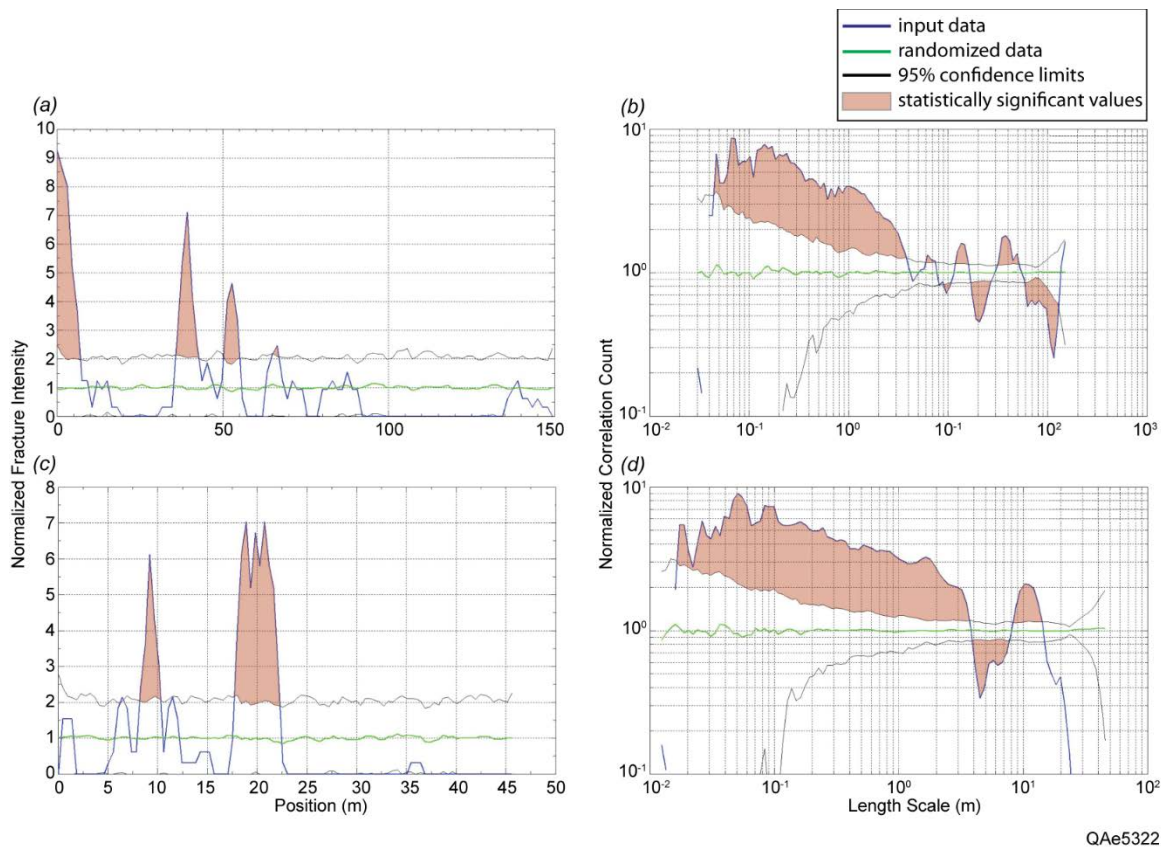
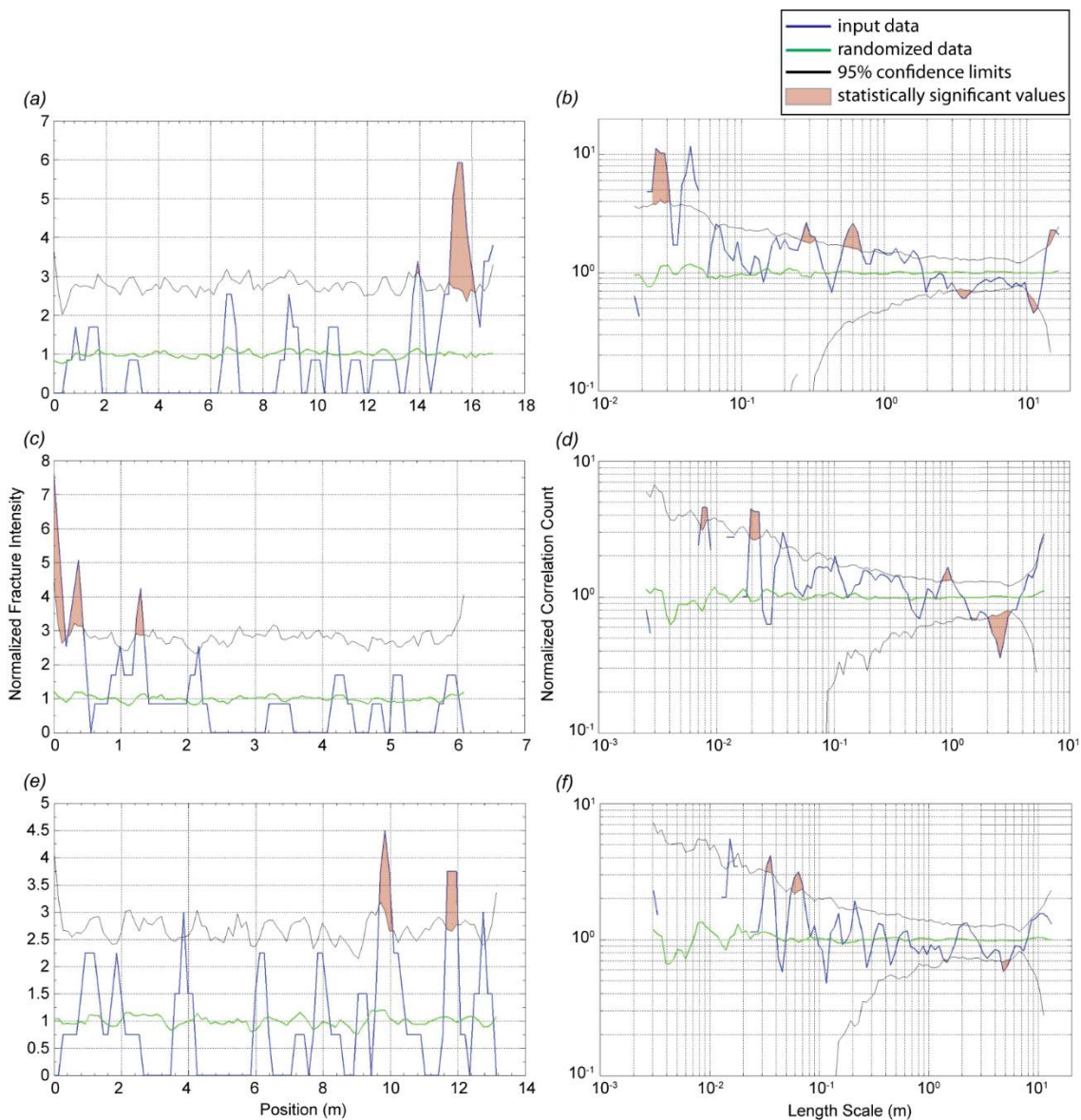


Figure 4-3 Sidewinder 2-H conductive fracture sets CorrCount results. (a) Intensity of Set 1. (b) Correlation count of Set 1. There is a minor trough over 9.5 m and a major trough over 20 m. (c) Intensity of Set 2. (d) Correlation count of Set 2. All correlation count results have a decreasing elevated section followed by peaks and troughs over larger length scales. Highlighted areas mark parts of curve outside 95% confidence interval.

Set 1 fracture intensities in Cores 1 and 2 from RI4H (Figure 4-4a) show a major peak near one end of the core. A minor peak is located at 14 m right before the major peak. The fracture intensity variation in approximately the first 13 m of the core is similar to that of a random fracture arrangement. In the NCC plot (Figure 4-4b), there are several peaks at 0.03 m, 0.04 m, 0.3 m, 0.6 m and two minor peaks at 1.2 m and 1.6 m. A trough is present over the length scale of 3.5 m. No significant elevated correlation count plateau is present.

In Core 3 from RI4H (Figure 4-4c), the largest fracture intensity peak is at the beginning of the core, followed by two successive peaks at 0.4 m and at 1.3 m. The rest of the intensity curve is indistinguishable from that of a random fracture arrangement. In the NCC plot (Figure 4-4d), small length scales around 0.02, 0.035, and 0.9 m appear to be statistically significant. This pattern means that there is a significant lack of spacing values at the 2-3 m length scale.

In the normalized fracture intensity plot of Core 4 from SW1H (Figure 4-4e), the largest intensity peak is at 9.8 m, followed by another peak at 11.8 m. These three peaks occur toward the end of the core. Minor peaks not exceeding the upper confidence limit appear periodic. In the NCC plot (Figure 4-4f), peaks for sub-meter scale spacings of 0.035 m and 0.6 m are present; this pattern is similar to that of the other cores. A trough beneath the lower confidence limit appears at length scale of 5 m. Much of the curve is bounded within the 95% confidence limits.



QAe5323

Figure 4-4 Cores, Frontier Formation sandstone, CorrCount results. (a) Intensity for Cores 1 and 2. (b) Correlation count of Cores 1 and 2. (c) Intensity of Core 3. (d) Correlation count of Core 3. (e) Intensity of Core 4. (f) Correlation count of Core 4. All correlation count results exhibit distinctive peaks for small length scales but are overall confined within the 95% confidence interval. Highlighted areas mark parts of curve outside 95% confidence interval.

Set 2 fractures strike at a low angle to wellbore trajectories, so fracture sampling per wellbore length is not as complete as for Set 1. The scanline of SW1H Set 2 corrected for obliquity is shorter than that for Set 1. The fracture intensity plot for SW1H Set 2 (Figure 4-2c), shows major peaks at 12 m, 124 m, and 138 m and minor peaks at 38 m, 105 m, 132 to 134 m, and 155 m. Unlike Set 1 fractures in SW1H, Set 2 fracture intensity peaks are bounded by near-zero intensity intervals; the peak edges are cluster boundaries. In the NCC plot (Figure 4-2d), the spatial correlation curve for length scales less than 0.9 m is above the upper confidence limit and has a generally negative slope. Spatial correlation decreases to 1 at approximately the 1 m length scale. Subsequent spatial correlation peaks center around the length scales of 3 m, 6 m, 15 m. A wide trough extends from 30 m to 90 m. The last peak above the length scale of 100 m, which is larger than half of the total scanline length, arises due to two clusters of fractures near the ends of the analyzed section.

The scanline for SW2H Set 2 (Figure 4-3c), also corrected for obliquity, has fracture intensity peaks around 9 and 18 m, with the latter formed by three closely spaced, overlapping peaks no more than 3 m apart. The normalized intensity falls to zero for most parts beyond 25 m. In the NCC plot (Figure 4-3d), a statistically significant elevated interval is present at length scales up to approximately 3.5 m. A trough extends from length scales of 4 to 8 m, followed by a single large peak at approximately 10 m.

4.6.2 Intensity and correlation count, Wyoming outcrop data

Outcrops Oc1 and Oc2 are highly similar, and therefore our analysis presentation focuses on Oc2, which has a slightly simpler fracture pattern and longer scanline. Fracture intensity of the east-striking fractures in the Frontier Formation outcrop Oc2 (Figure 4-5a), varies along the outcrop, with peaks and troughs. However, the intensity plots mostly fall within the 95% confidence interval, making the intensity variation indistinguishable from random. Minor peaks are present between 280 and 320 m and there is a small trough around 830 m. In the NCC plot (Figure 4-5b), the curve is also bounded within the 95% confidence interval for length scales over 0.45 m. Two very small peaks are present at 0.95 and 1.5 m. The curve dips sharply beneath the lower confidence limit for length scales less than 0.45 m. The intensity patterns for each component scanline segment of the outcrop data are also indistinguishable from random.

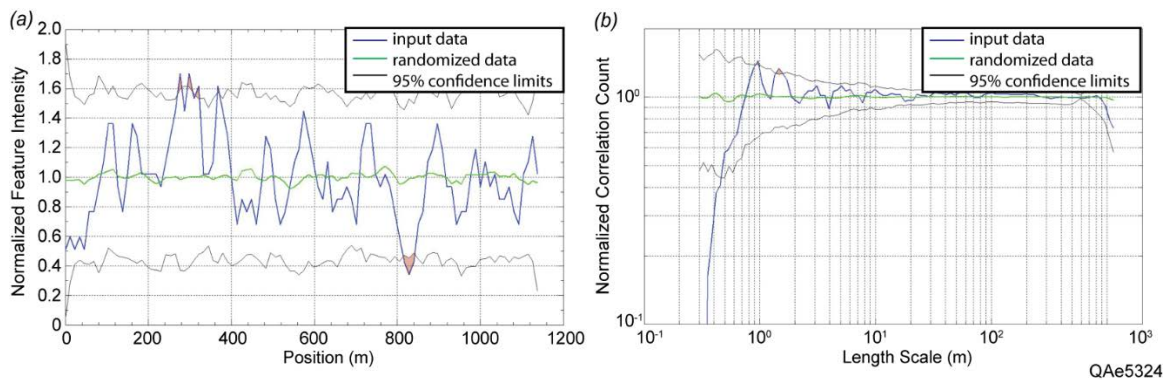


Figure 4-5 Outcrop, east-striking fractures, Frontier sandstone Oc2, CorrCount results. (a) Intensity result. (b) Correlation count result. Both plots Well VM-Confined within upper- and lower confidence limits and are therefore practically indistinguishable from random. Highlighted areas mark parts of curve outside 95% confidence interval.

Chapter 5: Discussion: Tight Gas Sandstone

5.1 CLUSTER PATTERNS IN SANDSTONE EXAMPLE

A fracture set's spatial arrangement can be inferred from the NCC curve. Marrett et al. (2017, their Figure 10) interpret eight characteristic patterns: indistinguishable from random, clustered individuals, anti-clustered individuals, regularly spaced individuals, fractal cluster (locally close spacings containing smaller self-similar spacing patterns), log-periodic cluster, regularly spaced clusters, and regularly spaced fractal clusters. I interpret our NCC curves using the Marrett et al. terminology, and discuss the meaning of the curves in the context of the geology of the Frontier Formation in outcrop and the subsurface.

I first discuss the NCC results for the image log and core data sets (Table 3). For RI4H Set 1 (Figure 4-1b), the elevated section with a broadly constant negative slope at small length scales followed by broad peaks at 50 m and 90 m indicates regularly spaced fractal clusters. The width of the largest cluster is given by the point at which the curve crosses the spatial correlation value of 1, which in this case is at 35 m. The spatial correlation peaks at length scales of 50 m and 90 m represent inter-cluster spacing values; the 90 m peak possibly being a harmonic of the 50 m peak. The 35 m-wide clusters spaced approximately 50 or 90 m apart are seen in the fracture intensity plot, but the NCC allows us to determine the pattern is statistically significant, and also signals that the internal structure of the clusters is fractal—a property not discernable from the intensity plot.

Set 1 fractures in SW1H form a wide cluster with multiple internal intensity peaks spanning one third of the scanline (Figure 4-2a). This NCC curve is unlike the others in that a broad, statistically significant elevated peak occurs across length scales from approximately 0.08 m to 120 m, falling off to a trough at greater length scales (Figure 4-

2b). This signal indicates one broad cluster about 120 m wide, within which there is a fractal arrangement at length scales below ~ 3 m, narrow clusters with fractal arrangement within the broad cluster of individuals. There are few fractures spaced at very small length scales below 7 cm or at long length scales above 120 m. The pattern is a hybrid between ‘clustered individuals’ and ‘fractal clusters’ (Marrett et al., 2017).

Data Type	Data Set*	Class[†]	NCC Interpretation	Cluster Width (m)	Cluster Spacing (m)
Image logs	RI4H	EW Set 1	Regularly spaced fractal clusters	35	50 & 90
	SW1H	EW Set 1	Clustered individual (+ fractal clusters)	120 (3)	one large cluster
		NS Set 2	Regularly spaced fractal clusters (+ log periodic cluster)	8.5 (1)	15 & 100
	SW2H	EW Set 1	Regularly spaced fractal clusters	4	6, 12, 36
		NS Set 2	Regularly spaced fractal clusters	4	10
	Cores	RI4H Core 1&2	EW Set 1	Indistinguishable from random (weak clusters?)	—
Core 3		EW Set 1	Indistinguishable from random (weak clusters?)	—	—
SW1H Core 4		EW Set 1	Indistinguishable from random (weak clusters?)	—	—
Outcrop	Hogsback Oc2	EW ‘J2’	Anti-clustered individuals	—	—

Table 5-1 Summary of NCC interpretation for fractures in Frontier image logs, cores, and outcrop. RI4H = Rock Island 4H; SW1H = Sidewinder 1H; SW2H = Sidewinder 2H. Cluster width within parenthesis indicates width of internal clusters. *Well name or outcrop locality. †Average orientation and local set classification.

The Set 1 NCC curve for SW2H also shows an elevated section with negative slope at small length scales. The curve crosses the spatial correlation value of 1 at 4 m length scale, which is the width of the largest clusters in this set (Figure 4-3b). Peaks in the NCC curve at 6, 12, and 36 m reflect the spacing of clusters, with the strongest signal at ~36 m. The largest two peaks in the intensity plot are spaced at ~36 m (Figure 4-3a). The spatial arrangement type resembles regularly spaced fractal clusters.

Although Set 2 fractures and spacing values are less numerous owing to low angle of fracture strike to wellbore trajectory, some patterns are evident. The Set 2 NCC in SW1H is similar to that for RI4H Set 1 with an elevated section with negative slope at small length scales indicating regularly spaced fractal clusters. However, the slope has some internal peaks and troughs similar to Marrett et al. (2017)'s "log periodic cluster". Some internal clusters are ~1 m wide, whereas the main clusters are ~8.5 m wide; these widths are indicated where the curve crosses the spatial correlation equal to 1 line (Figure 4-2d). An approximately periodic distribution of spatial correlation peaks at length scale > 8.5 m suggests periodically spaced fractal clusters with spacing of ~15 m. There is also a peak at ~100 m. The two largest peaks in the intensity plot are spaced ~100 m apart, and the smaller peaks are spaced at ~15 m (Figure 4-2c).

The Set 2 NCC pattern for SW2H is similar to SW2H Set 1 in the elevated section (Figure 4-3d), where the cluster width is also approximately 4 m, corresponding to the length scale at which the correlation count decreases to 1. The large peak after the elevated section at length scale 10 m represents the inter-cluster spacing, marked by the approximately 10 m gap between the two largest fracture intensity peaks (Figure 4-3c).

The discrepancy between the arrangement types inferred from the cores and the image logs may be because the cores are shorter so that the signal is weak. The Set 1 and 2 NCC curves for the cores retrieved in the mid- to upper- and lower-shoreface sandstones differ from their image log counterparts in that they lack the elevated, negatively sloped or plateau-shaped portion over small length scales (Figure 4-4b, d, f). Instead, the patterns overall are indistinguishable from random, although there are weak peaks and troughs at all length scales. In each case, the smallest length scales plot just above the 95% confidence limit, indicating more common spacing on the centimeter scale than would be the case for a random distribution. So although the overall pattern is indistinguishable from random, there is a weak signal of regularly spaced clusters. The coefficients of variation of the core spacings average approximately 1.51, corroborating that fracture clusters are present. The combined length of Cores 1 and 2 in RI4H is 17.7 m, and the length of Core 3 is 6.2 m, distances that together are less than the 50 m inter-cluster spacing and the 35 m cluster width inferred from the image log correlation count result for RI4H. The latter result is obviously based on a much longer sampling interval. The scale of the pattern inferred from image log data implies that the cores are unlikely to capture sufficient data to define complete fracture clusters, at least for macro-fractures.

East-west-striking fractures along the Oc2 outcrop have approximately the same orientation as Set 1 in core. For outcrop fractures, gradual variations are evident along strike. East-west fractures in Oc1 are dominantly ENE-striking (Figure 2-2), whereas ESE-striking are prevalent in Oc2 (Figure 2-3). However, as noted, these outcrops differ in structural setting from the cored areas and outcrop sets differ in relative timing from those

in core. In outcrop at least some of the east-west-striking fractures are younger than north-striking fractures based on crosscutting and abutting relations (Laubach and Lorenz, 1992).

For east-west-striking fractures in outcrop the NCC signal is mostly confined within the 95% confidence interval, indicating a spatial arrangement indistinguishable from random (Figure 4-5b). The pattern is one of anti-clustered individuals if the lack of spacings at this small length scale is real. The statistically significant absence of fracture pairs at length scales less than 0.45 m might be an artifact from low satellite image resolution preventing observation of closely spaced fractures, but field observations in the area analyzed shows that here probably such closely spaced fractures have not been missed.

A comparison of NCC results shows that image logs exhibit a common pattern: regularly spaced clusters where NCC decreases from length scales less than 0.1 m up to approximately 10 m (Table 3; Figure 5-1a). The peaks and troughs at length scales >10 m indicate periodic cluster spacing. The one exception is the pattern for Set 1 in the SW1H, which arises because the image log passes through one very wide (120 m) cluster.

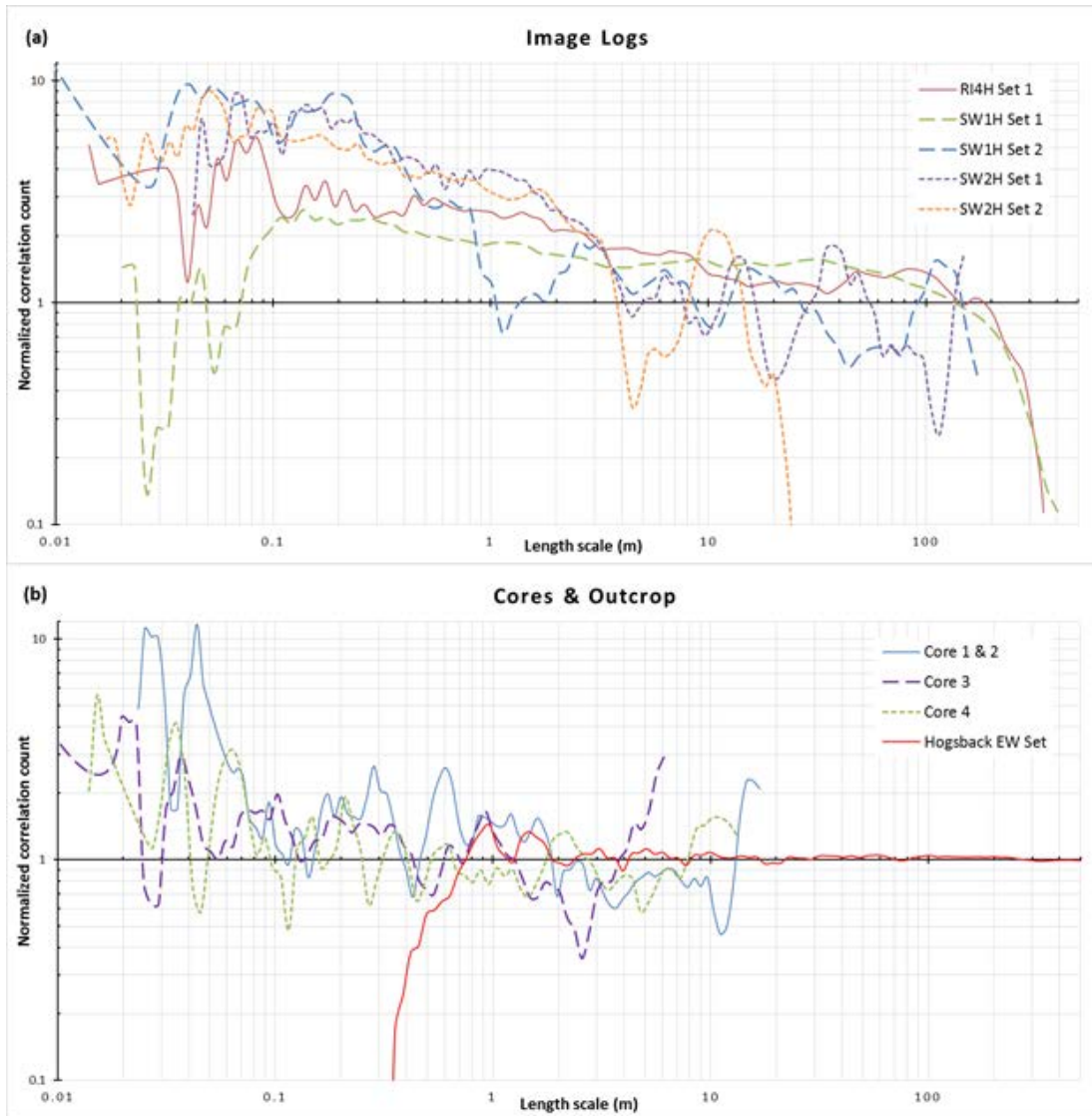


Figure 5-1 Comparison of CorrCount results. Normalized correlation count = 1 suggests correlation indistinguishable from random. Log scale, windowing set to 1. Highlighted areas mark parts of curve outside 95% confidence interval. (a) Comparison of normalized correlation count results between image logs. All results show similar exponential decrease in spatial correlation for length scales less than 10 m. RI4H = Rock Island 4-H, SW1H = Sidewinder 1-H, SW2H = Sidewinder 2-H. (b) Comparison of normalized correlation count results between cores and outcrop. Peak-and-trough signals differ from the continuous interval pattern for image log results.

The cores (Figure 5-1b) show similar patterns to most of the image logs, but with a weaker signal at long length scales, and a stronger signal at centimeter length scales. For example, in Cores 1 and 2 from RI4H the spatial correlation over length scales <0.1 m is higher than the spatial correlation over the corresponding image log result interval. Image logs, when optimally positioned and of adequate resolution, have an advantage over cores in providing reliable and abundant spacing measurements over long distances, in this case hundreds of meters.

I attribute the core NCC patterns to shorter scanlines, insufficient to give signals beyond random. However, cores capture a few more small fractures increasing resolution relative to image logs at small spacing values. The validity of correlation count inferences depends on the quality and quantity of input data. Correlation count for small length scales of meters to millimeters, depends on spacing resolution – results are valid down to the smallest measurable image log fracture spacing value. For large length scales of tens to hundreds of meters, output accuracy is controlled by the total scanline length, which limits the largest length scale – one half of the total scanline length – at which two or more pairs of fracture can be matched without any spacing overlap that violates the correlation sum principle. Correlation count for spacings larger than half the scanline are artifacts (e.g. Figure 4-2d).

The NCC for outcrop Oc2 east-west-striking fractures, though covering a larger range of spacings from < 1 to 100s of meters, is statistically indistinguishable from random. However, the weak peaks and troughs, and the significant lack of spacings below 0.45 m suggest individual fractures spaced between 0.45 to 1 m apart with weak clusters spaced

on the 60 to 120 m scale. Marrett et al. (2017) class this pattern as anti-clustered individuals, a regular spacing pattern compatible with visual impressions (Figure 2-2).

In addition to data quality, fracture spacing and intensity estimation can be affected by sampling bias and changing observation scales. For example, fracture sizes (height) can affect the number of fractures that intersect a scanline depending on scanline location (Ortega et al., 2006). If a wellbore trajectory is gradually cutting across a hierarchical fracture spacing pattern that varies with stratigraphy, this effect could be present in 'horizontal' well data because such wells are rarely precisely in the same part of a bed. The effect of this bias is particularly acute if a wide fracture size range is present, since small fractures could be preferentially missed. Although in our example core data shows that a range of kinematic aperture sizes is present (Laubach et al., 2016), implying a range of heights and lengths, the kinematic aperture size range is narrow, and I infer that size-related sampling bias is probably not important.

Though C_v values above 1 and the raw distributions and dimensions of fracture intensity peaks qualitatively indicate irregular fracture spacing, without aperture size information we could not quantify the heterogeneity of fracture strain with conventional approaches (i.e., Putz-Perrier and Sanderson, 2008). NCC analysis, however, rigorously quantifies statistically significant departures from randomness. Moreover, the NCC approach highlights the presence or absence of systematic clusters, cluster dimensions, cluster internal structures, and overall fracture spatial arrangement hierarchies.

5.2 CAUSES OF SPATIAL ARRANGEMENT PATTERNS, WYOMING

Fractures can be arranged in apparent clusters even in a statistically random sequence (Priest and Hudson, 1976). Fractures in non-random arrangements can be statistically more strongly clustered, or they may have spacings that are more regular than expected for a random arrangement (Marrett et al., 2017). Non-random distributions imply mechanisms that either promote localized close spacing (clusters) or regular spacing (Marrett et al., 2017). Correlation count results for Frontier Formation image log data sets—but not the outcrop data set—document clustering too concentrated to be due to random arrangement, differences that are not apparent from other types of spacing analysis (Figures 3-1 to 3-3; Table 1). As Watkins et al. (2017) and Hooker et al. (2017) show, many structural processes can produce localized fractures and clustering. Regional fracture arrays are low-strain features potentially arising from a range of loading paths during burial and uplift (Engelder, 1985), so without fracture timing information mechanisms governing patterns are hard to pin down. Our results constrain why differing clustering patterns exist here.

Our NCC patterns do not resemble those for ‘forced clustering’ (Marrett et al., 2017) arguing against folding or faulting as the cause of spatial arrangements I found, despite the occurrence of the fractures within folds and near faults. This assessment is consistent with previous interpretations that the outcrop and cored fractures are not the result of folding. Although within the leading edge of the fold-thrust belt, west-dipping beds (ca. 10-15 degrees) of outcrop Oc2 were tilted and likely did not pass through a fold hinge (Delphia and Bombolakis, 1988). (Although not sampled by our limited field scanlines, the outcrops likely contain other types of clusters, including forced clusters. The pervasive non-clustered patterns we analyzed contrast with abruptly more concentrated

fractures in the steep east-dipping fold limb adjacent to tear faults and higher fracture densities associated with along-strike dip changes (Lorenz and Laubach, 1994). These east-striking 'J2' fractures have been interpreted to result from deformation adjacent to the limits of thrusting (Laubach, 1991).

Based on their orientation orthogonal to the thrust front and their timing, regional fractures in the Frontier Formation have been interpreted to result from regional deformation in the thrust belt foreland (Laubach, 1992; Hennings et al., 2000; Lorenz, 2003; Laubach et al., 2016). Pervasive arrays having spatial arrangements indistinguishable from random may reflect stress fields associated with this structural setting, which also may exhibit mutual cross-cutting relations between orthogonal fracture sets as documented by Dunne and North (1990).

Another factor that could influence these outcrop fracture patterns is uplift and unloading. The outcrop fractures I measured are probably not primarily the result of near-surface unloading and weathering, based on calcite fracture fills of subsurface origin in fresh outcrops (Laubach, 1992) (Figure 2-2b), but such cements cannot be demonstrated for all fractures and I cannot rule out that some east-striking fractures formed after thrusting ceased, or even much later with exhumation. For outcrops fracture growth by thermoelastic contraction is likely, as this process affects other uplifted areas in the Rockies (English and Laubach, 2017). In our samples from the eastern Green River Basin, fluid inclusion sequences document late, probably uplift-related reactivation of some north-striking Set 2 fractures (Laubach et al., 2016). Evidence from outcrop fracture petrology and thus fracture timing is needed to test this idea.

Another difference between outcrops and our subsurface example is likely to be rock mechanical properties at the time of fracturing. During slow, subcritical crack growth (Atkinson, 1984) where mechanical layer thickness are held constant, numerical simulations of propagation show that differences in total strain or in rock mechanical properties produce either evenly spaced or clustered patterns (Olson, 1993; 2004). Currently, induration and average mechanical properties of core and outcrop samples differ because of their differing burial and thermal histories. As is the case with other Cretaceous sandstones in the Rockies (e.g., Ozkan et al., 2011), sandstones in Late Cretaceous to early Tertiary uplifts now in outcrop experienced lower thermal exposure and generally have less cement than equivalent rocks that have been persistently at depth. Consequently, mechanical properties differ. Nevertheless, Frontier sandstone likely has similar within-formation patterns of mechanical property variation. Rocks examined in this study are from the same part of the Frontier Formation stratigraphic section, deposited in shallow marine depositional environments, and have similar compositional range. Mechanical properties of the subsurface and outcrop sandstones at the time of fracture growth are needed to help test whether differences in mechanical properties in this case might account for differing spatial patterns. Contrasts in mechanical properties and loading history are likely part of the explanation for why the two areas differ.

Speculatively, in the distal foreland basin setting of our cores, mechanisms promoting close spacing may include cement accumulation affecting fracture growth and spacing (Hooker et al., 2012; Hooker and Katz, 2015). Set 1 and Set 2 fractures formed at depth concurrently with copious quartz cement precipitation in the fractures (Laubach et al., 2016). Evidence for fracture timing from fluid inclusions suggests that Set 1, concurrent

with regional Eocene-Oligocene foreland shortening, involved slow, intermittent fracture growth over millions of years (Laubach et al., 2016). Clustering may be favored where uneven partitioning of progressive opening displacement occurs within a fracture spacing population as a result of the mechanical effects of different types and amounts of cement deposited during fracture. Reconstructed fracture histories and models suggest that the adhesion effects of cement can modify fracture spacing and other attributes (Caputo and Hancock, 1988; Hooker et al., 2012; 2013; 2017; Hooker and Katz, 2015). Differences in amounts of spanning quartz could reflect depth of burial and temperature at the time of fracture (Lander and Laubach, 2015), which fracture petrology indicates differed for east-west-striking fractures in core and those fractures now in outcrop. For our Frontier Formation subsurface examples, clustered fractures of Set 2 and 2 have ample spanning quartz that could have interfered with fracture opening. In contrast, calcite-bearing outcrop fractures lack spanning quartz and have negligible quartz contemporaneous with fracture opening.

5.3 COMMENT ON FRACTURED LAYER/BED THICKNESS FROM WYOMING OUTCROP

Near-surface barren joints commonly show a proportionality between average fracture spacing and fractured-layer thickness (e.g. Ladeira and Price, 1981; Narr and Suppe 1991). Experiments and mechanical models have been proposed to explain the proportionality (e.g. Wu and Pollard, 1995; Bai et al., 2000). Observations of spacing-thickness proportionality (Ladeira and Price, 1981) and mechanical models predict a spacing to layer thickness ratio of approximately 0.3 (Bai and Pollard, 2000). Proportionality varies over a wide range of values, partly as a function of lithology (e.g.,

Laubach et al., 2009; McGinnis et al., 2017), and some studies show absence of a consistent relationship (McGinnis et al., 2015).

Distances between fractures in both horizontal wells and outcrop have a wide range of values, so using averages is of questionable value, but average spacing to layer thickness ratios are widely applied in reservoir characterization and flow modeling (Narr and Lerche, 1984; Pan et al., 2017). In Frontier outcrops, fractures primarily terminate at shale beds that bound sandstones, defining fractured beds having thicknesses of tens of meters (about 15 m for Oc2) (e.g. Laubach and Lorenz, 1992) (Figure 2-2c). Although in the Frontier Formation gross sandstone intervals can be thicker, fractured beds are this dimension or thinner. Some outcrops contain shorter fractures, defining thinner fractured layers, but these are generally barren, probably near-surface joints that do not extend away from outcrop margins and are not part of the array I measured.

Intervals sampled with cores and image logs are in comparable stratigraphic settings and within-formation contrasts in mechanical stratigraphy are likely similar. Thus, fractured units and layer thicknesses are likely to be similar, with fractures layers as thick as those measured in outcrop. These inferences allow estimates of the relation of fracture spacing to fractured layer thickness. Using our averages, fracture spacing relative to layer thickness is narrower than predicted by the spacing/bed thickness relation of about 0.3 (Figure 3-2) for both outcrop and subsurface examples. Even if assuming that fractured bed thicknesses are only one third of the value observed in Oc2 (5 m), the spacing/thickness ratio is markedly smaller than expected but within the wide range of ratio values from less than 0.1 to greater than 10 that have been reported (Bai et al., 2000). Cluster spacings, on the other hand, are generally wider than the ratio predicts (Table 3).

Subsurface spacing observations violate the assumption that an average spacing is meaningful. For subsurface data my observations do not of course rule out some form of fracture occurrence/bed thickness proportionality, since fracture height observations for horizontal wells are unobtainable. These findings together with evidence for non-trivial clustering suggests that for populating fracture models, a generalized fracture spacing/bed thickness relationship needs to be used with caution. Instead, more nuanced NCC spatial arrangement data could be useful for comparison with and improvement of mechanical models (e.g., Bai et al., 2000; Olson, 2004) and chemical-mechanical models (Hooker and Katz, 2015) that predict spacing patterns.

5.4 IMPLICATIONS FOR RESERVOIR CHARACTERIZATION, FRONTIER FORMATION TGS

Differences in spatial arrangement have implications for reservoir characterization. Fracture clusters, or corridors as these features are referred to in industry, have been identified as widespread features in reservoir rocks (e.g., Questiaux et al., 2010) that need to be accounted for in reservoir modeling (Panza et al., 2016). The Marrett et al. method provides a way to define rigorously what constitutes a corridor. In my subsurface example, core observations show that both Set 1 and Set 2 are open and potentially capable of contributing to fluid flow. Clustering characterizes both sets. Both sets are open in the subsurface, and the connections between clusters of the same or different sets could impact flow patterns. For example, clusters separated by unfractured or less fractured rock could explain differences between copious gas production from the RI4H and water production from the adjacent SW1H (DeJarnett et al., 2001; Coleman, 2008).

Chapter 6: Conclusions: Tight Gas Sandstone

I found spatial arrangements that are more clustered than would be expected for random arrangements in some fracture arrays but not others in Cretaceous Frontier Formation marine sandstones. I use an analytical and statistical approach called Normalized Correlation Count (NCC) and associated NCC software (Marrett et al., 2017) that accounts for sequential fracture occurrence and that defines statistical significance of the calculated spatial correlation values. Subsurface fractures sampled using image logs and cores in three horizontal wells are clustered. For image logs, which have the largest spacing samples, the most extensively sampled east-west-striking Set 1 opening-mode fractures are arranged in clusters that are hierarchical and probably fractal with the largest clusters, from meters to tens of meters wide, possibly distributed periodically. This result is broadly consistent with elevated C_v values and previous qualitative observations of unevenly spaced fractures in the Rock Island 4-H and Sidewinder 1-H cores.

Results from horizontal logs and cores contrast sharply with patterns of fractures of the same broadly east-west strike in outcrop, where spatial arrangements are indistinguishable from random. Although the origin of these differences is unknown, discrepancies could be due to contrasts in location-dependent burial and structural histories. Although sharing approximately the same strike, the fracture sets are from widely separated parts of the basin and likely formed under contrasting structural and diagenetic conditions.

My results have implications for reservoir characterization. For these and other tight gas sandstones, quantitative information on fracture spatial arrangement can help constrain reservoir models and thus contribute to efficient resource extraction. By

demonstrating non-random clustering in subsurface fractures and by showing contrasts in spacing patterns between outcrops and reservoirs, my example underlines that outcrop analogs and fracture spacing/bed thickness proportionality need to be used carefully, and that they can be misleading, even where fractures in outcrop and core superficially resemble each other. Patterns of clustered open fractures in at least two nearly orthogonal orientations typify Frontier Formation tight gas sandstone in part of the Green River Basin. Patterns of similar complexity can be expected elsewhere. Assessment of fluid flow at depth needs to account for the presence of such patterns.

SECTION III: FRACTURE SPATIAL ARRANGEMENT IN SHALES

The Vaca Muerta Formation shale, the Devonian shales of the Horn River Basin, and the Marcellus Formation shale are prominent hydrocarbon bearing unconventional reservoirs in their respective basins. NCC analyses of image logs fractures in the three shale reservoirs provide further information on fracture clusters and spatial arrangements and the potential correlation with reservoir properties. Results from the Vaca Muerta Formation shale show strong control on fracture cluster locality by reservoir mechanical stratigraphy. In the Horn River Basins shales, statistically significant and commonly fractal fracture clusters concentrate in preferred wellbore intervals. Results of Marcellus Formation shale fractures show clusters correlated with mechanical bed thickness.

Chapter 7: Geologic Backgrounds of Shale Studies

7.1 VACA MUERTA FORMATION SHALE, ARGENTINA

Vertical fractures were analyzed within three horizontal wells VM-A, VM-B, and VM-C (aliases due to confidentiality) drilled in the Neuquén Basin, Argentina targeting the Vaca Muerta Formation shale. The Neuquén Basin is a highly prolific oil and gas basin located in the eastern foothills of the Andes in west-central Argentina (Vergani et al., 1995; Howell et al., 2005) (Figure 7-1). Present-day S_{Hmax} in the basin broadly trends E-W (Guzmán et al., 2007). The Late Jurassic-Early Cretaceous Vaca Muerta Formation micritic shale ranges from 30 to 1200 m in thickness and is the primary hydrocarbon source rock in the Neuquén Basin (Rodrigues et al., 2009). Image log fracture depths and orientation information along with reservoir mechanical property categories – mechanical zones – to are used study fracture spatial arrangement in the Vaca Muerta Formation shale.

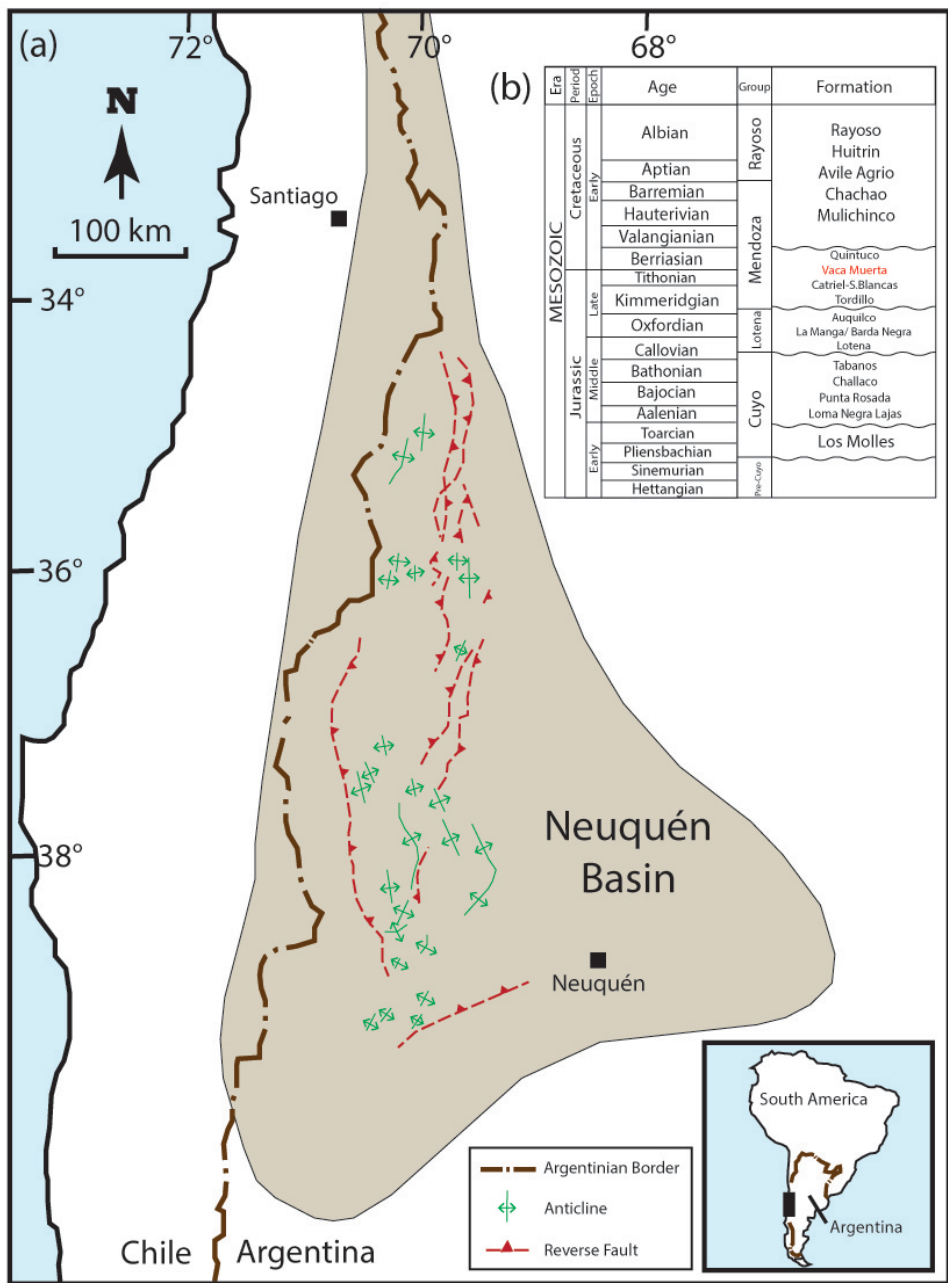


Figure 7-1 (a) Neuquén Basin location map with distribution of selected major compressional structures. Present-day S_{Hmax} trends approximately E-W. Modified from Howell et al. (2005) and Guzmán et al. (2007). (b) Generalized Early Jurassic to Early Cretaceous basinal stratigraphic column. Vaca Muerta Formation shale in red. Modified from Vergani et al. (1995).

At least two sets of vertical fractures are observed in selected Vaca Muerta Formation shale outcrops and cores. Optical microscopic examination of natural fractures captured in eight 3 in by 2 in petrographic thin-sections made from selected Vaca Muerta Formation shale cores confirms filling of fractures predominantly by anhedral calcite cements (Figure 7-2). Stylolites from dissolution are also observed. Fracture thin section and petrographic descriptions are provided in Appendix.

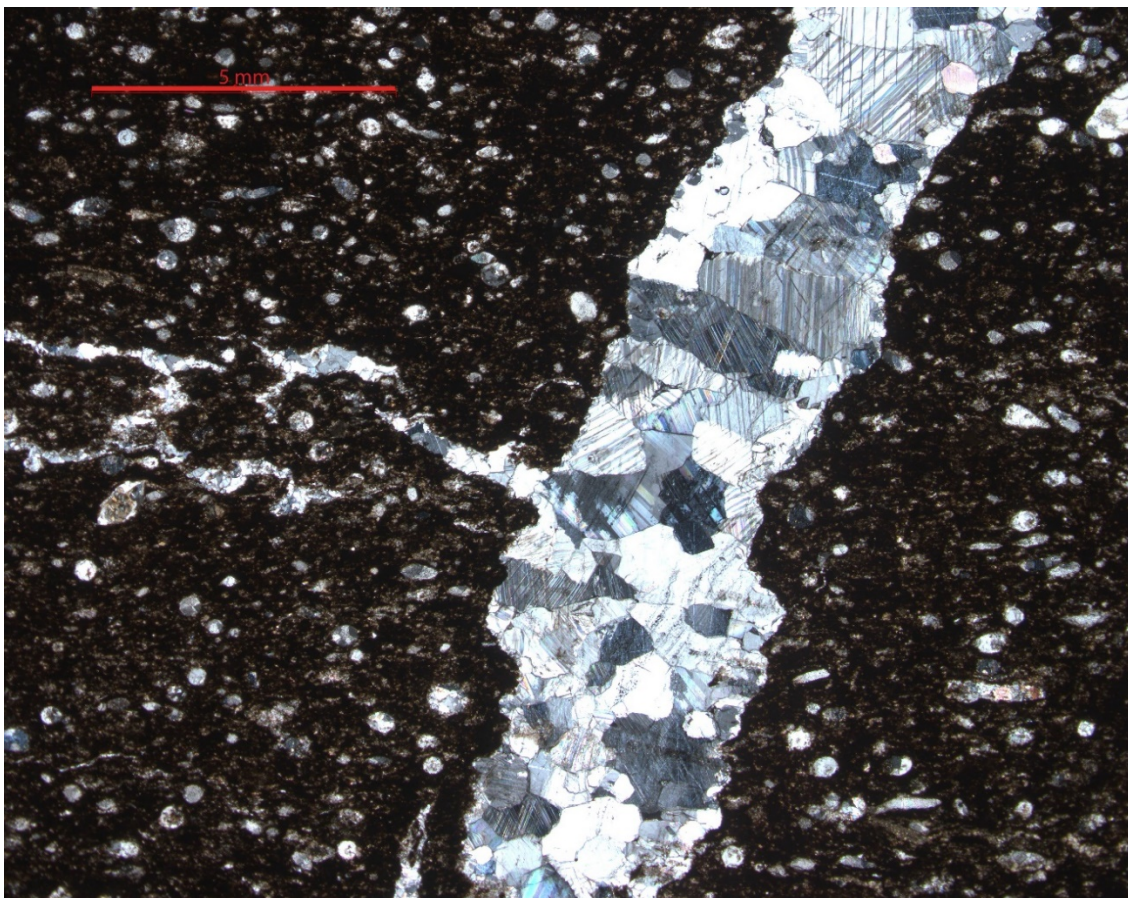


Figure 7-2 Subvertical opening-mode natural fracture in Vaca Muerta Formation shale petrographic thin section under optical microscope in crossed polar view. Wall-to-wall distance in figure averages approximately 3.5 mm. Fracture is filled by twinned anhedral calcite cements.

7.2 MIDDLE AND LATE DEVONIAN SHALES, CANADA

Vertical fractures were analyzed within horizontal wells HRB-1 and HRB-2 (aliases due to confidentiality) drilled in the Horn River Basin in northeastern British Columbia, Canada. Significant shale gas reservoirs present in the Horn River Basin include the Middle Devonian Evie, Otter Park and the Late Devonian Muskwa siliceous organic-rich black shales (e.g. Ross and Bustin, 2008; Reynolds and Munn, 2010; Dunphy and Campagna, 2011) (Figure 7-3). Present-day S_{Hmax} in the basin broadly trends NE-SW (Rogers et al., 2010). Two to three sets of natural fracture are present in outcrops and cores of the Horn River Basin shales depending on geographic location. Natural fractures in the Devonian shales are variably cemented by calcite, pyrite, and quartz (Ross and Bustin, 2008; Dunphy and Campagna, 2011). Fracture spacing data analyzed with NCC are from horizontal wellbore image logs of HRB-1 and HRB-2.

7.3 MARCELLUS FORMATION SHALE, USA

Vertical fractures were analyzed within the horizontal well Gulla 10H by Range Resources Corporation in SW Pennsylvania in the Appalachian Basin, eastern USA; the well targets the gas-rich Middle Devonian Marcellus Formation marine black shale (Ciezobka, 2013; Engelder et al., 2009) (Figure 7-4). Two cross-cutting sets of vertical-to-subvertical natural fractures, the ENE-striking J1 and the NW-striking J2 joint sets, are prevalent in Marcellus Formation shale outcrops; J1 is coincidentally along the direction of the present-day S_{Hmax} which trends NE-SW (Engelder et al., 2009). Petrographic examination of selected Marcellus Formation shale outcrop and core samples identify opening-mode natural fractures filled by crack-seal, fibrous, blocky, sub-euhedral, or amorphous calcite cements (Pommer, 2013). Stable isotope and fluid inclusion analyses of

Marcellus Formation shale fracture cements suggest fracture opening during Acadian or early Alleghenian burial (Pommer, 2013). Primary dataset used for NCC analysis is Marcellus Formation shale fracture information from the image log of Gulla 10H.

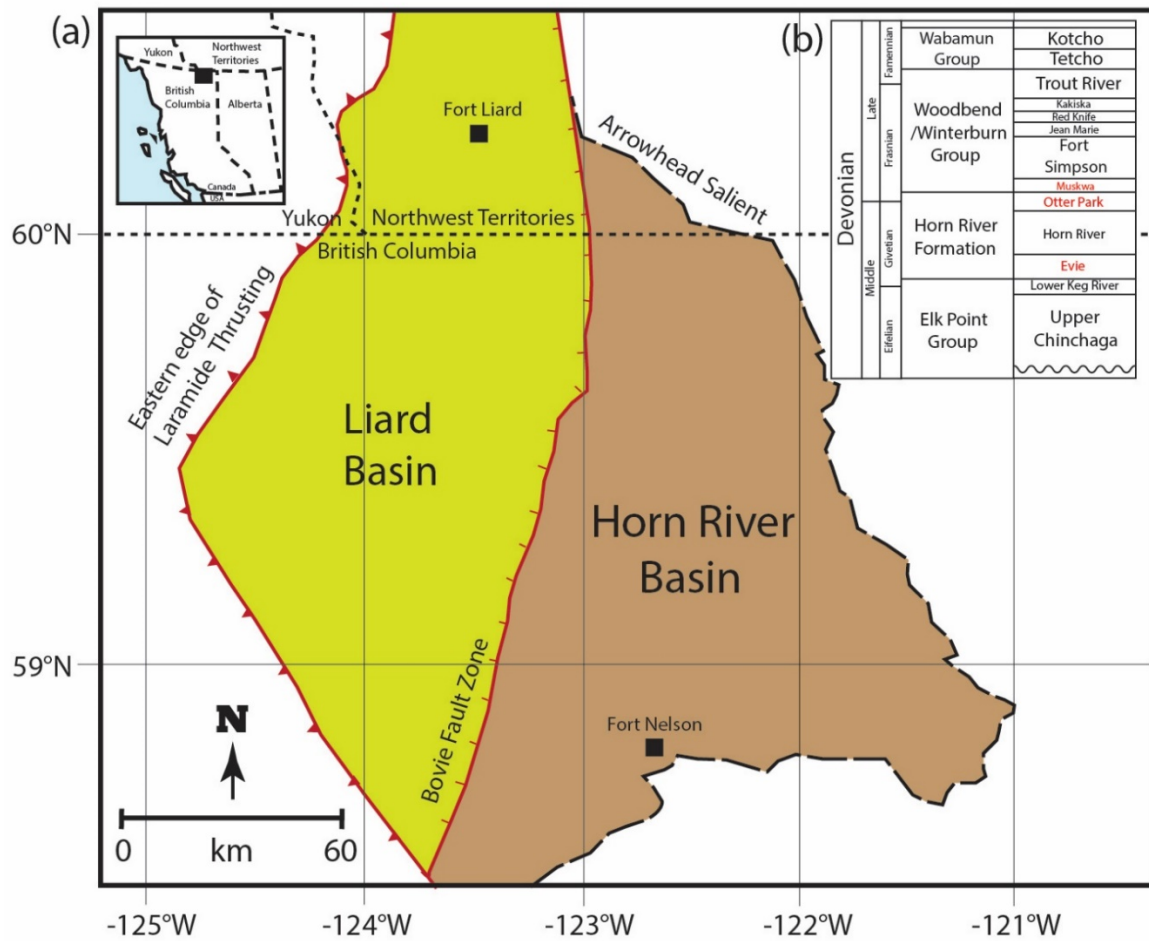


Figure 7-3 (a) Horn River Basin and the Liard Basin to its west, northeastern British Columbia, western Canada. The west-dipping Bovie normal fault zone divides the two basins. Modified from Wright et al. (1994), Ross and Bustin (2008), and Dunphy and Campagna (2011). (b) Generalized Middle to Late Devonian stratigraphic section of the Horn River Basin. Muskwa, Otter Park, and Evie Shales highlighted in red. Modified from Ross and Bustin (2008).

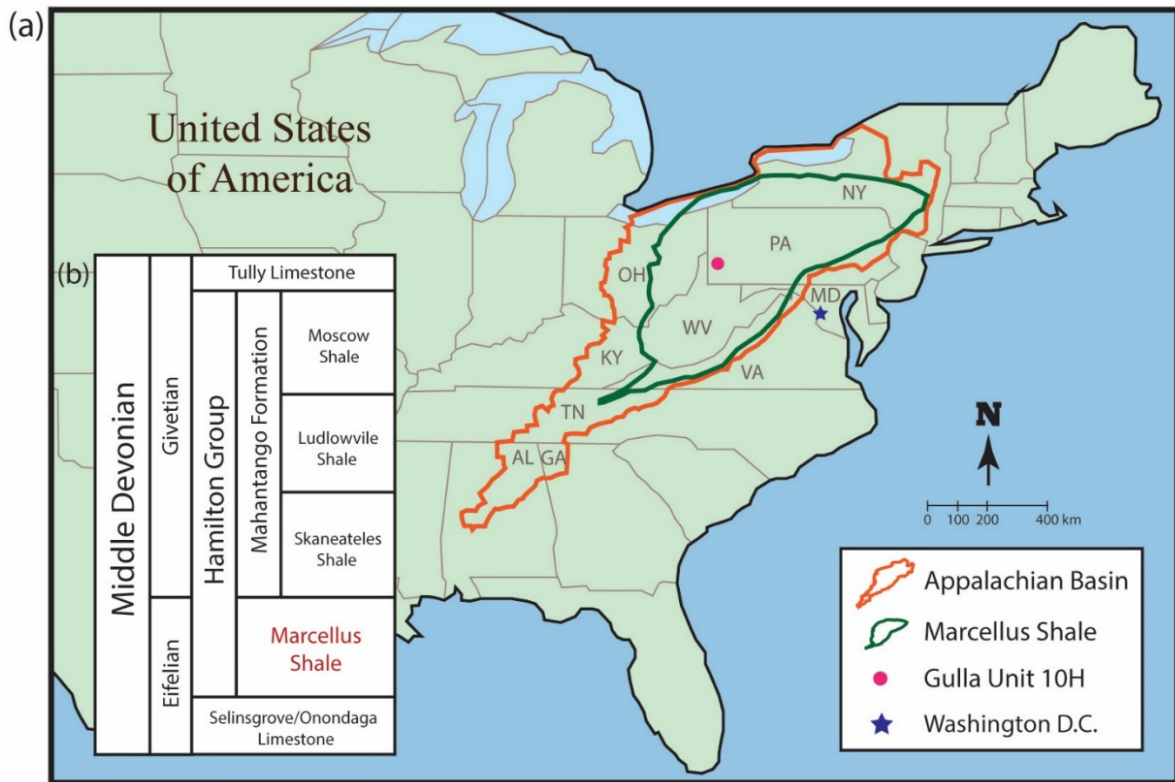


Figure 7-4 (a) Location of the Appalachian Basin and the surface and subsurface extent of the Marcellus Formation shale, eastern USA. Modified from USGS Marcellus Shale Assessment Team (2011) and Ciezobka (2013) (b) Generalized Middle Devonian stratigraphic section of Northern Central Appalachian Basin. Marcellus Formation shale highlighted in red. Modified from USGS Marcellus Shale Assessment Team (2011).

Chapter 8: Datasets and Methods for Shale Studies

Similar to the spatial arrangement analyses of fractures in the Frontier Formation tight gas sandstone presented in Section II, I use spacings of subsurface fracture sequences in shale reservoirs to analyze their spatial arrangement patterns. Horizontal cores are unavailable in the shale oil and gas wells of interests, and therefore focus is exclusive on analyzing horizontal image log data. Unlike the Frontier Formation fracture sequences derived from fracture trace measurements by hand using paper image logs, fracture sequences in the shale formations are based on operator-provided depth and orientation measurements directly from image log fracture traces picked originally using computer workstation. Quality control can be done when digital image logs are available for examination of the interpreted fractures such as in the case of the Vaca Muerta Formation shale. In the Horn River Basin wells, original image logs are unavailable for examination though the operator has provided additional information on fracture picking criteria and general observations of the image log fractures. For the shale reservoirs of interests, the pattern of fracture traces visible on the shale image logs as well as regional context (Gale et al., 2014) suggests that the features analyzed are predominantly near-vertical opening-mode fractures.

A given fracture sequences analyzed for spatial arrangement consists of fracture spacings calculated from image log fractures sorted and grouped by orientations and/or operator-classified feature types, e.g. conductive, resistive or “sealed”, or drilling-induced fractures; faults; bedding planes. A key methodological step is to identify discrete intervals of rock within each image log as a basis for parsing the fracture data. In other words, fracture populations along a long inclined wellbore are expected to vary depending on the

underlying mechanical property patterns of host shales, their mechanical stratigraphy (Laubach et al., 2009). Therefore fracture populations in each mechanically distinct interval should be analyzed separately. Provided in the case of the Vaca Muerta Formation shale, “mechanical zone” picks used to further parse fracture data are based on sonic logs and other operator-specific proprietary measurements, aimed at finding intervals of differing Young’s modulus, Poisson ratio and related factors (e.g., Bakulin et al., 2000; Rickman et al., 2008; Dunphy and Campagna, 2011). Mechanical zone picks are unavailable for the Horn River Basin’s Devonian shales though should be factor into consideration when interpreting fracture spatial arrangement and distribution along wellbores. The specific criteria for determining mechanical zones are outside the scope of this study. The major effect of changing such criteria would be to lengthen or shorten scanlines and increase or decrease fracture data included in my analysis.

I use the Normalized Correlation Count (NCC) technique and the associated CorrCount software (Marrett et al, 2017) to analyzed and quantify spatial arrangements among fractures in shale reservoirs. The principles of NCC analysis and the interpretation of CorrCount results are discussed previously in Section II. As in the case of analyzing fracture sequences in the Frontier Formation tight gas sandstone, apertures and heights of subsurface fractures in shale formations cannot be reliably or systematically obtained using image logs, nor are fracture aperture information available through associated cores. Therefore the NCC analyses of the shale fracture spacings use preset nominal aperture values as arbitrary placeholders similar to the Frontier tight gas sandstone fracture study. These aperture values are at least an order of magnitude smaller than the smallest fracture spacing in each sequence and thus have minimal influence on the NCC results.

Chapter 9: Results and Discussion: Neuquén Basin

9.1 INTENSITY AND SPATIAL ARRANGEMENT, NEUQUÉN BASIN

Fracture sets in horizontal wells VM-A, VM-B, VM-C are categorized using fracture orientations and their designated mechanical zones. Analytical results from CorrCount and Microsoft Excel include descriptive statistics, coefficients of correlation (Table 4), as well as normalized fracture intensity and correlation count plots (Figures 9-1 to 9-18). The Terzaghi correction has been applied to each fracture spacing dataset prior to correlation count analysis to adjust for fracture obliquity with respect to the wellbores approximately trend N-S. Since true fracture spacing is always less than or equal to the apparent spacing, the total scanline lengths calculated in the CorrCount application as the sum of the corrected spacings reflects distances less than the original interval along the wellbores.

Schlumberger provides OBMI image logs for Well VM-A and Well VM-B, while Baker Hughes provides for Well VM-C. Image log data quality may vary due to different service providers. Qualitatively, the images seem to be comparable, but the potential for differences arising from any contrasts in image log resolution could not be assessed.

9.1.1 Intensity and correlation count, Well VM-A

Natural fractures in the image log of Well VM-A are located between MD 2690 m and 4591 m. Fractures in the log are found in in three mechanical zones: Zone 2, 3, and 4. Zone 3 appears in the log both before and after Zone 4 due to the trajectory of the horizontal wellbore shifting in and out of Zone 4 during drilling (J.F.W. Gale, personal communication, 2016). Zone 3, where it reappears after Zone 4, is labeled “Zone 3-2” in this study (Table 4).

Well VM-A's image log contains a total of 514 natural fractures. Fractures that strike approximately WNW-ESE categorized as Set 1, and fractures that strike broadly ENE-WSW are as Set 2. Approximately 62% (319) of the fractures in Well VM-A are in Set 1. Fractures in each of Set 1 and 2 can be further divided into subsets by the mechanical zones they are found in. Here I present the fracture intensity and NCC results for the fracture sequences mostly with statistically meaningful plots. They include: Set 1 Zone 2, Set 1 Zone 4, Set 2 Zone 4, and Set 2 Zone 3-2. The sequences Set 1 All and Set 2 All that contain fractures in all mechanical zones are also analyzed and presented for reference.

Well	Fracture Set (strike)	Fracture Zone	# of fractures	Scanline length (m)	Mean spacing (m)	Standard deviation (m)	Min. spacing (m)	Max. spacing (m)	Cv	NCC figure #
VM-A		All	319	2031.29	6.35	31.35	0.085	411.83	4.94	9-2
	Set 1 (WNW-ESE)	2	30	514.68	16.60	58.93	0.094	326.46	3.55	9-4
		4	266	703.17	2.64	8.33	0.085	100.91	3.15	9-6
	Set 2 (ENE-WSW)	All	195	1673.76	8.54	23.49	0.057	213.52	2.75	9-8
		4	148	601.14	4.06	5.65	0.057	30.22	1.39	9-10
		3-2	30	507.06	16.36	34.96	0.368	129.73	2.14	9-12
VM-B	One set (ENE-WSW)	All	79	1394.27	17.43	38.91	0.028	216.78	2.23	9-14
		5	68	1071.77	15.76	37.60	0.028	216.78	2.38	9-16
VM-C	Mixed (~WNW-ESE)	Closed	77	1786.43	22.90	54.71	0.156	263.94	2.39	/
		Closed & in UVM	61	1344.83	21.69	52.27	0.156	263.94	2.41	9-18

Table 9-1 Statistical summaries of selected image log fracture sets in Well VM-A, VM-B, and VM-C. UVM = Upper Vaca Muerta.

Set 1 fractures, VM-A

Set 1 All has 319 fractures over a Terzaghi-corrected interval of 2031.29 m. The average fracture spacing is 6.35 m, and the Cv is 4.94. The normalized intensity plot (Figure 9-1) contains four statistically significant peaks above the upper 95% confidence limit at the positions of 550, 850, 1100, and 1400 m from the beginning of the interval. The broad central high intensity interval from 1000 to 1200 m is formed by at least three overlapped narrower intensity peaks. Intensity troughs are found between the large peaks. In the NCC plot (Figure 9-2), a broad, statistically significant correlation interval spans is present between the length scales of 0.15 m and 100 m. The curve dips to indistinguishable from random near 100 m. A broad correlation peak then reemerges centering at 300 m.

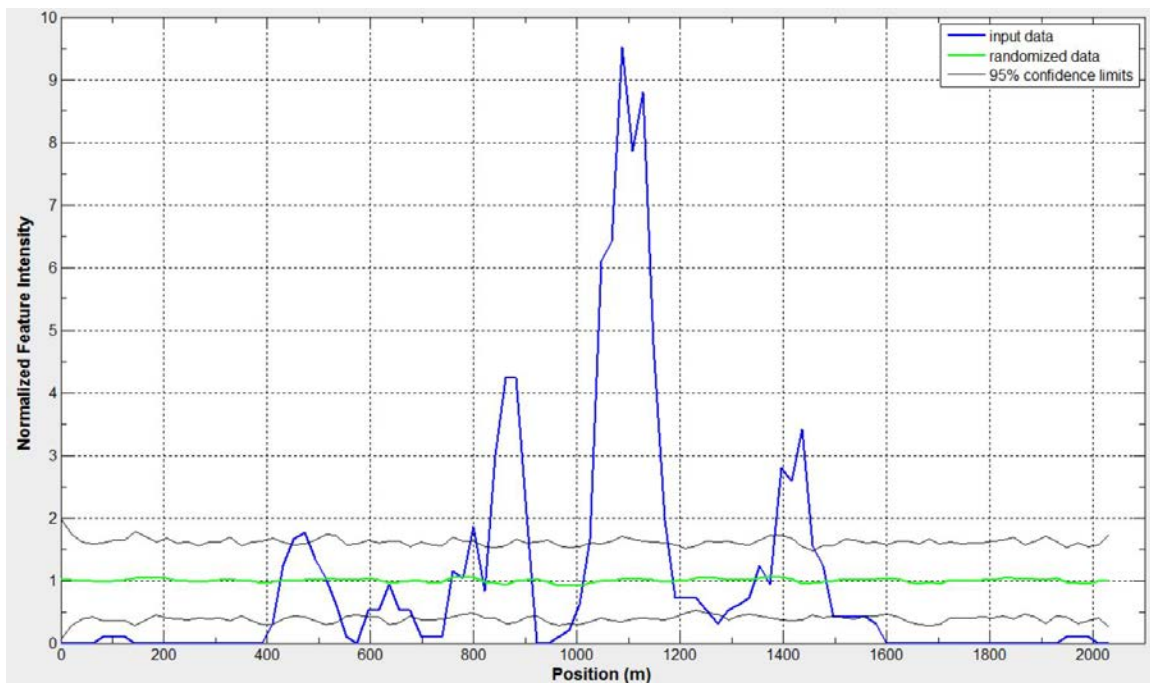


Figure 9-1 Intensity of all Set 1 natural fractures, Well VM-A

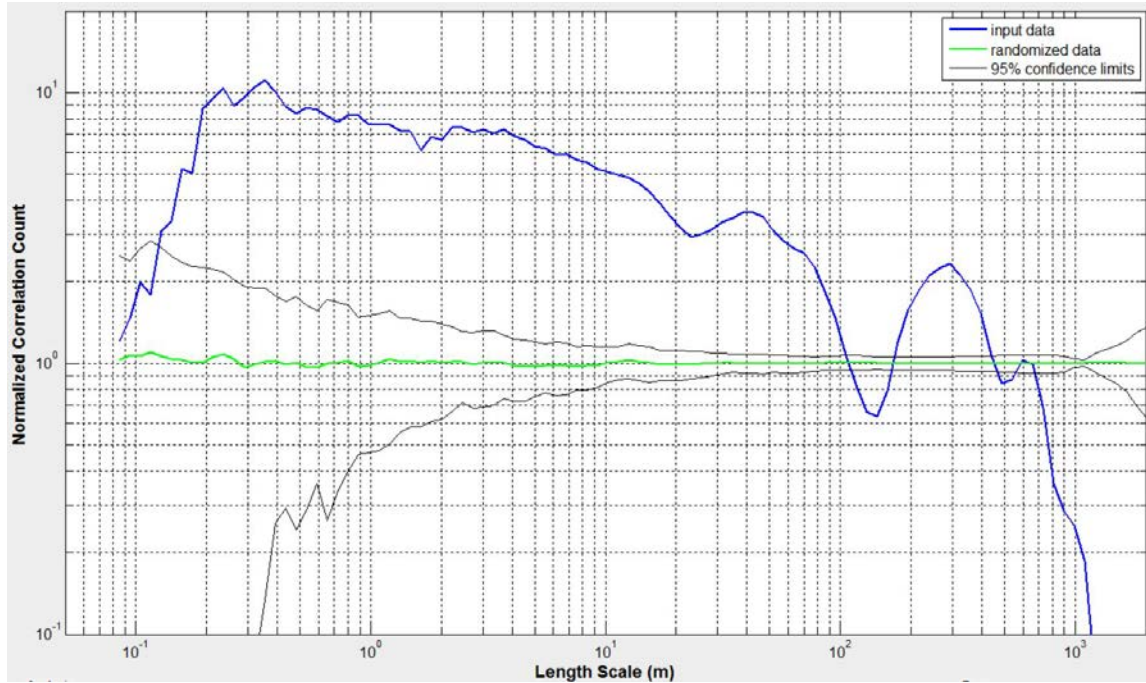


Figure 9-2 Correlation count of all Set 1 natural fractures, Well VM-A.

Set 1 Zone 2 contains 30 fractures over a Terzaghi-corrected interval of 514.68 m. The average fracture spacing is 16.60 m, and the C_v is 3.55. In the normalized intensity plot (Figure 9-3), three approximately periodically distributed intensity peaks with decreasing magnitudes are present at 340, 375, and 410 m. Another intensity peak also appears at the end of the interval. In the NCC plot (Figure 9-4), multiple statistically significant and consecutive correlation intervals are found before the 80 m length scale. The NCC curve intersects the randomized results at approximately 85 m.

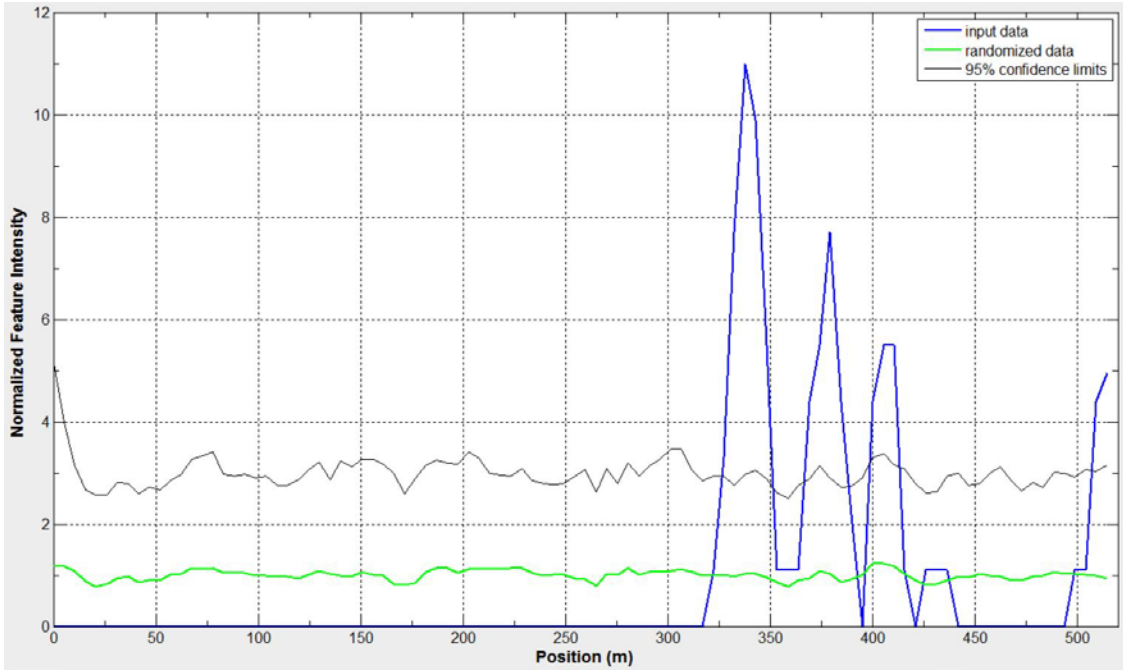


Figure 9-3 Intensity of Set 1 natural fractures in Zone 2, Well VM-A.

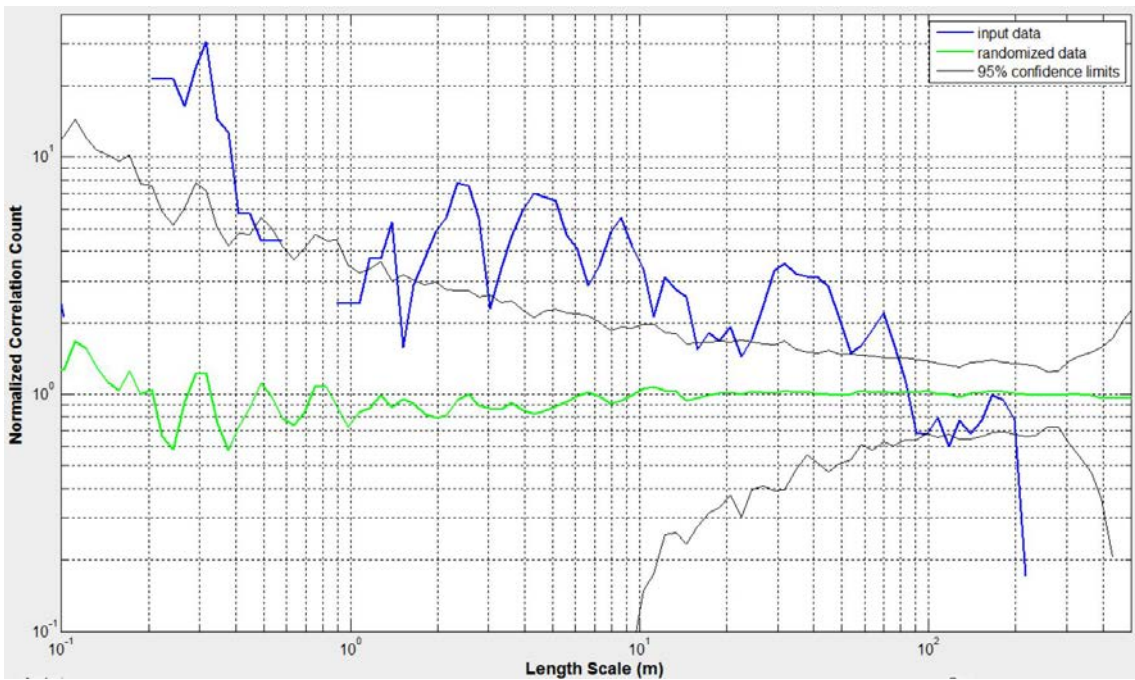


Figure 9-4 Correlation count of Set 1 natural fractures in Zone 2, Well VM-A.

Set 1 Zone 4 contains 266 fractures over a Terzaghi-corrected interval of 703.17 m. The average fracture spacing is 2.64 m, and the Cv is 3.15. In the normalized intensity plot (Figure 9-5), four peaks are found at 90 m, 280 m, 320 m, and 640 m, respectively. The two central peaks are approximately 50 m wide and may contain smaller overlapped peaks. Much of elsewhere along the intensity curve falls beneath the lower 95% confidence limit. The NCC plot of Set 1 Zone 4 fractures (Figure 9-6) resembles that of all Set 1 fractures. It similarly has a broad elevated section over smaller length scales before 80 m followed by a trough at 150 m and a significant peak at 300 m.

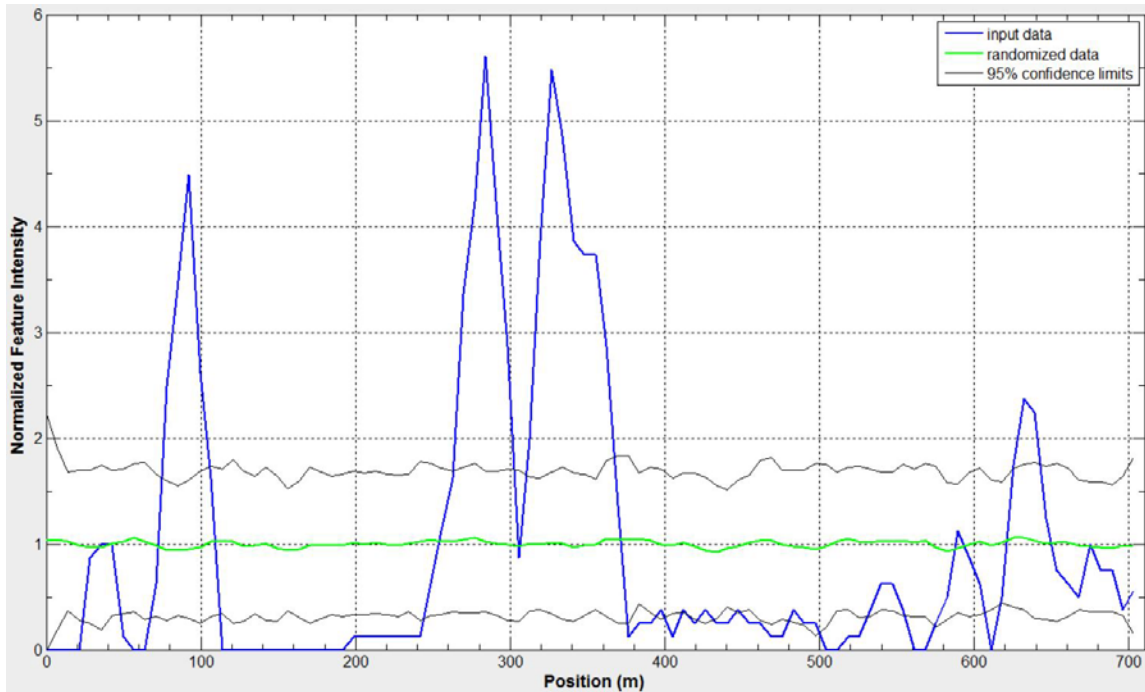


Figure 9-5 Intensity of Set 1 natural fractures in Zone 4, Well VM-A.

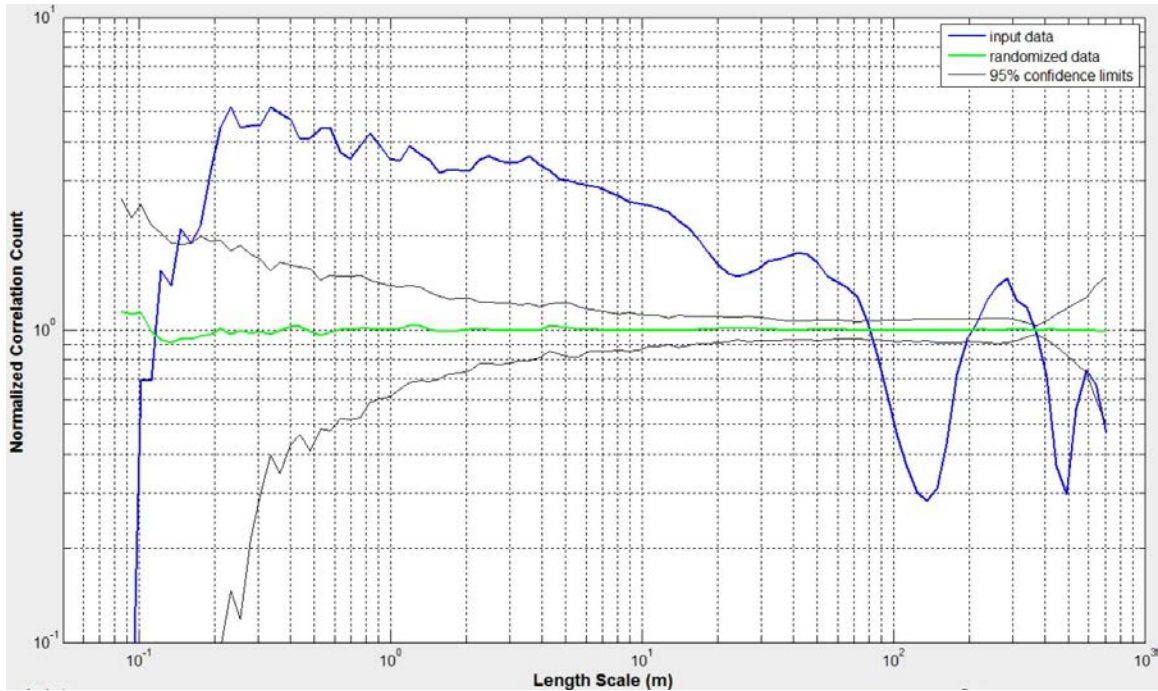


Figure 9-6 Correlation count of Set 1 natural fractures in Zone 4, Well VM-A.

Set 2 fractures, VM-A

Set 2 contains a total of 195 fractures over a Terzaghi-corrected interval of 1673.76 m. The average fracture spacing is 8.54 m, and the Cv is 2.75. In the normalized intensity plot (Figure 9-7), at least five intensity peaks concentrate in the middle third of the interval between 560 m and 1120 m. The NCC plot for all Set 2 fractures (Figure 9-8) remains above the upper 95% confidence limit for all length scales approximately less than 550 m and greater than 0.2 m. The trend of the curve roughly follows that of the upper confidence limit.

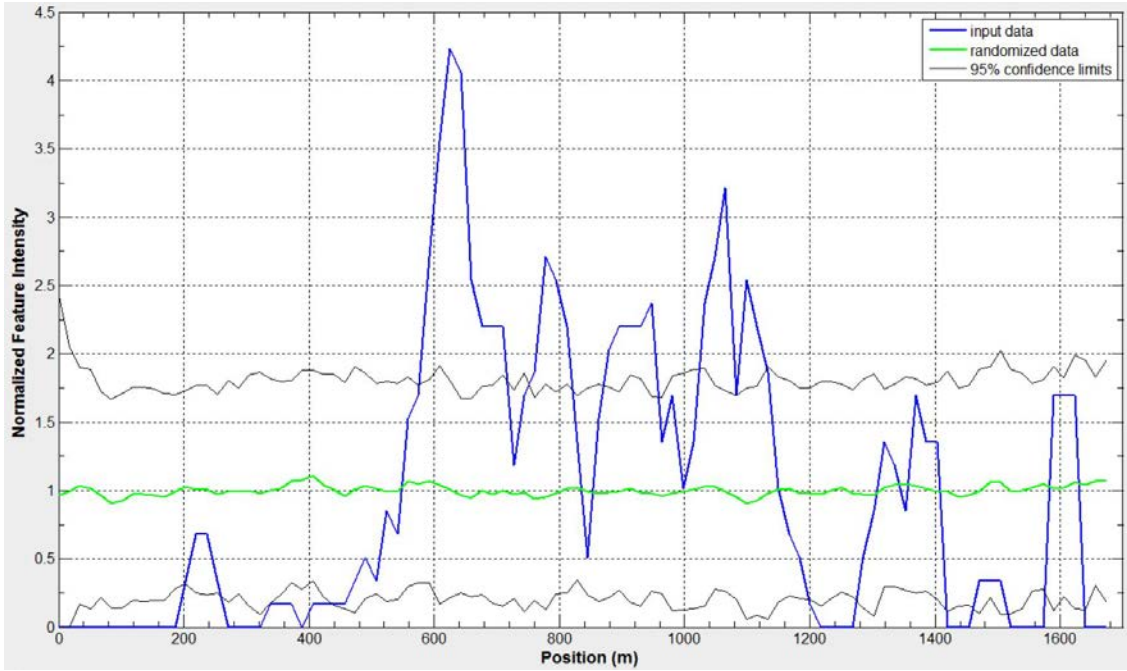


Figure 9-7 Intensity of all Set 2 natural fractures, Well VM-A.

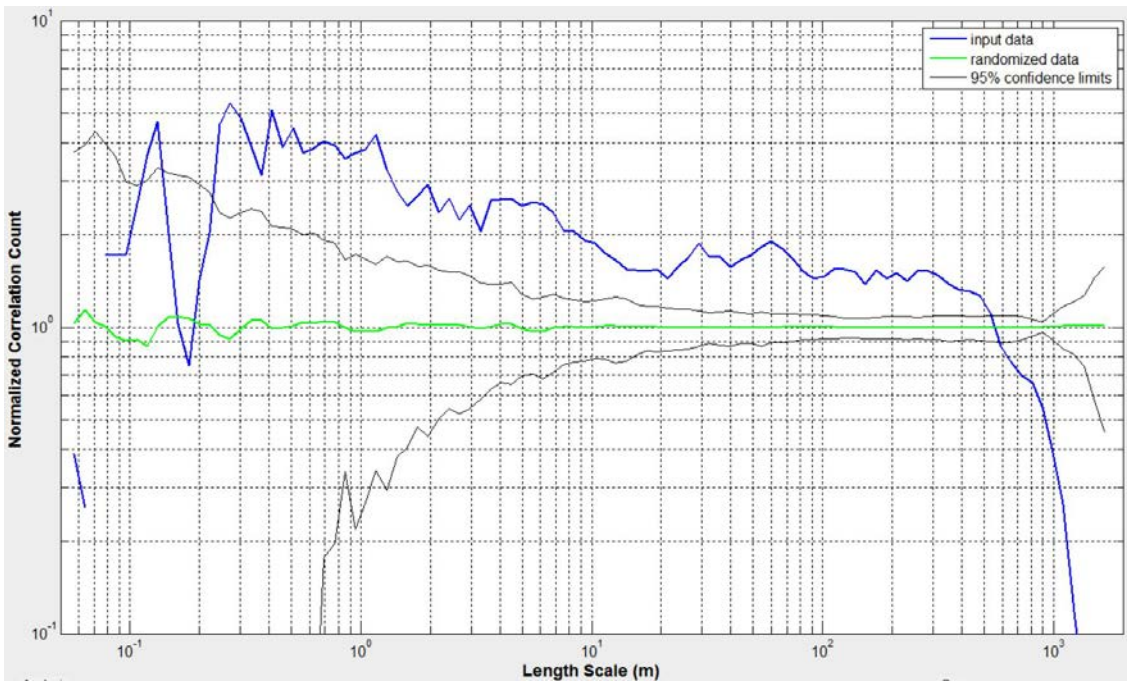


Figure 9-8 Correlation count of all Set 2 natural fractures, Well VM-A.

Set 2 Zone 4 contains 148 fractures over a Terzaghi-corrected interval of 601.14 m. The average fracture spacing is 4.06 m, and the Cv is 1.39. Two major normalized intensity peaks are present at positions 80 and 480, respectively (Figure 9-9). Each is about 20 m wide. A very minor peak is found at about 240 m. The NCC plot (Figure 9-10) is mostly bounded between the upper and the lower confidence limits for larger length scales. Small length scales up to 2 m exhibit multiple correlation peaks, however.

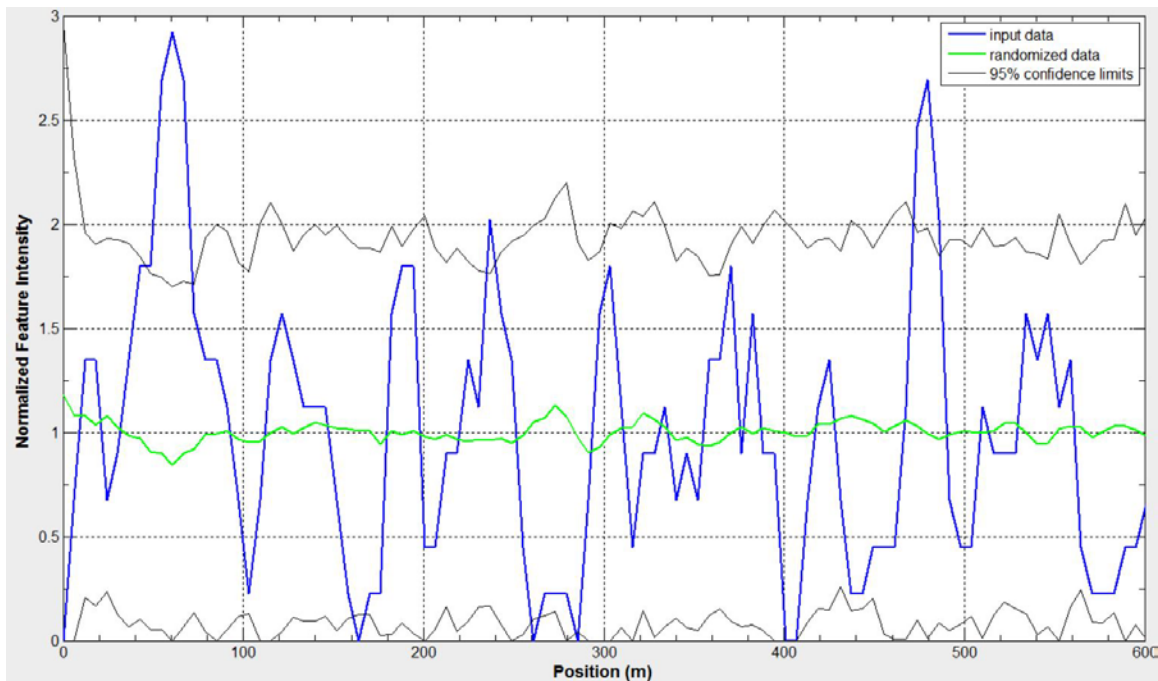


Figure 9-9 Intensity of Set 2 natural fractures in Zone 4, Well VM-A.

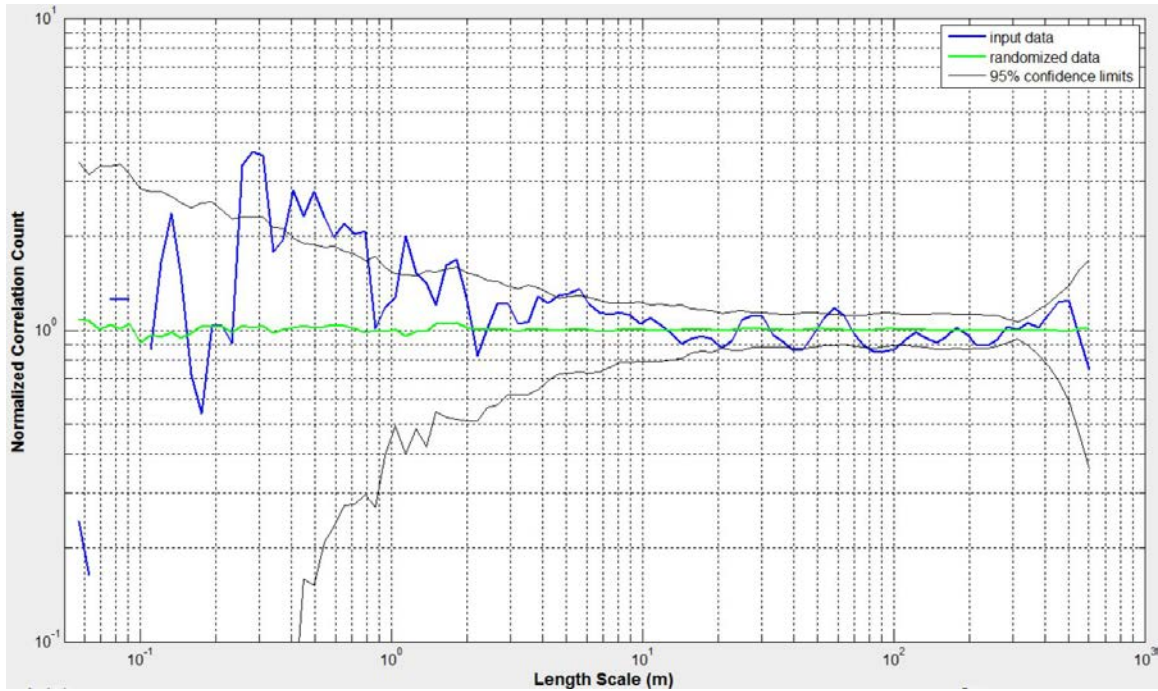


Figure 9-10 Correlation count of Set 2 natural fractures in Zone 4, Well VM-A.

Set 2 Zone 3-2 contains 30 fractures over a Terzaghi-corrected interval of 507.06 m. The average fracture spacing is 16.36 m, and the Cv is 2.1377. The normalized intensity curve (Figure 9-11) contains four statistically significant peaks. The first three of which are almost periodically distributed at 135, 170, and 210 m. The last is at 425 m close to the end of the interval. All peaks are about 40 m wide. In the NCC plot (Figure 9-12), the correlation curve is statistically significant for length scales less than 9 m. The curve also peaks at 40 m and at about 220 m. Note that the curve is incomplete at length scales approximately between 11 m and 25 m.

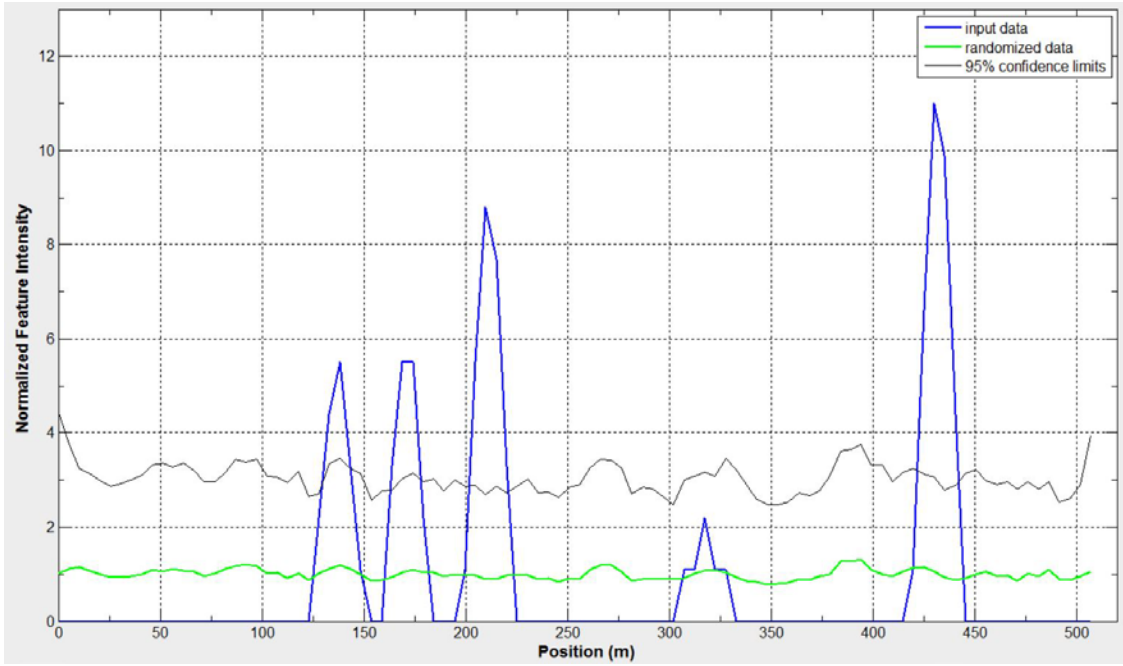


Figure 9-11 Intensity of Set 2 natural fractures in Zone 3-2, Well VM-A.

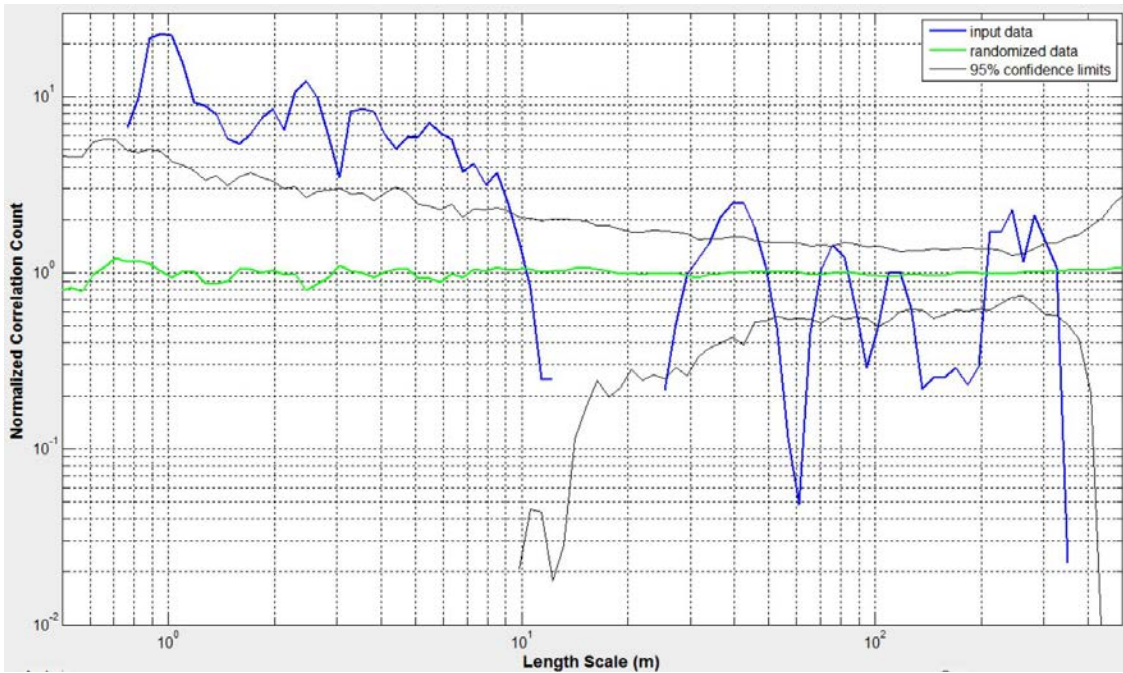


Figure 9-12 Correlation count of Set 2 natural fractures in Zone 3-2, Well VM-A.

9.1.2 Intensity and correlation count, Well VM-B

In Well VM-B, 79 image log natural fractures are recorded between MD 3072 and 4507 m within deepening mechanical zones 2, 3, 4, and 5. Unlike in Well VM-A, all the image log fractures are in one set striking ENE-WSW. Here I present results for all the fractures as well as for those exclusively in Zone 5 which contains about 86% of all the Well VM-B image log fractures.

A total of 79 image log natural fractures in Well VM-B are present over a Terzaghi-adjusted interval of 1394.27 m. The average fracture spacing is 17.43 m, and the C_v is 2.23. The normalized fracture intensity plot (Figure 9-13) contains high intensity peaks concentrating in the last 400 m of the interval. Two of the peaks at 1000 and 1080 m respectively, each 30 to 40 m wide, are followed by three overlapped narrow peaks between positions 1160 and 1240 m. The highest intensity interval is between positions 1300 and 1360 m. The NCC plot (Figure 9-14) is almost entirely statistically between length scales 1 and 200 m though the magnitude of correlation varies throughout.

Zone 5 in Well VM-B contains 68 fractures over a Terzaghi-adjusted interval of 1071.77 m. The average fracture spacing is 15.76 m, and the C_v is 2.38. The normalized fracture intensity plot (Figure 9-15) reveals the high intensity peaks that resemble those found in the last 400 m segment of the scanline for all fractures in Well VM-B. The shape of the NCC curve (Figure 9-16) is also similar to that for all the Well VM-B image log fractures.

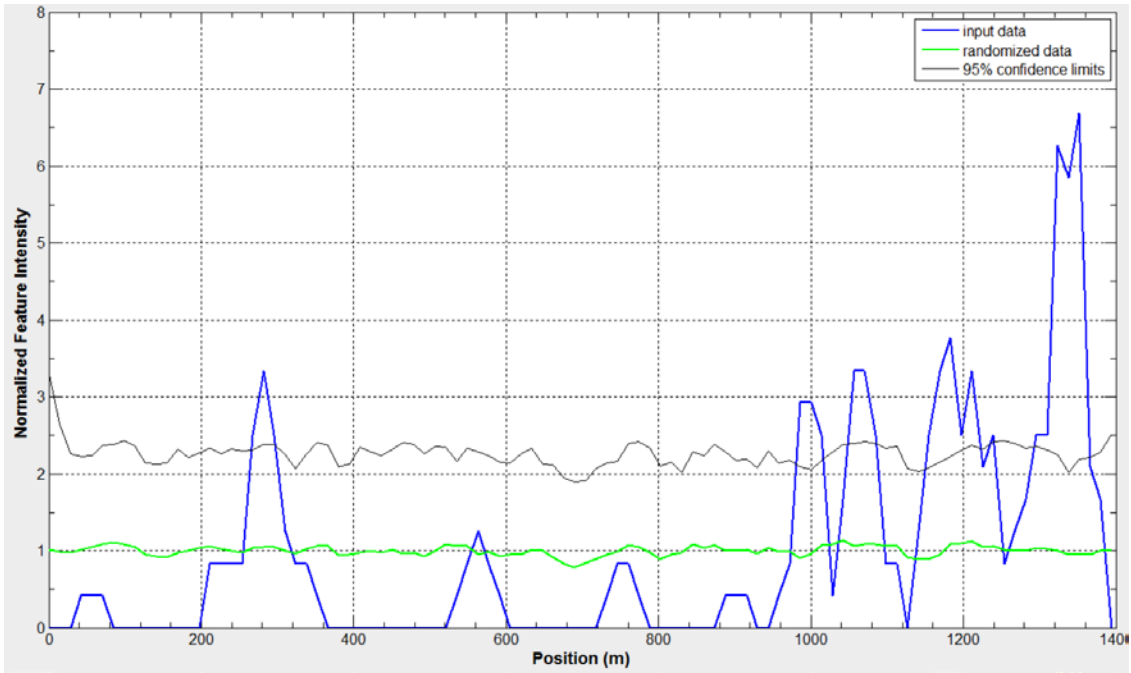


Figure 9-13 Intensity of all image log natural fractures, Well VM-B.

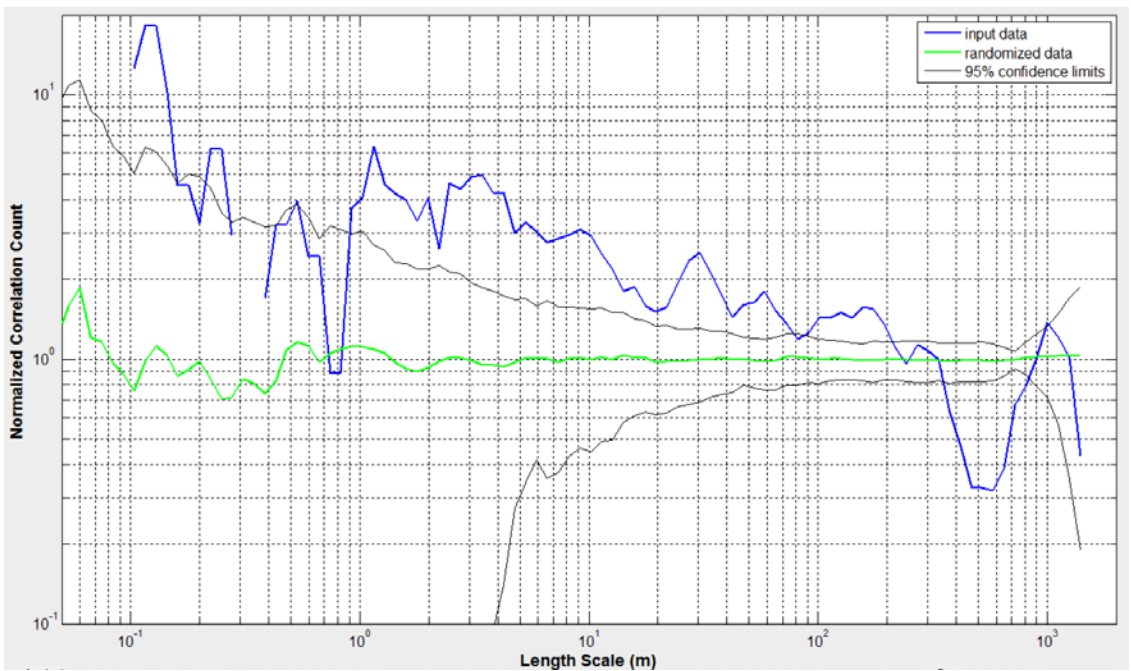


Figure 9-14 Correlation count of all image log natural fractures, Well VM-B.

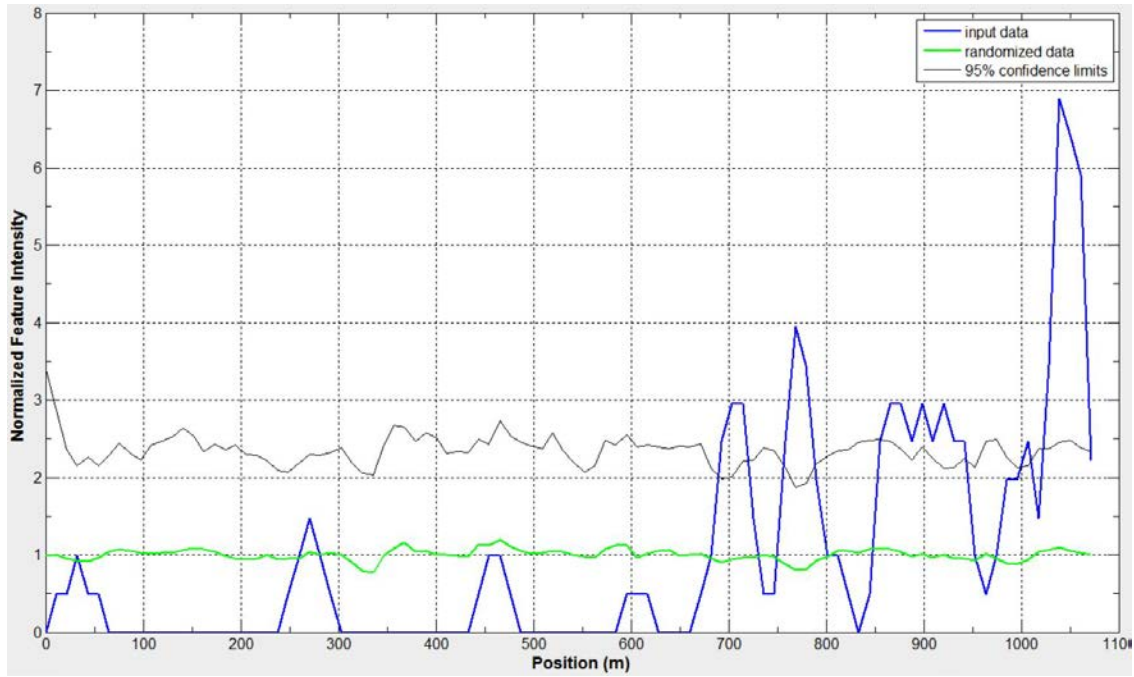


Figure 9-15 Intensity of natural fractures in Zone 5, Well VM-B.

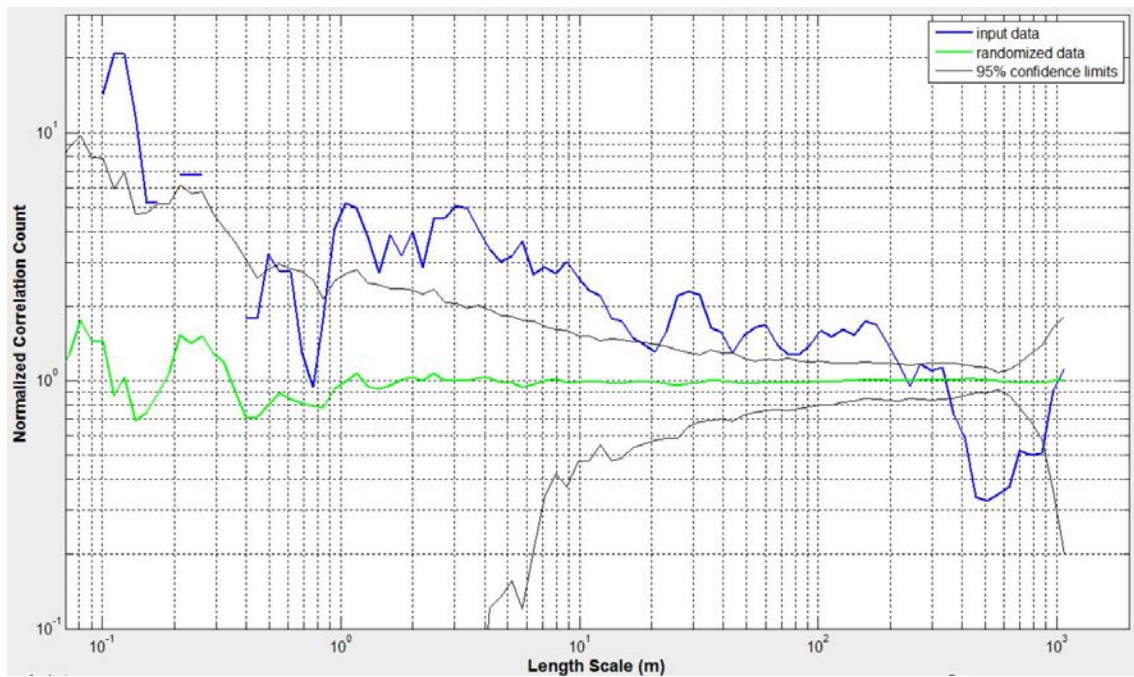


Figure 9-16 Correlation count of natural fractures in Zone 5, Well VM-B.

9.1.3 Intensity and correlation count, Well VM-C

A total of 103 natural fractures are present in the image log of Well VM-C. The measured depths of the first and the last image log fractures are 2255 and 4389 m, respectively. Among all image log natural fractures, 26 are picked as open and the other 77 are as closed. The more abundant closed fractures have varying strikes with the majority striking broadly WNW-ESE. Natural image log fractures in VM-C are further classified by the geological formation such as the Quintuco formation that overlies the Vaca Muerta Formation (Rodrigues et al., 2009) and the upper member of the Vaca Muerta Formation (e.g. Garcia et al., 2013) (Upper Vaca Muerta hereinafter) where the fractures are located. In the image log are also seven drilling induced fractures striking E-W and 116 wellbore breakouts striking N-S.

I present the NCC result for the 61 closed fractures in the Upper Vaca Muerta, the only geologically meaningful image log fracture sequence in Well VM-C that contains sufficient fractures for complete NCC evaluation. This fracture sequence present over a Terzaghi-corrected interval of 1344.83 m has an average fracture spacing of 21.69 m and a C_v of 2.41. In the normalized fracture intensity plot, two major intensity peaks, each about 70 m wide, are present in first 200 m of the scanline (Figure 9-17). Two minor peaks follow at 240 and 330 m. The remaining of the intensity interval is indistinguishable from random. The NCC plot (Figure 9-18) contains a negatively sloped elevated correlation interval for length scales less than approximately 35 m. It is followed by a double hump peaking at 60 and 90 m. Statistically significant troughs appear at 150, 250, and 500 m.

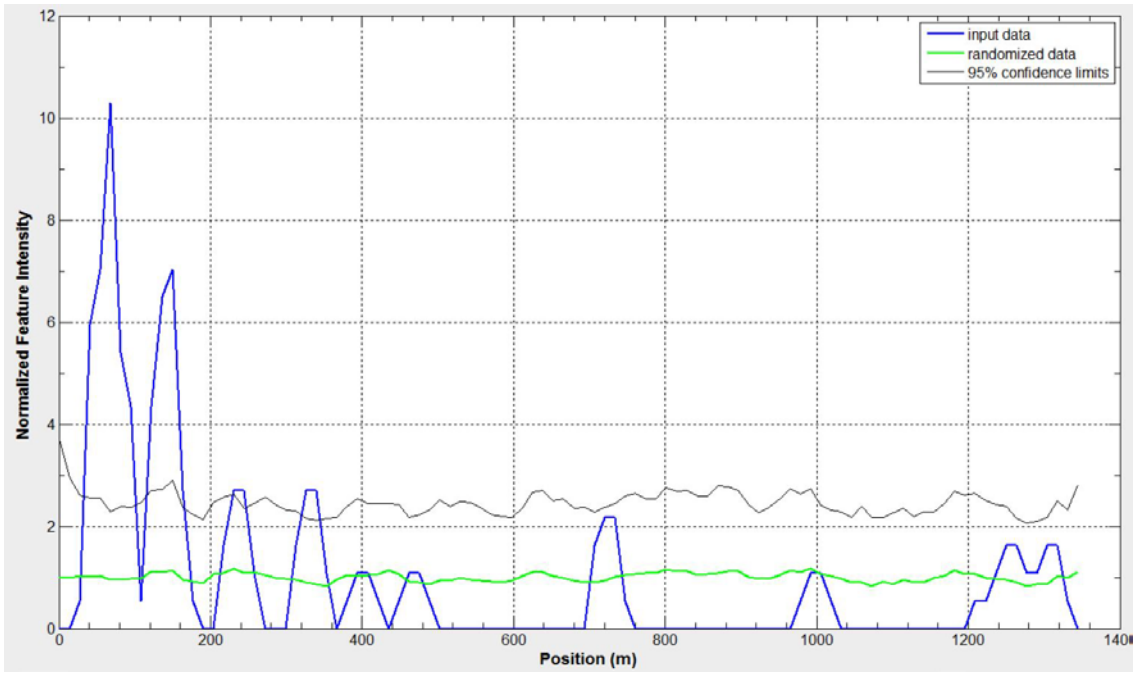


Figure 9-17 Intensity of Upper Vaca Muerta closed fractures, Well VM-C.

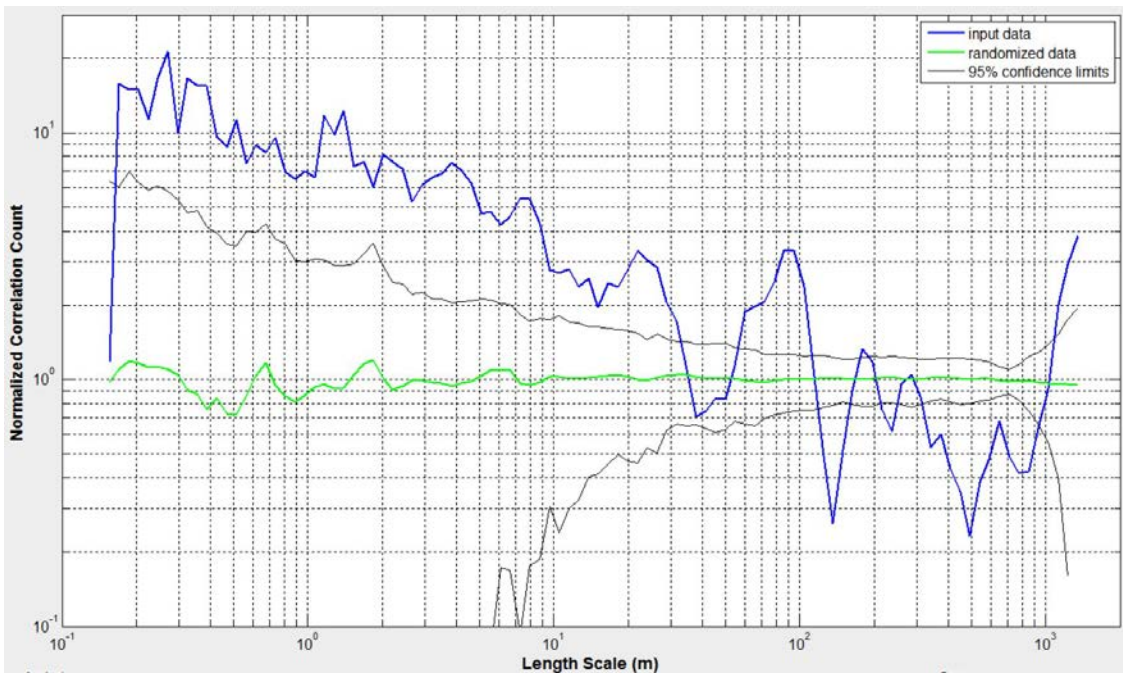


Figure 9-18 Correlation count of Upper Vaca Muerta closed fractures, Well VM-C.

9.2 INTERPRETATION AND DISCUSSION, NEUQUÉN BASIN

Interpretation of the NCC results for Vaca Muerta Formation shale fracture focuses on those within geologically meaningful sequences such that they represent fractures within the same strike set that are located in a single mechanical zone (and formation member). The NCC results for sequences Set 1 Zone 2 and Set 2 Zone 3-2 in Well VM-A, though are included in earlier results for completeness, do not reflect the true spatial arrangement of the fracture sequence due to few fractures available for complete NCC characterization and are not included for interpretation.

9.2.1 Interpretation: Well VM-A

Preliminary observation of the fracture intensity plot for the sequence Set 1 Zone containing 266 fractures suggests that fractures clusters are present throughout the scanline interval (Figure 9-5). The NCC pattern shows that the curve crosses the line corresponding to the spatial correlation value of 1 at the length scale of 80 m, which indicates the width of the largest fracture cluster present in the sequence (Figure 9-6). The peak at approximately 290 m indicates the value of the regular spacing between individual large clusters. Both attributes are broadly consistent with the widths of the corresponding fracture intensity peaks and the spacings between them. The consistently negative slope of the elevated NCC interval before length scale corresponding the largest cluster width suggest that the internal organization of the largest clusters is likely fractal.

Approximately 76% (148) of the Set 2 image log fracture in Well VM-A are in Zone 4, which is in line with the high percentage of fractures present in Set 1 Zone 4 (Table 4). The fracture intensity curve for the sequence of Set 2 Zone 4, largely bound within the upper and lower confidence limits, show fewer peaks and troughs relative to their Set 1

counterparts (Figure 9-9). Similarly, the corresponding NCC curve is largely bounded within the central 95% confidence interval for most length scales above 2 m. The spatial arrangement of fractures in this sequence is therefore best interpreted as statistically indistinguishable from random.

Though as the second most numerous fracture sequences in each of Set 1 and Set 2, fractures present in Zone 2 and Zone 3-2 are too few for their respective NCC results to be statistically meaningful.

9.2.2 Interpretation: Well VM-B

For the one set of ENE-striking fractures in Zone 5 of Well VM-B, the NCC pattern suggests that all fractures in Zone 5 may be considered part of a large cluster that is as wide as 350 m which is determined from the length scale where the NCC curve crosses the spatial correlation value of one (Figure 9-14). The broadly negative slope for the NCC curve segment before the length scale of 20 m indicates the presence of internally fractal clusters within the overarching cluster, and 20 m may be the width of such clusters. The interpretation of the 350-m-wide cluster is broadly consistent with width of the intensity interval bounding the four largest intensity peaks near the end of the scanline (Figure 9-13), and that the 20 m width for potentially fractal clusters is consistent with the widths of the peaks inside the interval. The rise in spatial correlation near the length scale of 1000 m is from matching fractures within the small intensity peak at position 280 and fractures found near the end (Figure 9-13).

9.2.3 Interpretation: Well VM-C

In Well VM-C, the NCC pattern for the closed fractures in the Upper Vaca Muerta suggests that the fractures are arranged in regularly spaced fractal clusters that are up to 35

m in width with a common inter-cluster spacing of 90 m (Figure 9-18). The small statistically significant correlation signal at 180 m likely is a harmonic of the dominant 90 m spacing. The interpretation of fracture cluster distribution is broadly consistent with the separation and dimension of the major intensity peaks in the associate plot (Figure 9-17).

9.2.4 Discussion: Neuquén Basin wells

The observation of the Cv's of the Set 1 fracture sequences versus the Cv's of the Set 2 sequences (Table 4) suggests that Set 1 fractures in each mechanical zone are statistically more clustered than the Set 2 fractures within the same zone. Interpretation of the respective NCC results for Set 1 and Set 2 fractures in Mechanical Zone 4 of Well VM-A suggests drastically different fracture spatial arrangements: whereas the WNW-striking Set 1 fractures are concentrated in fractal clusters, no statistically significant cluster is formed by the ENE-striking Set 2 fractures (Table 5).

Well	Fracture Set	Zone	NCC Interpretation	Cluster Width (m)	Cluster Spacing (m)
VM-A	Set 1 (WNW-ESE)	4	Regularly spaced fractal clusters	80	290
	Set 2 (ENE-WSW)	4	Indistinguishable from random	n/a	n/a
VM-B	One set (ENE-WSW)	5	Clustered individuals (+ fractal clusters)	350 (20)	One big cluster
VM-C	Mixed (~ WNW-ESE)	Closed & in UVM	Regularly spaced fractal clusters	3.5	9

Table 9-2 Summary of NCC interpretation for selected fracture sequences in Vaca Muerta image logs. Numbers within parentheses indicates attributes of internal clusters. UVM = Upper Vaca Muerta.

For Well VM-A, the association wellbore mechanical stratigraphy from the operator suggests that Mechanical Zone 4 correlates with a carbonate bed beneath the targeted black shale. The horizontal wellbore of VM-A briefly deviated into this underlying limestone layer during drilling before subsequently returning to the shale above (personal communication, 2015), leading to Mechanical Zone 3 representing the black shale interval to appear both before and after the Zone 4 carbonate layer along the wellbore. The information on the wellbore trajectory of VM-A explains the reemergence of Mechanical Zone 3 behind Zone 4 that may otherwise be interpreted as due to lateral reservoir heterogeneity. It also allows for the interpretation of the origin behind the inferred fracture cluster exclusive to central scanline interval of VM-A (Figures 9-1 and 9-5). As discussed previously, a correlation exists between rock mechanical properties and fracture cluster styles and attributes (e.g. Laubach et al., 2009). In the case of Set 1 natural fractures, the mechanical contrast-driven preferred fracture clustering in VM-A is suggested through both the greater number of fracture clusters and the degree of statistically significant non-random clustering within the fracture-prone carbonate of Zone 4 relative to conditions in the black shale of Zone 3, as indicated by the NCC results. For Well VM-C, the NCC results suggest that statistically significant, regularly spaced fractal clusters of closed natural fracture are present near the top of the Upper Vaca Muerta, the stratigraphically upper-most member of the Vaca Muerta Formation that represents a carbonate platform (Garcia et al., 2013). The style of clustering among the analyzed broadly WNW-striking fractures in the carbonate-rich Upper Vaca Muerta are in line with the presence similarly orientated fracture clusters inferred in the carbonate layer of Well VM-A, though fracture cluster dimensions and spacings differ likely due to differing subsurface conditions.

Chapter 10: Results and Discussion: Horn River Basin

10.1 INTENSITY AND SPATIAL ARRANGEMENT, HORN RIVER BASIN

For spacing datasets of Well HRB-1 and HRB-2 categorized by fracture types and orientations, I present analytical results include descriptive statistics, Cv's, as well as statistically meaningful normalized intensity and NCC plots from sufficient spacing input. The Terzaghi correction is not applied to datasets from Well HRB-1 or Well HRB-2 at the time of spacing collection. Fracture spacings or length scale values discussed in the results represent differences between the raw measured depths of two fractures in the image logs. In other words, the patterns are valid but the absolute values need correction for obliquity.

10.1.1 Intensity and correlation count, Well HRB-1

In Well HRB-1, a total of 6124 image log fractures are categorized as conductive, resistive, drilling induced, or as faults. The fractures can be subcategorized by their orientations: Set 1 for NE-striking fractures and Set 2 for NW-striking. In addition, the operator has pre-classified each image log fracture as continuous, discontinuous (fractures not conductive/resistive throughout its trace), or bed-bound (fracture terminating against a bedding plane). Spacings, descriptive statistics, and the coefficients of variation are calculated for the fracture sequences categorized by the scheme above (Table 6). Figure 10-2 to Figure 10-34 show the normalized fracture intensity and the correlation count results for selected image fracture sequences in Well HRB-1. The scanline lengths of each fracture sequence, without the Terzaghi correction, represent true measured distances along the wellbore. The true vertical depths (TVD) of the image log's interval is plotted against the associated measure depths (MD) for horizontal wellbore trajectory approximation and for reference of fracture intensity peak positions (Figure 10-1c).

Well	Fracture type	Set (average strike)	# of fractures	Scanline length (m)	Mean spacing (m)	Standard deviation (m)	Min. spacing (m)	Max. spacing (m)	Cv	NCC figure #
HRB-1	Conductive	Continuous (NE-SW)	965	1104.64	1.14	3.05	0.015	61.48	2.68	10-3
		Discontinuous (NE-SW)	3052	1112.04	0.36	0.57	0.015	8.78	1.59	10-7
		Bed-bound (NE-SW)	113	919.44	8.13	22.44	0.028	105.34	2.76	10-9
		All (NE-SW)	4130	1112.10	0.27	0.42	0.013	8.76	1.56	10-11
	Resistive	All (Mixed)	1188	1109.47	0.93	1.52	0.005	19.72	1.63	10-14
		Set 1 (NE-SW)	872	1100.61	1.26	2.26	0.010	19.72	1.80	10-16
		Set 2 (NW-SE)	497	990.07	1.99	4.21	0.015	39.72	2.12	10-18
		Continuous Set 2 (NW-SE)	293	988.25	3.38	7.11	0.015	68.11	2.10	10-21
		Discontinuous (~ NW-SE)	95	899.82	9.47	15.51	0.071	95.21	1.64	10-23
		Bed-bound (NW-SE)	133	915.00	6.88	12.61	0.048	59.59	1.83	10-25
		Natural (Conductive w/ Healed)	All Set 1 (NE-SW)	5002	1105.82	0.22	0.31	<0.001	8.78	1.39
	Drilling-induced	Single set (NE-SW)	556	1096.06	1.97	7.70	0.023	81.34	3.91	10-27
		w/ conductive continuous (NE-SW)	1521	1099.42	0.72	2.00	0.015	52.23	2.77	10-30
	Fault	Single set (~ NE-SW)	22	952.41	43.29	64.75	0.310	241.48	1.50	10-34

Table 10-1 Statistical summaries on image log fracture sets in Horn River Basin Well HRB-1. Fracture sets in red contain NCC results for select internal high intensity interval(s) and are presented in Figures 10-64 to 10-67 for cross-well comparison.

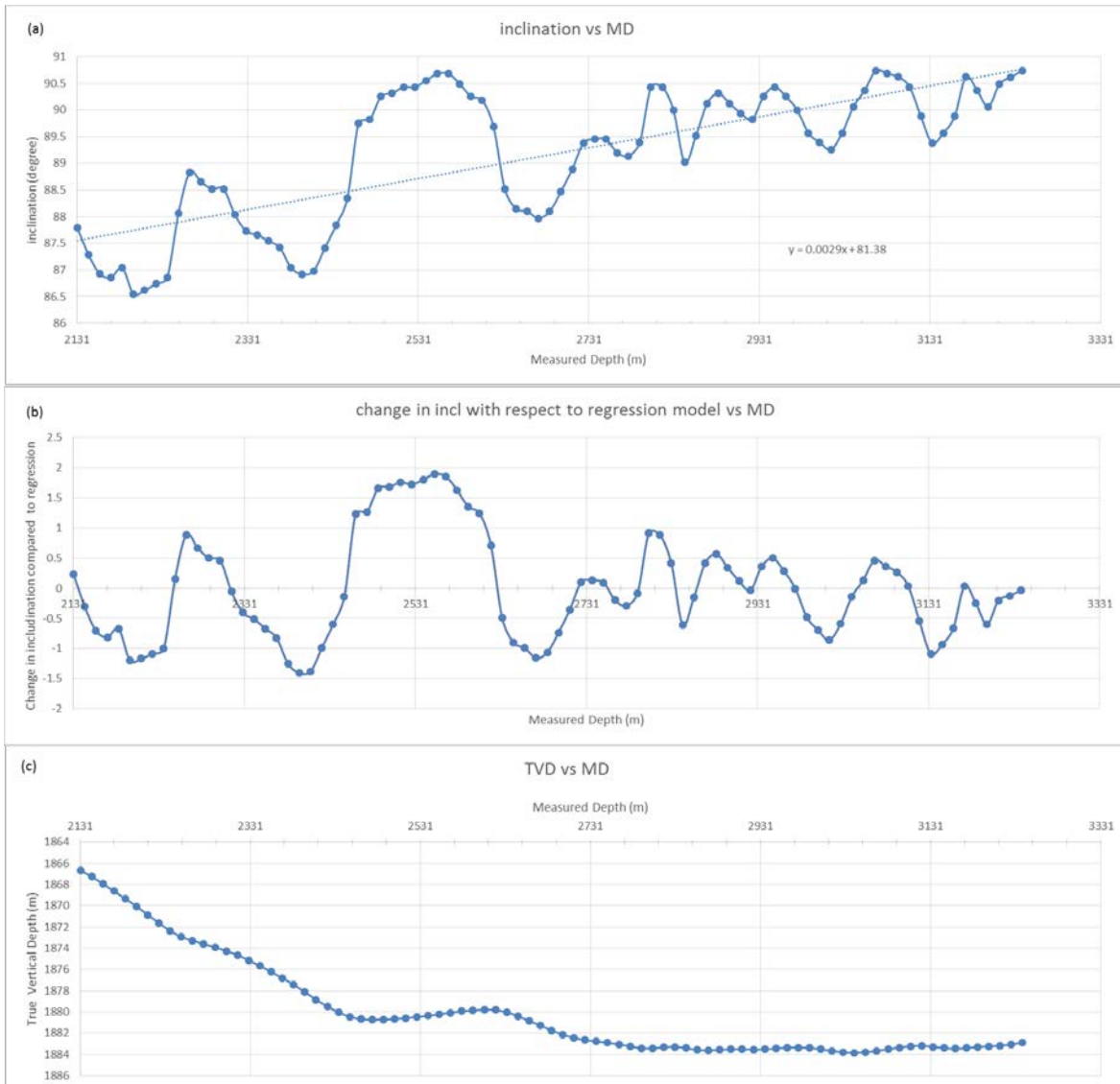


Figure 10-1 (a) Well HRB-1 inclination versus Measured Depth (m). (b) Change in inclination value with respect to best fit regression value. (c) True Vertical Depth (TVD) of the wellbore with respect to Measured Depth. Measured Depth interval begins at the first healed fracture observed.

Conductive fracture sets, HRB-1

Conductive fractures in Well HRB-1 are divided into three subsets: continuous, discontinuous, and bed-bound. All conductive fractures broadly strike NE-SW and therefore there is no further need for set-subdivision by strikes.

There are 965 conductive continuous fractures over an interval of 1104.64 m. The average fracture spacing is 1.14 m, and the Cv is 2.68. The normalized fracture intensity plot (Figure 10-2) shows four composite intensity peaks with 60 to 80 m widths. The first pair of peaks is located between 400 and 600 m in the middle of the scanline, and the second pair is near the end of the scanline after 900 m. Troughs appear semi-periodically between the peak pairs along the scanline. The NCC plot (Figure 10-3) is statistically significant and negatively sloped for length scales less than 20 m. The curve has a double hump interval over 50 and 90 m before it intercepts the randomized data curve at approximately 150 m. The curve also has an individual peak at 500 m. NCC analysis of the 266 fractures in the high intensity interval between positions 200 m and 400 m reveals statistically significant high spatial correlation for length scales between 0.15 and 20 m (Figure 10-4). Two prominent peaks are present at the length scales 6 m and 12 m. The correlation peak at approximately 120 m should be regarded as an artifact, for the corresponding length scale over half of the total interval length. Correlation count analysis of the 351 fractures in high intensity interval between positions 900 m and 1100 m reveals a decreasing elevated interval between length scale 0.2 to 15 m and a single peak at 50 m (Figure 10-5).

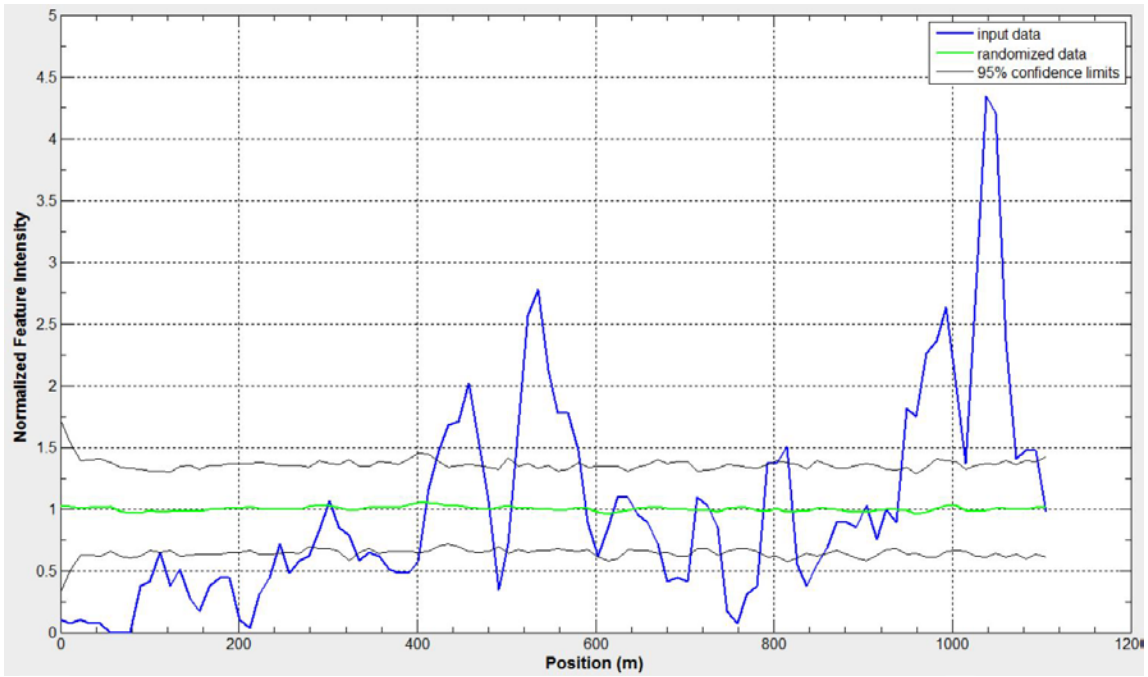


Figure 10-2 Intensity of conductive continuous fractures, Well HRB-1.

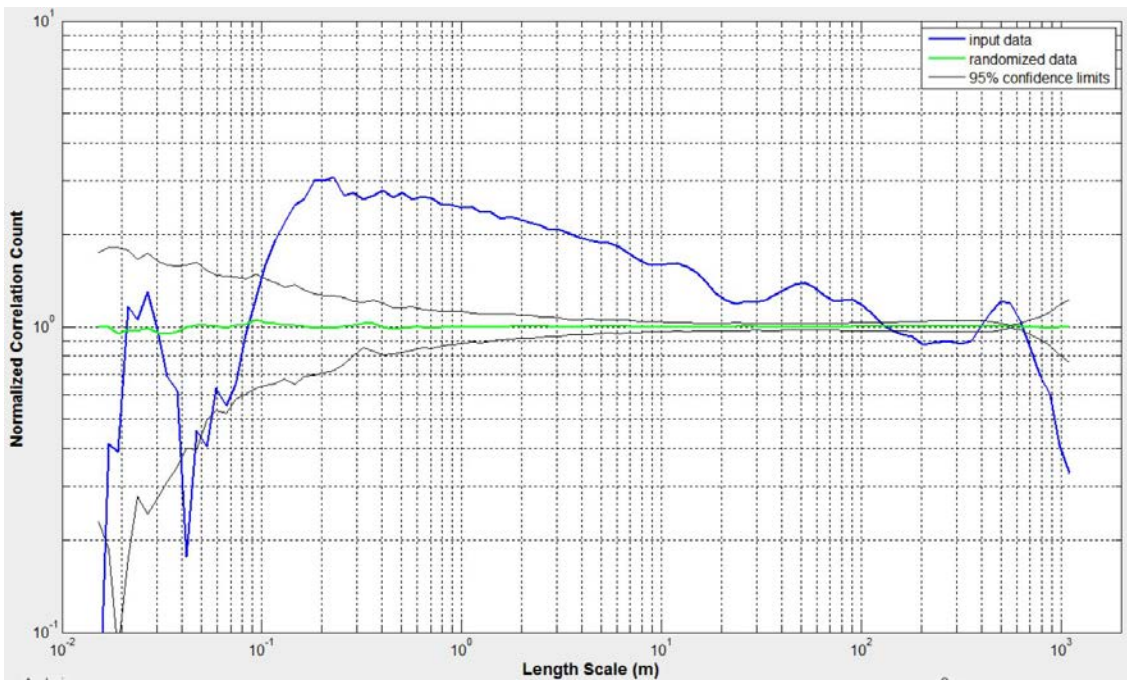


Figure 10-3 Correlation count of conductive continuous fractures, Well HRB-1.

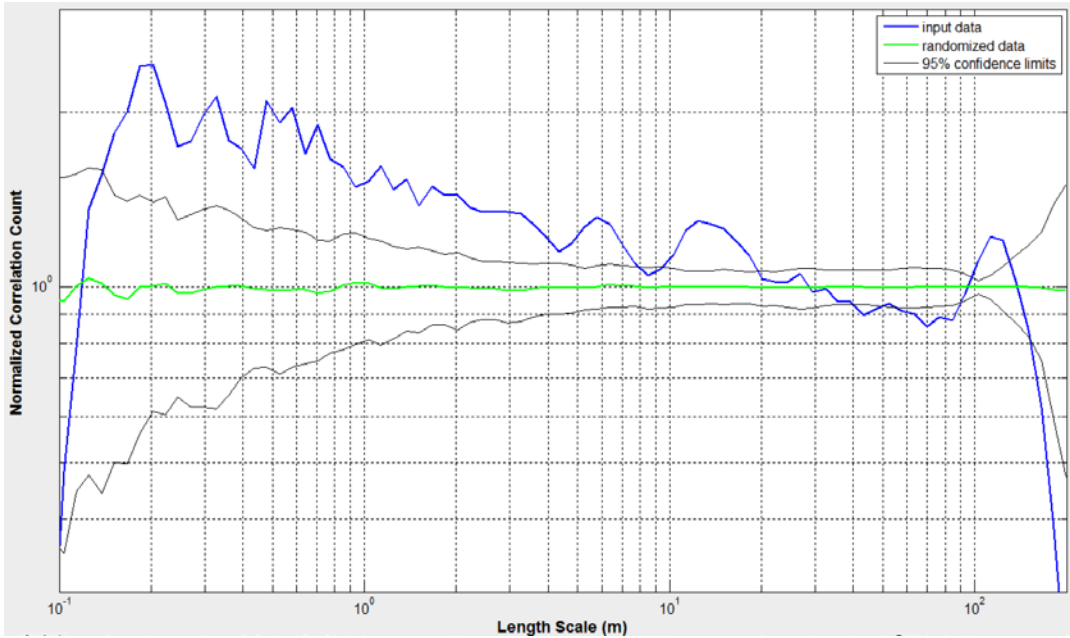


Figure 10-4 Correlation count of conductive continuous fractures, intensity plot position 400 to 600 m, Well HRB-1.

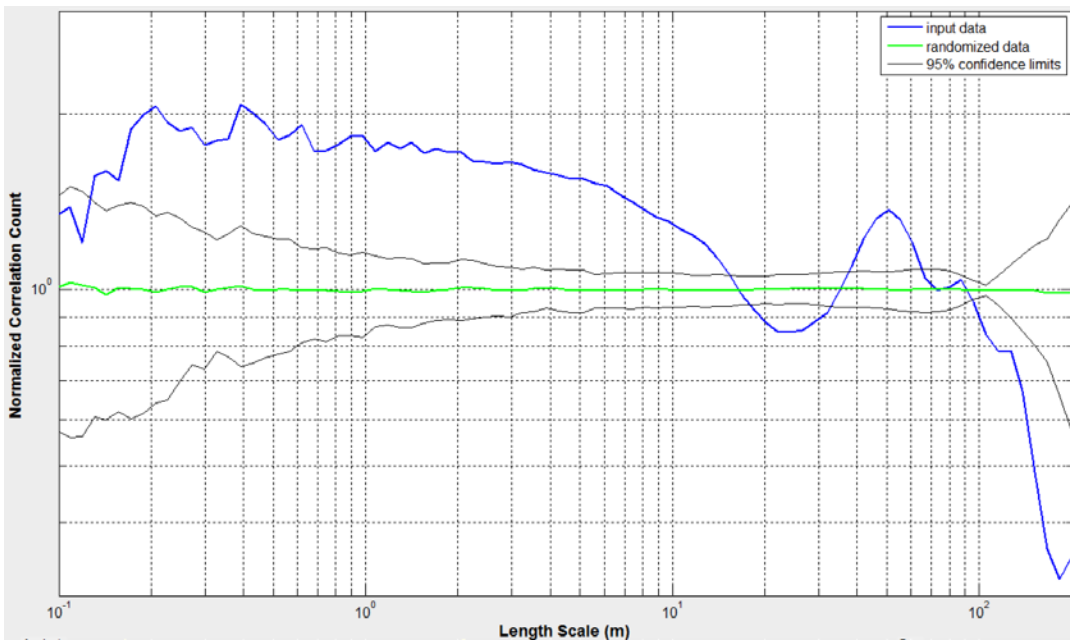


Figure 10-5 NCC of conductive continuous fractures, intensity plot position 900 to 1100 m, Well HRB-1.

There are 3052 conductive discontinuous fractures over an interval of 1112.04 m. The average fracture spacing is 0.36 m, and the Cv is 1.58. Discontinuous conductive fractures account for approximately 74% of all conductive fractures in Well HRB-1. The normalized fracture intensity plot (Figure 10-6) shows alternative placement of statistically significant peaks and troughs within the interval. Individual peaks and troughs are approximately 40 m wide on average. The NCC plot (Figure 10-7) remains statistically significant above the upper 95% confidence limit through approximately the 300 m length scale where it intercepts the randomized data curve. The correlation curve has a consistently negative slope for length scales less than 10 m. The trend of the curve flattens after 10 m, and multiple wide, statistically significant correlation humps subsequently appear centering above 30, 70, and 200 m.

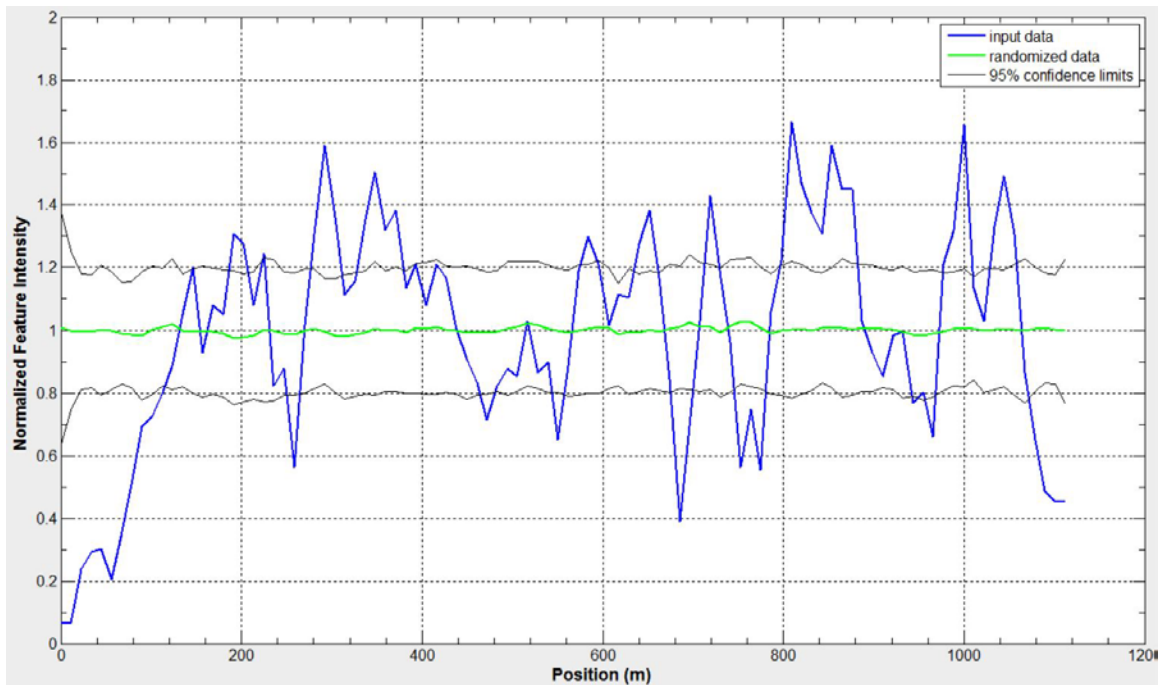


Figure 10-6 Intensity of conductive discontinuous fractures, Well HRB-1.

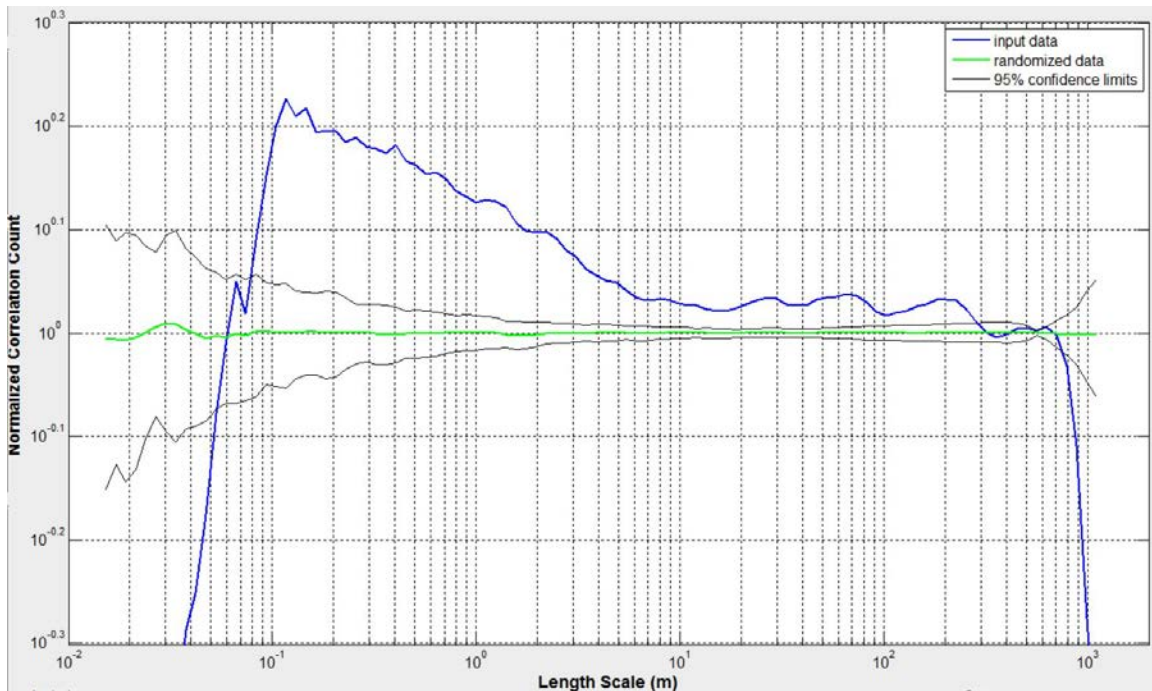


Figure 10-7 Correlation count of conductive discontinuous fractures, Well HRB-1.

There are 113 conductive bed-bound fractures over an interval of 919.44 m. The average fracture spacing of 8.13 m, and the C_v is 2.76. The normalized fracture intensity plot (Figure 10-8) contains multiple narrow intensity peaks approximately at positions 280, 520, 570, 690, 760, and 850 m. The peaks are approximately 30 m on average. The NCC curve (Figure 10-9) has a decreasing elevated portion before 6 m. Low amplitude yet statistically significant correlation peaks also appear at length scales 25, 50, 80, and 180 m. A sharp drop in correlation count appears as a missing curve segment is present between length scales 30 and 40 m.

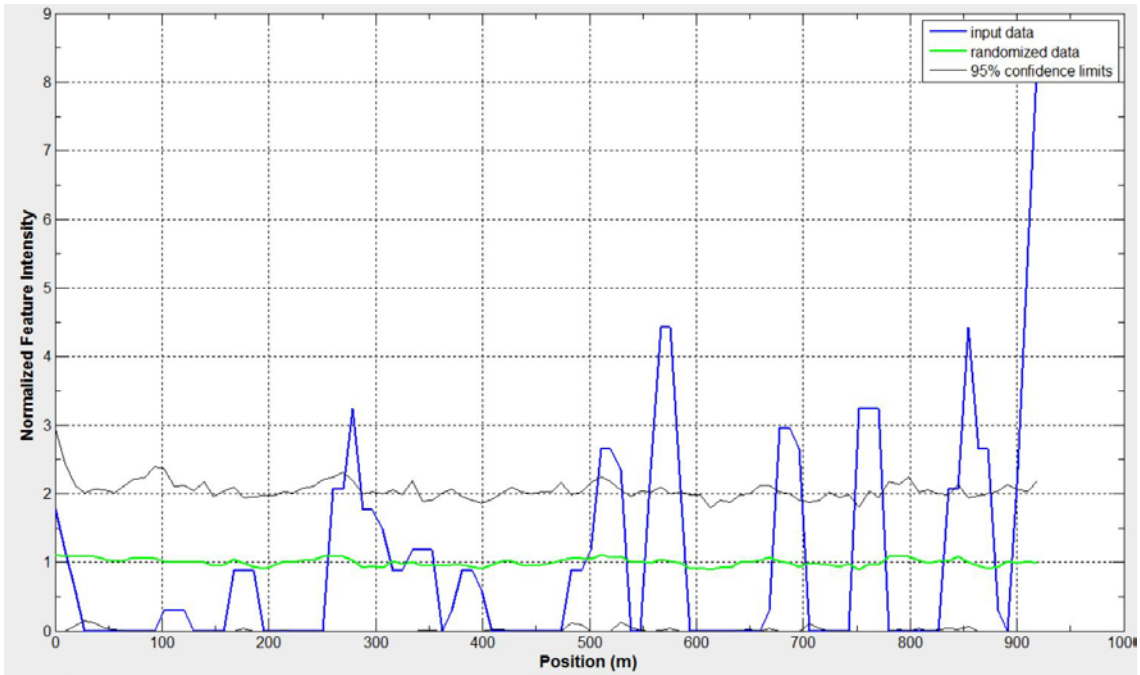


Figure 10-8 Intensity of conductive bed-bound fractures, Well HRB-1.

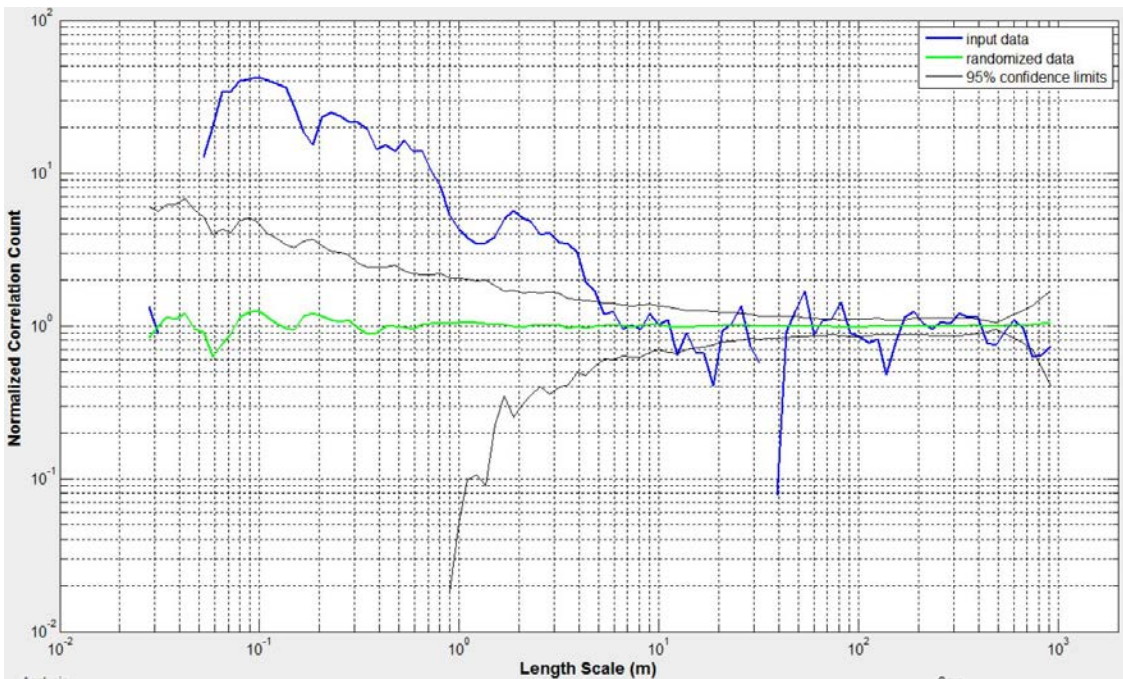


Figure 10-9 Correlation count of conductive bed-bound fractures, Well HRB-1.

The fracture superset of all 4130 continuous, discontinuous, and bed-bound conductive fractures spans an interval of 1112.10 m. The average fracture spacing is 0.27 m, and the C_v is 1.56. The normalized fracture intensity plot contains peak intervals separated by individual troughs (Figure 10-10). The two highest peaks concentrate in the end portion of the interval between 900 and 1100 m. The correlation curve in the NCC plot (Figure 10-11) remains statistically significant for all length scales up to approximately 300 m where it intercepts the randomized data curve, and a peak reappears then at near 450 m. The curve is negative in slope and approximately linear until length scale 6m, and peaks rise at 50 and 200 m in the flat-trending curve segment beyond. NCC analysis of the 936 fractures in the high intensity peak interval between positions 900 and 1100 m (Figure 10-12) reveals a low-amplitude, statistically significant spatial correlation curve segment decreasing to 1 between length scales 0.1 and 25 m. It then rises above the upper confidence limit and peaks at 50 m.

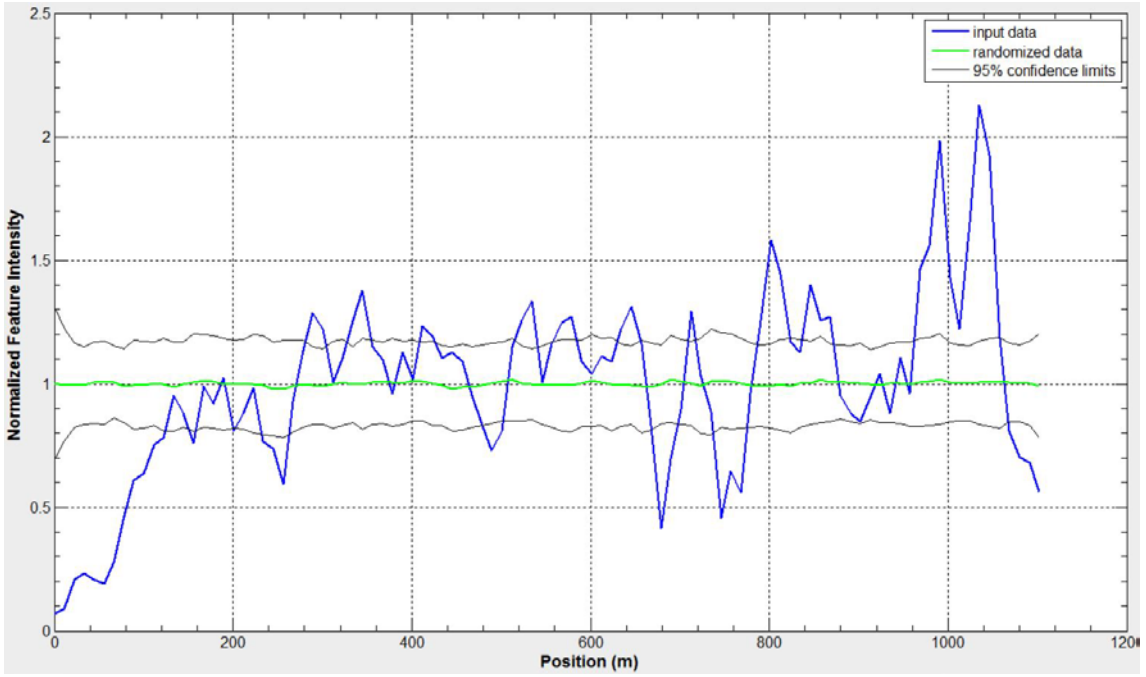


Figure 10-10 Intensity of all conductive fractures, Well HRB-1.

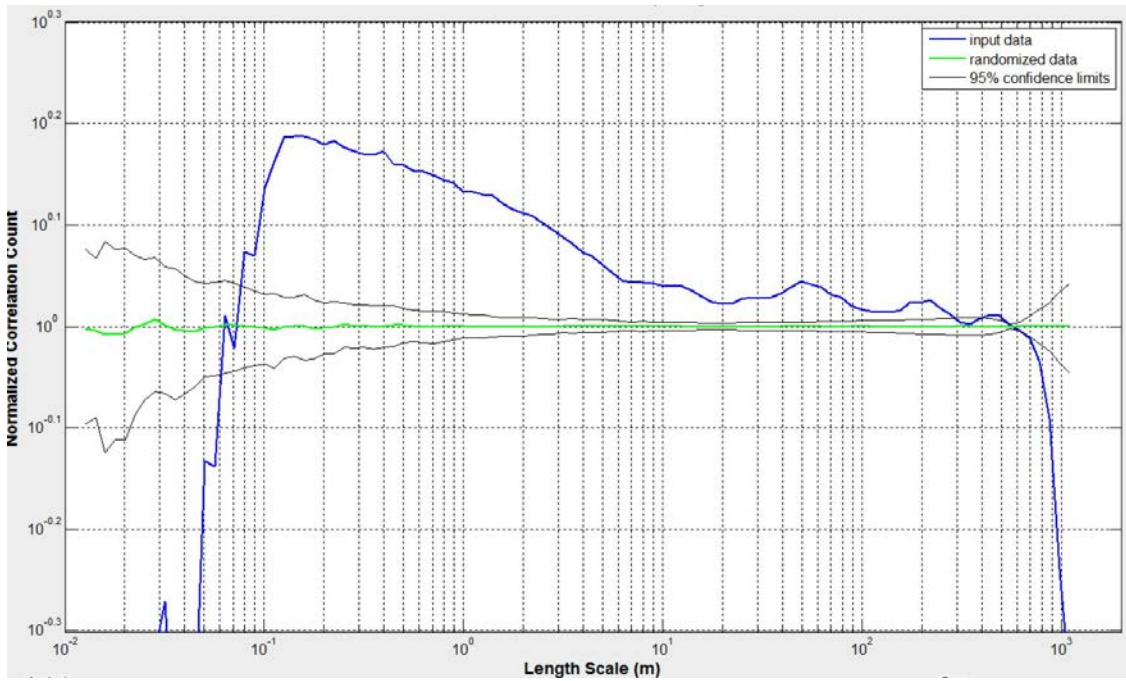


Figure 10-11 Correlation count of all conductive fractures, Well HRB-1.

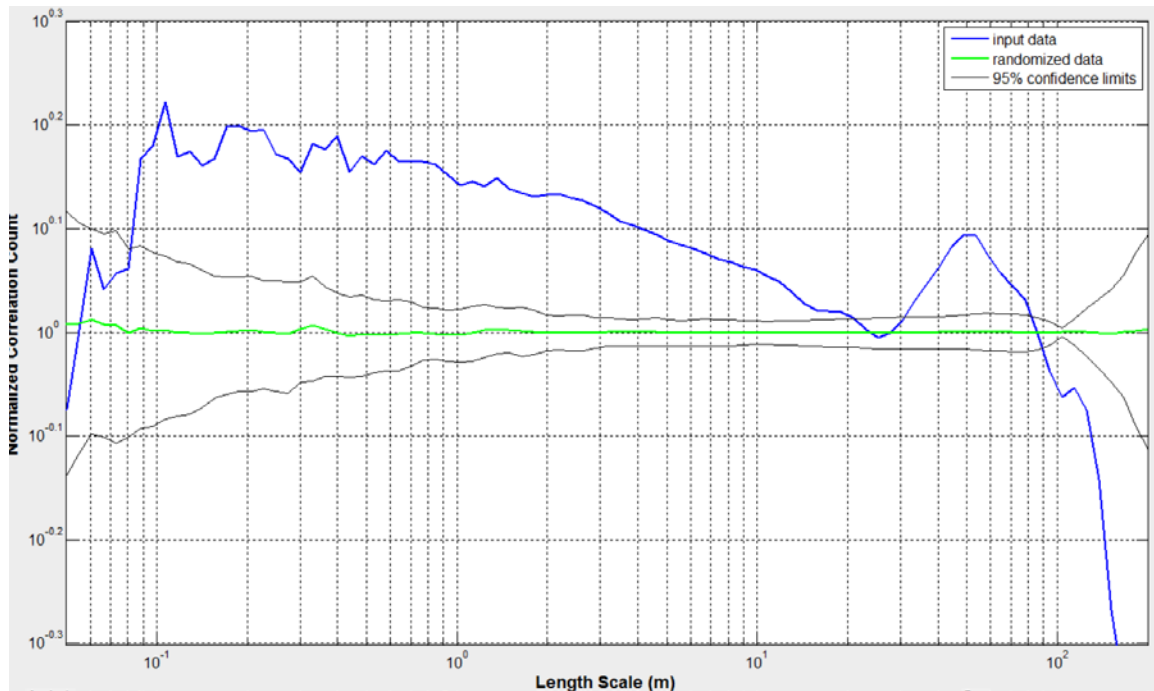


Figure 10-12 Correlation count of all conductive fractures, intensity plot position 900 to 1100 m, Well HRB-1.

Resistive fracture sets, HRB-1

Resistive fractures in Well HRB-1 are categorized as two sets by fracture orientations: Set 1 for NE-striking fractures and Set 2 for NW-striking fractures. There are approximately twice as many Set 1 resistive fractures as Set 2 (Table 6).

There is a total of 1188 resistive fractures of all orientations over an interval of 1109.47 m. The average fracture spacing is 0.93 m, and the Cv is 1.63. The normalized fracture intensity plot (Figure 10-13) contains three large intensity peaks at 240, 640, and 1080 m and multiple smaller peaks and troughs in between. The NCC curve (Figure 10-14) is statistically significant and has a negative slope for length scales less than 30 m. After the two troughs at 40 and 90 m, the curve peaks at 200 and 400 m.

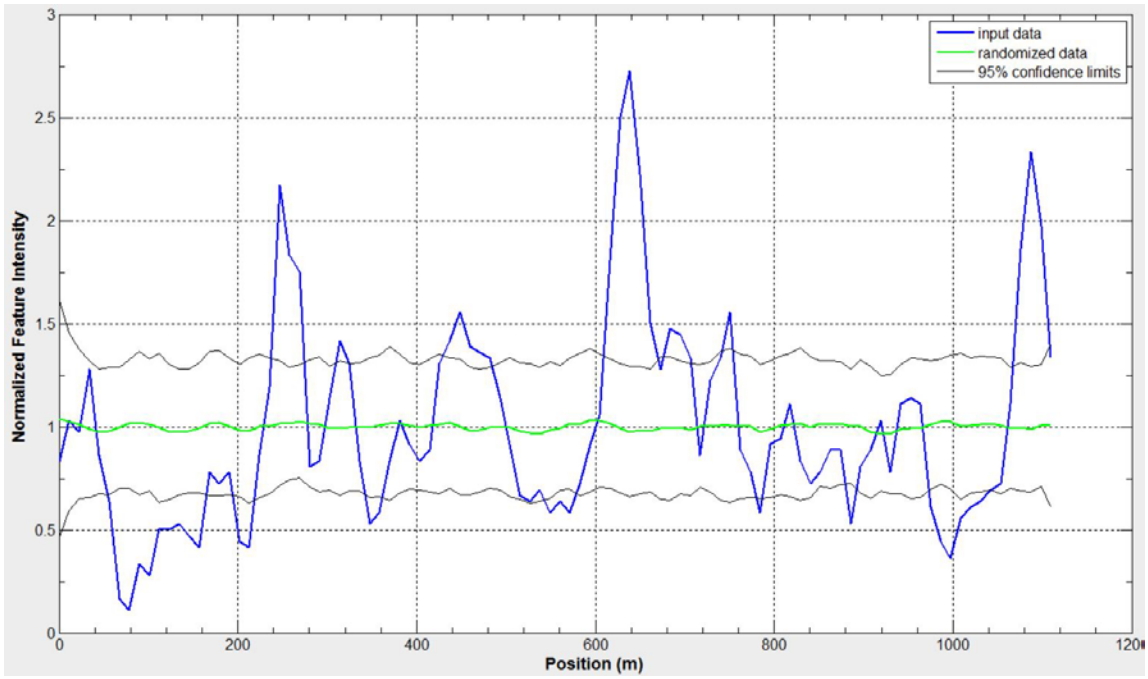


Figure 10-13 Intensity of all resistive fractures, Well HRB-1.

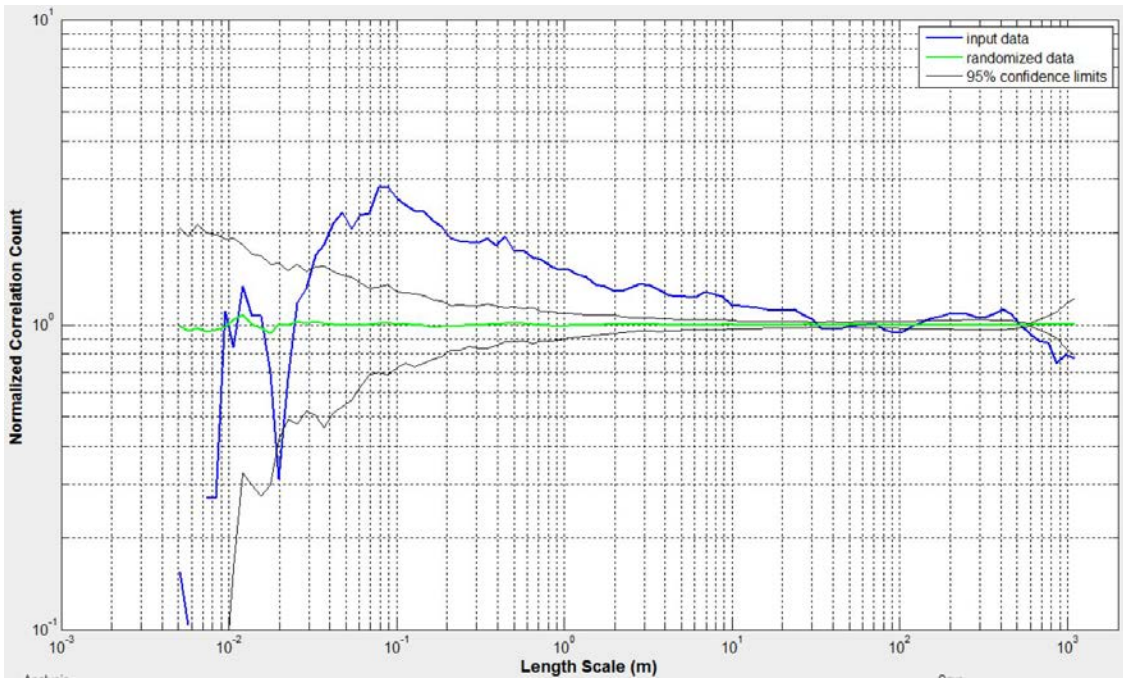


Figure 10-14 Correlation count of all resistive fractures, Well HRB-1.

There are 872 resistive Set 1 fractures over an interval of 1100.61 m. The average fracture spacing is 1.26 m, and the Cv is 1.80. Both the normalized fracture intensity plot (Figure 10-15) and the NCC plot (Figure 10-16) mirror those for all resistive fractures. Note that an absolute majority (73.4%) of all the resistive fractures are in Set 1. Also note that, while fracture spacings in resistive Set 1 are geologically meaningful, those in resistive Set All (as analyzed in Figures 10-14 and 10-14) are not and are included for completeness sake.

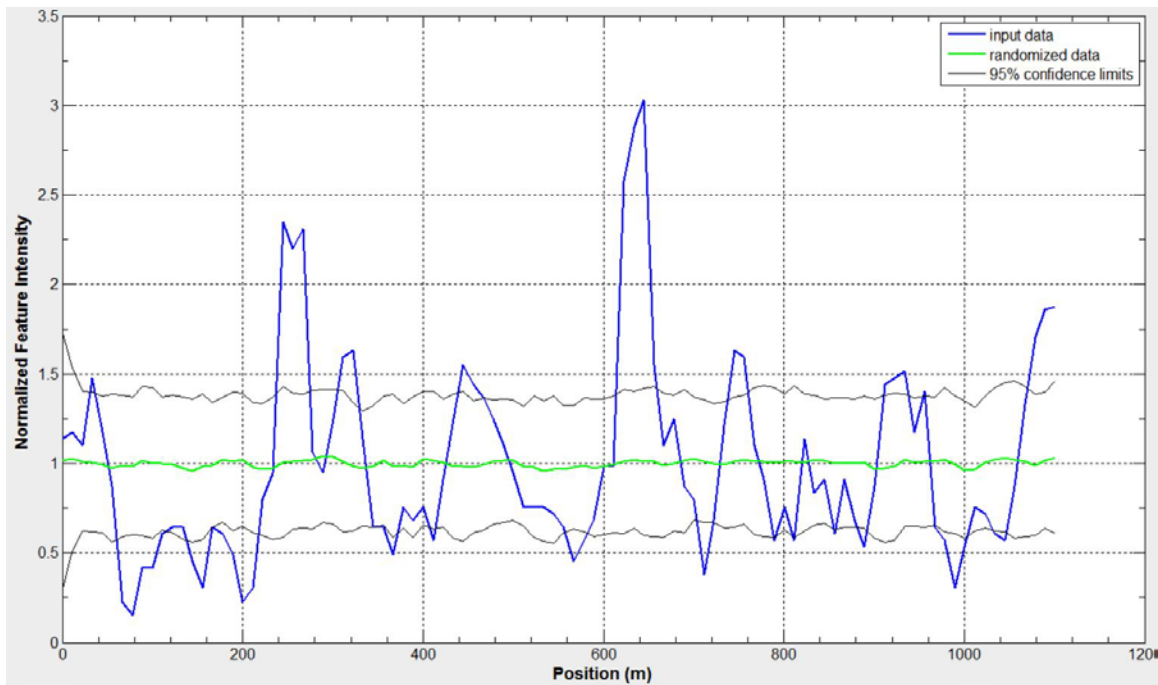


Figure 10-15 Intensity of resistive Set 1 fractures, Well HRB-1.

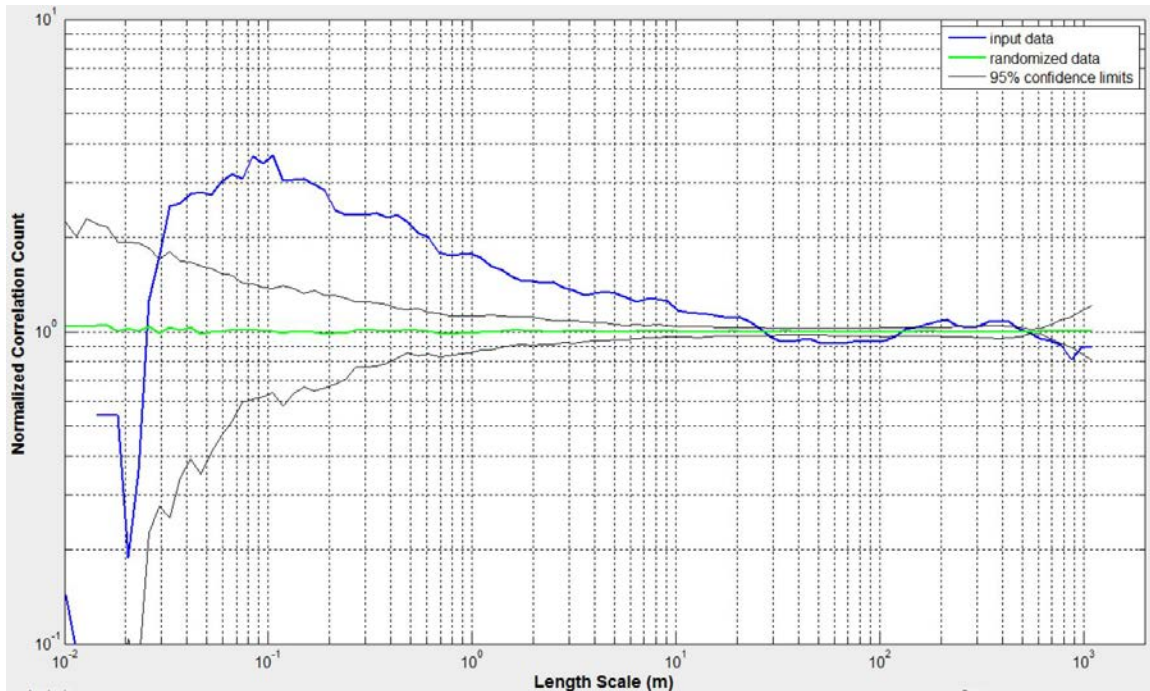


Figure 10-16 Correlation count of resistive Set 1 fractures, Well HRB-1.

There are 497 resistive Set 2 fractures over an interval of 990.07 m. The average fracture spacing is 1.99 m, and the Cv is 2.12. The normalized fracture intensity plot (Figure 10-17) contains a large central high intensity interval between 500 and 600 likely formed by overlapped neighboring peaks. Three smaller peaks appear at 260, 680, and 970 m along the scanline. Six major troughs are present centering positions 20, 220, 420, 620, 820, and 900 m. The statistically significant elevated interval in the NCC plot (Figure 10-18) ends approximately at length scale 50 m. It is followed by two troughs at 70 and 140 m and two peaks at 200 and 430 m. NCC analysis of the 153 fractures in the peak intensity interval between positions 450 and 650 m reveals that the spatial correlation curve remains mostly statistically significant for all length scales between 0.06 and approximately 60 m

(Figure 10-19). The curve's saw-tooth pattern for length scales less 2 m contrasts with the smooth plateau pattern for those exceeding 2 m.

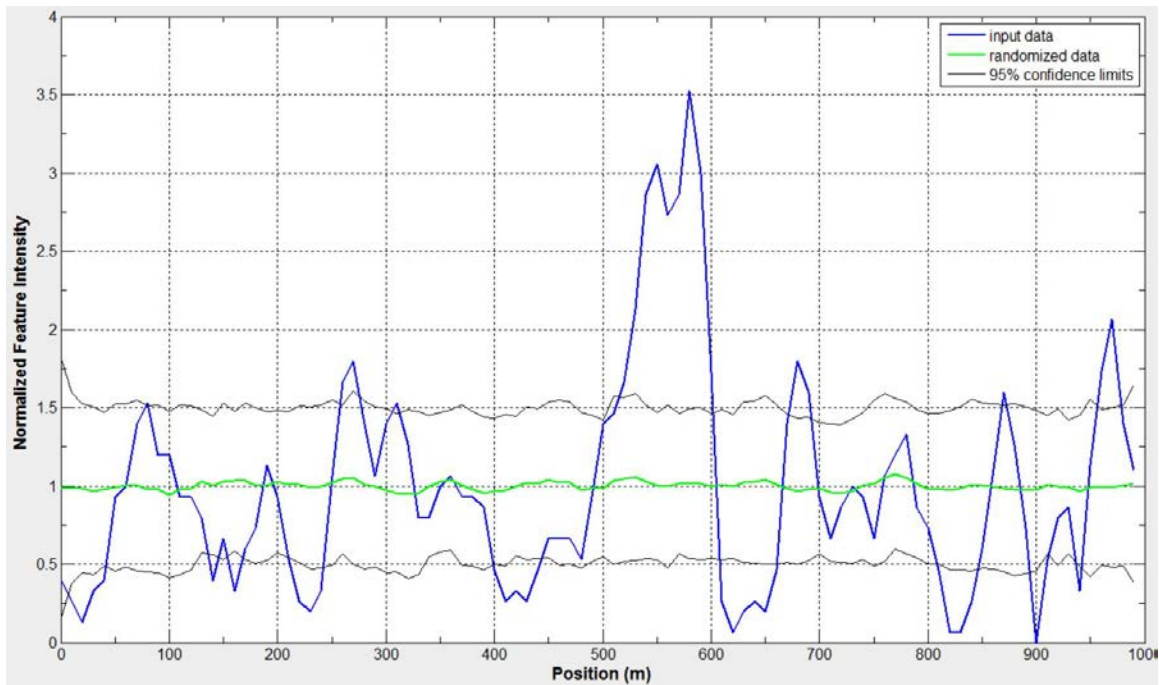


Figure 10-17 Intensity of resistive Set 2 fractures, Well HRB-1.

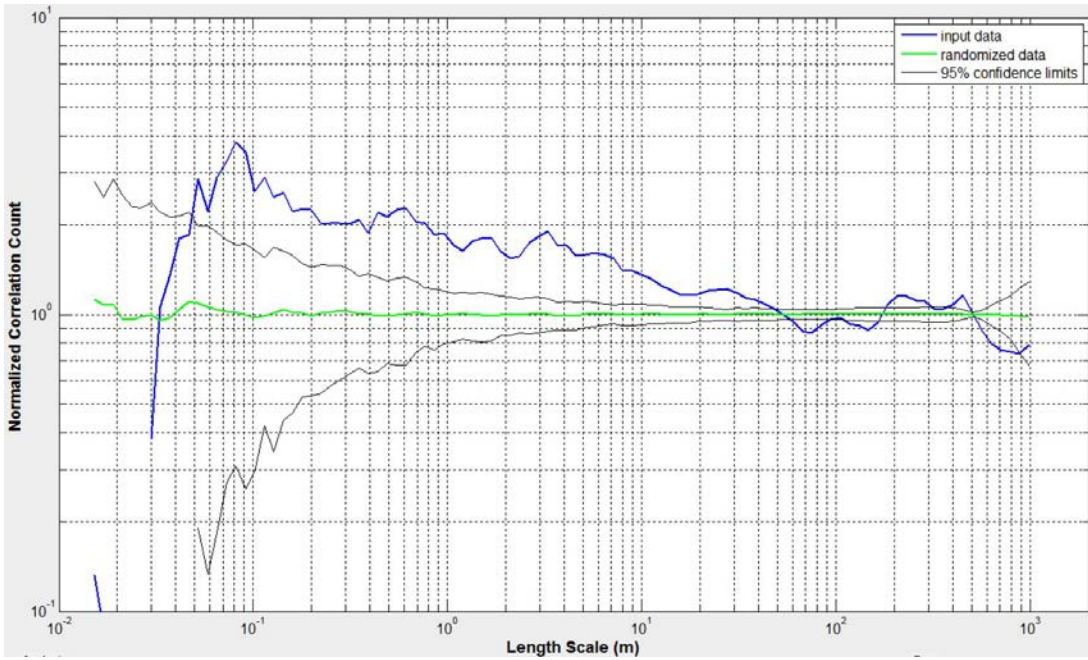


Figure 10-18 Correlation count of resistive Set 2 fractures, Well HRB-1.

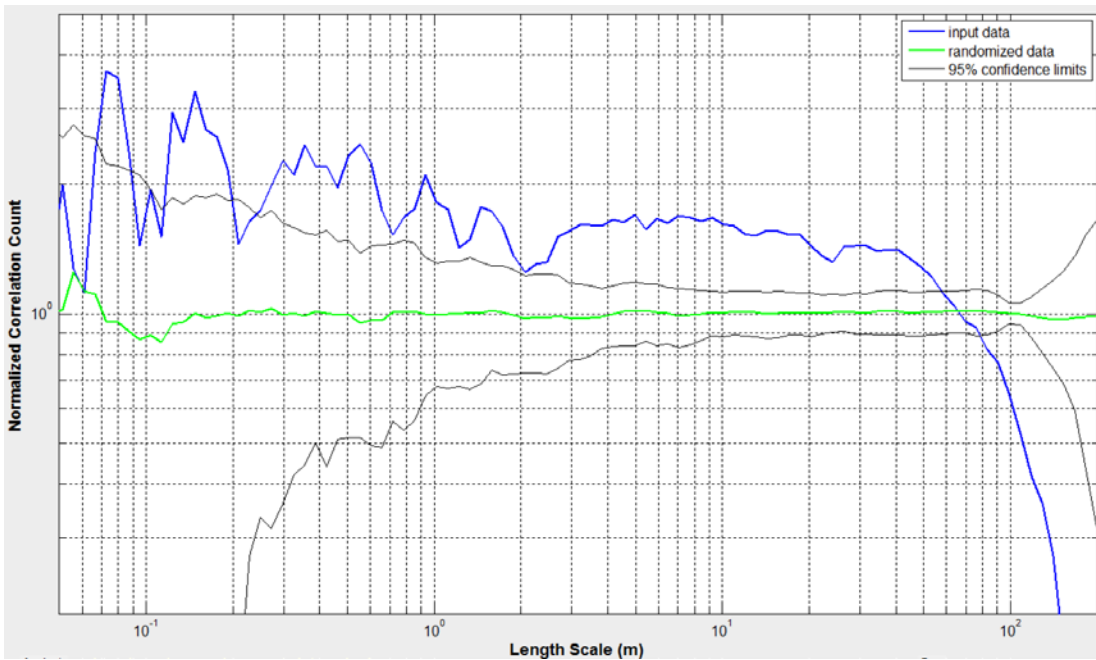


Figure 10-19 Correlation count of resistive Set 2 fractures, intensity plot position 450 to 650 m, Well HRB-1.

The NW-SE striking Set 2 resistive fractures can be further categorized into three fracture subsets: continuous, discontinuous, and bed-bound. Note that certain resistive Set 2 fractures have been assigned as both discontinuous and bed-bound by the operator, and therefore the sum of the fractures in the three subsets exceeds the number in the original undivided set.

There are 293 resistive continuous fractures over an interval of 988.25 m. The average fracture spacing is 3.38 m, and the Cv is 2.10. The normalized fracture intensity plot (Figure 10-20) contains peaks in the intervals between positions 250 and 350 m, 500 and 600 m, and 950 and 1000 m. The NCC curve (Figure 10-21) features a linearly decreasing elevated interval ending at length scale 10 m. Two singular peaks are then found at 40 and 450 m with a troughs appearing in between at 80 and 150 m.

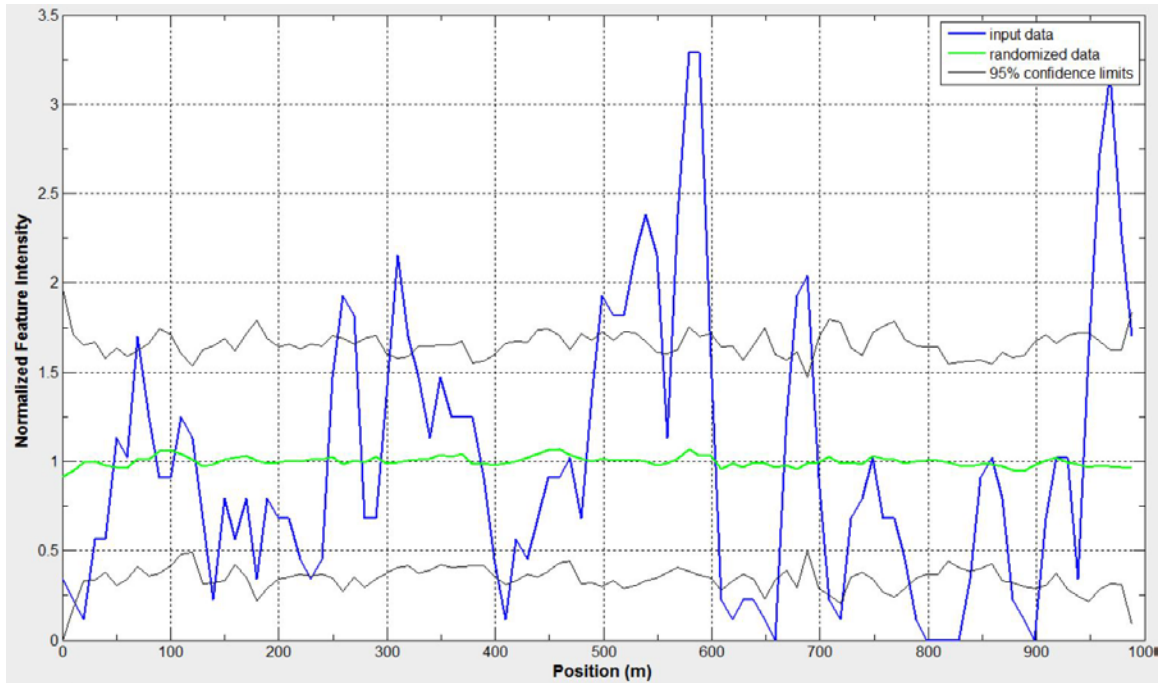


Figure 10-20 Intensity of Set 2 resistive continuous fractures, Well HRB-1.

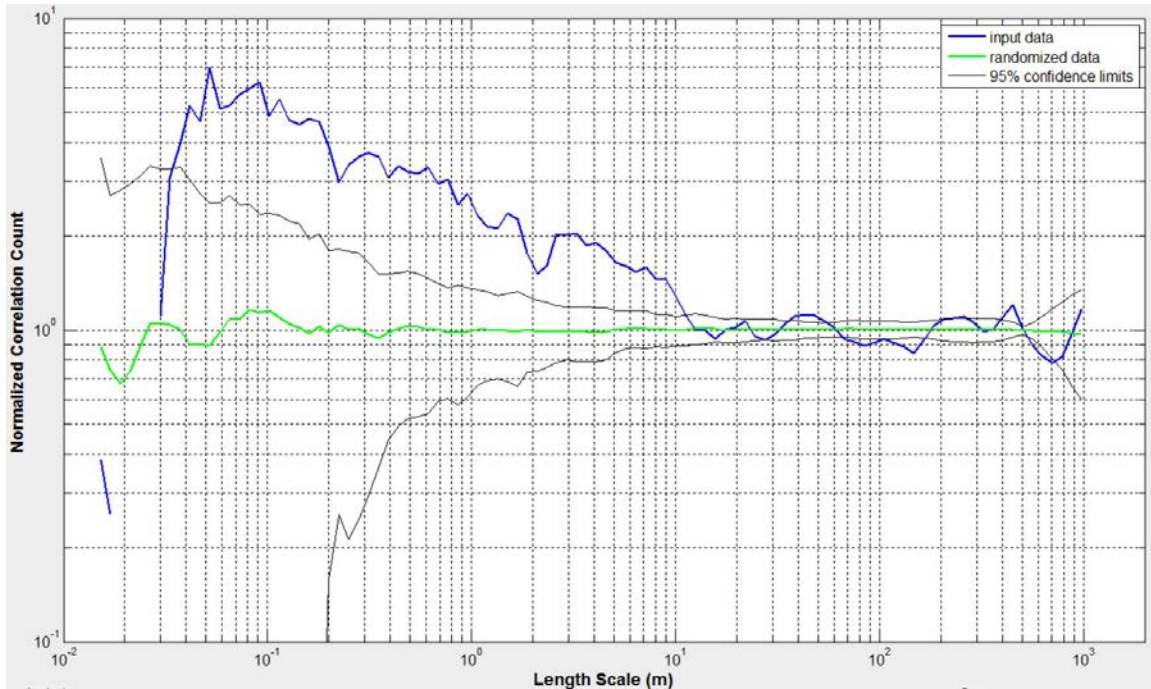


Figure 10-21 Correlation count of Set 2 resistive continuous fractures, Well HRB-1.

There are 95 resistive discontinuous fractures over an interval of 899.82 m. The average fracture spacing is 9.47 m, and the Cv is 1.64. The normalized fracture intensity plot (Figure 10-22) features a short, narrow peak at 160 m and two high and wide composite peak intervals centering over positions 600 and 840 m. The latter two are each approximately 70 m wide. The NCC curve (Figure 10-23) is statistically significant for most length scales less than 40 m except for close to 0.2 or 1.5 m. The curve first drops beneath the lower confidence limit into an extended trough from 50 to approximately 180 m after crossing the randomized data curve at length scale 45 m. It then peaks at approximately 250 m and bottoms again at 350 m.

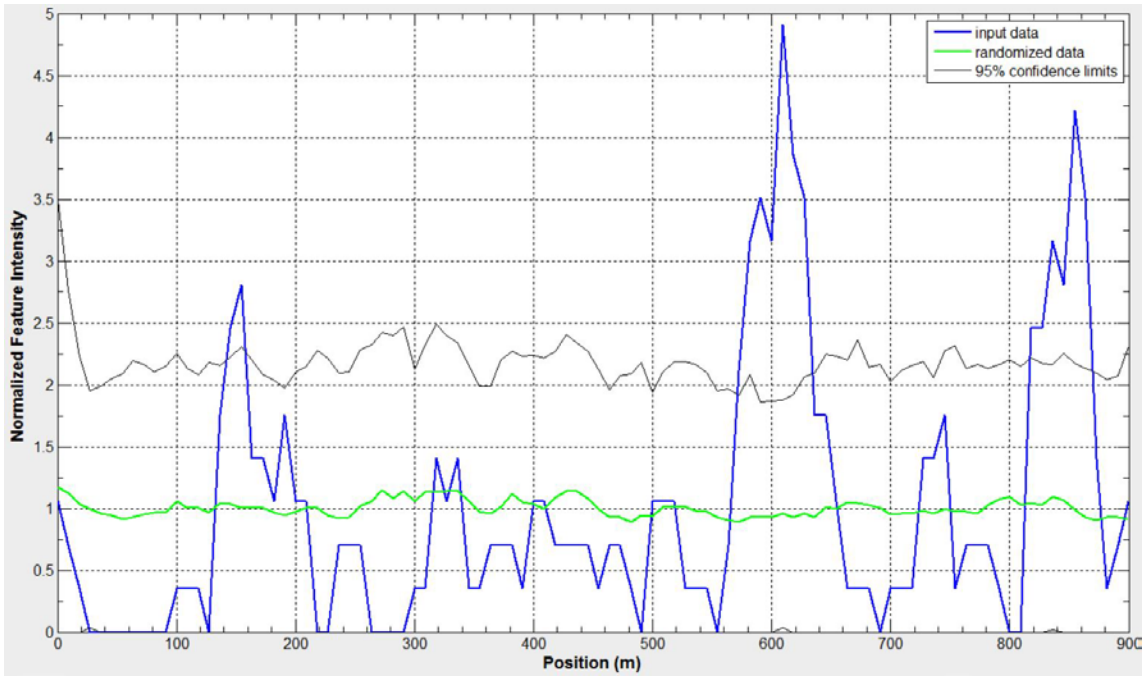


Figure 10-22 Intensity of resistive discontinuous fractures, Well HRB-1.

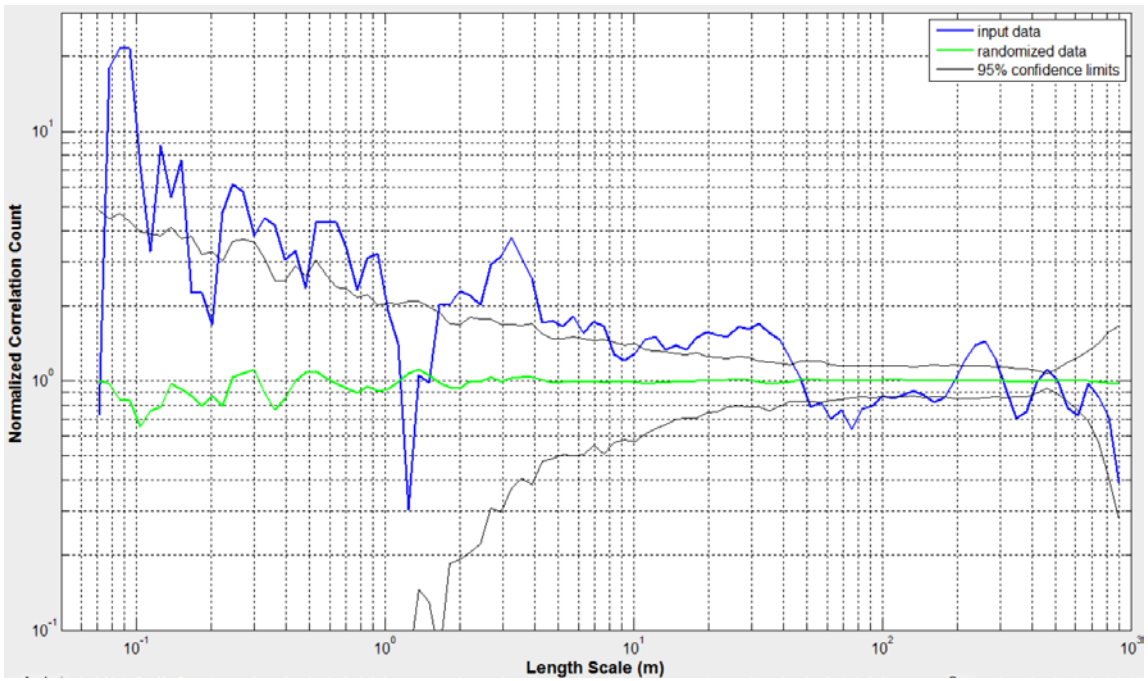


Figure 10-23 Correlation count of resistive discontinuous fractures, Well HRB-1.

There are 133 resistive bed-bound fractures over an interval of 915.00 m. The average fracture spacing is 6.88 m, and the Cv is 1.83. The normalized fracture intensity plot (Figure 10-24) contains three large intensity peak intervals near positions 220 m, 520 m, and 820 m with the middle one formed by at least two overlapped peaks. The NCC curve (Figure 10-25) contains a statistically significant and decreasing correlation interval that first crosses the randomized data curve approximately at length scale 45 m. The curve peaks at again near 300 m.

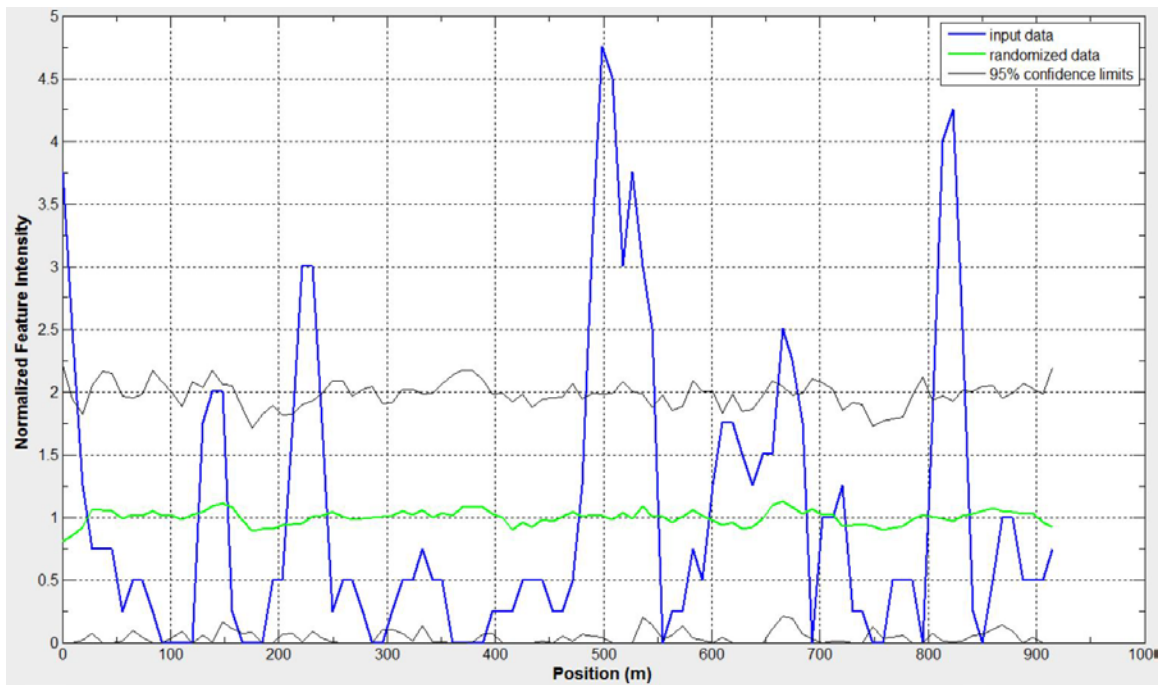


Figure 10-24 Intensity of resistive bed-bound fractures, Well HRB-1.

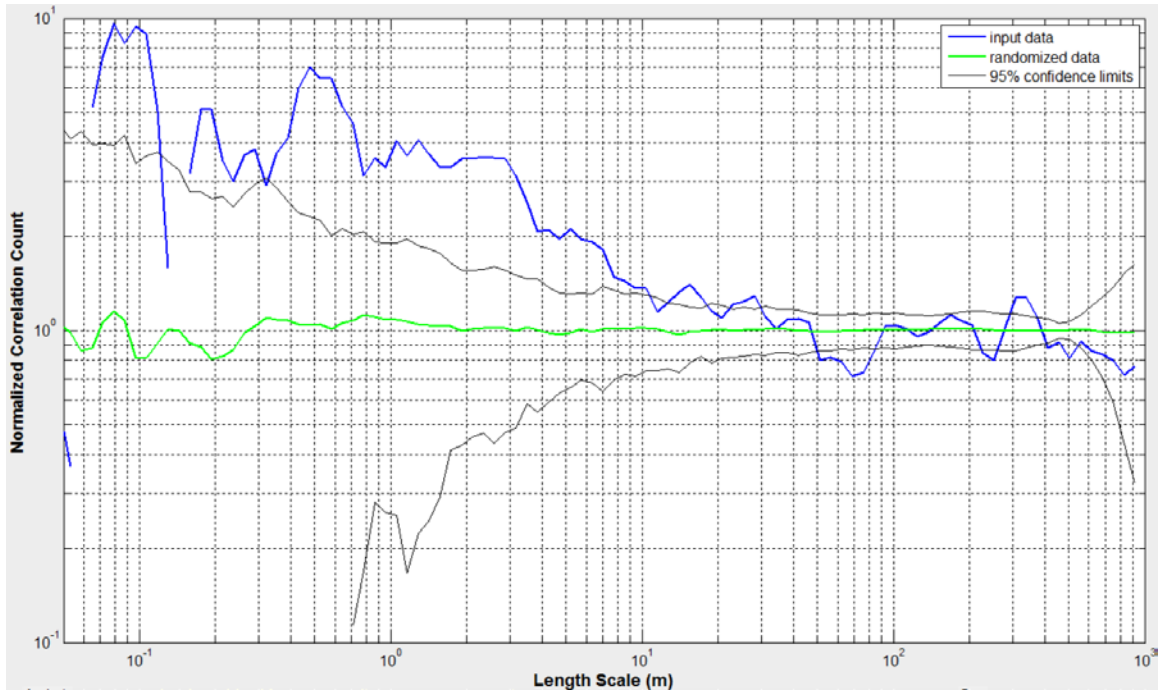


Figure 10-25 Correlation count of resistive bed-bound fractures, Well HRB-1.

Other fracture sets, HRB-1

Other sinusoidal features classified in Well HRB-1's image log include drilling induced fractures and faults. This study also creates and analyzes two fracture supersets. One superset includes all drilling induced fractures and all the conductive fractures that similarly strike NE-SW, and the other includes all NE-striking natural (i.e. non-drilling-induced) fractures.

There are 556 drilling induced fractures over an interval of 1096.06 m. The average fracture spacing is 1.97 m, and the Cv is 3.91. The normalized fracture intensity plot (Figure 10-26) contains a singular intensity peak at position 320 m that is approximately 50 m wide. The central portion of the plot extending approximately from 560 to 720 m is a broad, high intensity band formed by at least three neighboring peaks with increasing

magnitude. Intensity troughs are present semi-regularly elsewhere in the plot. The NCC plot (Figure 10-27) contains a relatively smooth and negatively sloped high correlation interval. It crosses the random data curve at 150 m, bottoms into a trough at 200 m, and peaks again at 350 m. NCC analysis of the 289 fractures in the dominant peak intensity interval between positions 550 and 750 m reveals an elevated and decreasing correlation count curve that briefly dips beneath the upper confidence limit at 25 m before peaking again at 40 m (Figure 10-28).

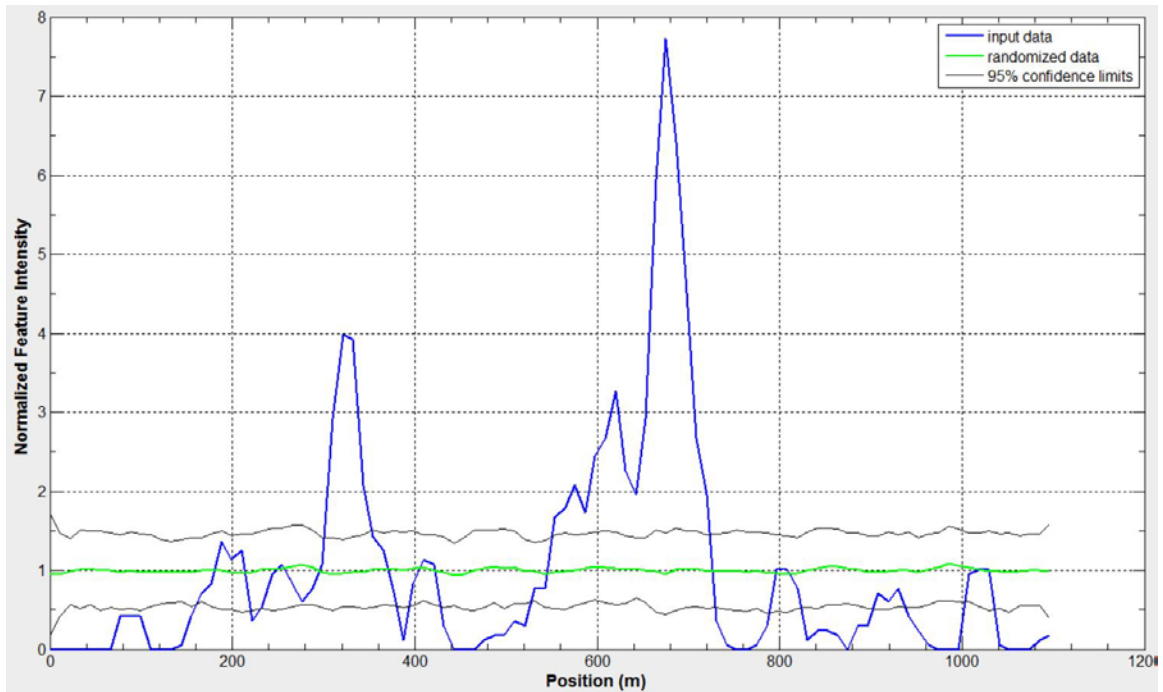


Figure 10-26 Intensity of drilling induced fractures, Well HRB-1.

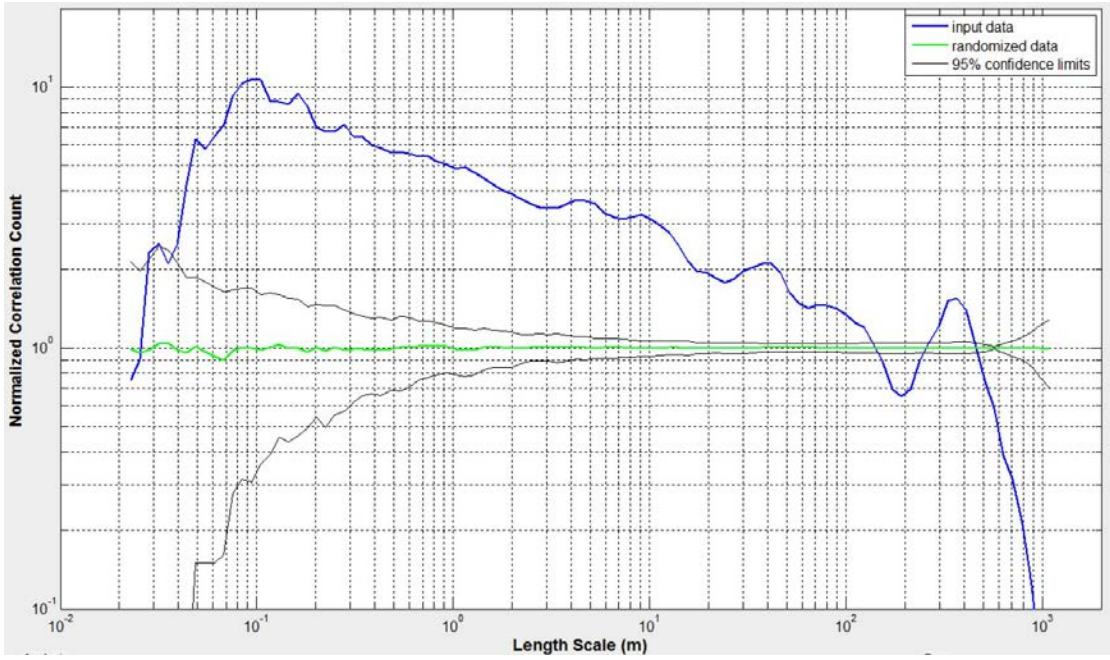


Figure 10-27 Correlation count of drilling induced fractures, Well HRB-1.

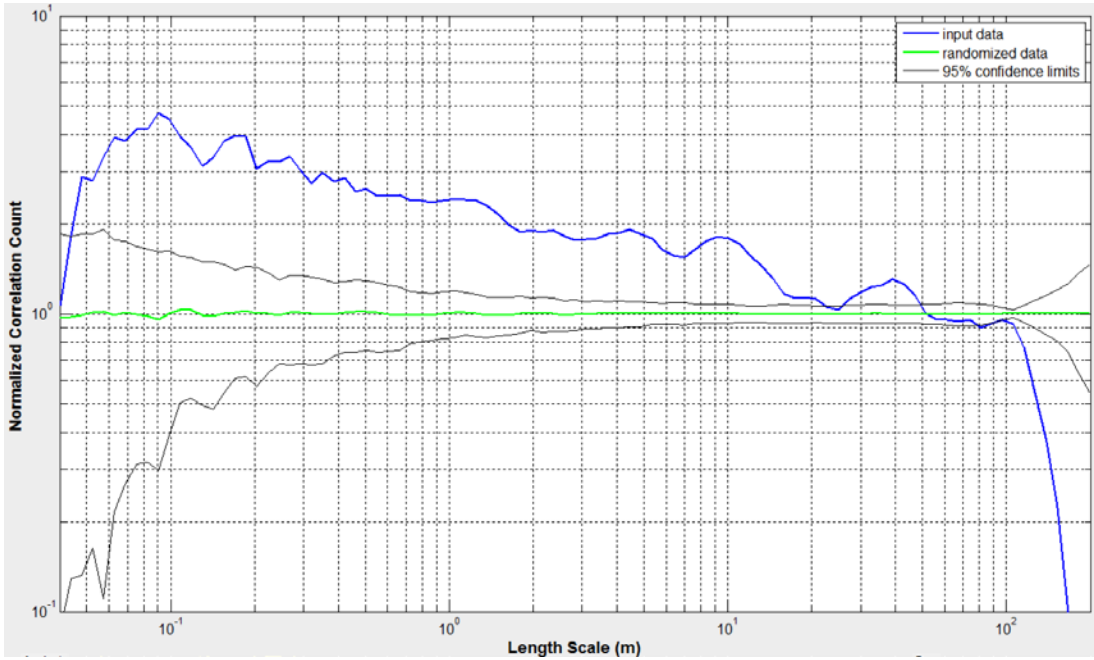


Figure 10-28 Correlation count of drilling induced fractures, intensity plot position 550 to 750 m, Well HRB-1.

The fracture superset containing all drilling-induced and all continuous conductive fractures was created to investigate the hypothetical extreme case scenario where all continuous conductive fractures are in fact incorrectly categorized drilling induced fractures. The set contains 1521 fractures over an interval of 1099.42m. The average fracture spacing is 0.72 m, and the C_v is 2.77. The normalized intensity plot (Figure 10-29) shows three statistically significant, high intensity portions separated by troughs: first an intensity peak at position 310 m after an extended saw-toothed trough interval, then a broad band of overlapping peaks between 520 and 720 m with the largest peak at 660 m, and lastly two adjacent peaks at 980 and 1030 m near the end of the scanline. The NCC plot (Figure 10-30) consists of a smooth, near-linearly decreasing and elevated interval. It crosses the randomized data at length scale 180 m, bottoms at 200 m, and then peaks again at 400 m after. The segment from 20 to 180 m appears to be have at least two peaks embedded within.

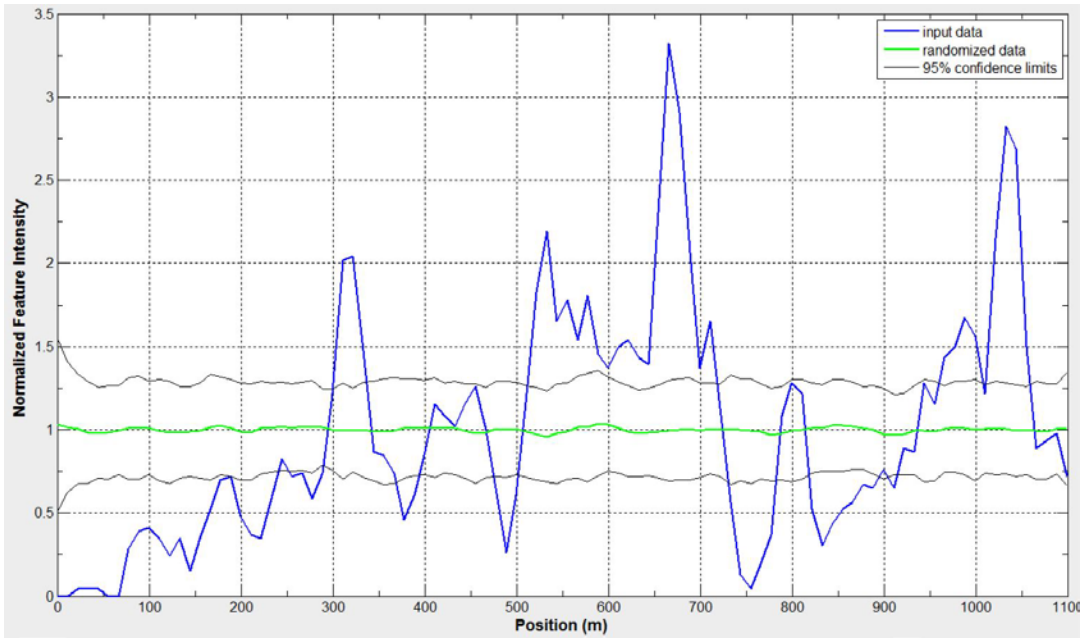


Figure 10-29 Intensity of drilling induced fractures and continuous conductive fractures, Well HRB-1.

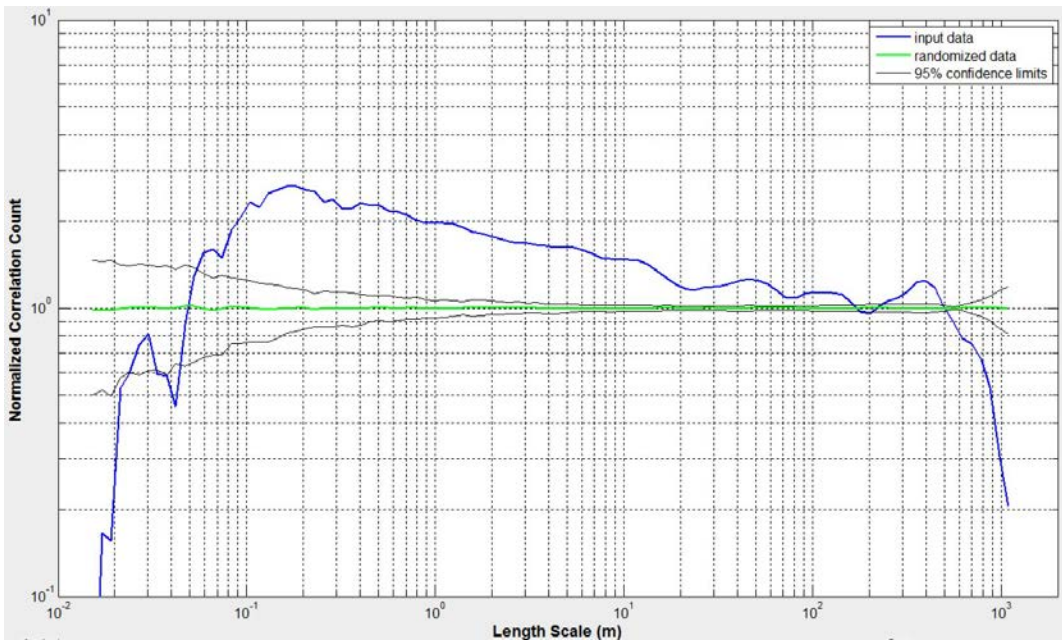


Figure 10-30 NCC plot of Well HRB-1 drilling fractures & continuous conductive fractures.

The superset of 5002 natural fracture in Well HRB-1 contains 4130 NE-striking conductive fractures and 872 NE-striking resistive fractures (few NW-striking Set 2 conductive fractures are present) in a 1105.82 m interval. The average fracture spacing is approximately 0.22 m, and the C_v is approximately 1.39, which lower than those of the constituent sets. The normalized fracture intensity curve (Figure 10-31) contains primarily troughs between positions 0 and 200 m. The subsequent segment before 600 m containing is mostly bounded between the upper and lower 95% confidence limits with sporadic minor peaks and troughs. The first major peak is found at 640 m and is immediately followed by moderate troughs at 680 m and 750 m. Two intermediate peaks then follows at 800 and 850 m, and the two largest peaks emerge lastly near positions 1000 and 1050 m. The highly smooth NCC curve (Figure 10-32) is above the upper 95% confidence limit everywhere between 0.09 and 550 m. The negatively sloped portion of the curve flattens for length scales over 8m.

There are 22 faults over an interval of 952.41 m. The average spacing between the faults is 43.29 m, and the C_v is 1.49. Due to limited fault spacing data, the corresponding fracture intensity (Figure 10-33) and the NCC curves (Figure 10-34) are incomplete and are therefore uninformative.

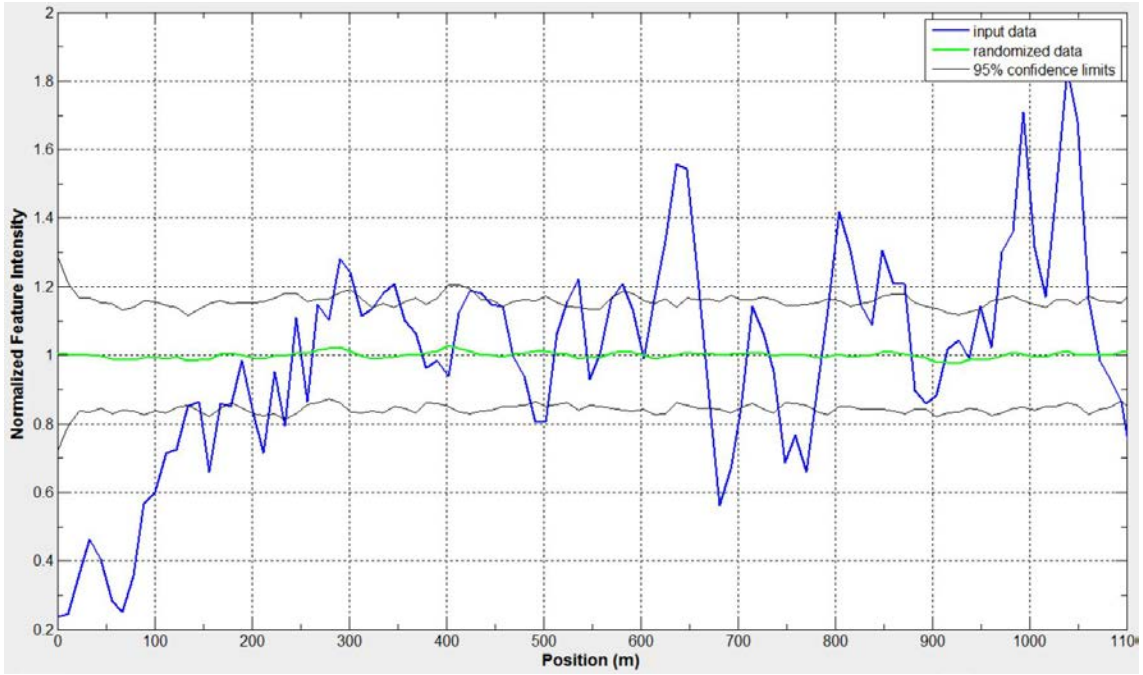


Figure 10-31 Intensity of all natural Set 1 fractures, Well HRB-1.

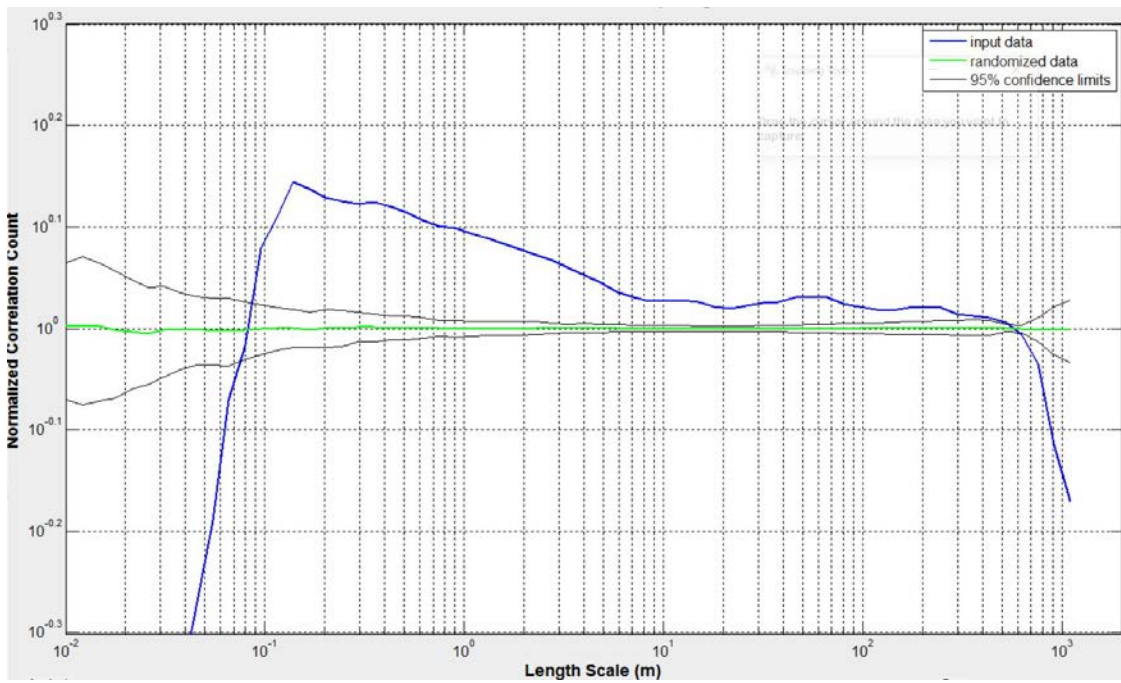


Figure 10-32 Correlation count of all natural Set 1 fractures, Well HRB-1.

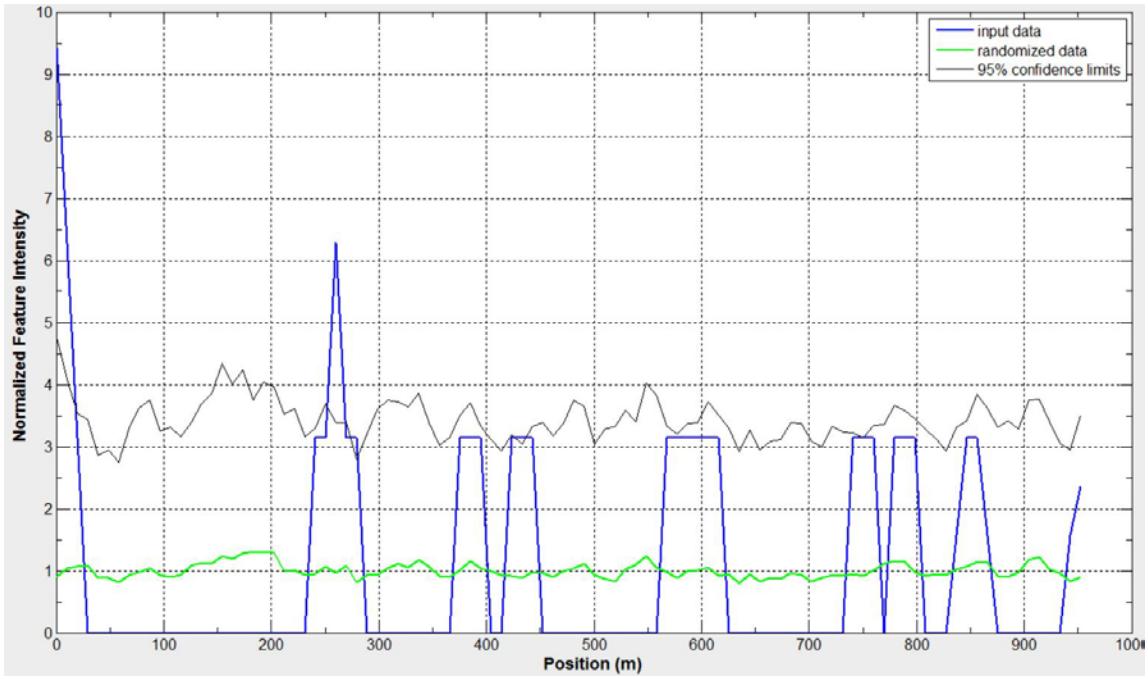


Figure 10-33 Intensity of faults, Well HRB-1.

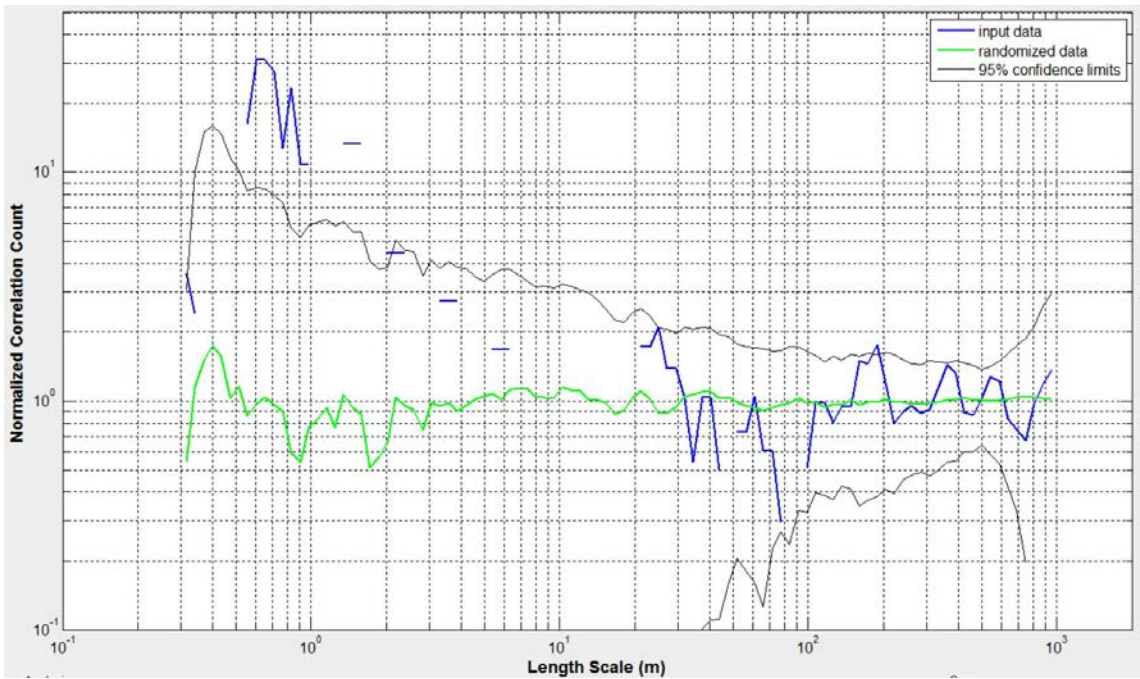


Figure 10-34 Correlation count of faults, Well HRB-1.

10.1.2 Intensity and correlation count, Well HRB-2

A total of 7086 fractures in Well HRB-2 are categorized as either conductive or 'healed' in the original image log. The healed fractures are resistive image log fractures that are presumably sealed and will be referred to as "sealed" hereinafter. No fracture in Well HRB-2 was picked as "drilling induced". Each conductive or sealed fracture can be further categorized into subsets by their strikes: Set 1 if striking NE-SW, Set 2 if NW-SE, and Set 3 if E-W. Table 7 summarizes the CorrCount-calculated statistics of the fracture subsets along with those of the three supersets containing all conductive and sealed fractures in the same strike subset. Figure 10-36 to Figure 10-63 show the normalized fracture intensity and the correlation count results for selected image fracture sequences in Well HRB-1. The true vertical depths (TVD) of the image log's interval is plotted against the associated measure depths (MD) for horizontal wellbore trajectory approximation and for reference of fracture intensity peak positions (Figure 10-35).

Well	Fracture type	Set (average strike)	# of fractures	Scanline length (m)	Mean spacing (m)	Standard deviation (m)	Min. spacing (m)	Max. spacing (m)	Cv	NCC figure #
HRB-2	Conductive	All (Mixed)	4416	1260.05	0.28	0.75	0.001	32.32	2.67	10-37
		Set 1 (NE-SW)	3967	1250.45	0.31	0.84	0.007	32.32	2.68	10-39
		Set 2 (NW-SE)	296	1246.77	4.19	16.39	0.031	204.19	3.91	10-42
		Set 3 (E-W)	153	1246.63	8.09	16.62	0.026	121.64	2.05	10-45
	Healed (i.e. sealed)	All (Mixed)	2670	1255.87	0.47	1.33	0.001	32.53	2.84	10-48
		Set 1 (NE-SW)	118	1246.60	10.47	19.72	0.043	124.03	1.88	10-50
		Set 2 (NW-SE)	1111	1247.59	1.12	5.36	0.002	141.00	4.78	10-53
		Set 3 (E-W)	1441	1247.92	0.87	2.00	0.004	32.53	2.31	10-56
	Natural (Conductive w/ Healed)	Set 1 (NE-SW)	4085	1249.05	0.30	0.83	0.002	32.32	2.71	10-59
		Set 2 (NW-SE)	1407	1106.88	0.79	2.06	0.002	34.94	2.62	10-61
Set 3 (E-W)		1594	1248.06	0.78	1.75	0.002	32.53	2.24	10-63	

Table 10-2 Statistical summaries on image log fracture sets in Horn River Basin Well HRB-2. Fracture sets in red contain NCC results for select internal high intensity interval(s) and are presented in Figures 10-64 to 10-67 for cross-well comparison.

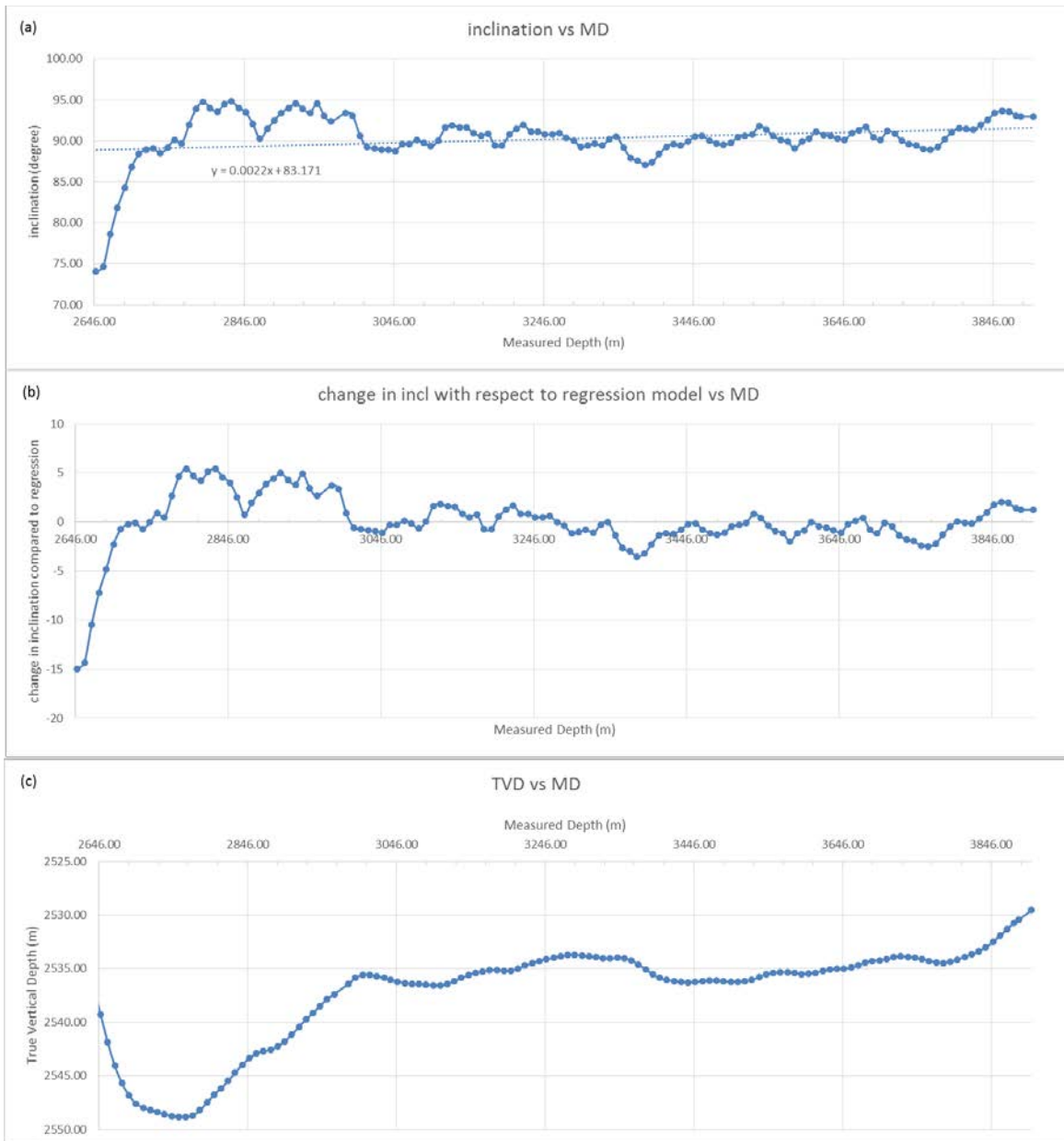


Figure 10-35 (a) Well HRB-2 inclination versus Measured Depth (m). (b) Change in inclination value with respect to best fit regression value. (c) True Vertical Depth of the wellbore with respect to Measured Depth. Measured Depth interval begins at the first sealed fracture observed.

Conductive fracture sets, HRB-2

A total of 4416 conductive fractures in three subsets by strikes are present in a 1260.05 m long wellbore interval. The average fracture spacing is 0.28 m, and the Cv is 2.67. The normalized fracture intensity curve contains numerous neighboring peaks that form a statistically significant high intensity interval extending approximately from the beginning of the interval to position 500 m (Figure 10-36). The portion of the curve from 600 m to the end largely fall beneath the lower confidence limit, indicating a statistically significant lack of fractures in the deeper half of the image log interval. The NCC curve (Figure 10-37) contains a single broad, smooth, and predominantly linearly decreasing elevated interval between length scales 0.07 m and 450 m.

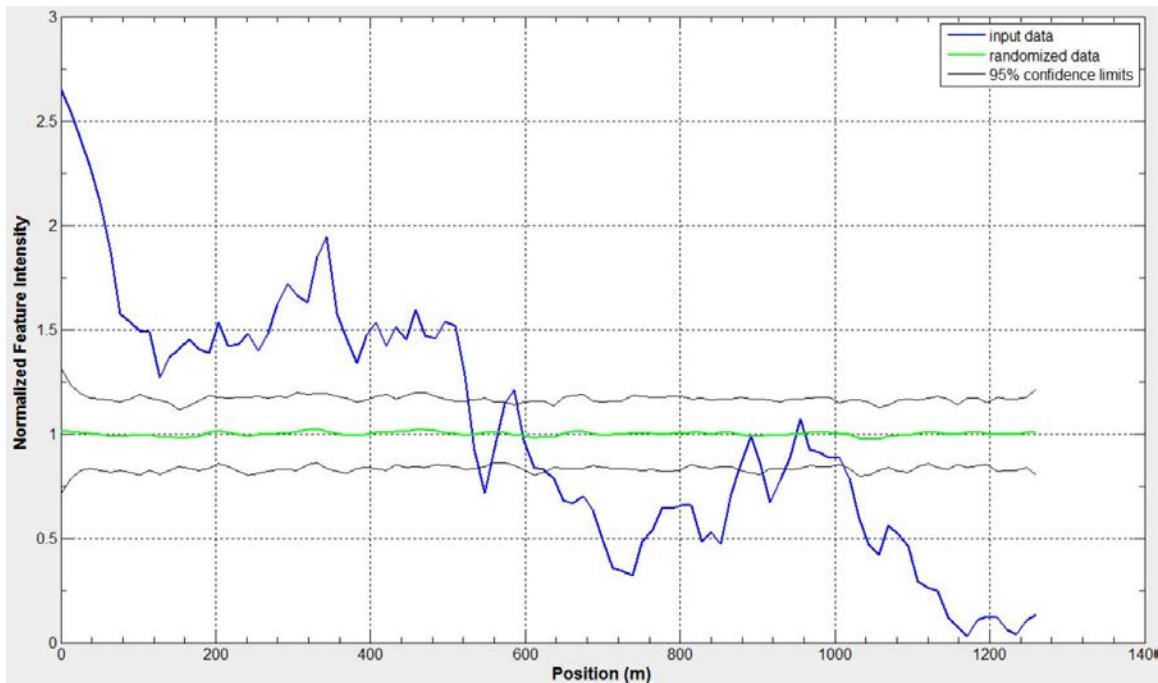


Figure 10-36 Intensity of all conductive fractures, Well HRB-2.

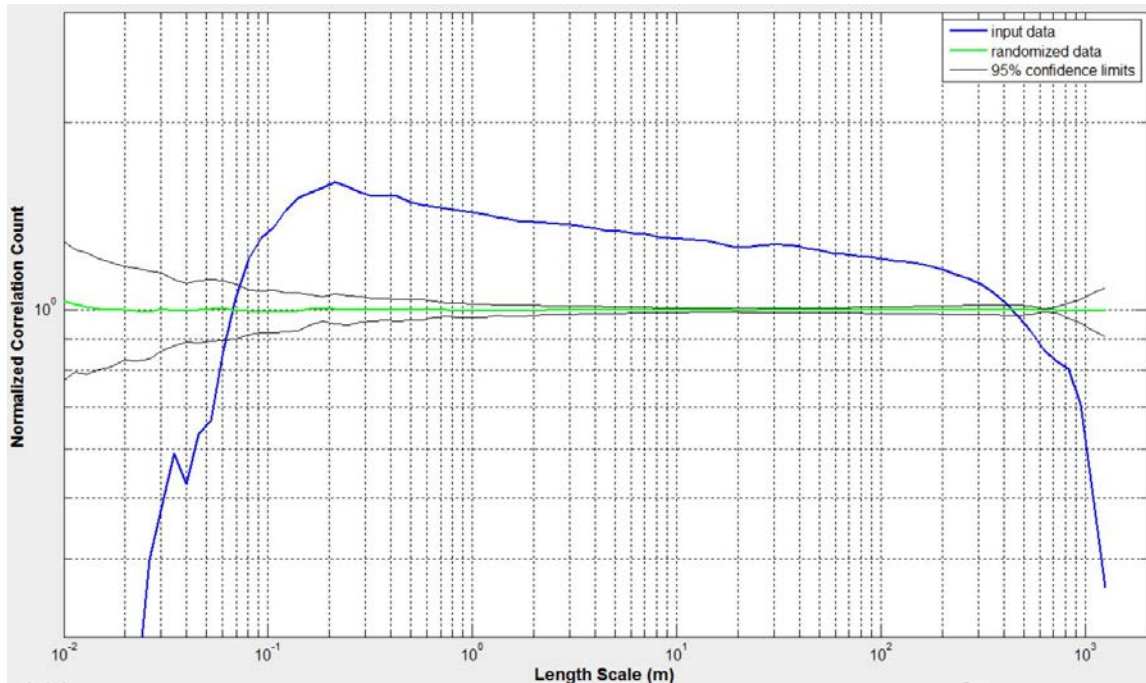


Figure 10-37 Correlation Count of all conductive fractures, Well HRB-2.

Conductive fractures in Well HRB-2 are divided into the NE-striking Set 1, NW-striking Set 2, or E-striking Set 3. Set 1 contains approximately 90% of all the conductive fractures whereas Set 3 only contains approximately 3.5%. Note that the Cv of Set 2 fractures is the highest of the three sets while the Cv of Set 3 is the lowest (Table 7).

There are 3967 conductive Set 1 fractures over an interval of 1250.45 m. The average fracture spacing is 0.31 m, and the Cv is 2.68. Both the normalized fracture intensity plot (Figure 10-38) and the NCC plot (Figure 10-39) for conductive Set 1 fractures mirror those for all conductive fractures (Figures 10-36, 10-37). Note that although the results for Set 1 and Set “All” of the conductive fractures (and of the sealed fractures to be presented soon) are visually similar, those for Set 1 are geologically meaningful while those for the latter are not and are included for completeness sake. NCC analysis of the

3066 conductive Set 1 fractures concentrated in high intensity interval between positions 0 and 600 m reveals a negatively sloped elevated correlation interval from length scale 0.2 to 15 m followed by a peak at 30 m (Figure 10-40). Note that the correlation count peak at 30 m can be seen embedded in the NCC curve for the overall set (Figure 10-39).

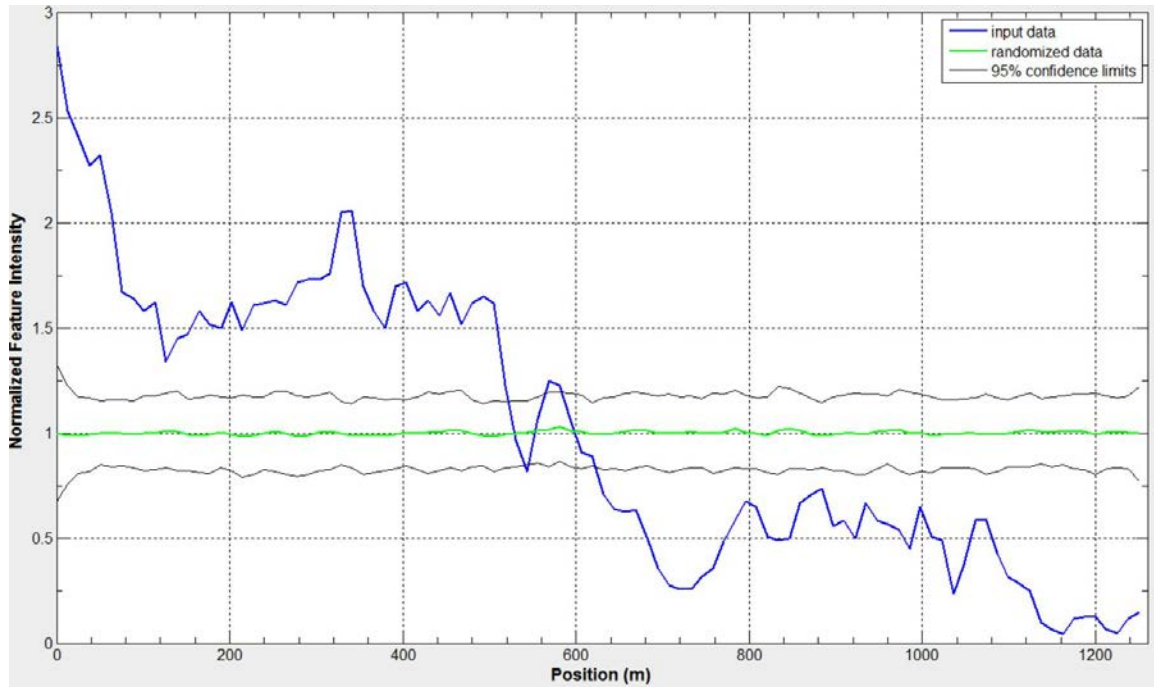


Figure 10-38 Intensity of conductive Set 1 fractures, Well HRB-2.

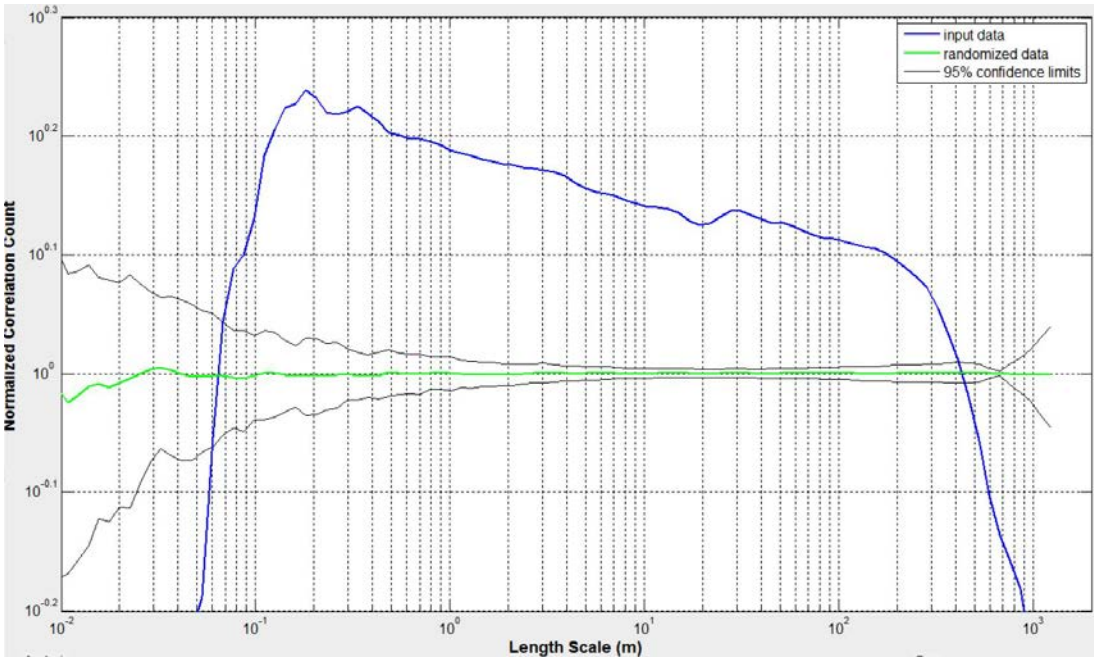


Figure 10-39 Correlation count of conductive Set 1 fractures, Well VM-A.

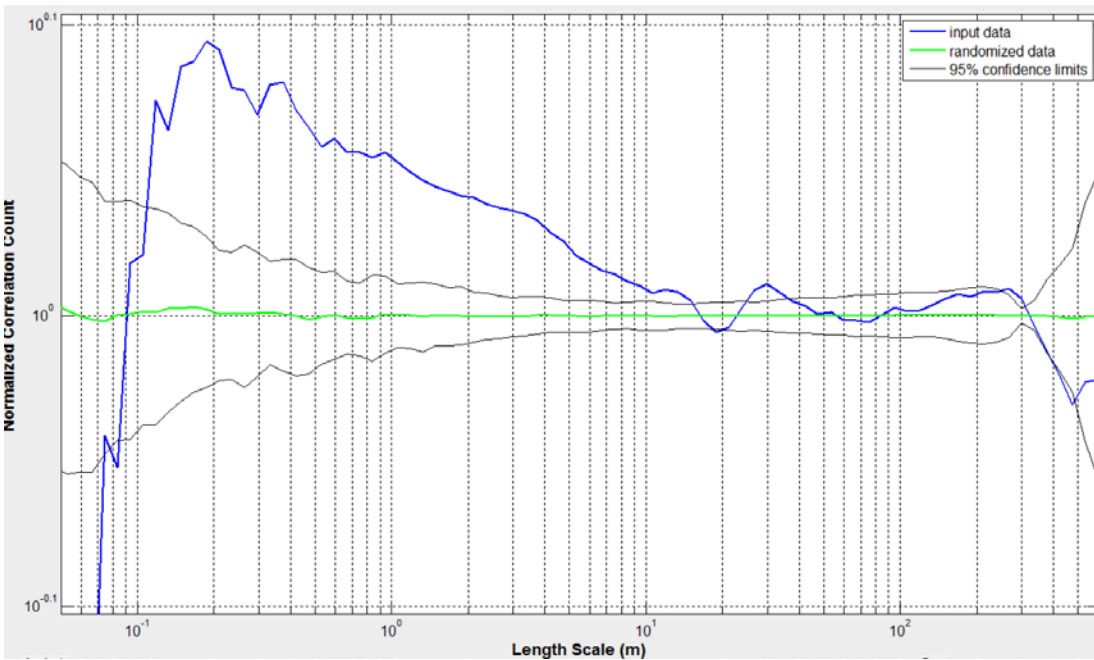


Figure 10-40 Correlation count of conductive Set 1 fractures, intensity plot position 0 to 600 m, Well HRB-2.

There are 296 conductive Set 2 fractures over an interval of 1246.77 m. The average fracture spacing is 4.19 m, and the Cv is 3.91. The normalized fracture intensity curve is mostly beneath the lower confidence limit in the 600 m of the interval (Figure 10-41). The first peak is located approximately at position 760 m, and the intensity curve remains above the upper limit from 840 m to 1040 m due to multiple overlapped tall peaks. The NCC plot (Figure 10-42) is statistically significant for all length scales greater than 0.06 m and less than 280 m. The curve overall trends negatively and has visible internal peaks at length scales 30 m, 60 m, and 200 m. NCC analysis of the 204 fractures (~70% of the 296 fractures) in the high intensity interval between positions 820 and 1060 m reveals a negatively sloped correlation interval for length scales less than 10 m followed by a double hump at length scales 30 and 65 m (Figure 10-43).

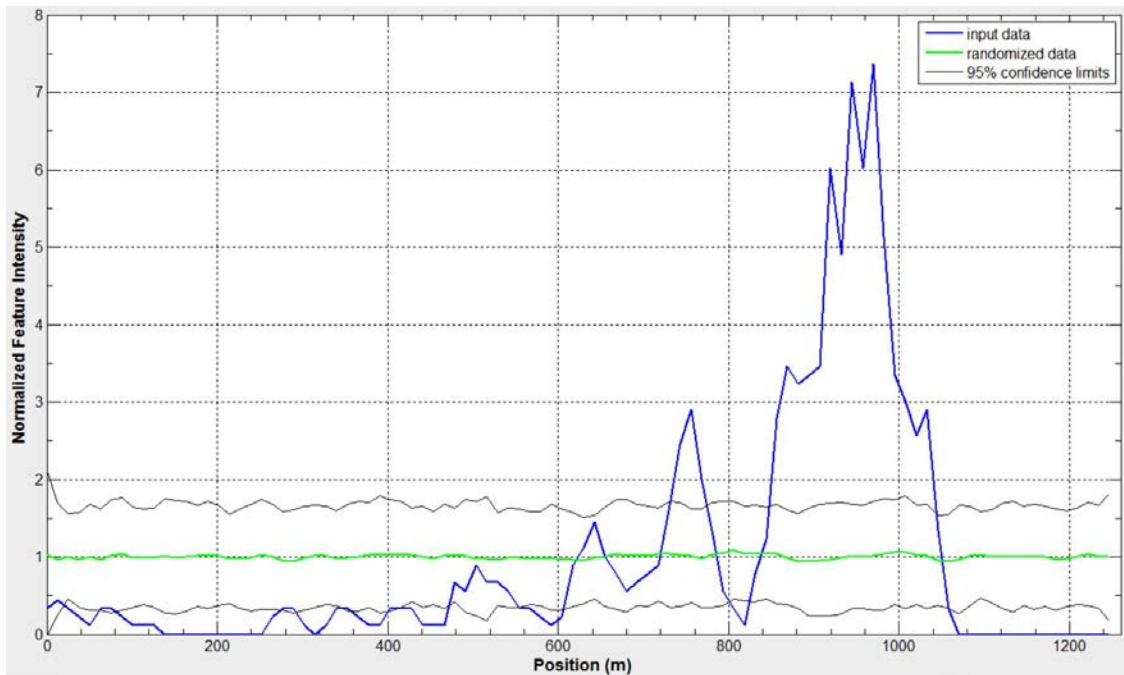


Figure 10-41 Intensity of conductive Set 2 fractures, Well HRB-2.

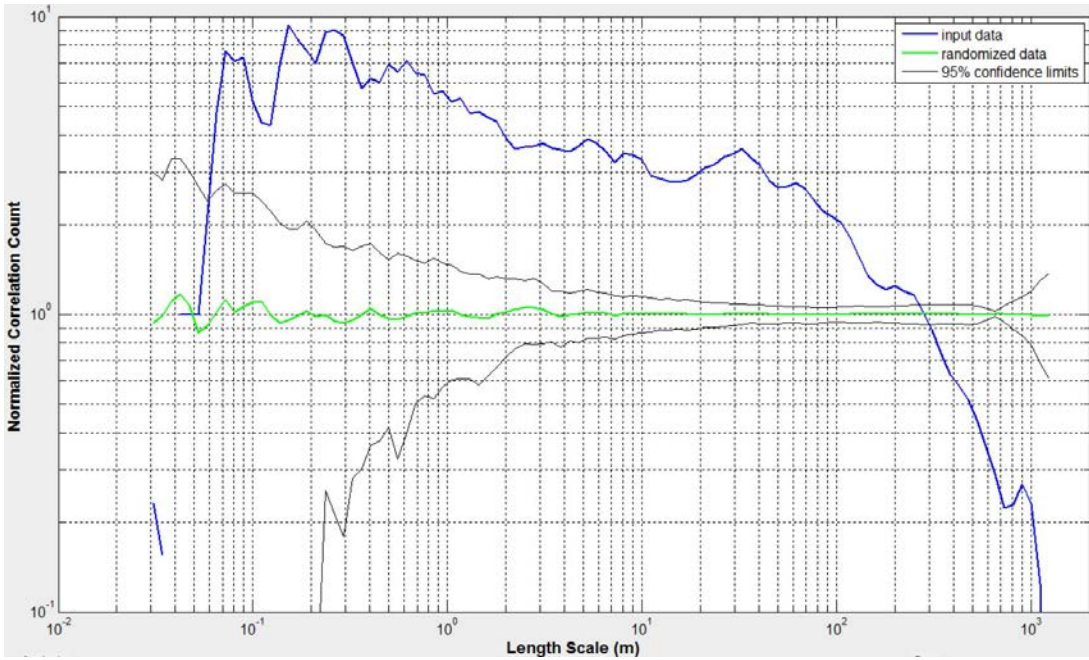


Figure 10-42 Correlation count of conductive Set 2 fractures, Well HRB-2.

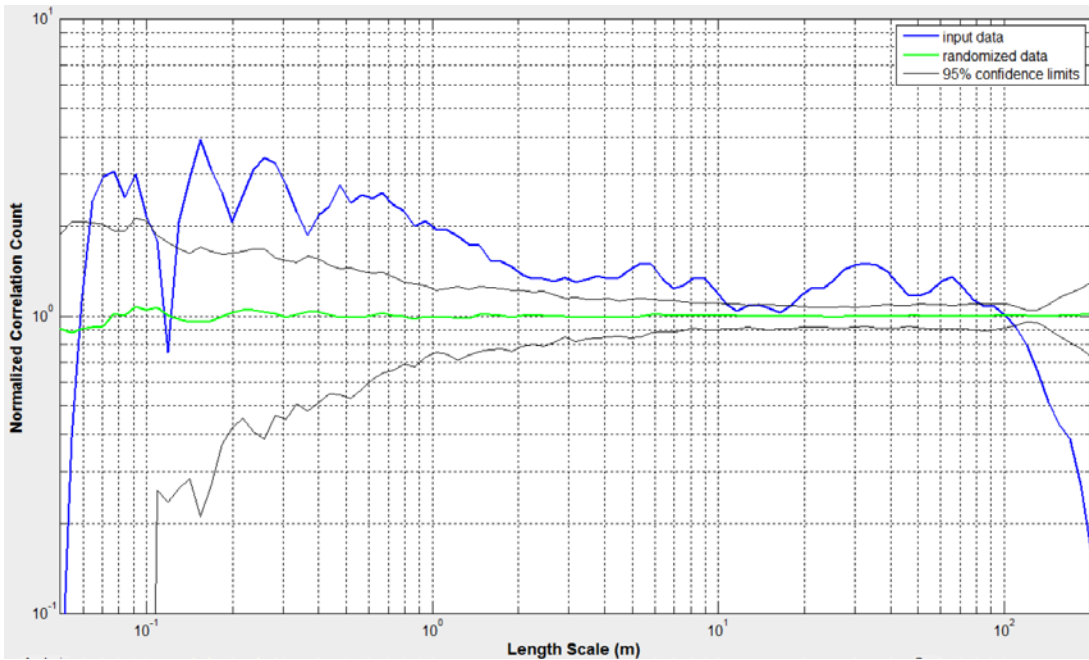


Figure 10-43 Correlation count of conductive Set 2 fractures, intensity plot position 820 to 1060 m, Well HRB-2

There are 153 conductive Set 3 fractures over an interval of 1246.63 m. The average fracture spacing is 8.09 m, and the Cv is 2.05. The normalized fracture intensity curve (Figure 10-44) peaks greatly at the beginning of the scanline and, after four smaller yet still statistically significant peaks approximately at positions 90, 140, 190 m, and 280 m, becomes statistically indistinguishable from random in the remaining of the interval. The NCC plot (Figure 10-45) contains a broad elevated section for length scales less than 4 m. The slope of the interval rapidly decreases between 1 m and 4 m. Multiple statistically significant and sometimes overlapped peaks appear subsequently at 6, 7.5, 9, 20, 35, 70, 100, and 170 m, and troughs appear near 45, 200, 350, and 500 m. NCC analysis of the 35 fractures in the highest intensity peak before position 80 m reveals an elevated correlation region that crosses the random data curve at approximately 3.5 m and is followed by a broad peak near 8 m (Figure 10-46). There is a statistically significant lack of correlation count for length scales larger than approximately 22 m.

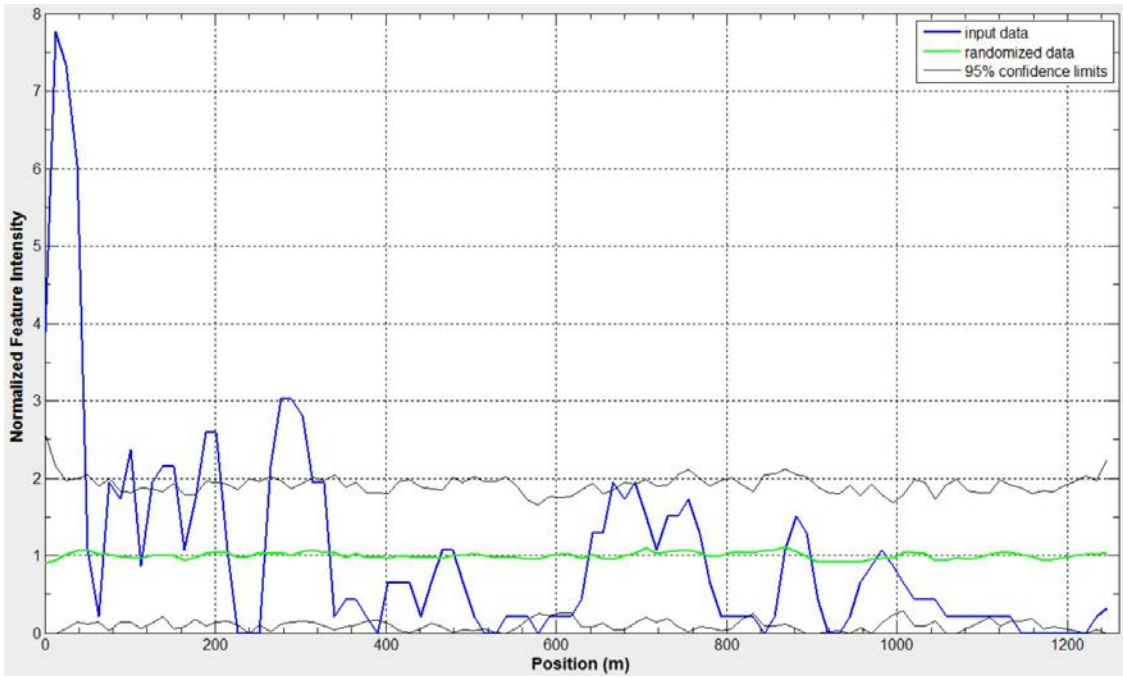


Figure 10-44 Intensity of conductive Set 3 fractures, Well HRB-2.

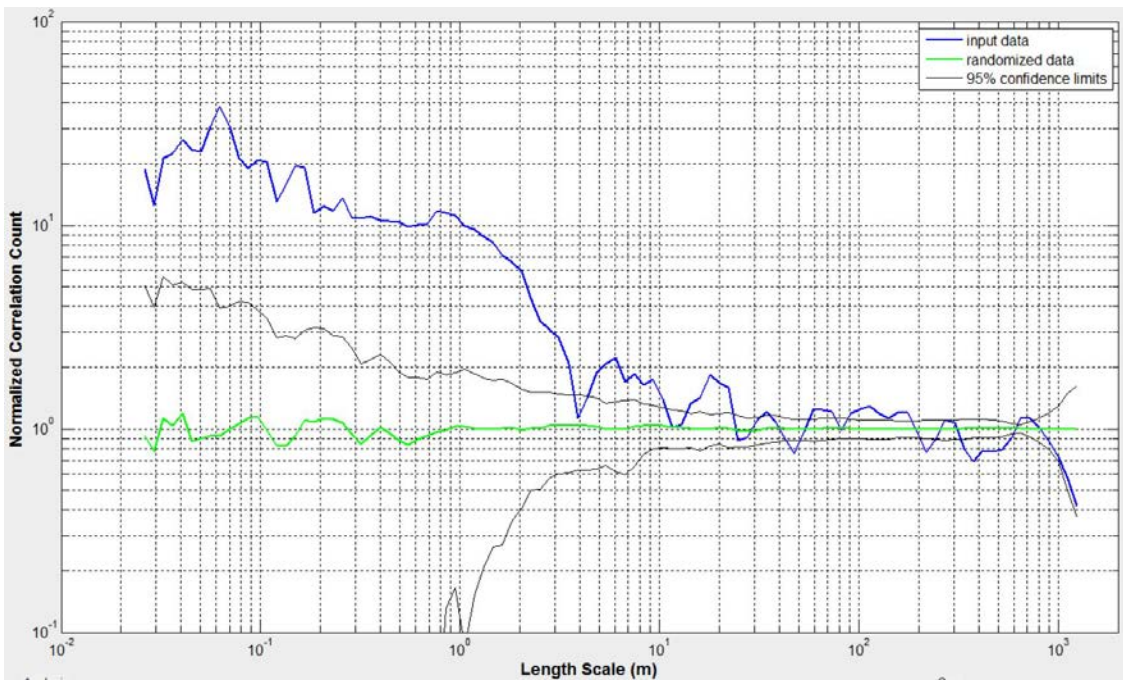


Figure 10-45 Correlation count of conductive Set 3 fractures, Well HRB-2

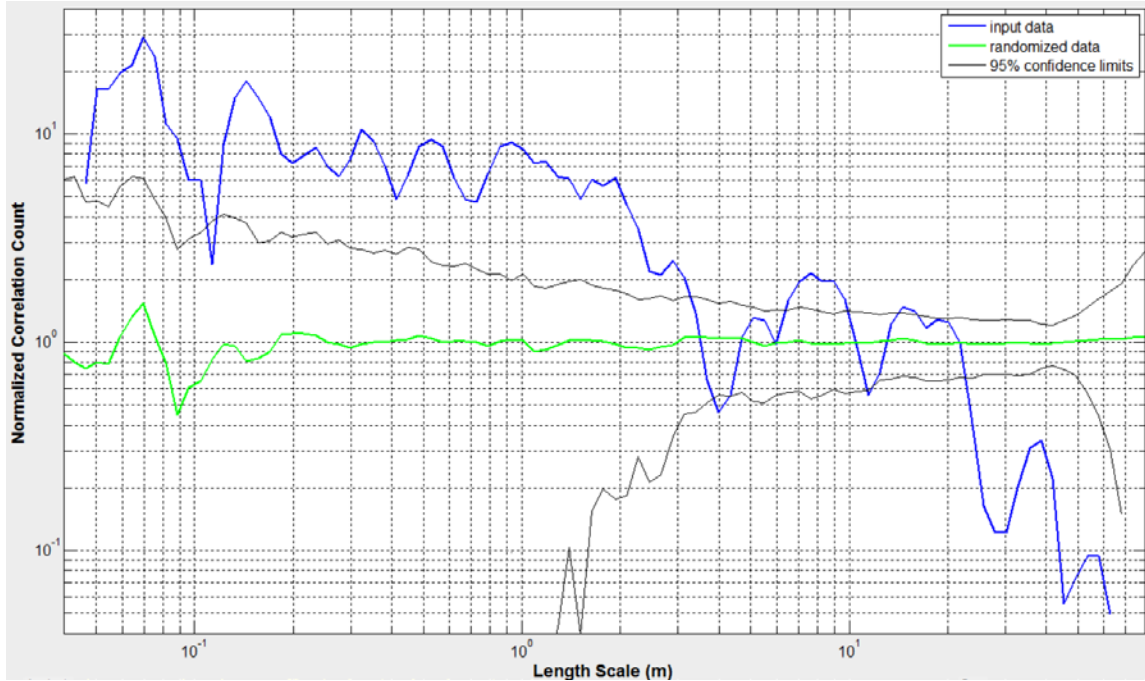


Figure 10-46 Correlation count of conductive Set 3 fractures, intensity position 0 to 80 m, Well HRB-2.

Sealed fracture sets, HRB-2

A total of 2670 sealed fractures were found over an interval of 1255.87 m. The average fracture spacing is 0.47 m, and the Cv is 2.84. The normalized fracture intensity plot (Figure 10-47) shows four high intensity intervals between 0 and 600 m with widths decreasing from 180 m for the first interval to 30 m for the last. An extended trough is present between position 760 m and the end of the interval. The NCC plot (Figure 10-48) shows a smooth, broad elevated section for length scales between 0.02 to 400 m. Spatial correlation for length scales less than approximately 0.002 m is statistically indistinguishable from random.

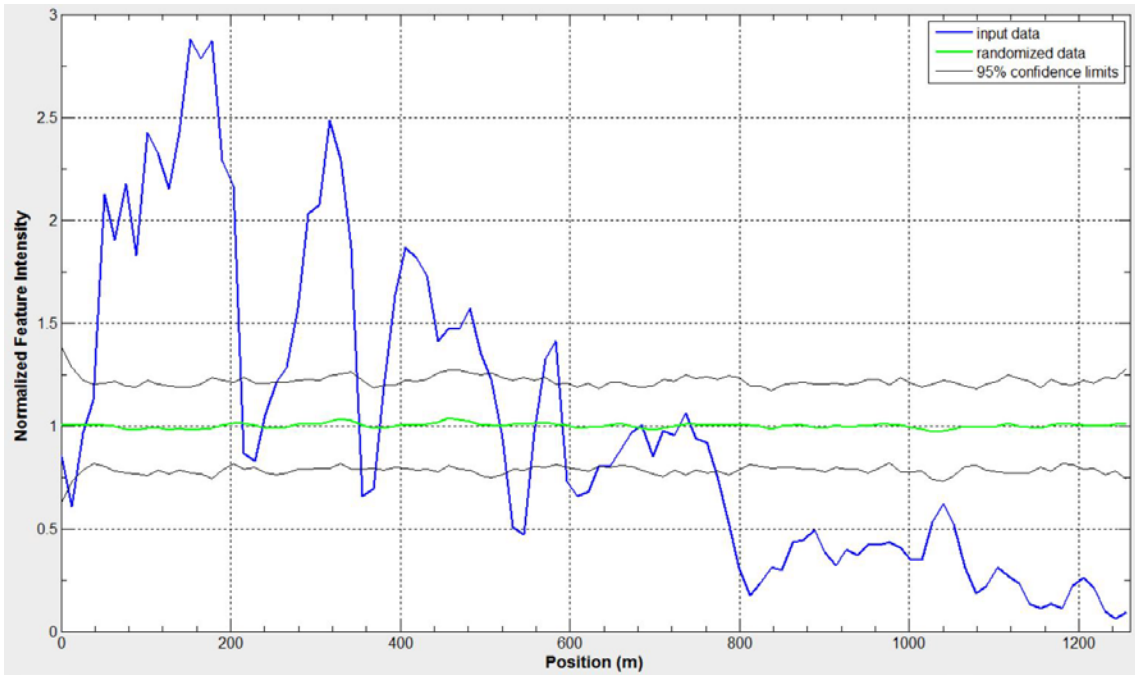


Figure 10-47 Intensity of all sealed fractures, Well HRB-2

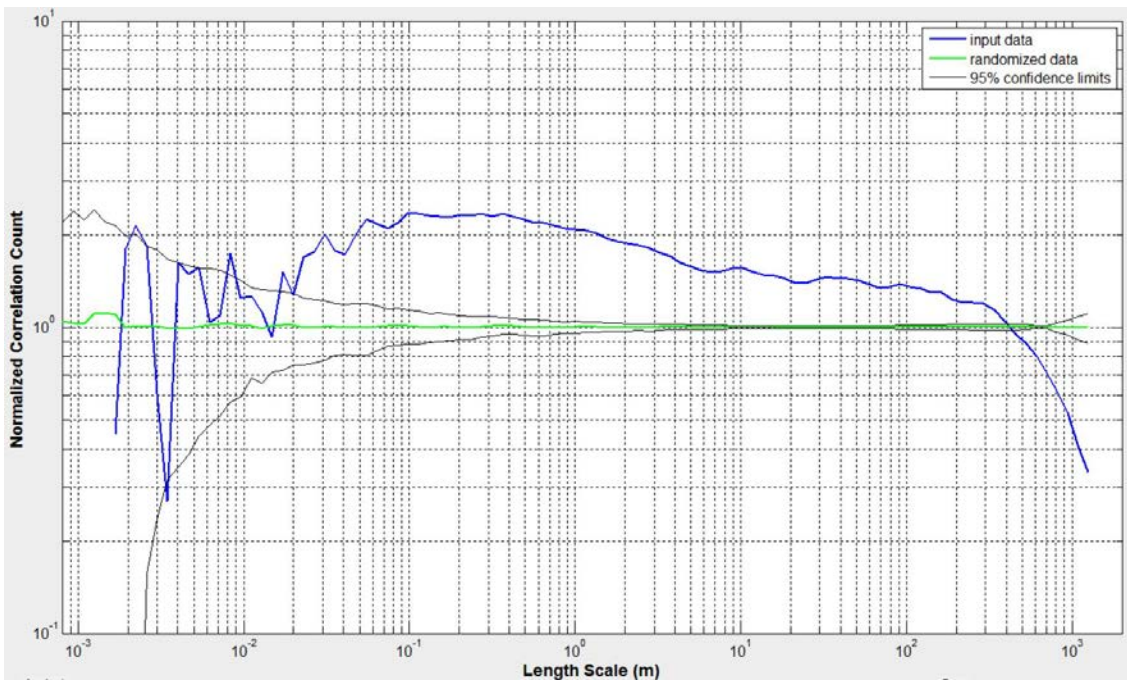


Figure 10-48 Correlation count of all fractures, Well HRB-2.

Sealed fractures in Well HRB-2 can also be separated into three sets by fracture strikes similar to the categorization of the conductive fractures (Table 7). Opposite of the distribution of Well HRB-2's conductive fractures where most of them are found in Set 1 and fewest are in Set 3, less than 5% of all the sealed fractures in Well HRB-2 belong in Set 1 while more than half (54%) are in the E-striking Set 3. Note that, similar to how the Cv of conductive Set 2 fractures rank, sealed Set 2 fractures also has the highest Cv out of the three sets.

There are 118 sealed Set 1 fractures over an interval of 1246.60 m. The average fracture spacing is 10.47 m, and the Cv is 1.88. The normalized fracture intensity plot (Figure 10-49) contains a single high intensity peak between positions 200 m and 300 m. Fracture intensity values elsewhere in the curve are statistically indistinguishable from those of a random set. The NCC curve is (Figure 10-50) statistically significant for length scales less than 90 m that contains multiple internal peaks. Spatial correlation overall decreases steadily from length scale 0.4 m to 7 m, at which point the curve reverses the trend and rises to a significant peak at 14 m where it again begins descending. The curve crosses the randomized data curve at length scale 100 m and peaks afterward near 180 m. NCC analysis of the 71 fractures (60% of the original 118 fractures) in the high intensity interval between positions 100 and 350 m two elevated, decreasing correlation intervals (Figure 10-51). It resembles the shape of correlation curve from the complete set except that the length scales from 6 to 8 m are no longer statistically significant and that the previous peak at length scale 180 m is absent.

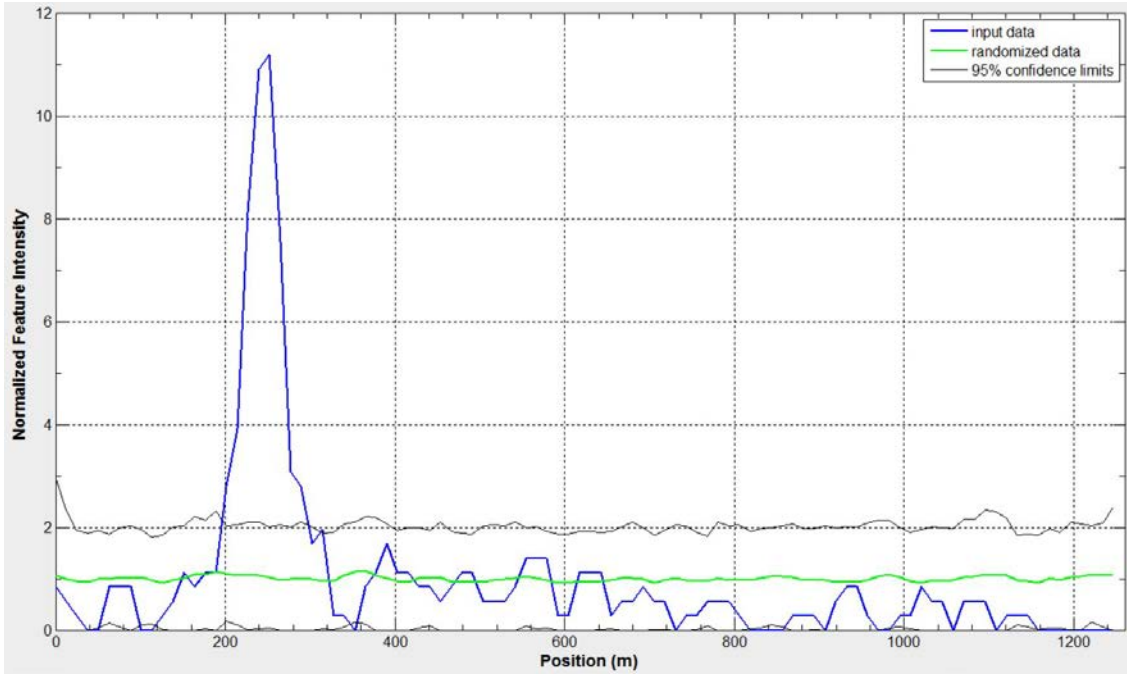


Figure 10-49 Intensity of sealed Set 1 fractures, Well HRB-2.

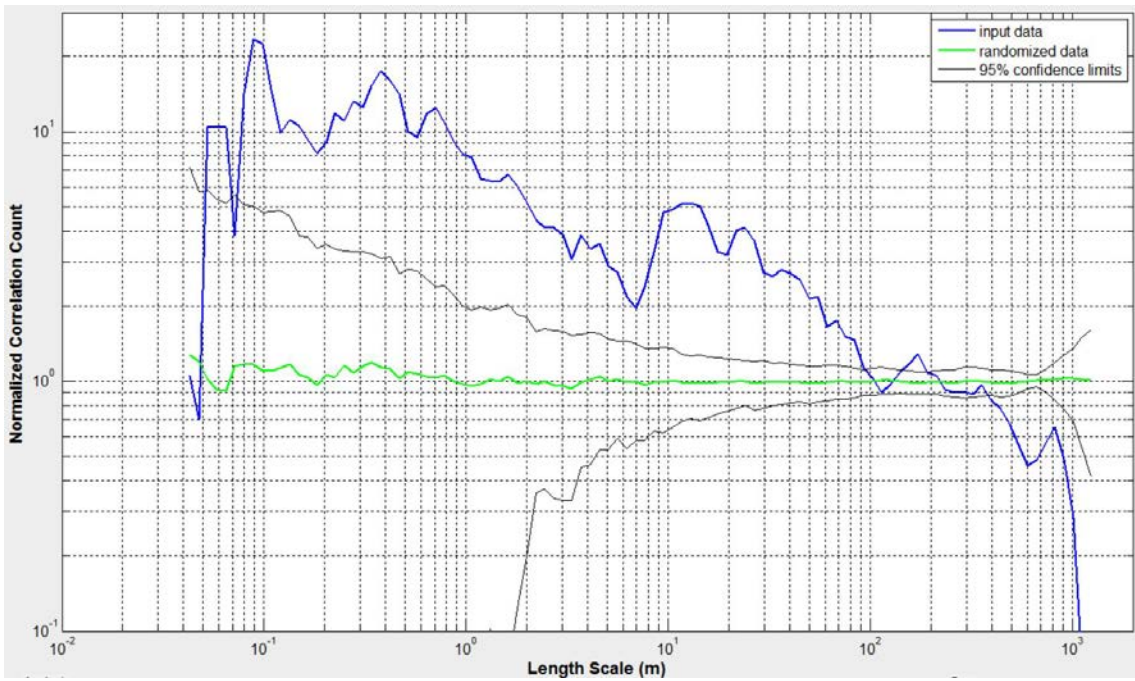


Figure 10-50 Correlation count of sealed Set 1 fractures, Well HRB-2.

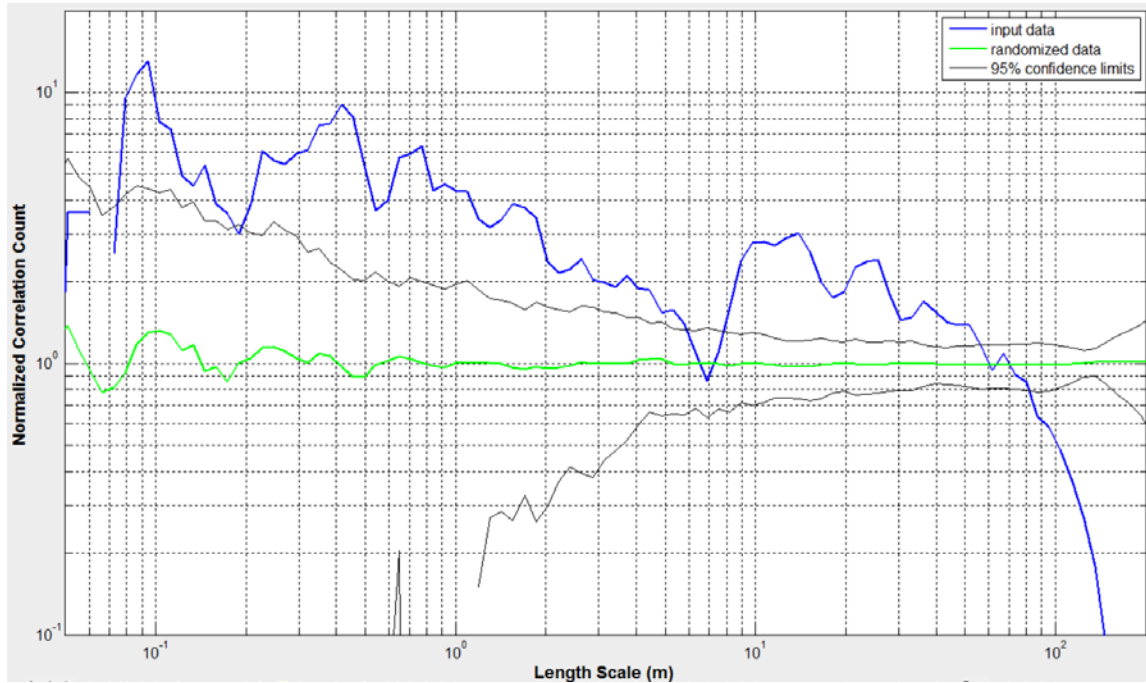


Figure 10-51 Correlation count of sealed Set 1 fractures, intensity position 100 to 350 m, Well HRB-2.

There are 1111 sealed Set 2 fractures over an interval of 1247.59 m. The average fracture spacing is 1.12 m, and the C_v is 4.78. The normalized fracture intensity plot (Figure 10-52) contains multiple high intensity peaks in approximately four groups before position 600 m. There is a statistically significant lack of fractures at the 95% confidence level beyond position 640 m. The NCC plot (Figure 10-53) is statistically significant for all length scales between approximately 0.03 and 450 m. NCC analysis of the high intensity zone before position 650 m that collectively contains 1043 fractures (~ 94% of all sealed Set 2 fractures) reveals an elevated, decreasing correlation interval that crosses the random data curve at 20 m before peaking again at 30 m (Figure 10-54).

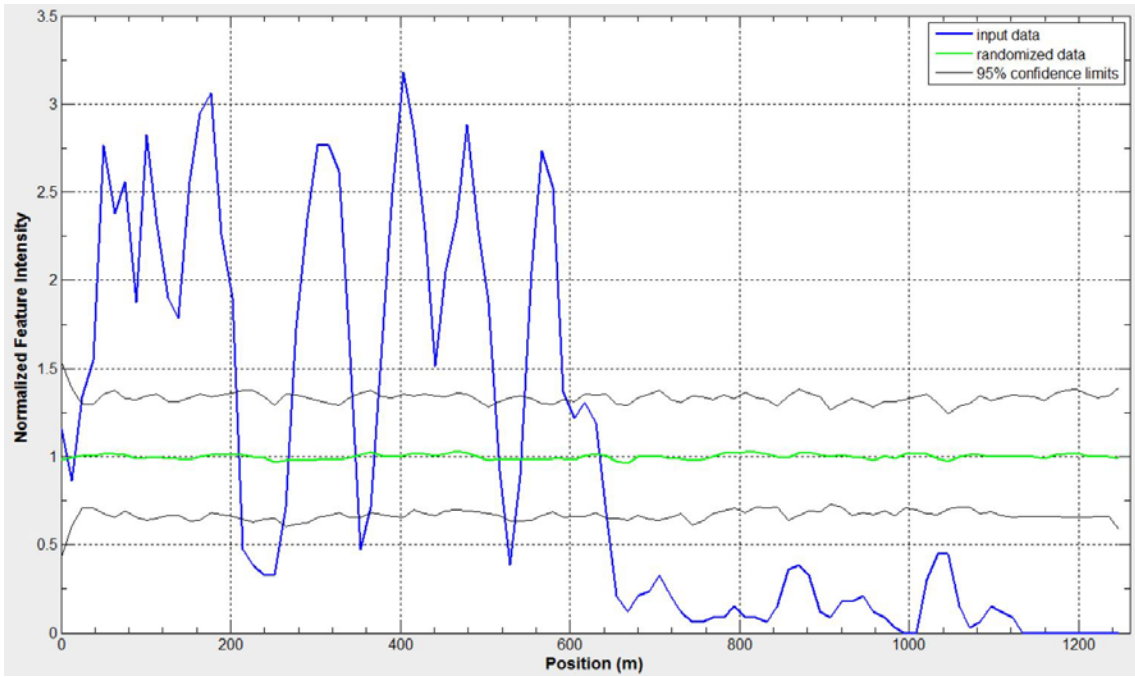


Figure 10-52 Intensity of sealed Set 2 fractures, Well HRB-2.

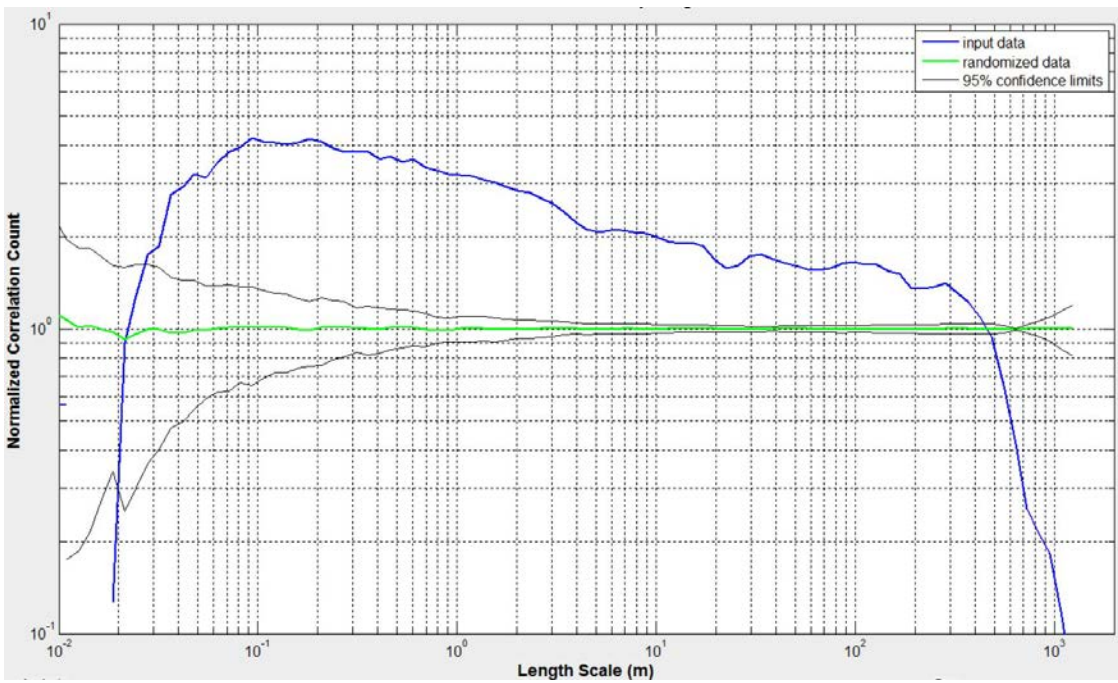


Figure 10-53 Correlation count of sealed Set 2 fractures, Well HRB-2

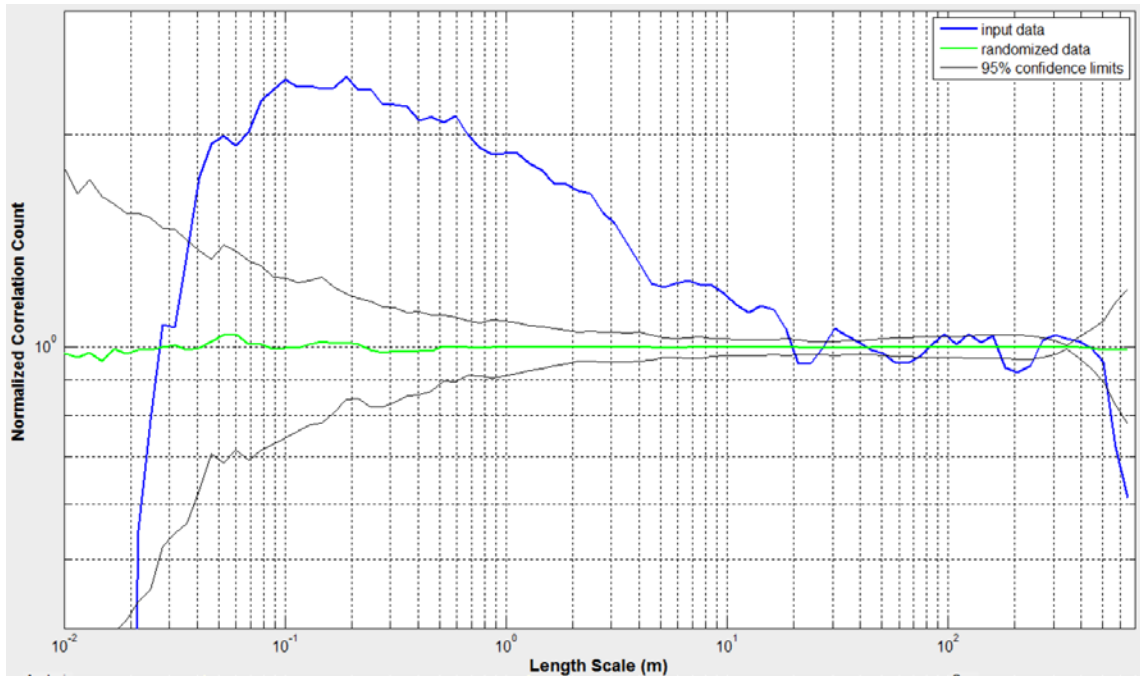


Figure 10-54 Correlation count of sealed Set 2 fractures, intensity position 0 to 650 m, Well HRB-2.

There are 1441 sealed Set 3 fractures over an interval of 1247.92 m. The average fracture spacing is 0.87 m, and the C_v is 2.31. The normalized fracture intensity plot (Figure 10-55) contains three separate high intensity intervals with widths from 180 to 60 m. The NCC plot (Figure 10-56) contains a wide elevated decreasing correlation interval from 0.05 to approximately 300 m. NCC analysis of the 495 fractures in the high intensity interval between positions 20 and 220 m reveals a saw-toothed and broad elevated correlation interval for length scales between 0.2 and 70 m (Figure 10-57). An off-trended drop in spatial correlation occurs for length scales between 10 and 20 m.

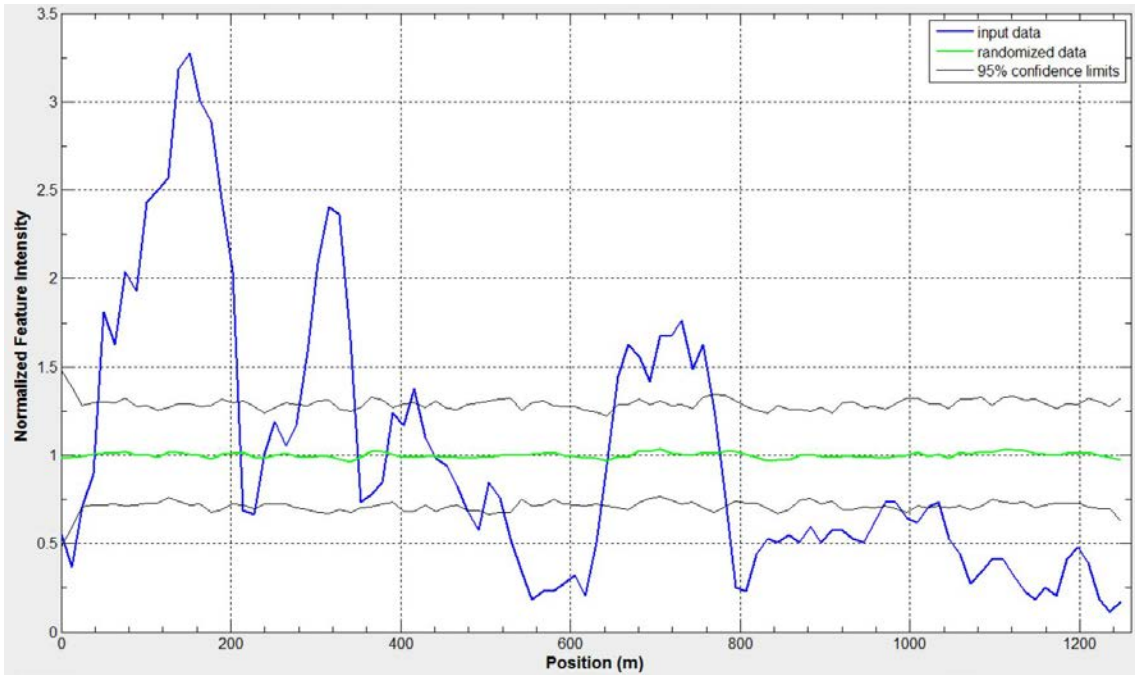


Figure 10-55 Intensity of sealed Set 3 fractures, Well HRB-2.

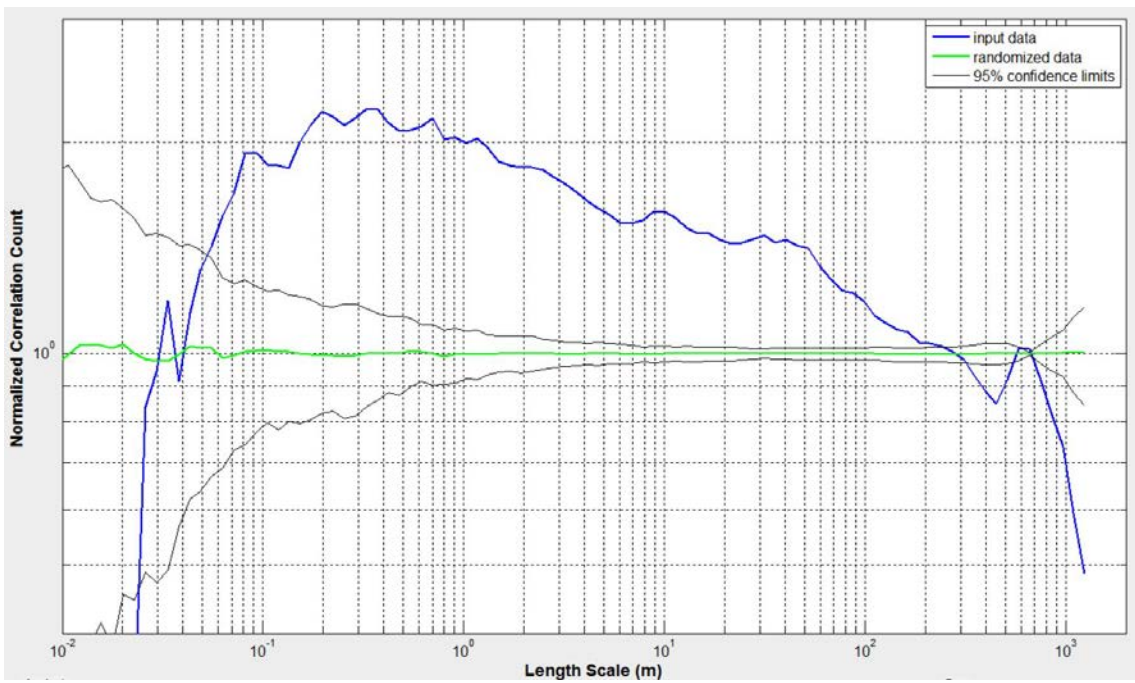


Figure 10-56 Correlation count of sealed Set 3 fractures, Well HRB-2.

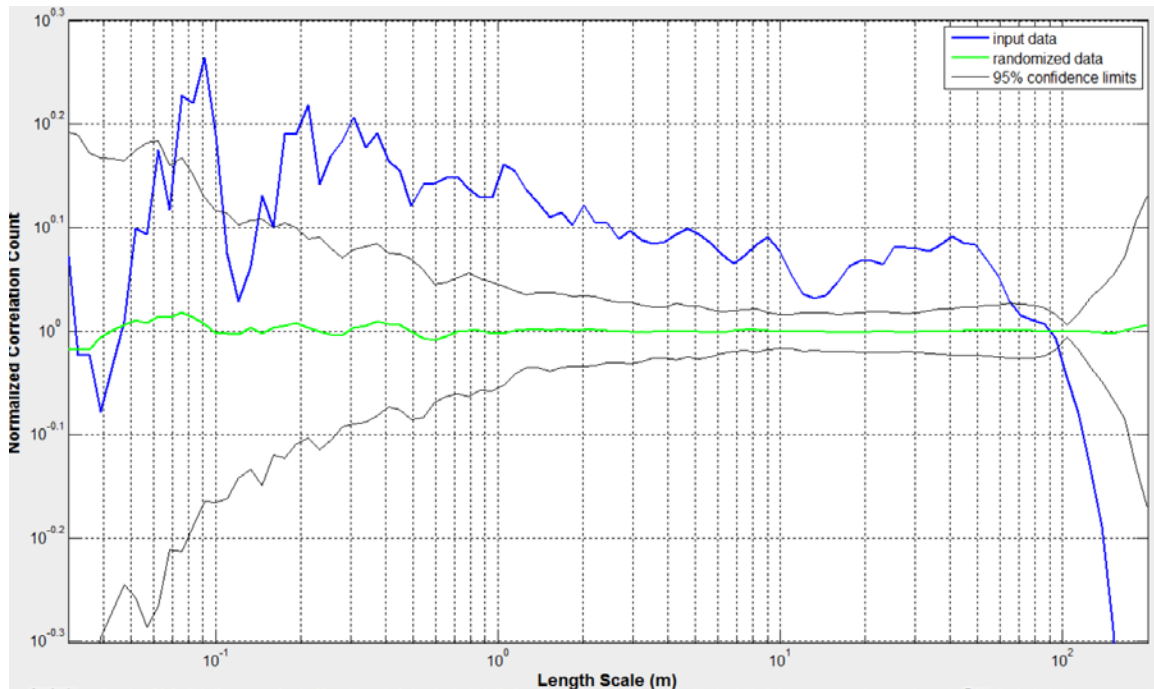


Figure 10-57 Correlation count of sealed Set 3 fractures, intensity position 20 to 220 m, Well HRB-2.

Natural fracture supersets, HRB-2

Three natural fracture supersets – Set 1, 2, and 3 – were created to study spacings between conductive and sealed fractures in Well HRB-2 that share similar orientations. The NE-striking superset, Set 1, contains 4085 fractures over a 1249.05 m interval. The average spacing is approximately 0.30 m, and the Cv is approximately 2.71. The Normalized intensity plot (Figure 10-58) contains a statistically significant high intensity interval from zero to approximately 550 m. A trough interval from near 600 m to the end of the scanline. The NCC curve (Figure 10-59) is above the upper 95% confidence limit for all length scales between 0.07 m and 400 m. The interval from 0.2 to 200 decreases near-linearly with a small internal peak visible at 30 m. Both the intensity and the NCC plots are similar in shapes to those of conductive Set 1 fractures (Figures 10-38, 10-39).

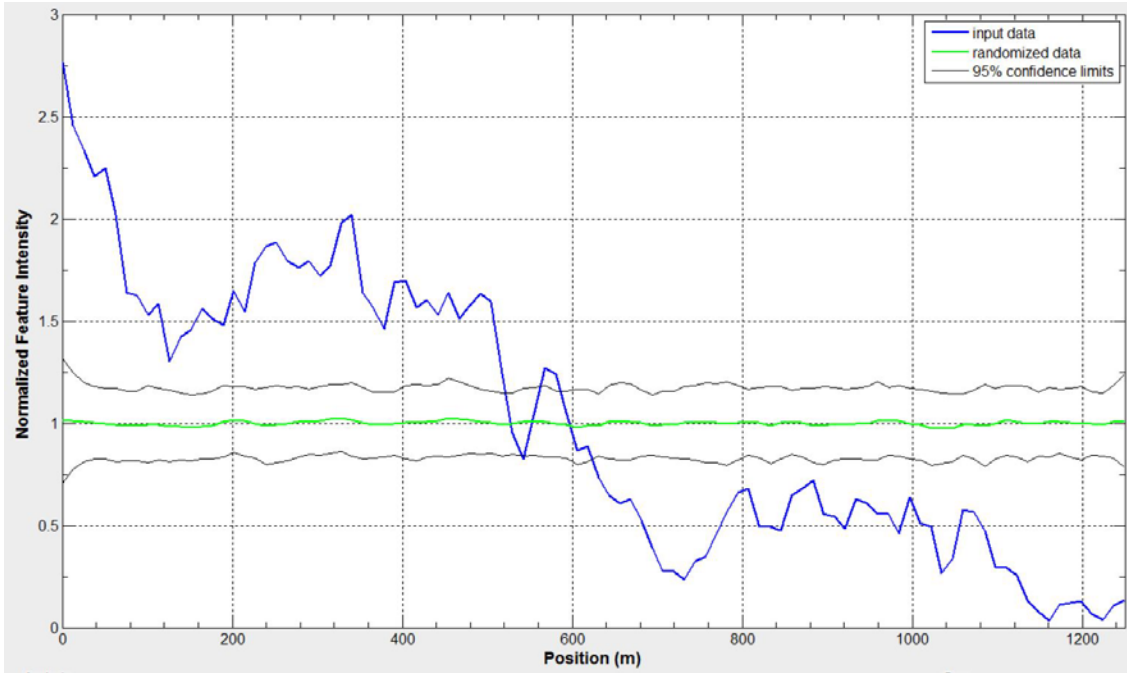


Figure 10-58 Intensity of all Set 1 natural fractures, Well HRB-2.

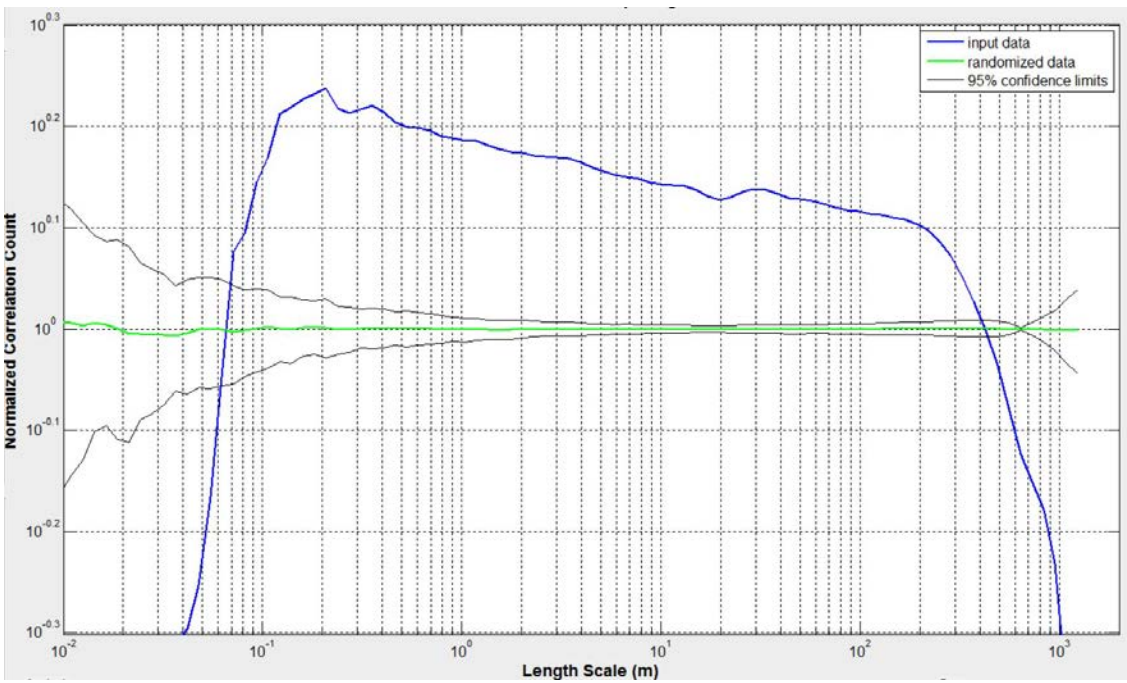


Figure 10-59 Correlation count of all Set 1 natural fractures, Well HRB-2.

The NW-striking superset Set 2 contains 1407 fractures over a 1106.88 m interval. The average spacing is approximately 0.79 m, and the Cv is approximately 2.62. The Normalized intensity plot (Figure 10-60) contains approximately 50-m-wide peaks distributed semi-periodically every 70 to 100 m in the first 600 m. Three troughs are present between the peaks. A wide trough interval extends from approximately 650 m to 850 m. The largest trough is present in the last 50 m of the scanline. The NCC curve (Figure 10-61) decreases approximately linearly over length scales less than 20 m. Two peaks are present at 30 and 80 m before the curve intercepts the randomize data curve at approximately 180 m. A broad hump then reemerges in the curve between length scales 300 and 400 m. This superset's intensity and NCC plots resemble those of sealed Set 2 fractures (Figures 10-52, 10-53).

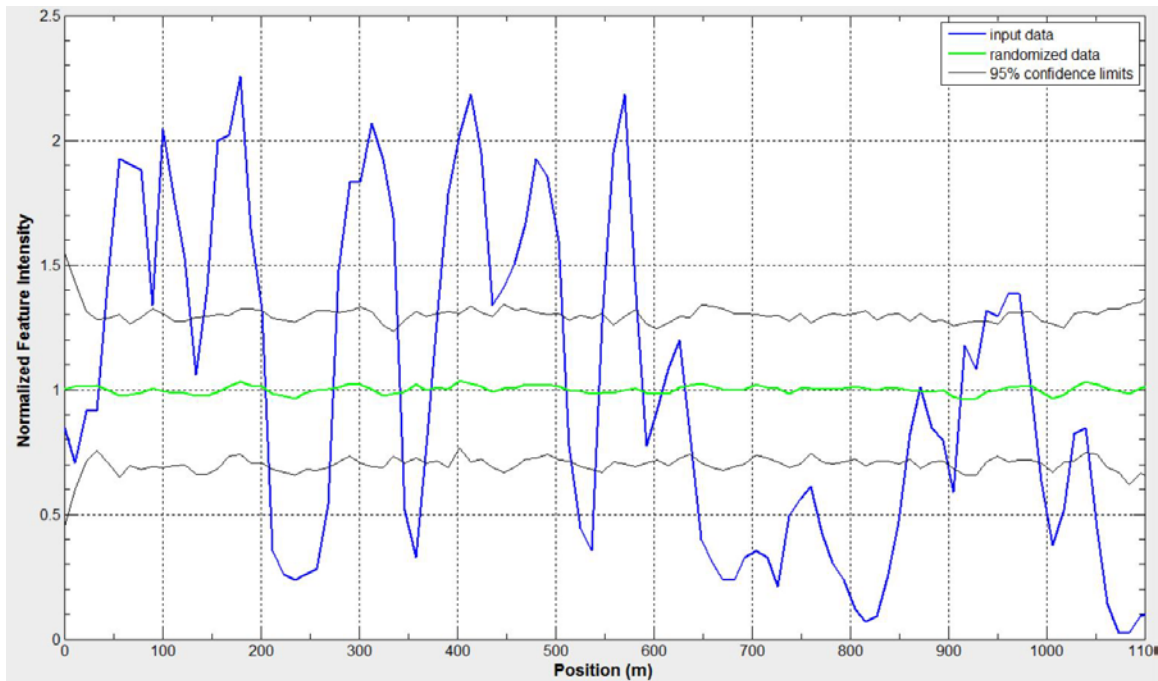


Figure 10-60 Intensity of all Set 2 natural fractures, Well HRB-2.

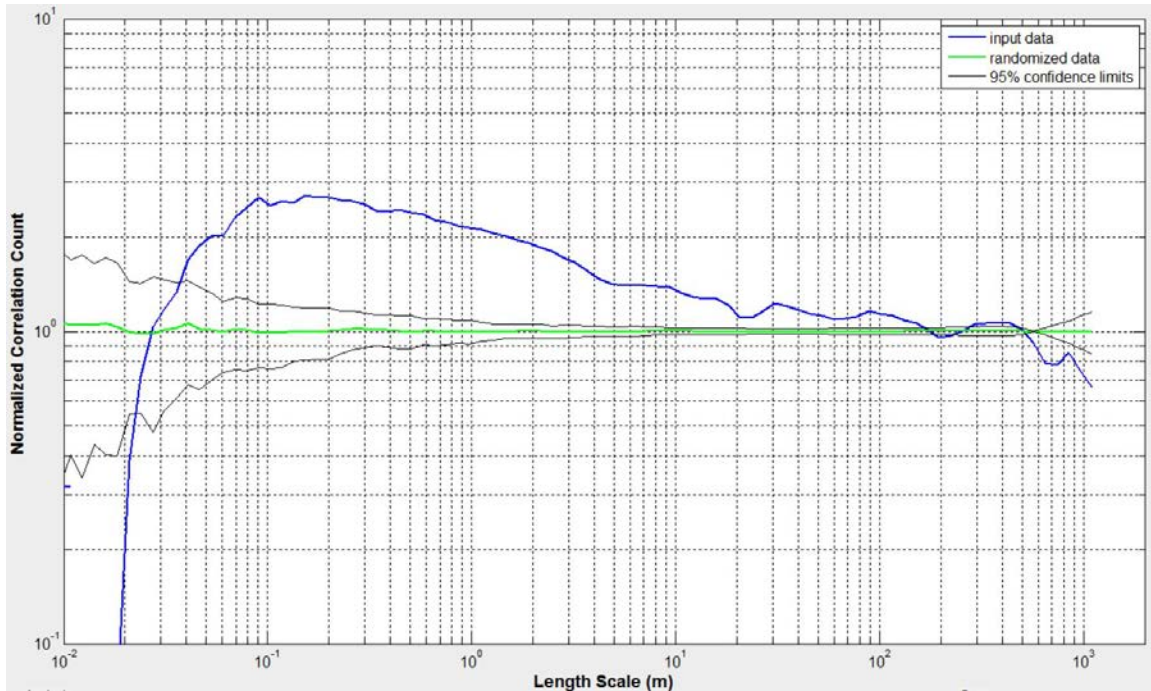


Figure 10-61 Correlation count of all Set 2 natural fractures, Well HRB-2.

The EW-striking superset Set 3 contains 1594 fractures over a 1248.06 m interval. The average spacing is approximately 0.78 m, and the Cv is approximately 2.24. The Normalized intensity plot (Figure 10-62) contains three peak intervals formed by smaller overlapped neighboring peaks and are centered on 120, 320, and 720 m, respectively. The intensity curve is under the lower 95% confidence limit for the scanline portion beyond 780 m. The NCC plot (Figure 10-63) contains a gradually decreasing elevated portion that crosses the randomized data curve at length scale 200 m and bottoms at 400 m subsequently. Both Figures resemble those of sealed Set 3 fractures (Figures 10-55, 10-56).

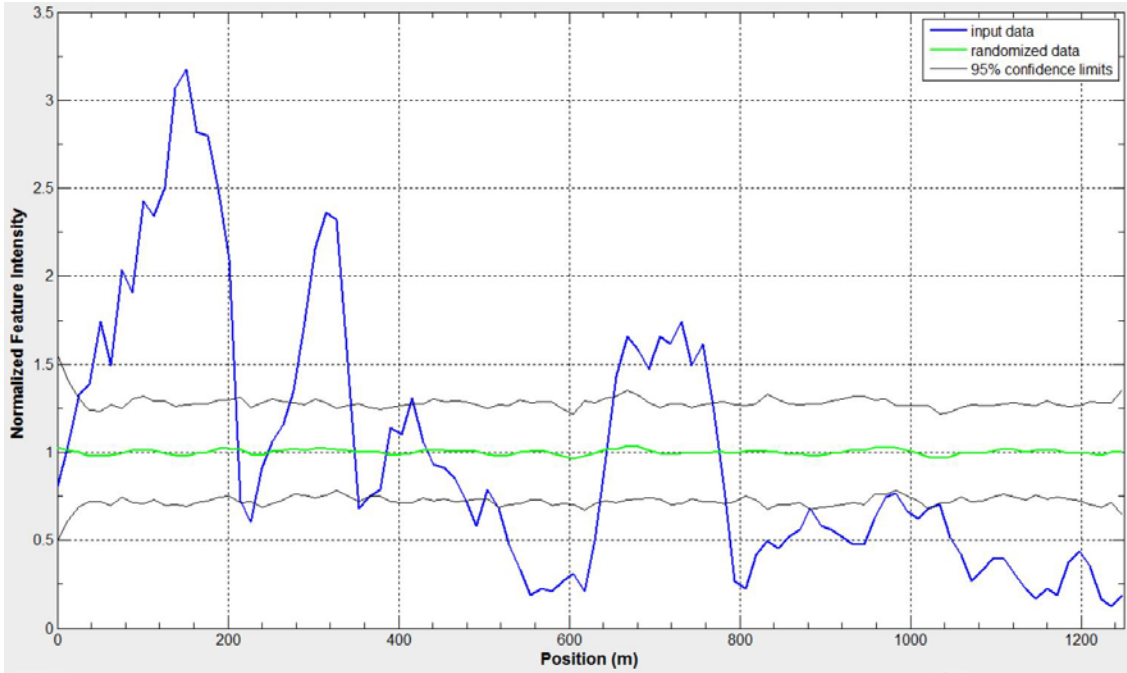


Figure 10-62 Intensity of all Set 3 natural fractures, Well HRB-2.

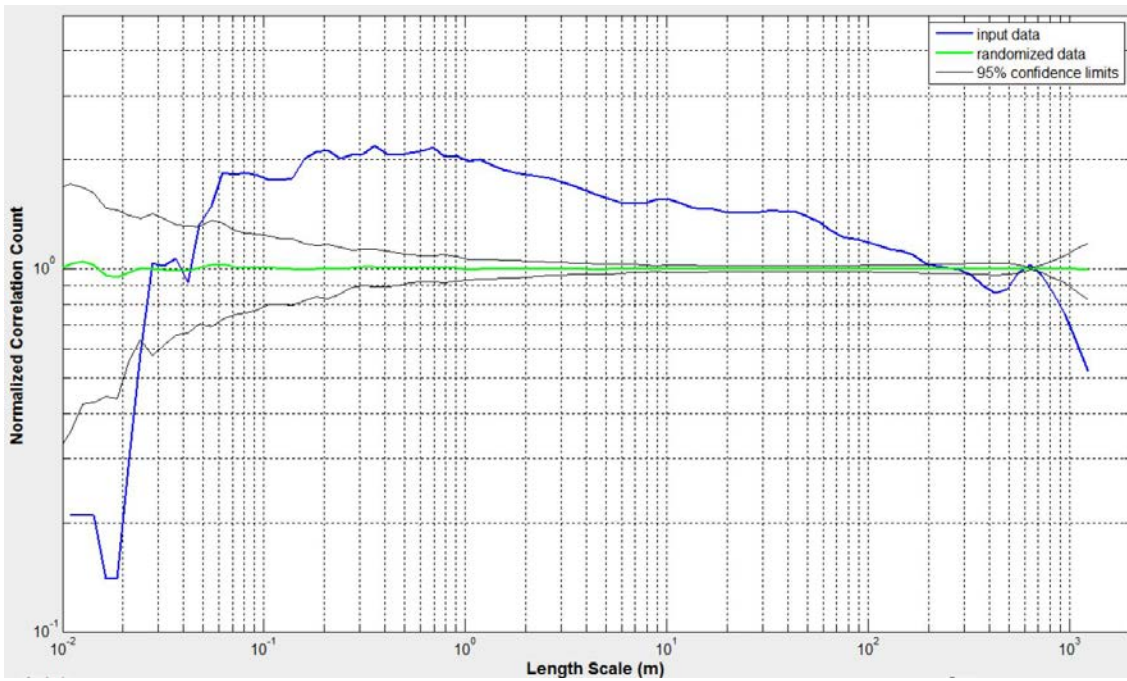


Figure 10-63 Correlation count of all Set 3 natural fractures, Well HRB-2.

10.2 INTERPRETATION AND DISCUSSION, HORN RIVER BASIN

The NCC results for fracture sets in wells HRB-1 and HRB-2 allow us to interpret the spatial arrangement styles of fractures in the Devonian shales of the Horn River Basin. The fracture intensity and Normalized Correlation Count (NCC) plots for the geologically meaningful and singular-typed fracture sequences in both wells, with corresponding horizontal wellbore trajectory analogue plots for reference, are rescaled and compiled for ease of comparison and interpretation (Figures 10-64 to 10-67). My NCC interpretation primarily focus on the results for the selected conductive and resistive fracture sequences in each well, since the non-selected fracture sequences generally either 1) have NCC results that are geologically unmeaningful and are only included earlier for completeness (e.g. for the “All” sequences containing fractures with all different orientations), or 2) are sequences with more than one type of fractures (e.g. the “Natural” sequences containing both conductive and resistive fractures with similar orientations) whose NCC results in most cases simply resemble the NCC of each one’s most numerous constituent fracture sequence.

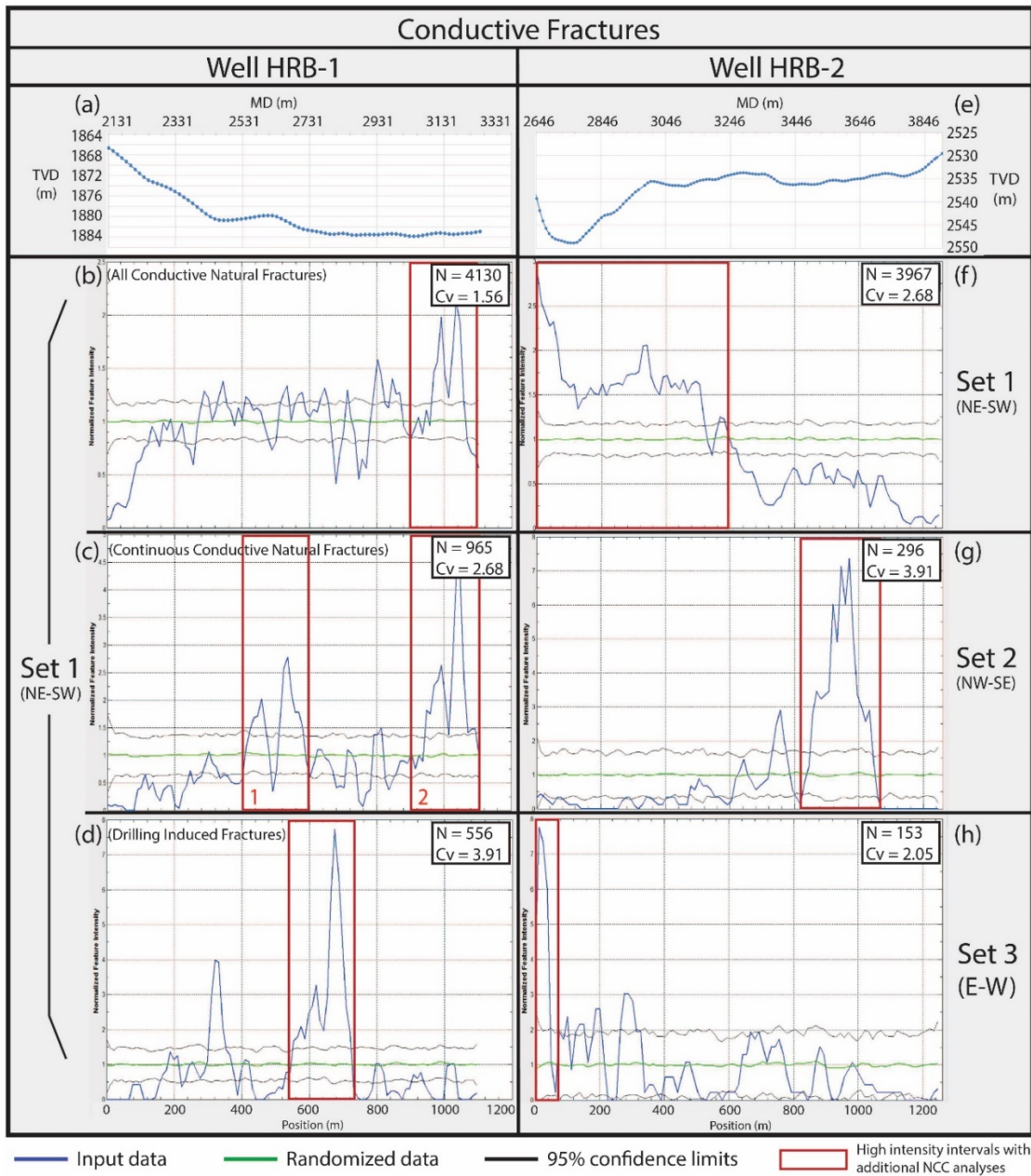


Figure 10-64 Comparing fracture intensities from conductive fracture sets in Wells HRB-1 and HRB-2. TVD vs MD plots (a) and (e) provided as horizontal wellbore trajectory approximation. N = number of fractures in a given sequence. Cv = coefficient of variation. Red boxes indicate high fracture intensity intervals further analyzed separately with NCC. Horizontal axes are column-wise aligned. Vertical axes are not aligned.

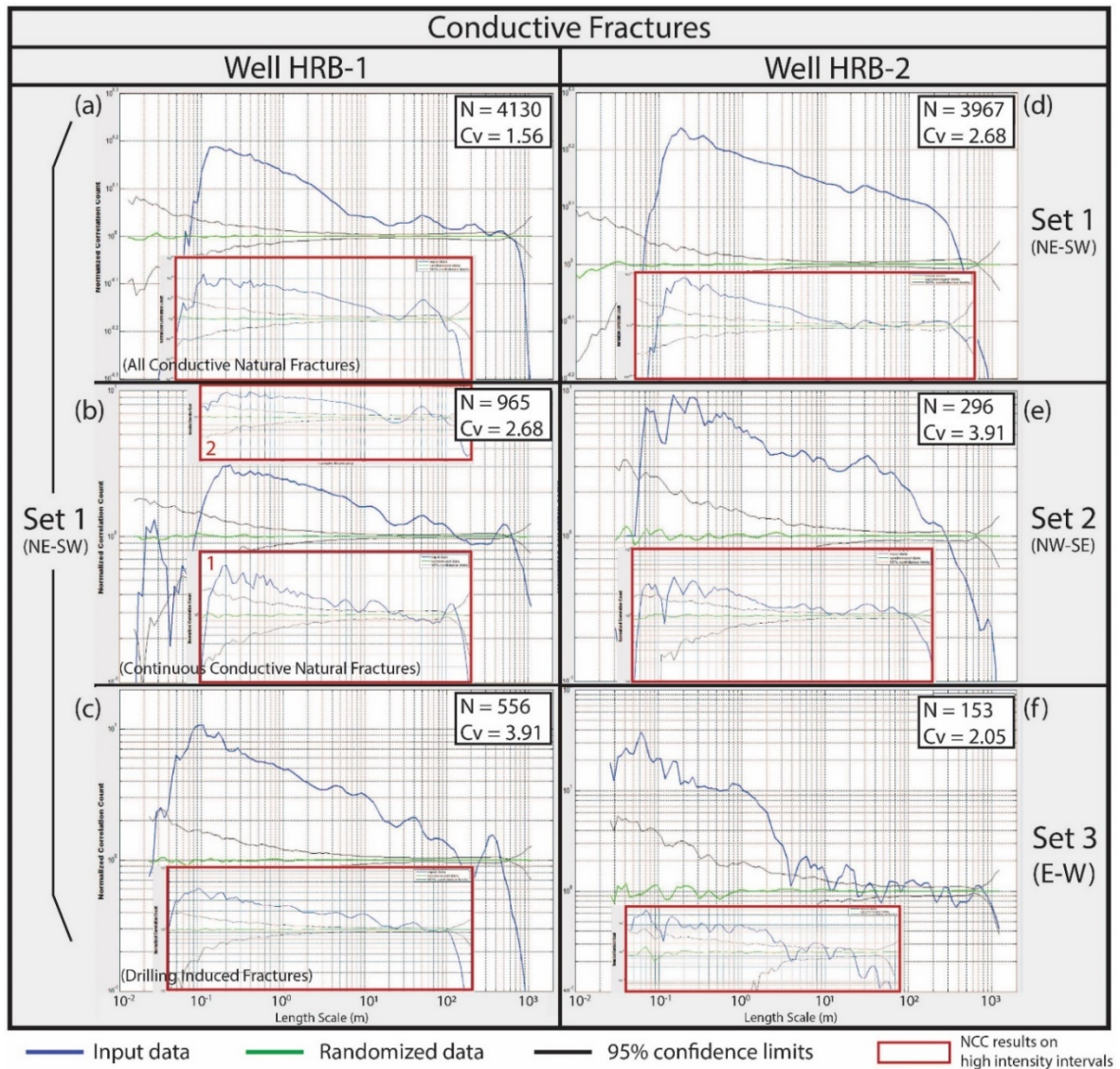


Figure 10-65 Comparing NCC results from conductive fracture sets in Wells HRB-1 and HRB-2. N = number of fractures in a given sequence. Cv = coefficient of variation. Red insets show correlation count results from analyzing high fracture intensity intervals in individual sets. Horizontal axes are column-wise aligned. Vertical axes not aligned.

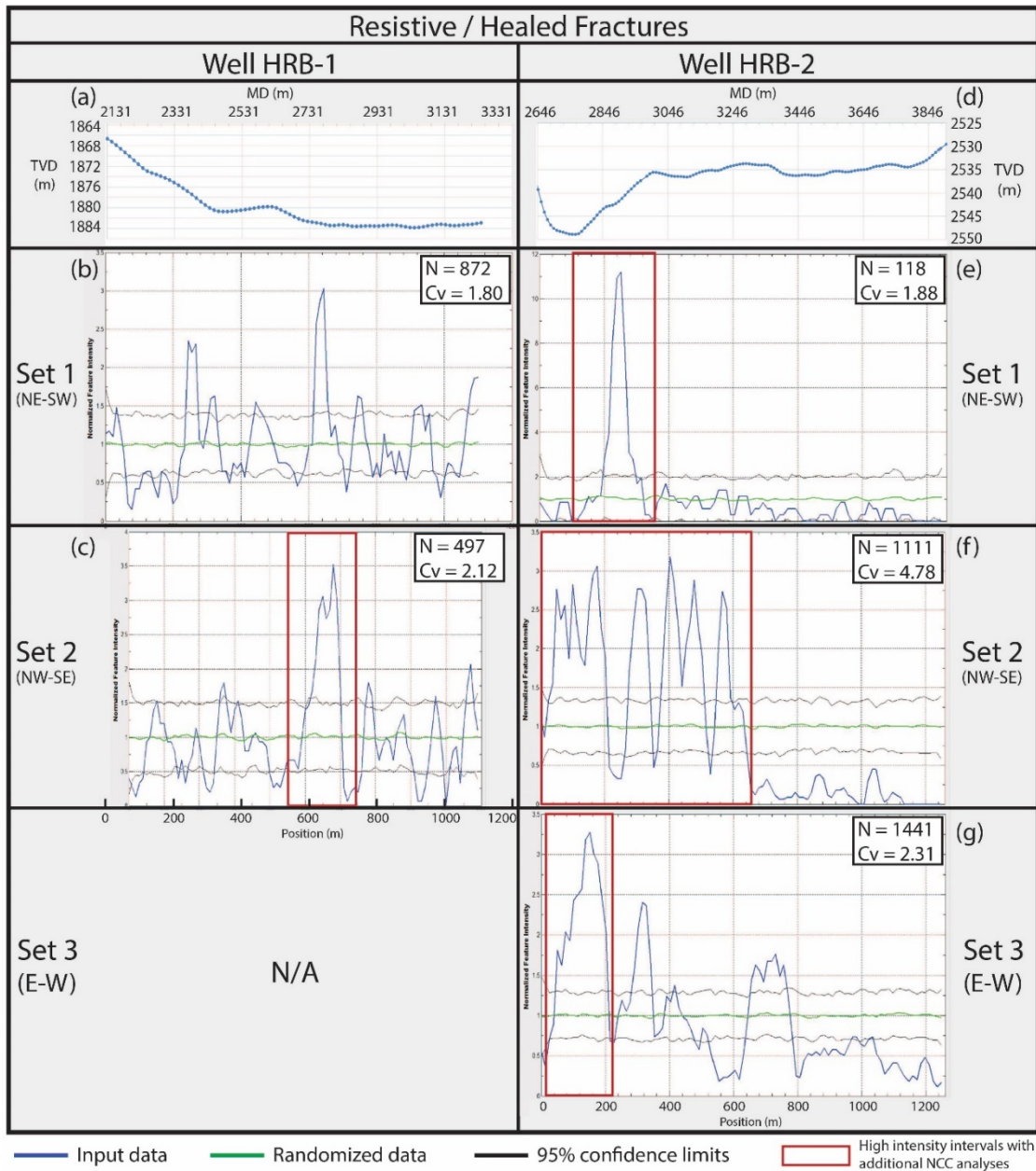


Figure 10-66 Comparing fracture intensities from resistive or healed (i.e. sealed) fracture sets in Wells HRB-1 and HRB-2. TVD vs MD plots (a) and (d) provided as horizontal wellbore trajectory approximation. N = number of fractures in a given sequence. Cv = coefficient of variation. Red boxes indicate high fracture bintensity intervals further analyzed separately with NCC. Horizontal axes are column-wise aligned. Vertical axes not aligned.

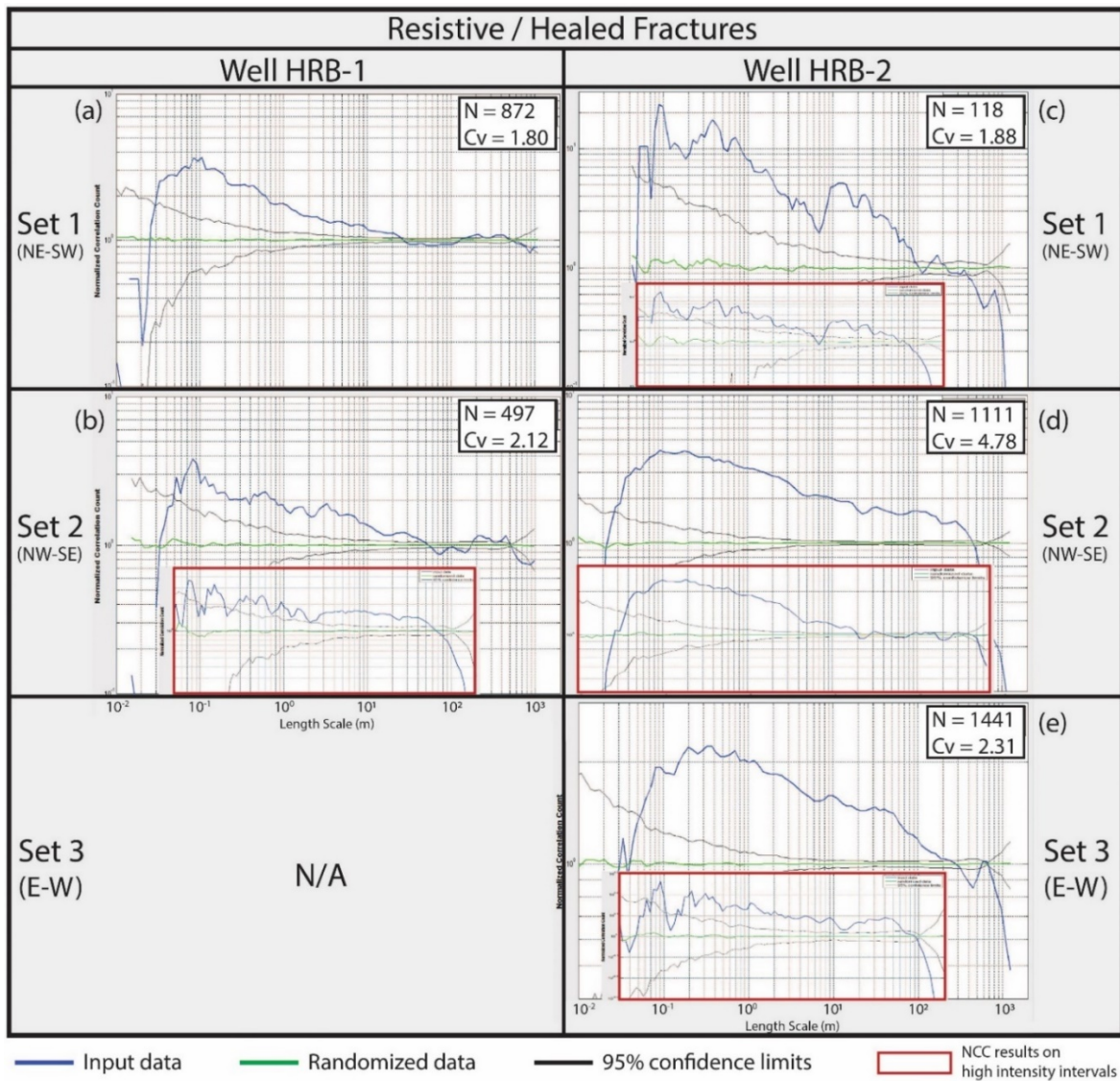


Figure 10-67 Comparing NCC results from resistive or healed (i.e. sealed) Set 1, 2, 3 fractures in Wells HRB-1 and HRB-2. N = number of fractures in a given sequence. Cv = coefficient of variation. Red insets show correlation count results from analyzing high fracture intensity intervals within individual sets. Horizontal axes are column-wise aligned. Vertical axes not aligned.

10.2.1 Interpretation: Well HRB-1

Conductive fracture sets, HRB-1

Analyzed all together, Well HRB-1's 4130 conductive fractures (which all broadly strike NE-SW regardless of continuity) are reflected by the NCC result as a sequence of clusters that are individually as wide as approximately 300 m, the length scale at which the NCC curve crosses the spatial correlation value of 1 (Figure 10-65a). The largest clusters have a 450 m regular inter-cluster spacing based on the largest NCC peak length scale. Internal NCC analysis of the cluster with the highest intensity peaks near the end of the scanline (Figure 10-64b) suggests that within each 300-m-wide cluster are regularly spaced and internally fractal clusters that are as wide as 25 m individually, and that the regular spacings between individual fractal clusters are 50 and 200 m (Figure 10-65a inset).

The 965 continuous conductive fractures, though much fewer than the 3052 discontinuous fractures, are statistically more clustered as suggested by its higher C_v (2.68 vs 1.59). The fracture intensity plot indicates two distinct high intensity intervals (Clusters 1 and 2), each containing at least two narrower intensity peaks (Figure 10-64c). The overall NCC plot suggests that the two high intensity intervals represent two 500-m-apart fracture clusters that are each approximately 150 m wide (Figure 10-65b). The NCC result of Cluster 1 suggests that the cluster contains regularly spaced fractal clusters as wide as 30 m (Figure 10-65b inset 1). The NCC result of Cluster 2 suggests the presence of 15-m-wide, regularly spaced fractal clusters that are 50 m apart (Figure 10-65b inset 2).

The analytical results of the drilling induced fractures (which are also conductive in image log), are shown along the results of the conductive natural fractures for comparison. The C_v of the drilling induced fractures (3.91) is the highest among all fracture sequences analyzed in HRB-1 which indicates a higher degree of statistically non-random

fracture clustering than the other types of fractures. The corresponding NCC plot (Figure 10-65c) suggests that the drilling induced fractures are arranged in regularly spaced fractal clusters with a maximum cluster width of 150 m and a regular spacing of 350 m. NCC analysis of the largest drilling induced fracture cluster (Figure 10-64d) suggests that the fractal clusters within (corresponding to the three internal intensity peaks) are individually as wide as 50 m (Figure 10-65c inset).

Resistive fracture sets, HRB-1

For the 872 NE-striking Set 1 resistive fractures in Well HRB-1, peaks in the fracture intensity plot indicate that multiple statistically significant and narrow fracture clusters are present (Figure 10-66b). The length scale of 25 m where the NCC result has a spatial correlation of one suggests that the clusters are up to 25 m wide individually. The consistent negative slope following which the curve decreases suggests that the internal organization of the clusters is fractal. The double peak in the NCC curve following a period of statistical low indicates regular inter-cluster spacings of 200 m and 350 m (Figure 10-67a).

Contrasting with few conductive fractures in Well HRB-1 striking NW-SE, a total of 497 resistive fractures are in the broadly NW-striking Set 2 sequence. Though approximately 50% fewer than the NE-striking Set 1 fractures, resistive fractures in Set 2 are statistically more clustered as indicated by a slightly higher Cv of 2.12 (Figure 10-66c). The overall shape of NCC result for the full sequence resembles that of Set 1 and suggests a spatial arrangement style of regularly spaced fractal clusters for Set 2. Individual fractal clusters are approximately up to 60 m wide, and the regular spacings among the largest clusters are 200 and 450 m (Figure 10-67b). NCC analysis for the central cluster as seen in

the corresponding intensity plot (Figure 10-66c) suggests a cluster width of approximately 60 m which confirms earlier interpretation. The internal arrangement of the cluster is also implied to be fractal, and that the length scale of 2 m where the trend of the NCC curve changes could reflect the width of the most common smaller internal clusters (Figure 10-66c inset).

10.2.2 Interpretation: Well HRB-2

Conductive fracture sets, HRB-2

Visual comparison of the intensity plots for the NE-striking Set 1, NW-striking Set 2, and E-striking Set 3 conductive fractures in Well HRB-2 indicate that fractures in each set are present within various clusters corresponding to the statistically significant peaks (Figure 10-64f-h). The peaks, or clusters, are visually the broadest within Set 1 and the narrowest in Set 3. The degree of statistically non-random clustering for each of the three fracture sets is indicated by the coefficient of variation, C_v , and is the highest (3.91) in Set 2 and the lowest (2.05) in Set 3.

In the NCC plot for the most numerous conductive Set 1 fractures in HRB-2, the length scale value where the curve intersects the spatial correlation of 1 suggests that the fractures are spatially arranged in an approximately 450-m-wide cluster (Figure 10-65d). The interpretation is supported by the approximate width of the continuous high fracture intensity interval (Figure 10-64f). The result of the NCC analysis on this interval alone suggests that the wide cluster is composed of fractal clusters that are individually up to approximately 15 m wide and have a regular inter-cluster spacing of 30 m (Figure 10-65d inset).

The NCC plot for the conductive Set 2 fracture sequence, statistically the most clustered among the three, suggests that the fractures are spatially organized in an approximately 280-m-wide cluster (Figure 10-65e). The interpretation matches the approximate width of the fracture intensity interval bounding the small and the broad separate high intensity bands (Figure 10-64g). NCC analytical result for the approximately 250-m-wide broad intensity band alone suggests that the corresponding cluster is composed of regularly spaced fractal clusters that are individually up to approximately 10 m wide and have regular spacings of approximately 33 and 65 m (the latter significant spacing may simply be a harmonic signal of the former) (Figure 10-65e inset).

The peaks in the intensity plot for conductive fractures in Set 3, the least abundant and statistically the least clustered set, suggest that fractures clusters are present predominantly within the first 300 m of the scanline (Figure 10-64h). The NCC plot suggests the presence of fractal clusters with multiple regular spacings e.g. 8 m, 20 m, 60, 100, and 160 m (Figure 10-65f). NCC analysis for largest cluster corresponding to the tallest fracture intensity peak further confirms the presence of regularly spaced fractal clusters within that are up to approximately 3.5 m wide and have inter-cluster spacings of approximately 8 m and 20 m (Figure 10-65f inset).

Sealed fracture sets, HRB-2

Inspection of the fracture intensity plots for sealed (or resistive) fractures in HRB-2 suggests that fracture clusters are present in all sets analyzed and are all present within the first 800 m of horizontal wellbore, or in other words there is statistically significant lack of sealed fractures in the last 400m of the wellbore (Figure 10-66e-g). Distribution of

the fracture intensity peaks varies from one tall narrow peak in Set 1, multiple widely distributed narrow peaks in Set 2, to multiple widely distributed wide peaks in Set 3.

For Set 1 which has the fewest fracture and the lowest C_v among the three sealed sets, the NCC plot indicates the presence of a 100-m-wide fracture cluster which matches the characteristic of the one and only fracture intensity peak in the Set (Figure 10-67c, 10-66e). The small NCC peak near 150 m may be from fractures within the cluster matching outside sparse fractures. NCC Analysis of the isolated intensity peak interval shows that within the cluster are regularly spaced fractal clusters that are proximately 7 m wide and have approximate inter-cluster spacings of 15, 25 and 35 m (Figure 10-66e inset).

Sealed Set 2 fractures are not only statistically the most clustered among fractures in the three sealed sets, but are also the most clustered among all natural and induced fractures in both Well HRB-1 and HRB-2 as indicated by the highest C_v (4.78) among all sequences analyzed. Closely spaced peaks with similar amplitudes present in the intensity plot show that the fractures predominately concentrate in the first 650 m of the horizontal wellbore (Figure 10-66f), and the NCC analysis suggests that a 450-m-wide, statistically significant cluster is present within this interval (Figure 10-67d). NCC analytical result for the statistically significant subinterval suggests that the wide cluster internally consists of regularly spaced fractal clusters that are as wide as 20 m and have a common inter-cluster spacing of 30 m (Figure 10-67d inset).

The intensity plot for sealed Set 3 fractures, the most abundant set among the three, suggests that the interval may contain multiple statistically significant wide fracture clusters with (Figure 10-66g). The NCC result suggests that a cluster with a width of approximately 300 m is present (Figure 10-67e). The cluster corresponds to the interval

between scanline positions 50 and 350 m that bounds the first two intensity peaks. The small NCC peak corresponding to the length scale of 600 m, which is less than half of the total scanline and therefore is not an artifact, indicates the statistically significant spacing between fractures in the first and the last intensity peak (Figure 10-66g). NCC Analysis of the part of identified cluster alone corresponding to the first peak suggests that the fractures within are organized in regularly spaced fractal clusters that are as wide as approximately 15 m and have significant inter-cluster spacings of 20, 25 and 40 m (with the last spacing likely a harmonic of the first) (Figure 10-67e inset).

10.2.3 Discussion: Horn River Basin wells

For the selected Horn River Basin fracture sequences interpreted where statistically more significant than fractures intensity peaks are present (Table 8), NCC subinterval analysis can quantify the statistical significance of off-trended spatial correlation peaks or troughs embedded in elevated NCC portions of the overall curves (e.g. Figure 10-65a-f, 10-67a-e). NCC subinterval analysis helps detecting the presence of statistically significant smaller clusters that is often overshadowed by spatial correlation signals of larger clusters, as well their internal organization which cannot be described through intensity plots. Detailed analysis generally requires a high number of fracture spacings available within the interval of interest in order to yield statistical meaningful NCC results. In cases such as the Frontier Formation cores or in Well VM-B and VM-C where the number of fractures present in the geologically meaningful sequences are fewer than 100 where fractures, individual fracture intensity peak or high intensity interval generally do not contain sufficient fracture for complete NCC plots.

Well	Fracture Type	Fracture Set	NCC Interpretation	Cluster Width (m)	Cluster Spacing (m)
HRB-1	Conductive	All Set 1 (NE-SW)	Clustered individual (+ regularly spaced fractal clusters)	300 (25)	450 (50, 200)
		Continuous Set 1 (NE-SW)	Clustered individual (+ regularly spaced fractal clusters)	150 (15, 30)	500 (50, 100)
	Drilling Induced	Set 1 (NE-SW)	Regularly spaced fractal clusters (+ fractal clusters)	150 (50)	350 (fractal)
	Resistive	Set 1 (NE-SW)	Regularly spaced fractal clusters	25	200, 350
Set 2 (NW-SE)		Regularly spaced fractal clusters (+ fractal clusters)	60 (2)	200, 450 (fractal)	
HRB-2	Conductive	Set 1 (NE-SW)	Clustered individual (+ regularly spaced fractal clusters)	450 (15)	one big cluster (30)
		Set 2 (NW-SE)	Clustered individual (+ regularly spaced fractal clusters)	280 (10)	one big cluster (33, 65)
		Set 3 (E-W)	Regularly spaced fractal clusters (+fractal clusters)	3.5 (3.5)	8, 20, 60, 100, 160 (8,20)
	Healed (i.e. sealed)	Set 1 (NE-SW)	Clustered individual (+ regularly spaced fractal clusters)	100 (7)	one big cluster (15, 25, 35)
		Set 2 (NW-SE)	Clustered individual (+ regularly spaced fractal clusters)	450 (20)	one big cluster (30)
		Set 3 (E-W)	Clustered individual (+ regularly spaced fractal clusters)	300 (15)	one big cluster (20, 25, 40)

Table 10-3 Summary of NCC interpretation for selected fracture sequences in Horn River Basin horizontal wellbore image logs. Spatial arrangement styles in parentheses are interpreted for NCC on selected internal clusters. Numbers within parentheses indicates attributes of internal clusters identified from corresponding NCC results.

Well HRB-1

As summarized in Table 8, image log fractures in HRB-1 are predominantly arranged in regularly spaced fractal clusters in all types or sets. The widths and the inter-cluster spacings of the fractal clusters within each sequence may vary but are generally on the order of tens of meters for the former and up to 100 to 200 meters for the latter (Table 8). For the conductive fractures including the drilling induced fractures, the regularly spaced fractal clusters form statistically significant larger clusters that are up to 300 m wide each and that are up to 500 m apart. The continuous conductive fractures i.e. fractures that are mostly conductive throughout their image log traces are statistically more clustered than their more abundant discontinuous counterparts (which practically have the same NCC results as the “All” sequence interpreted earlier) as suggested both by the higher C_v and the NCC shape. It suggests a correlation between that the spatial clustering among conductive fractures in HRB-1 and the conductivity continuity (or resistivity discontinuity) along their image log traces which is an indicator of the porosity along the fracture aperture.

Though the spatial arrangement style for both the continuous conductive fractures and the drilling induced fractures the same that their cluster dimensions, both on the order of a few tens of meters, appear to be comparable, the drilling induced fractures in HRB-1 are significantly more clustered as indicated by the sequence’s much higher C_v (Table 6). Though one may question the accuracy of picking drilling induced fractures among the background of similarly oriented conductive fractures, inspection of the intensity peak positions for both sequences suggest that clusters within the two sequences are offset (Figure 10-64c, d). The lack of overlapping between the sequences’ statistically significant clusters suggest that the conductive fractures and the drilling induced fracture picked in the original image log may indeed be fractures from distinct populations such

that the spatial organization of the drilling induced fractures is not a result of mispicked conductive natural fractures and vice versa.

Observation of the fracture intensity plots for HRB-1's resistive fractures in Set 1 and in Set 2 suggests that the fractures in both sequences have similar intensity distributions along the well bore though Set 1 has nearly twice as many fractures as Set 2 (Figure 10-66b&c). As observed, the spatial arrangement style of both set are also the same and that the cluster widths and spacings are on the same orders of magnitudes across the two sets. The largest fracture clusters in both sets are present within the same central interval around position 600 m along the horizontal wellbore, and similar central cluster is present within in Set 2 regardless of the type of fracture resistivity continuity (Figures 10-20, 22, 24). Also, it should be note that this shared cluster interval within both sets of resistive fractures coincides with the same wellbore interval where the largest NE-striking drilling induced fracture cluster is present (Figure 10-64d). These observations suggest that for all resistive fractures and drilling induced fractures present in HRB-1, the apparent source of regularly spaced fractal clustering comes from a localized, approximately 200-m-wide interval behind MD 2731 m within horizontal wellbore (Figures 10-64a, 10-66a). The interval corresponds to a TVD of 1884 m that is first reached here in HRB-1 directly after the interval where the horizontal wellbore has the largest decrease in inclination dropping approximately 5 m in vertical depth (Figure 10-1). This interval of rapid depth decline from TVD 1880 to 1884 m, on the other hand, corresponds with the occurrence of the first major cluster in the continuous conductive fracture sequence; the second occurs at the very end of the wellbore (Figure 10-64c). Overall, the results indicate that there is a statistically significant localization of fracture clusters along the horizontal wellbore of HRB-1, such

that the occurrence of drilling induced fractures coincide with a major resistive/sealed natural fracture cluster that is directly preceded by a zone approximately 5 m shallower in true vertical depth that contains large clusters of continuous conductive or open natural fractures.

Well HRB-2

In each of the interpreted major conductive and sealed fracture sequence of Well HRB-2, fractures are organized in a statistically significant, single large cluster that contains interval(s) of regularly spaced fractal clusters or is itself organized in such style (Table 8). The dimensions and the positions of the statistically significant clusters vary across fracture types and sets even the same well, however. For the conductive fractures, the interval where a Set 1 cluster that is nearly 500 m in width is present corresponds to a statistically significant lack of Set 2 fractures; the presence of a major Set 2 cluster in the second half of the wellbore similarly correlates with a statistical lack of Set 1 fractures (Figure 10-64f, g). Examination of the intensity plots show that localization of fracture cluster appears to link to certain regions within the horizontal wellbore (Figures 10-64e-h and 10-66d-g). Well HRB-2's horizontal trajectory shows that the well travels from TVD 2538 m down to 2548 m and back up to 2533 m between MD 2646 and 3346 m, after which it stays approximately within 1 m away from TVD 2535 until it begins to shallow near MD 3750 m (Figure 10-64e). The wide cluster of conductive Set 1 fractures intercepted by the wellbore largely correspond to the interval where the well is beneath TVD 2535 m, and the cluster of conductive Set 2 fractures is broadly consistent to the wellbore that steadies around 2535 m. Current observation indicates that the end of the conductive Set 2 cluster correlates with a statistical lack of all other conductive and sealed fractures in the interval

beyond MD 3750 m that coincides within the rising of the wellbore above TVD 2535 m (Figure 10-64e). As for conductive Set 3 fractures, the clusters correlated exclusively with the interval of the wellbore approximately beneath TVD 2540, and that the fractal cluster at the beginning coincides with the most steepest portion of the wellbore analyzed (Figure 10-64e, h). Note that this steep wellbore interval also associates with the highest intensity value in Set 1 (Figure 10-64f).

The intensity plots for all three sealed fractures sets suggests that sealed fractures in HRB-2, regardless of orientations, predominantly concentrate in the first 800 m of the scanline that associates with the undulatory portion of the wellbore (Figure 10-66d-g). As for sealed Set 1 fractures, the single wide cluster is limited to the portion of the wellbore that rises from TVD 2548 to 2533 m. Fracture clusters in Set 2 are prevalent in the first 600 m of the wellbore that coincide with occurrence of conductive Set 1 fractures (Figures 10-66f, 10-64f) through the two fracture sequences have opposite types and approximately orthogonal orientations. Note that the fracture intensity peak in resistive Set 1 corresponds with intensity troughs in the other two sealed sets, which indicates that the corresponding interval is mechanically conducive to the growth of only the resistive fracture population that have a present-day strike of NE-SW.

As for the overall distribution of HRB-2's fractures that are within the same sets by strike, there is complete lack of overlap between the high intensity intervals or clusters of the conductive Set 2 and the sealed Set 2 fractures (Figures 10-64g, 10-66f). It indicates that the NW-striking conductive fractures in HRB-2 are different from their resistive counter parts internals of their origins. As discussed earlier, the latter appears to be physically associated with the conductive, NE-striking Set 1 fractures. The current lack of

cores from said interval hinders further understanding of any potential association between the two. Unlike Set 2 fractures, fractures in the other two sets all are concentrated in the first half of the wellbore. It has been observed previously that Set 1 fractures are predominantly conductive and that Set 3 fractures are predominantly sealed and that the number of fractures in the major type is approximately an order of magnitudes or above more than the minor type (Table 7). Unlike fractures in HRB-1, fractures in HRB-2 have not been categorized by the continuity or their trace resistivity, and therefore there's no further information on the picking of the minor components of fractures in the same Set. However, since the NCC results for the Natural fracture superset #1 and 3 (Figures 10-59, 63) indicate that combining each Set's major and minor type components does not markedly affect the spatial arrangement outcome (which reflect the results of the major types), it may be safe to conclude that the sealed Set 1 fractures and the conductive Set 3 fractures share origins with their conductive or sealed counterparts, respectively. Note that the statement does not apply to Set 2 fractures, for, other than our earlier discussion on the non-overlapping clusters between the two types, the NCC result (Figure 10-61) as well as the Cv (Table 7) also show significant increase in statistical randomness comparing the Natural superset #2 to each of its constituent sets.

Causes of spatial arrangement patterns, Horn River Basin

It is interpreted that fractures in the major conductive and resistive sequences in both HRB-1 and HRB-2 are preferentially arranged in wide clusters that contain regularly spaced fractal clusters within (Table 8). Whist conductive fractures in both wells preferentially strike NE-SW, resistive or sealed fractures in HRB-1 predominantly strike NE-SW while those in HRB-2 mostly strike E-W, a fracture set that is not present in HRB-

1 (Table 6, 7). Though both wells target the Middle Devonian Evie, Otter Park and the Late Devonian Muskwa shales, note that the trajectory of the wells show that the target shales are present at drastically different depths (TVD 1884 m vs 2535 m) within each well (e.g. Figure 10-66a, d). It is likely that the marked differences in the orientations between the sealed fracture populations of the two wells are associated with varying diagenetic and burial histories experienced by the shales at different depths. The theory of multiple generations of fractures is supported by an unpublished study based on other confidential well logs and relevant outcrops, which suggests that an older set of orthogonal sealed fractures originally striking N-S and E-W may have formed during the initial burial of the shales and later rotated to NE-SW and NW-SE in places before the opening of a new set of NE-striking fractures during the Laramide burial (Hartwell, 2008) coincidentally along present-day S_{Hmax} as well as potential formation or reaction of orthogonal fractures (J.F.W. Gale and R. Dunphy, personal communication, 2010)

As supported by observations of peaks in the fracture intensity plots, fracture cluster dimensions and localities inferred from the NCC patterns for fracture sequences in HRB-1 and HRB-2 are strongly linked to high intensity interval(s) that of often preferentially located within each well. It is also observed that these high intensity intervals can overlap across fractures sequences differ by types and orientations, and that these intervals often correspond to portions of the wellbores with particular trajectories associated with drastic (or in certain case, the lack of) changes in true vertical depths. As discussed in earlier sections, localization of fracture cluster may be linked to reservoir mechanical property variation along well path. Since mechanical stratigraphic information are not made available for Wells HRB-1 and HRB-2 nor are relevant mud logs, further investigation in

this study on the potential correlation between the fracture cluster locality, dimension, and internal organization, and wellbore litho/mechanical stratigraphy is precluded. However, well log observation and core analyses from relevant studies suggest that changes in the Horn River Basin shales' mechanical properties associate strongly with reservoir lithology, and that natural fracture density is the highest in the carbonate-rich shale intervals or limestones with high hardness measurements, such as the Evie shale with limestone interbedding and the Lower Keg River limestone beneath the Evie. (Dunphy and Campagna, 2011; Yang et al., 2015). The hypothesized association between preferential fracture clustering in the Devonian shales intervals in the Horn River Basin and reservoir lithology variation could be a result of lateral facies change (Dunphy and Campagna, 2011) or due to well path traveling through mechanically different shale beds with changing TVD, the latter of which is in line with the implication of the Vaca Muerta Formation shale NCC results such as in the case of Well VM-A where the carbonate-rich mechanical zone #4 correlates with the interval of strongly clustered WNW-striking natural fractures.

Preferential clustering of natural fractures in the Devonian shales of the Horn River Basin suggests control on fracture spatial arrangements by lithology-based mechanical property variations along well paths. Interpretation of regional fracture set spatial arrangement should account for fracture sampling bias arise from undulations. As observed in HRB-1, fractures clusters potentially associated with mechanical stratigraphic variation appear to coincide with localized drilling induced fracture clusters (e.g. Figures 10-64d, 10-66b,c). Reservoir characterization may benefit from full understanding of fracture spatial arrangement patterns associated with of rock mechanical property variation and reservoir heterogeneity in the context of regional diagenetic and burial histories.

Chapter 11: Results and Discussion: Appalachian Basin

11.1 INTENSITY AND SPATIAL CORRELATION RESULTS, APPALACHIAN BASIN

Among a total of 103 opening-mode fractures in the 487-m-long image log of Gulla 10H, three are picked as WNW-striking conductive fractures, 59 as WNW-striking partially sealed fractures, 25 as WNW-striking resistive fractures, and 16 as ENE-striking drilling induced fractures. The spacing statistics as well as the coefficients of variation for each type of image log fractures are calculated using CorrCount and Microsoft Excel (Table 9). The results have also been discussed in part in a previously published extended abstract (Li et al., 2016)

Well	Fracture type	Set (average strike)	# of fractures	Scanline length (m)	Mean spacing (m)	Standard deviation (m)	Min. spacing (m)	Max. spacing (m)	Cv
Gulla 10H	Natural	All (~WNW-ESE)	88	236.36 (Terzaghi corrected)	2.69	5.14	0.017	32.19	1.91
		Partially Healed (WNW-ESE)	59	487.47	8.26	13.68	0.210	66.41	1.66
		Resistive (WNW-ESE)	25	374.38	14.98	21.71	0.333	87.98	1.45
	Drilling Induced	One set (ENE-WSW)	16	465.00	29.06	55.41	0.427	214.4	1.91

Table 11-1 Statistical summaries on image log fracture sets in Gulla 10H. Note that the NCC results for sets other than Natural-All are omitted due to incomplete curves from small sample sizes.

The largest single image log fracture sequence in Gulla 10H analyzed using is one containing all 88 WNW-striking, non-drilling-induced (or “natural”) fractures present along a Terzaghi-adjusted interval of 236.36 m. The adjustment for obliquity accounts for the 29 degree angle between the WNW-striking set and the horizontal wellbore. The

scanline length before correction is approximately 487.5 m. Analysis of all natural fractures produces statistically similar yet more complete spatial correlation result than those from the partial healed or resistive subsequences. The average image log fracture spacing is 2.69 m, and the Cv is 1.91. This Cv value is larger than those of the subsequences, and it is the same as the Cv of the much less abundant ENE-striking drilling induced set (Table 9). The normalized fracture intensity plot (Figure 11-1) contains few statistically significant intensity peaks other than two minor ones near the position of 160 m. The NCC plot (Figure 11-2) contains five identifiable non-overlapped correlation peaks above the upper confidence limit at length scales 0.85, 3.5, 6.8, 12.5, and 100 m, respectively.

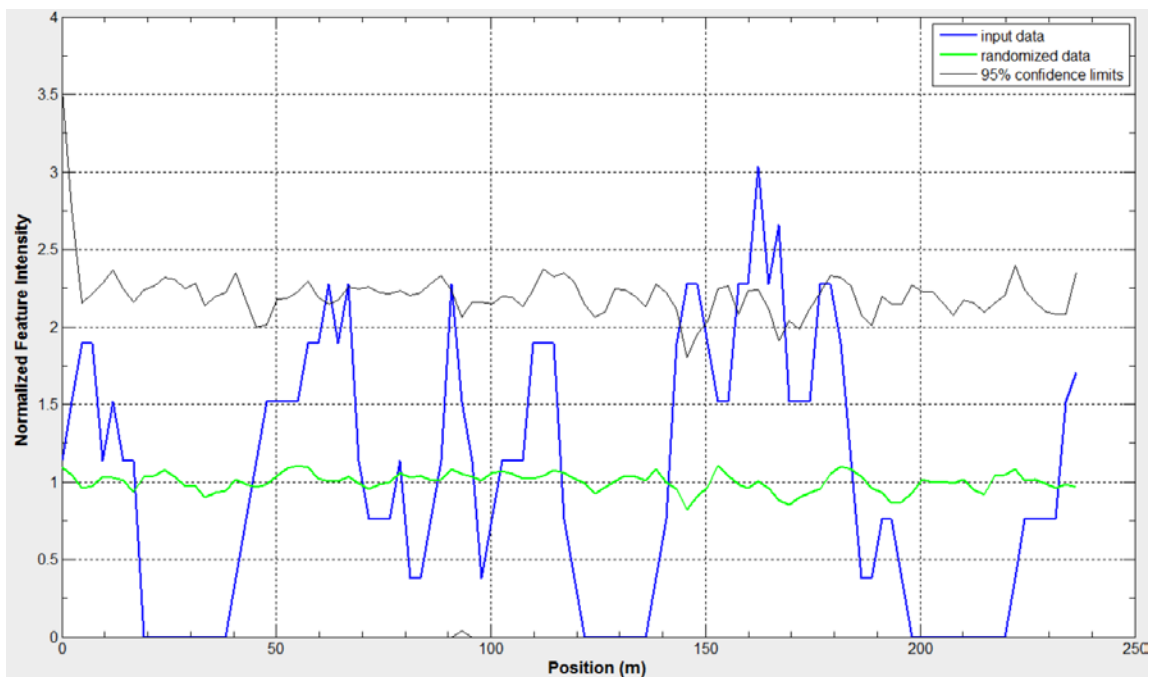


Figure 11-1 Intensity of all natural fractures, Gulla 10H.

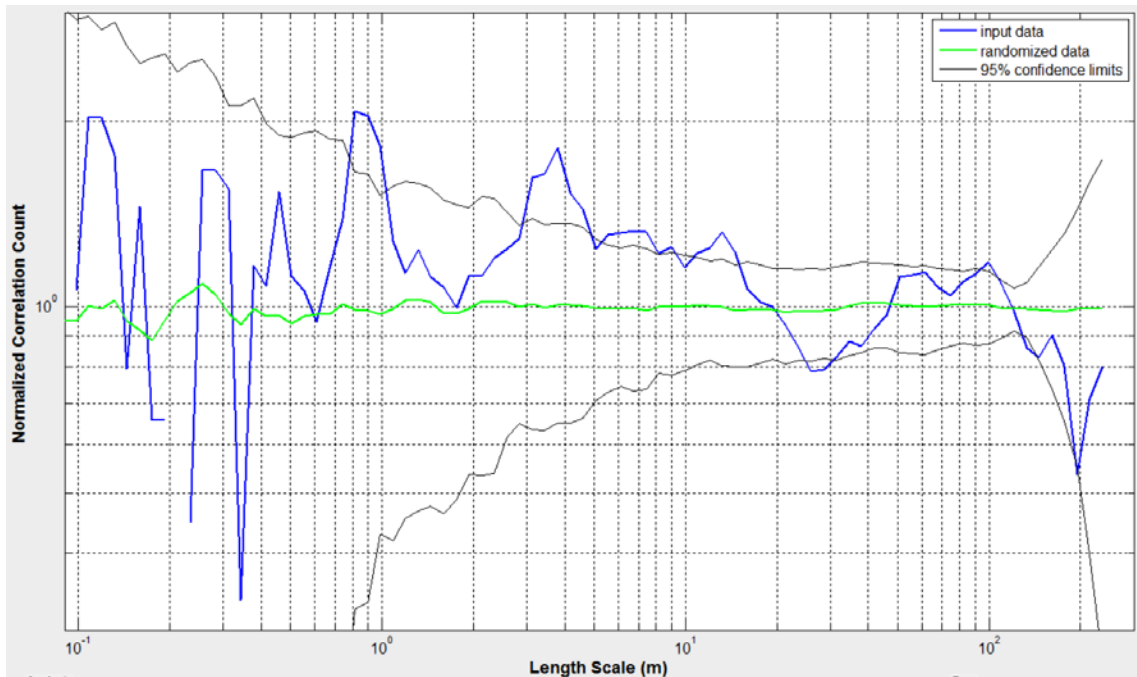


Figure 11-2 Correlation count of all natural fractures, Gulla 10H.

Since few fractures are found in the drilling-induced fracture sequence, the corresponding intensity and NCC plots are incomplete and statistically meaningless and are omitted.

11.2 INTERPRETATION: GULLA 10H

The NCC peaks at length scales 0.85 m, 3.5 m and 12.5 m reflect statistically significant spacings among the image log fractures, whereas the peak at 6.8 m may likely a harmonic of the 3.5 m spacing (Figure 11-2). These meter to sub-meter statistically significant length scales reflect spacings within smaller fracture clusters present in the sequence. The small spatial correlation peak at length scale 100 m reflects the distance between the significant intensity peaks near position 160 m and the much smaller peak at 60 m (Figure 11-1). The NCC curve intersects the spatial correlation value of 1 at the length

scale of 20 m which corresponds to a local maximum in fracture cluster width. The trough for length scales between 20 and 50 m suggests a statistically significant absence of fracture spacing values within this length scale range in this fracture sequence. Overall, the NCC result may indicate that evenly spaced fractures are in clusters with widths up to approximately 20 m that are spaced 50 to 100 m apart.

11.3 DISCUSSION: GULLA 10H

The 88 WNW-striking image log natural fractures are likely analogous to the WNW-striking J2 fractures observed in Marcellus Formation shale outcrops (e.g. Engelder et al., 2009). As noted by Gale et al. (2014), measurements of the subcritical crack index, a property that influences fracture clustering (Olson, 2004), from Marcellus core in a nearby well indicates a low degree of mechanical tendency for fractures to cluster. The observation is consistent with the interpreted fracture spatial arrangement patterns from image log data (Figure 11-2). Though fractures in the ENE orientation are picked as drilling induced because they coincide with the ENE-trending present day S_{Hmax} , image log interpretation is ambiguous such that uncertainty remains about whether the ENE-striking image log fractures are induced, natural, or reactivated natural fractures (Gale et al., 2012).

As previously discussed, interpretation of subsurface fracture spatial arrangement origin should take into consideration reservoir geology along well path. In adjacent vertical wells, it is noted that the spacing at small length scales up to 12.5 m matches the thickness of shale intervals in facies interpretations (Gale et al., 2012). Assuming that fracture height is bound by the shale intervals as commonly observed in outcrop, fracture spacing at statistically significant length scales may be controlled predominantly by shale layer thickness, with carbonates acting as barriers to height growth (Gale et al., 2012).

SECTION IV: SUMMARY

Chapter 12: Fracture Spatial Arrangement Insights through Normalized Correlation Count

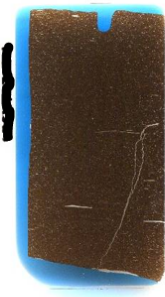
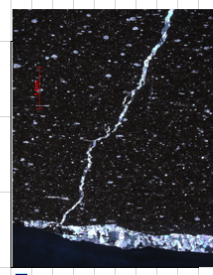
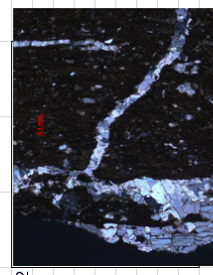
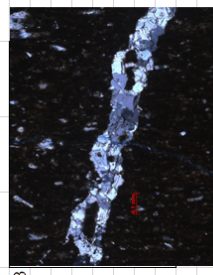
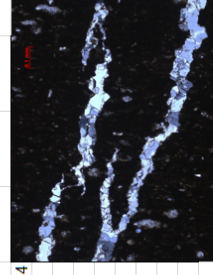
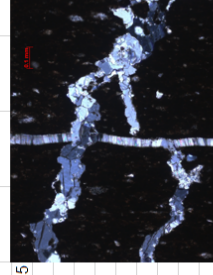
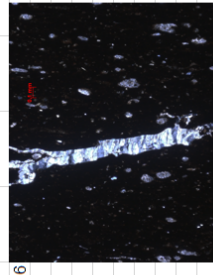
Using the Normalized Correlation Count (NCC) method and the associated CorrCount software by Marrett et al. (2017), I analyzed fracture spacing data from unconventional tight gas sandstone and shale reservoirs to statistically quantify spatial arrangement patterns among opening-mode reservoir fractures. Analyses of fracture spatial arrangement in the Frontier Formation tight gas sandstone based on image log, core, and satellite outcrop imageries show opening-mode fractures are arranged in clusters that are hierarchical and probably fractal with the largest clusters, from meters to tens of meters wide, possibly distributed periodically. Results from horizontal logs and cores contrast sharply with patterns of fractures of the same broadly east-west strike in outcrop, where spatial arrangements are indistinguishable from random. Although the origin of these differences is unknown, discrepancies could be due to contrasts in location-dependent burial and structural histories.

I found more significant than random and commonly fractally organized fractures clusters prevalent in the image log fracture sequences within selected shale reservoirs. Results of the Vaca Muerta Formation shale in the Neuquén Basin suggest statistically significant fracture clustering along wellbore preferentially within high-hardness carbonate beds. Results of the Middle and Late Devonian shale reservoirs in the Horn River Basin similarly indicate preferential clustering of fractures in selected intervals likely linked to reservoir lithology and mechanical stratigraphy associated with vertical depth variation along well paths. Correlation between particular lithology and fracture cluster localization

cannot be pinpoint due to unavailable wellbore geological information though relevant studies observed preferential clustering of natural fractures within carbonate-rich reservoir members. In the Marcellus Formation shale in the Appalachian Basin, correlation count result suggests evenly spaced fracture clusters in shale with potential correlation with bed thicknesses and that fracture growth may be controlled by carbonate barriers.

My results on fracture spatial arrangement in selected unconventional petroleum reservoirs demonstrated the analytical power of the Normalized Correlation Count method in inferring reservoir fracture array geometry through image log data that are commonly available in modern-day horizontal wells. The method of study avoids uncertainty in using outcrop analogues and provides direct quantitative information on subsurface fracture organization, and the accuracy of the results can be improved through calibration using cores when available. Quantitative information on fracture spatial arrangement from NCC can help constrain reservoir models and thus contribute to efficient resource extraction.

Appendix: Vaca Muerta Formation Shale Fracture Petrography

Petrographic Summary	
DATE 1/23/2015 STUDY:	
Well Name: [REDACTED] Depth (ft): [REDACTED] Sample Number: 1114 Formation: Vaca Muerta Depth (ft): 2670.2 ROCK TYPE: GRAIN SIZE: Thin Section Map: Mark key features: Mark traverse location: Label "up direction":	Date Rec'd: [REDACTED] Date processed: [REDACTED] Analyst 1: [REDACTED] Project: [REDACTED] Contact: [REDACTED] Other Info: No. Counts: I O X Porosity (point count): Dag%: Perm mD: Porosity %: Main cements: TS Storage Location: TS Info: Circle Polished: <input checked="" type="checkbox"/> OR Conventional: <input type="checkbox"/> Stained: <input type="checkbox"/> Oriented thin section? YES Orientation method (core): Notch indicates= deep end (down): Carbonates: Feldspar: Sidewall? Full Diameter? Rock Mass (Notes) (IDX Inspection): Visible porosity: YES/NO Visible: (postkinematic cement) Cement sequence: Fracture (Notes): Visible fractures: 3 Phases in fractures: Sequence: Comments: subvertical fracture with crystalline cement branches out into two top of the fracture terminates against high-relieved large mineral grains part of a slickenside multiple small short fibrous beef present at least one was cut across by the large fracture one thin cement-free horizontal fracture cuts across the central fracture it's a vertical thinsection Diagrams of key relations (Note location on reference map). Note Appx. Scale.
Thin Section Map II	
	
	
	
	
	
	

Petrographic Summary

DATE: 12/29/2016
 STUDY: Eb, John, LJ

Well Name: [REDACTED] Date Rec'd: [REDACTED] TS Storage Location: [REDACTED]

Depth (ft): [REDACTED] No. Counts: 1

Sample Number: 12-14 Date processed: [REDACTED] Analyst 1: [REDACTED] Analyst 2: [REDACTED]

Formation: Vaca Muerta Project: [REDACTED] Contact: [REDACTED]

Depth (ft): 2751.75 Porosity (point count): [REDACTED] Other Info: [REDACTED]

ROCK TYPE: [REDACTED] Dq%: [REDACTED] Perm mD: [REDACTED] (from.....)

GRAIN SIZE: [REDACTED] Porosity %: [REDACTED] Main cements: [REDACTED] (from.....)

Thin Section Map: [REDACTED] 6


Mark key features: 3 4 5

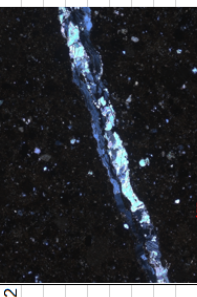
Mark traverse location: 1 2

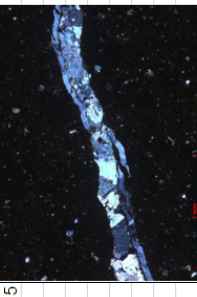
Label "up direction": [REDACTED]

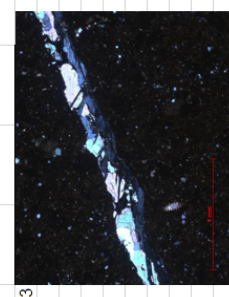
TS Info: Polished IR Conventional Stained Carbonates Feldspar Sidewall? Full Diameter?

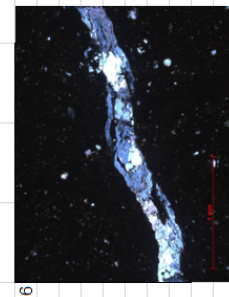
Match indicates: Well center


Thin Section Map I: 


Thin Section Map II: 

Thin Section Map III: 

Thin Section Map IV: 

Thin Section Map V: 

Thin Section Map VI: 


Thin Section Map VII: 

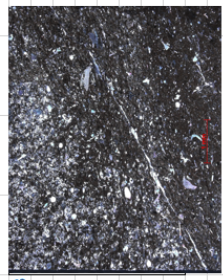
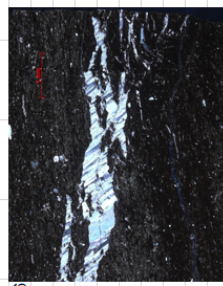
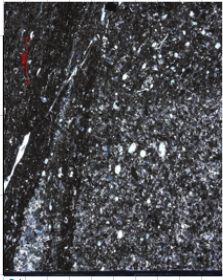
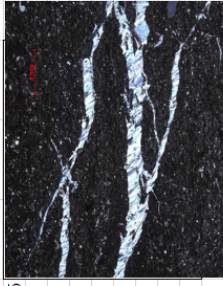
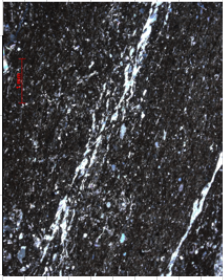
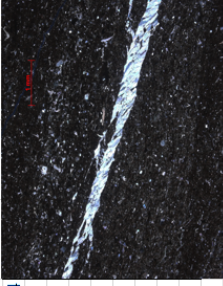
Comments: fracture filled with various crystalline cement with clear cleavages
 it's a horizontal thin section through a vertical fracture

Diagrams of key relations (Note location on reference map). Note Appx. Scale.


Petrographic Summary

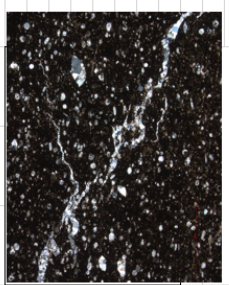
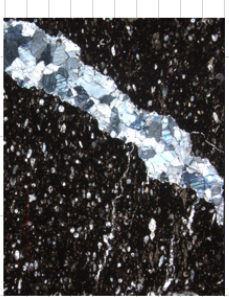
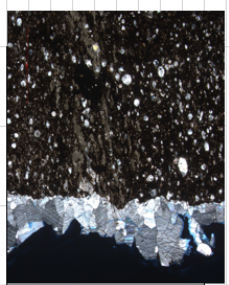
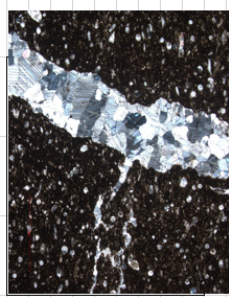
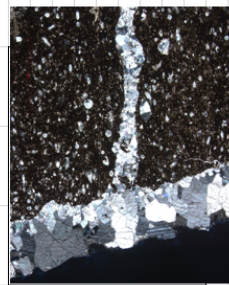
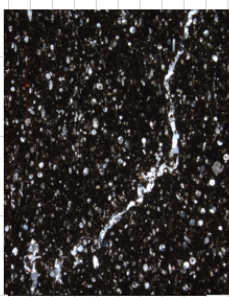
DATE: 1/29/2016
 STUDY: By John LI

Well Name	Date Rec'd	No. Counts	TS Storage Location
Depth (ft)	Date processed	I	
Sample Number 2-1241	Analyst 1	O	
Formation Vaca Muerta	Project	X	
Depth (ft) 2741.52m	Contact		Other Info
ROCK TYPE		Dg%	(from.....)
GRAIN SIZE		Perm md	(from.....)
Thin Section Map		Porosity %	
Mark key features	1	Main cements	
Mark traverse location	2		
Label "up direction"	3	6	
TS Info-----Circle:	Polished <input type="checkbox"/> OR Conventional <input type="checkbox"/> Stained <input type="checkbox"/>	Carbonates	Faldispar
	Oriented thin section? YES <input type="checkbox"/> NO <input type="checkbox"/>	Orientation method (core).....	Sidewall? Full Diameter?
	Match indicates.....shallow end (up).....		
Thin Section Map II		Rock Mass (Notes) IDX Inspection	
	X	Visible porosity YES <input type="checkbox"/> NO <input type="checkbox"/>	
	X	Visible _____ (post/intrinsic cement)	
	X	Cement sequence.....	
		Fracture (Notes)	
		Visible fractures... Multiple ...	
		Phases in fractures.....	
		Sequence.....	
		Comments: A vertical slide with a portion of an elliptical nodule bounded by thin fibrous fractures.	
		1mm thick low-angled fibrous beef going through the middle of the thin section	
		2 to 3 thin fibrous fractures branching out from the beef	
		2 long, 50micron thick cement-free horizontal fractures partially overlap with cemented thin fractures	
		Diagrams of key relations (Note location on reference map). Note Appx. Scale.	




Petrographic Summary

DATE 1/23/2016 STUDY: By John Li					
Well Name [redacted]	Date Rec'd	No. Counts	TS Storage Location		
Depth (ft) [redacted]	Date processed	1			
Sample Number 33A	Analyst 1	0			
Formation Yaca Muerta	Project	X			
Depth (ft) 2974m	Contact		Other Info		
ROCK TYPE		Dq%	(from.....)		
GRAIN SIZE		Perm md	(from.....)		
Thin Section Map		Porosity %			
Mark key features	1	Main cements			
Mark traverse location	3				
Label "up direction"	4				
2	6				
TS Info-----Circle	Polished [] OR []	Conventional	Stained	Carbonates	Feldspar
	Oriented thin section? YES	Orientation method (core).....			Sidewall? Full Diameter?
Notch indicates-----up					
Thin Section Map II					
	Rock Mass (Notes) IDX Inspection Visible porosity YES NO Visible _____ (postkinematic cement) Cement sequence.....				
	Fracture (Notes) Visible fracture 5 Phases in fractures..... Sequence.....				
	Comments: Vertical thin section through a subvertical fracture (1mm aperture) with crystalline (calcite) multiple smaller horizontal/low angle calcite-cemented fracture left edge of the thinsection is part of the broken face in core with calcite				
	Diagrams of key relations (Note location on reference map). Note Appx. Scale.				



DATE 10/30/2016										STUDY: By John, LJ										Petrographic Summary																	
Well Name		[REDACTED]		Date Rec'd		No. Counts		TS Storage Location		1										4																	
Depth (ft)		[REDACTED]		Date processed		Analyst 1		O		[REDACTED]										[REDACTED]																	
Sample Number		3-3B		Analyst 1		Project		X		[REDACTED]										[REDACTED]																	
Formation		Vaca Muerta		Contact		Porosity (point count)		Other Info		[REDACTED]										[REDACTED]																	
Depth (ft)		297.4m		ROCK TYPE		Perm mD		(from.....)		[REDACTED]										[REDACTED]																	
GRAIN SIZE		[REDACTED]		Porosity %		(from.....)		Main cements		[REDACTED]										[REDACTED]																	
Thin Section Map		1		3		4		5		[REDACTED]										[REDACTED]																	
Mark traverse location		[REDACTED]		6		[REDACTED]		[REDACTED]		[REDACTED]										[REDACTED]																	
Label "up direction"		[REDACTED]		[REDACTED]		[REDACTED]		[REDACTED]		[REDACTED]										[REDACTED]																	
TS Info-----Circle		Polished		OR		Conventional		Stained		Carbonates		Feldspar		Sidewall?		Full Diameter?		[REDACTED]										[REDACTED]									
Oriented thin section?		YES		Orientation method (core)		[REDACTED]		[REDACTED]		[REDACTED]		[REDACTED]		[REDACTED]		[REDACTED]		[REDACTED]										[REDACTED]									
Notch indicates=		up		[REDACTED]		[REDACTED]		[REDACTED]		[REDACTED]		[REDACTED]		[REDACTED]		[REDACTED]		[REDACTED]										[REDACTED]									
Thin Section Map II		[REDACTED]		[REDACTED]		[REDACTED]		[REDACTED]		[REDACTED]		[REDACTED]		[REDACTED]		[REDACTED]		[REDACTED]										[REDACTED]									
Rock Mass (Notes) IX Inspection		Visible porosity		YES		NO		Visible		[REDACTED]		[REDACTED]		[REDACTED]		[REDACTED]		[REDACTED]										[REDACTED]									
Cement sequence		[REDACTED]		[REDACTED]		[REDACTED]		[REDACTED]		[REDACTED]		[REDACTED]		[REDACTED]		[REDACTED]		[REDACTED]										[REDACTED]									
Fracture (Notes)		Visible fractures		[REDACTED]		[REDACTED]		[REDACTED]		[REDACTED]		[REDACTED]		[REDACTED]		[REDACTED]		[REDACTED]										[REDACTED]									
Phases in fractures		[REDACTED]		[REDACTED]		[REDACTED]		[REDACTED]		[REDACTED]		[REDACTED]		[REDACTED]		[REDACTED]		[REDACTED]										[REDACTED]									
Sequence		[REDACTED]		[REDACTED]		[REDACTED]		[REDACTED]		[REDACTED]		[REDACTED]		[REDACTED]		[REDACTED]		[REDACTED]										[REDACTED]									
Comments:		vertical thin section through multiple sub-verticle fractures		fully filled with crystalline calcite cement		[REDACTED]		[REDACTED]		[REDACTED]		[REDACTED]		[REDACTED]		[REDACTED]		[REDACTED]										[REDACTED]									
Diagrams of key relations		[REDACTED]		[REDACTED]		[REDACTED]		[REDACTED]		[REDACTED]		[REDACTED]		[REDACTED]		[REDACTED]		[REDACTED]										[REDACTED]									
Note location on reference map		[REDACTED]		[REDACTED]		[REDACTED]		[REDACTED]		[REDACTED]		[REDACTED]		[REDACTED]		[REDACTED]		[REDACTED]										[REDACTED]									
Note Appx. Scale		[REDACTED]		[REDACTED]		[REDACTED]		[REDACTED]		[REDACTED]		[REDACTED]		[REDACTED]		[REDACTED]		[REDACTED]										[REDACTED]									

DATE 11/30/2016										STUDY: By John Li										Petrographic Summary									
Well Name		Date Rec'd		No. Counts		TS Storage Location		1		4		1		4		2		5		6									
Depth (ft)		Date processed		No. Counts		TS Storage Location		1		4		1		4		2		5		6									
Sample Number E3A		Analyst 1		O																									
Formation Vaca Muerta		Project		X																									
Depth (ft)		Contact		Porosity (point count)		Other info																							
ROCK TYPE		Dg%		Perm mD		(from.....)																							
GRAIN SIZE		Porosity %		Porosity %		(from.....)																							
Thin Section Map		Main cements																											
Mark traverse location		2		3		4		5		6																			
Label "up direction"																													
TS Info-----Circle		Polished		DR		Conventional		Stained		Carbonates		Feldspar		Sidewall?		Full Diameter?													
Oriented thin section? YES		UP		Orientation method (core).....																									
Notch indicates--		UP																											
Thin Section Map II																													
Comments:		subvertical thinsection through a 2 to 4mm thick vertical stylolite		between shale and the overlying coarse-grained portion (see 4)		multiple cement-free thin vertical and horizontal fractures present (e.g. 6)		stylolite is thicker in the coarser layer																					
Diagrams of key relations (Note location on reference map). Note Appx. Scale.																													

DATE 11/30/2016
STUDY: By John LI

Well Name: [REDACTED] Date Rec'd: [REDACTED] No. Counts: 1 TS Storage Location: [REDACTED]

Depth (ft): [REDACTED] Analyst 1: O Analyst 2: [REDACTED]

Sample Number: 53B Project: Contact Porosity (point count): [REDACTED]

Formation: Vacca Muerta Other Info: [REDACTED]

Depth (ft): [REDACTED] Dg%: [REDACTED] Perm mD: [REDACTED] Porosity %: [REDACTED] Main cements: [REDACTED]

ROCK TYPE: [REDACTED]

GRAIN SIZE: [REDACTED]

Thin Section Map: [REDACTED]

Mark traverse location: 1 2 3 4 5 6


Label "up direction": [REDACTED]

TS Info: Circle [REDACTED] CR Conventional [REDACTED] Stained [REDACTED] Carbonates [REDACTED] Feldspar [REDACTED] Sidewall? [REDACTED] Full Diameter? [REDACTED]

Oriented thin section? YES [REDACTED] Orientation method (core): [REDACTED]

Notch indicates: UP [REDACTED]

Thin Section Map II



Polished [REDACTED] Rock Mass (Notes) [REDACTED] IODX Inspection [REDACTED]

Visible porosity: YES NO [REDACTED]

Visible [REDACTED] (postkinematic cement)

Cement sequence: [REDACTED]

Fracture (Notes) [REDACTED]

Visible fractures: 2 [REDACTED]

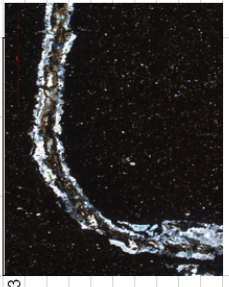
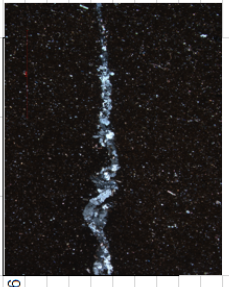
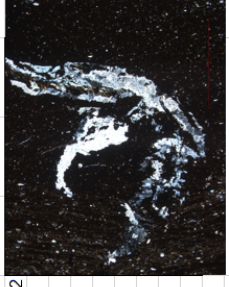
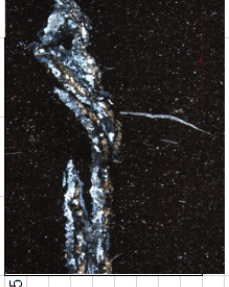
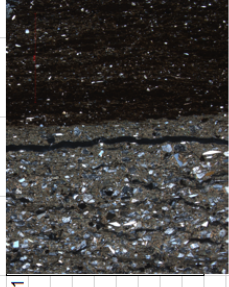
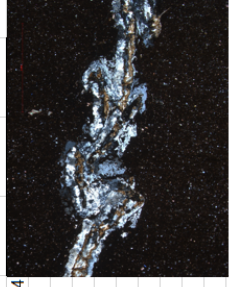
Phases in fractures: [REDACTED]

Sequence: [REDACTED]

Comments: vertical thin section through a vertical stylolite with a cement-free horizontal fracture in the upper coarse part near the lithologic contact (see 1)

Diagrams of key relations (Note location on reference map). Note Appx. Scale.

Petrographic Summary




Petrographic Summary

DATE: 1/30/2016
 STUDY: By John Li

Well Name: [REDACTED] TS Storage Location: [REDACTED]
 Depth (ft): [REDACTED] No. Counts: 1
 Date Rec'd: [REDACTED] Date processed: [REDACTED]
 Analyst 1: [REDACTED] Analyst 2: [REDACTED]
 Project: [REDACTED] Project: [REDACTED]
 Contact: [REDACTED] Contact: [REDACTED]
 Formation: Vaca Muerta
 Depth (ft): [REDACTED] Porosity (point count): [REDACTED]
 Other Info: [REDACTED]
 ROCK TYPE: [REDACTED] Dg%: [REDACTED]
 GRAIN SIZE: [REDACTED] Perm mD: [REDACTED]
 Thin Section Map: [REDACTED] Porosity %: [REDACTED]
 Mark key features: 3 4 5 6 Main cements: [REDACTED]
 Mark traverse location: [REDACTED]
 Label "up direction": 2 1

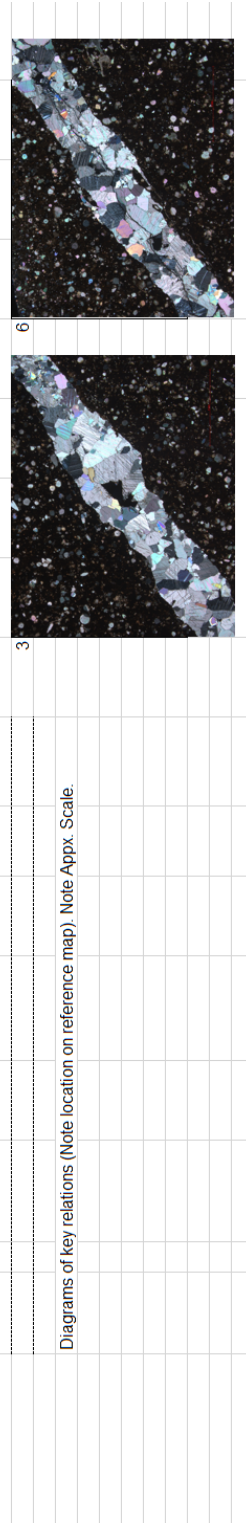
TS Info: Circle: [REDACTED] OR: Conventional: [REDACTED] Stained: [REDACTED] Carbonates: [REDACTED] Feldspar: [REDACTED]
 Oriented thin section? YES [REDACTED] Orientation method (core): [REDACTED]
 Notch indicates: core center [REDACTED] Sidewall? Full Diameter? [REDACTED]

Thin Section Map II



Rock Mass (Notes) I/OX Inspection
 Visible porosity: YES NO
 Visible: [REDACTED] (postkinematic cement)
 Cement sequence: [REDACTED]
 Fracture (Notes)
 Visible fractur: 1
 Phases in fractures: [REDACTED]
 Sequence: [REDACTED]

Comments: horizontal thin section through the width of a calcite-filled subvertical fracture
 transgranular fracture through the center of the fracture cements at 6



Diagrams of key relations (Note location on reference map). Note Appx. Scale.

References

- Anders, M.H., Laubach, S.E., and Scholz, C.H., 2014. Microfractures: a review. *Journal of Structural Geology* 69(B), 377-394.
- Atkinson, B.K., 1984. Subcritical crack growth in geological materials. *Journal of Geophysical Research* 89, 4077-4114.
- Bai, T., and Pollard, D.D., 2000. Fracture spacing in layered rocks: a new explanation based on the stress transition. *Journal of Structural Geology* 22(1), 43-57.
- Bai, T., Pollard, D.D., and Gao, H., 2000. Explanation for fracture spacing in layered materials. *Nature* 403, 753-756. doi:10.1038/35001550
- Bakulin, A., Grechka, V. and Tsvankin, I., 2000. Estimation of fracture parameters from reflection seismic data - Part I: HTI model due to a single fracture set. *Geophysics* 65, 1788-1802.
- Bonnet, E., Bour, O., Odling, N.E., Davy, P., Main, I., Cowie, P., and Berkowitz, B., 2001. Scaling of fracture systems in geological media. *Reviews of Geophysics* 29, 347-383.
- Caputo, R., and Hancock, P.L., 1998. Crack-jump mechanism of microvein formation and its implications for stress cyclicity during extension fracturing. *Journal of Geodynamics* 27(1), 45-60.
- Ciezobka, J., 2013. Marcellus shale gas project final report, RPSEA 09122-04.FINAL. <http://www.netl.doe.gov/File%20Library/Research/Oil-Gas/Natural%20Gas/shale%20gas/09122-04-final-report.pdf>
- Cobban, W.A., and Reeside, J.B., Jr., 1952. Frontier Formation, Wyoming and adjacent areas. *AAPG Bulletin* 36, 1913-1961.
- Coleman Jr., J.L., 2008. Tight-gas sandstone reservoirs: 25 years of searching for the answer. In: Cumella, S.P., Shanley, K.W., Camp, W.K., (Eds.), *Understanding, exploring, and developing tight-gas sands-2005 Vail Hedberg Conference*. AAPG Hedberg Series, No. 3, 221-250.
- Copley, L.K., 2015. Fracture sets, timing, and size distribution in the Cretaceous Frontier Formation, Greater Green River Basin, Wyoming. M.S. thesis, The University of Texas at Austin.
- Cumella, S.P., and Scheevel, J., 2008. The influence of stratigraphy and rock mechanics on Mesaverde gas distribution, Piceance Basin, Colorado. In: Cumella, S.P., Shanley, K.W., Camp, W.K., (Eds.), *Understanding, exploring, and developing tight-gas sands-2005 Vail Hedberg Conference*. AAPG Hedberg Series, No. 3, 137-155.

- DeJarnett, B.B., Lim, F.H., Krystinik, L.F., and Bacon, M.L., 2001. Greater Green River Basin Production Improvement Project, Final Report. U. S. Department of Energy, Federal Energy Technology Center, Contract no. DE-AC21-95MC31063.
- Delphia, J.G., and Bombolakis, E.G., 1988. Sequential development of a frontal ramp, imbricates, and a major fold in the Kemmerer region of the Wyoming thrust belt. *Geological Society of America Special Papers* 222, 207-222.
- Dunne, W.M., and North, C.P., 1990. Orthogonal fracture systems at the limits of thrusting: an example from southwestern Wales. *Journal of Structural Geology* 12(2), 207-215.
- Dunphy, R., and Campagna, D.J., 2011. Fractures, elastic moduli & stress: geological controls on hydraulic fracture geometry in the Horn River Basin. In: *Recovery-2011 CSPG CSEG CWLS Convention extended abstracts*.
- Dutton, S.P., Hamlin, H.S., and Laubach, S.E., 1995. Geologic controls on reservoir properties of low-permeability sandstone, Frontier Formation, Moxa Arch, southwestern Wyoming. *Bureau of Economic Geology Report of Investigations No. 234*, 89 p.
- Engelder, T., 1985. Loading paths to joint propagation during a tectonic cycle: an example from the Appalachian Plateau, USA. *Journal of Structural Geology* 7(3), 459-476.
- Engelder, T., Lash, G.G., and Uzcátegui R.S., 2009. Joint sets that enhance production from Middle and Upper Devonian gas shales of the Appalachian Basin. *AAPG Bulletin* 93(7), 857-889
- English, J.M., and Laubach, S.E., 2017. Opening-mode fracture systems – Insights from recent fluid inclusion microthermometry studies of crack-seal fracture cements. In: Turner, J.P., Healy, D., Hillis, R.R., and Welch, M. (Eds.), *Geomechanics and Geology: Geological Society, London, Special Publications*, 458. doi.org/10.1144/SP458.1
- English, J.M., and Johnston, S.T., 2004. The Laramide orogeny: what were the driving forces? *International Geology Review* 46(9), 833-838.
- Ekstrom, M.P., Dahan, C.A., Chen, M., Lloyd, P.M., and Rossi, D.J., 1987. Formation imaging with micro-electrical scanning arrays. *The Log Analyst* 28, 294-306.
- Garcia, M.N., Sorenson, F., Bonapace, J.C., Motta, F., Bajuk, C., and Stockman, H., 2013. Vaca Muerta shale reservoir characterization and description: The starting point for development of a shale play with very good possibilities for a successful project.. Presented at the *Unconventional Resources Technology Conference*, Denver, Colorado, 12-14 August, 2013. SPE 168666.

- Gale, J.F.W., Laubach, S.E., Pommer, L.E., Olson, J.E., Holder, J., and Naseem, K. 2012. Marcellus Shale Natural Fracture Project: The University of Texas at Austin, Final Report for RPSEA Marcellus Gas Shale Project, Project No. 09122-04, 134–181.
- Gale, J.F.W., Laubach, S.E., Olson, J.E., Eichhubl, P., and Fall, A. 2014. Natural Fractures in shale: a review and new observations. *AAPG Bulletin* 98, 2165-2216.
- Gillespie, P.A., Howard, C.B., Walsh, J.J., and Watterson, J., 1993. Measurement and characterization of spatial distributions of fractures. *Tectonophysics* 226, 114-141.
- Gillespie, P.A., Johnston, J.D., Loriga, M.A., McCaffrey, K.J.W., Walsh, J.J., and Watterson, J., 1999. Influence of layering on vein systematics in line samples. In: McCaffrey, K.J.W, Walsh, J.J., and Watterson, J. (Eds.), *Fracture, Fluid Flow, and Mineralization*. Geological Society [London] Special Publication 155, 35-56.
- Gillespie, P.A., Walsh, J.J., Watterson, J., Bonson, C.G, and Manzocchi, T., 2001. Scaling relationships of joint and vein arrays from The Burren, Co. Clare, Ireland. *Journal of Structural Geology* 23, 183-201.
- Guzmán, C., Cristallini, E., and Bottesi, G. 2007. Contemporary stress orientations in the Andean retroarc between 348 and 398S from borehole breakout analysis. *Tectonics*, 26, TC3016.
- Hartwell, L. 2008. Horn River horizontal well earnings: A case study. *Proceedings of Canadian Unconventional Gas 10th Annual Unconventional Gas Conference*.
- Hennings, P.H., Olson, J.E., and Thompson, L.B., 2000. Combining outcrop data and three-dimensional structural models to characterize fractured reservoirs: An example from Wyoming. *AAPG Bulletin* 84(6), 830-849.
- Hooker, J.N., Gomez, L.A., Laubach, S.E., Gale, J.F.W., and Marrett, R., 2012. Effects of diagenesis (cement precipitation) during fracture opening on fracture aperture-size scaling in carbonate rocks. In: Garland, J., Neilson, J.E., Laubach, S.E., Whidden, K.J. (Eds.), *Advances in Carbonate Exploration and Reservoir Analysis*. Geological Society, London, Special Publications 370, 187-206.
- Hooker, J.N., Laubach, S.E., and Marrett, R., 2013. Fracture-aperture size–frequency, spatial distribution, and growth processes in strata-bounded and non-strata-bounded fractures, Cambrian Mesón Group, NW Argentina. *Journal of Structural Geology* 54, 54-71.
- Hooker, J.N., and Katz, R.F, 2015. Vein spacing in extending, layered rock: The effect of synkinematic cementation. *American Journal of Science* 315, 557-588.
- Hooker, J.N., Laubach, S.E., and Marrett, R., 2017. Microfracture spacing distributions and the evolution of fracture patterns in sandstones. *Journal of Structural Geology*. doi.org/10.1016/j.jsg.2017.04.001

- Howell, J.A., Schwarz, E., Spalletti, L.A., and Veiga, G.D., 2005. The Neuquén Basin: an overview. In Veiga, G.D., Spalletti, L.A., Howell, J.A. and Schwarz, E., eds, *The Neuquén Basin, Argentina: A Case Study in Sequence Stratigraphy and Basin Dynamics*. Geological Society, London, Special Publications 252, 1-14.
- Jordan, T.E., 1981. Thrust loads and foreland basin evolution, Cretaceous, western United States. *AAPG Bulletin* 65(12), 2506-2520.
- Ladeira, F.L., and Price, N.J., 1981. Relationship between fracture spacing and bed thickness. *Journal of Structural Geology* 3, 179-183.
- Lander R.H., and Laubach, S.E., 2015. Insights into rates of fracture growth and sealing from a model for quartz cementation in fractured sandstones. *Geological Society of America Bulletin* 127(3-4), 516-538.
- Laubach, S.E., 1991. Fracture patterns in low-permeability-sandstone gas reservoir rocks in the Rocky Mountain Region. Society of Petroleum Engineers, SPE Conference Paper, 501–510. doi:10.2118/21853-MS
- Laubach, S.E., 1992. Fracture networks in selected Cretaceous sandstones of the Green River and San Juan Basins, Wyoming, New Mexico, and Colorado. In: Schmoker, J.W., Coalson, E.B., Brown, C.A. (Eds.), *Geological Studies Relevant to Horizontal Drilling: Examples from Western North America*. The Rocky Mountain Association of Geologists, Denver, 115-127.
- Laubach, S.E., 2003. Practical approaches to identifying sealed and open fractures. *AAPG Bulletin* 87, 561-579.
- Laubach, S.E., and Lorenz, J.C., 1992. Preliminary assessment of natural fracture patterns in Frontier Formation sandstones, southwestern Wyoming. Wyoming Geological Association 43rd Field Conference Guidebook, 87-96.
- Laubach, S.E., Olson, J.E, and Gross, M. R., 2009. Mechanical and fracture stratigraphy. *AAPG Bulletin* 93(11), 1413-1426.
- Laubach, S.E., Fall, A., Copley, L.K., Marrett, R., and Wilkins, S.J., 2016. Fracture porosity creation and persistence in a basement-involved Laramide fold, Upper Cretaceous Frontier Formation, Green River Basin, USA. *Geological Magazine* 153 (5/6), 887-910.
- Li, J.Z., Gale, J.F.W., Marrett, R.A., and Laubach, S.E., 2016. Quantifying natural fracture spatial organization in horizontal image logs: Application in Unconventional Reservoirs. Presented at the Unconventional Resources Technology Conference, San Antonio, Texas, 1-3 August, 2016. URTEC-2456264-MS
- Li, J.Z., Laubach, S.E., Gale, J.F.W., and Marrett, R.A., 2017. Quantifying opening-mode fracture spatial organization in horizontal wellbore image logs, core and outcrop:

- application to Upper Cretaceous Frontier Formation tight gas sandstones, USA. *Journal of Structural Geology*, in press.
- Lofts, J.C., Bedford, J., Boulton, H., Van Doorn, J.A., and Jeffreys, P., 1997. Feature recognition and the interpretation of images acquired from horizontal wellbores. In: Lovell, M.A and Harvey, P.K. (Eds.), *Developments in Petrophysics*. Geological Society Special Publication 122, 345-365.
- Lofts, J.C., and Bourke, L.B., 1999. The recognition of artifacts from acoustic and resistivity borehole imaging devices. In: Lovell, M., Williamson, G., and Harvey, P. (Eds.), *Borehole Imaging: Applications and Case Histories*. Geological Society Special Publication 159, 59-76. doi:10.1144/GSL.SP.1999.159.01.03
- Lorenz, J.C., and Laubach, S.E., 1994. Description and interpretation of natural fracture patterns in sandstones of the Frontier Formation along the Hogsback, Southwestern Wyoming. Topical Report to Gas Research Institute, GRI-94/0020.
- Lorenz, J.C., Krystinik, L.F., and Mroz, T.H., 2005. Shear reactivation of fractures in deep Frontier Sandstones: Evidence from horizontal wells in the Table Rock Field, Wyoming. In: Bishop, M.G., Cumella, S.P., Robinson, J.W., Silverman, M.R. (Eds.), *Gas in Low Permeability Reservoirs of the Rocky Mountain Region*, Rocky Mountain Association of Geologists Guidebook, 267-288.
- Luthi, S.M., and Souhaité, P., 1990. Fracture apertures from electrical borehole scans. *Geophysics* 55, 821–833.
- Marrett, R., Gale, J.F.W., Gomez, L.A., and Laubach, S.E., 2017. Correlation analysis of fracture arrangement in space. *Journal of Structural Geology*.
- McGinnis, R.N., Ferrill, D.A., Smart, K.J., Morris, A.P., Higuera-Diaz, C., Prawika, D., 2015. Pitfalls of using entrenched fracture relationships: Fractures in bedded carbonates of the Hidden Valley Fault Zone, Canyon Lake Gorge, Comal County, Texas. *AAPG Bulletin* 99, 2221-2245.
- McGinnis, R.N., Ferrill, D.A., Morris, A.P., Smart, K.J., Lehrmann, D., 2017. Mechanical stratigraphic controls on natural fracture spacing and penetration. *Journal of Structural Geology* 95, 160-170.
- Merewether, E.A., 1983. The Frontier Formation and Mid-Cretaceous orogeny in the foreland of southwestern Wyoming. *The Mountain Geologist* 20(4), 121-138.
- Narr, W., and Lerche, I., 1984. A method for estimating subsurface fracture density in core. *AAPG Bulletin* 68(5), 637-648.
- Narr, W., and Suppe, J., 1991. Joint spacing in sedimentary rocks. *Journal of Structural Geology* 13, 1037-1048.

- Olson, J.E., 1993. Joint pattern development: Effects of subcritical crack growth and mechanical interaction. *Journal of Geophysical Research* 98 (B7), 12251-12265.
- Olson, J.E., 2004. Predicting fracture swarms – the influence of subcritical crack growth and the crack-tip process zone on joint spacing in rock. In: Cosgrove, J.W., Engelder, T. (Eds.), *The Initiation, Propagation, and Arrest of Joints and Other Fractures*. Geological Society, London, Special Publications 231, 73-87.
- Olson, J. E, Laubach, S. E., and Lander, R. H., 2009. Natural fracture characterization in tight gas sandstones: Integrating mechanics and diagenesis. *AAPG Bulletin* 93(11), 1535-1549.
- Ortega, O., Marrett, R., and Laubach, S.E., 2006. A scale-independent approach to fracture intensity and average spacing measurement. *AAPG Bulletin* 90, 193-208.
- Ozkan, A., Cumella, S.P., Milliken, K.L., and Laubach, S.E., 2011. Prediction of lithofacies and reservoir quality using well logs, Williams Fork Formation, Mamm Creek Field, Piceance Basin. *AAPG Bulletin* 95(10), 1699-1723.
- Pan, Y., Hui, M.H., Narr, W., King, G.R., Tankersley, T., Jenkins, S., Flodin, E., Bateman, P., Laidlaw, C. and Vo, H.X., 2016. Integration of pressure-transient data in Modeling Tengiz Field, Kazakhstan—A new way to characterize fractured reservoirs. *SPE Reservoir Evaluation & Engineering* 19(1), 5-17. doi.org/10.2118/165322-PA
- Panza, E., Agosta, F., Rustichelli, A., Zambrano, M., Tondi, E., Prosser, G., Giorgioni, M. and Janiseck, J.M., 2016. Fracture stratigraphy and fluid flow properties of shallow-water, tight carbonates: The case study of the Murge Plateau (southern Italy). *Marine and Petroleum Geology* 73, 350-370.
- Pommer, L.E, 2013. Natural fracture cementation in the Marcellus Formation. M.S. thesis, The University of Texas at Austin.
- Pöppelreiter, M., García-Carballido, C., and Kraaijveld, M., 2010. Borehole image log technology: Application across the exploration and production life cycle. In: Pöppelreiter, M. García-Carballido, C., and Kraaijveld, M. (Eds.), *Dipmeter and borehole image log technology*. AAPG Memoir 92, 1–13.
- Ponziani, M., Slob, E.C., Luthi, S.M., Bloemenkamp, R.F., and Le Nir, I., 2013. Fracture characterization from Formation MicroImager Data. In 75th EAGE Conference & Exhibition incorporating SPE EUROPEC 2013.
- Price, N.J., 1996. *Fault and joint development in brittle and semi-brittle rock*: London, United Kingdom, Pergamon Press, 176 p.
- Priest, S.D., and Hudson, J.A., 1976. Discontinuity spacings in rock. *International Journal of Rock Mechanics* 13, 135-148.

- Putz-Perrier, M.W., Sanderson, D.J., 2008. The distribution of faults and fractures and their importance in accommodating extensional strain at Kimmeridge Bay, Dorset, UK. In: Wibberley, C.A.J., Kurz, W., Holdsworth, R.E., and Collettini, C. (Eds.), *The internal structure of fault zones: implications for mechanical and fluid-flow properties*. Geological Society [London] Special Publication 299, 97–111.
- Questiaux, J.M., Couples, G.D., and Ruby, N., 2010. Fractured reservoirs with fracture corridors. *Geophysical Prospecting* 58, 279–295.
- Reynolds, M.M., and Munn, D.L., 2010. Development update for an emerging shale gas giant field - Horn River Basin, British Columbia, Canada. In *SPE Unconventional Gas Conference*, 23-25 February, Pittsburgh, Pennsylvania, USA.
- Rickman, R., M. Mullen, E. Petre, B. Grieser, and D. Kundert, 2008. A practical use of shale petrophysics for stimulation design optimization: All shale plays are not clones of the Barnett shale. *Annual Technical Conference and Exhibition, SPE*, SPE115258.
- Rodrigues, N., Cobbold, P.R., Loseth, H., and Ruffet, G., 2009. Widespread bedding-parallel veins of fibrous calcite ('beef') in a mature source rock (Vaca Muerta Fm, Neuquén Basin, Argentina): evidence for overpressure and horizontal compression. *Journal of the Geological Society, London* 166, 695–709.
- Rogers, S., Elmo, D., Dunphy, R. and Bearinger, D., 2010. Understanding hydraulic fracture geometry and interactions in the Horn River Basin through DFN and numerical modeling. In *Canadian Unconventional Resources and International Petroleum Conference*. Society of Petroleum Engineers.
- Ross, D.J.K., and Bustin, R.M., 2008. Characterizing the shale gas resource potential of Devonian–Mississippian strata in the Western Canada sedimentary basin: Application of an integrated formation evaluation. *AAPG Bulletin* 92(1), 87–125.
- Solano, N., Zambrano, L., and Aguilera, R., 2011. Cumulative-gas-production distribution on the Nikannassin Tight Gas Formation, Alberta and British Columbia, Canada. *SPE Reservoir Evaluation & Engineering* 14, 357-376. doi:10.2118/132923-PA.
- Terzaghi, R., 1965. Sources of error in joint surveys. *Geotechnique* 15, 287-297.
- USGS Marcellus Shale Assessment Team, 2011, Information relevant to the U.S. Geological Survey assessment of the Middle Devonian Shale of the Appalachian Basin Province, 2011: U.S. Geological Survey Open-File Report 2011–1298, 22 p.
- Vergani, G.D., Tankard, A.J., Belotti, H.J., and Welsink, H.J., 1995. Tectonic evolution and paleogeography of the Neuquén basin, Argentina. In A. J. Tankard, R. Suárez S., and H. J. Welsink, *Petroleum Basins of South America*. AAPG Memoir 62, 383–402.

- Walsh, J.J., and Watterson, J., 1993. Fractal analysis of fracture patterns using the standard box-counting technique: valid and invalid methodologies. *Journal of Structural Geology* 15, 1509-1512.
- Watkins, H., Healy, D., Bond, C.E., and Butler, R.W., 2017. Implications of heterogeneous fracture distribution on reservoir quality; an analogue from the Torridon Group sandstone, Moine Thrust Belt, NW Scotland. *Journal of Structural Geology*. doi.org/10.1016/j.jsg.2017.06.002
- Wiltschko, D.V., Dorr, J.A., 1983. Timing of deformation in overthrust belt and foreland of Idaho, Wyoming, and Utah. *AAPG Bulletin* 67, 1304-1322.
- Wright, G.N., McMechan, M.E., Potter, D.E.G., and Holter, M.E., 1994. Structure and architecture of the Western Canada Sedimentary Basin. In of western Canadian Basins. In: Massop, G.D., and Shetsen, I. (Eds.), *Geological Atlas of the Western Canada Sedimentary Basin*. Canadian Society of Petroleum Geologists and Alberta Research Council, Special Report 4.
- Wu, H., and Pollard, D., 1995. An experimental study of the relationship between joint spacing and layer thickness. *Journal of Structural Geology* 17, 887-905.
- Yang, S., Harris, N., and Dong, T., 2015. Mechanical properties and natural fractures in a Horn River Shale core from well logs and hardness measurements. In SPE EUROPEC 2015. SPE-174287-MS